Upstream Approaches for Whole Heart Tissue Engineering

Inaugural-Dissertation

zur Erlangung des Doktorgrades
der Mathematisch-Naturwissenschaftlichen Fakultät
der Heinrich-Heine-Universität Düsseldorf

vorgelegt von

Jörn Hülsmann

aus Lohne

Düsseldorf, Oktober, 2017

aus der Forschungsgruppe Experimentelle Chirurgie,

Klinik für Kardiovaskuläre Chirurgie, Medizinische Fakultät

der Heinrich-Heine-Universität Düsseldorf.

Mentor: **Prof. Dr. med. Payam Akhari**

Gedruckt mit der Genehmigung der
Mathematisch-Naturwissenschaftlichen Fakultät der

Heinrich-Heine-Universität Düsseldorf

Referent: **Prof. Dr. med. Artur Lichtenberg**

Korreferent: **Prof. Dr. rer. nat. Eckhardt Lammert**

Tag der mündlichen Prüfung: 26.02.2018

Zusammenfassung

Erkrankungen des Herzens sind mit einem Anteil von mehr als 20 % für einen Großteil der Todesfälle in Europa verantwortlich [1]. Eine echte Heilung übersteigt bis heute leider noch die medizinischen Therapiemöglichkeiten. Allerdings gab es in der jüngsten Vergangenheit einen hoffnungsschöpfenden Durchbruch in der Kardiovaskulären Forschung indem der Ansatz des sog. *Whole Heart Tissue Engineerings* die komplexe Mikroarchitektur der Extrazellulärmatrix des Myokards dem mittlerweile sehr fortgeschrittenen Forschungsgebiet kardialer regenerativer Medizin eröffnete [2-4].

Diese Arbeit konzentriert sich auf Grundanforderungen für eine angestrebte pharmaindustrielle Produktion von Ganzherz-Konstrukten als Medizinprodukt und soll dafür Lösungsansätze auf dem Stand des wissenschaftlichen Fortschritts bereitstellen. In aktuellen Studien liefern die gängigen Methoden zur Herstellung und Prozessierung von Ganzherz-Konstrukten bereits vielversprechende Ergebnisse [5-9]. Allerdings scheint die Entwicklung hier im Grundkonsens einer Ein-Schritt-Gesamtoptimierung zu folgen. Dabei werden sowohl Donororgane als auch Zellen von möglichst klinischer Relevanz verwendet, um maximale Zellzahlen so lange wie technisch möglich unter Einsatz bewährter biophysikalischer Stimulation zu kultivieren. Im direkten Gegensatz dazu ist es die zentrale Arbeitshypothese dieser Arbeit, dass weder der gegebene wissenschaftliche Fortschritt noch der Stand der Technik dem hohen wissenschaftlichen Anspruch dieser Vorgehensweise bereits entspricht.

Bei der Bearbeitung dieser Arbeitshypothese musste zunächst der bisher undurchsichtige Prozess der Zellentfernung, die Dezellularisierung, aufgeklärt und verfahrenstechnisch greifbar gemacht werden. Dafür wurde die Dynamik und Kinetik des Biomasseaustrags ermittelt und mit Hilfe von Parametern und Variablen beschrieben. Über den Vergleich spezifischer Austragsraten zeigte sich, dass die Größe und Masse eines Organs offenbar weniger Einfluss auf die Dynamik der Dezellularisierung hat, sondern es vielmehr eine beachtliche individuelle Varianz zwischen einzelnen Organen vergleichbarer Biomasse gibt. Über Computersimulationen auf Basis eines vereinfachten Austragsmodels konnten diese Varianzen hauptsächlich auf Massentransportlimitierungen zurückgeführt werden. Während der Perfusions-Dezellularisierung zeigten sich charakteristische fluiddynamische Phänomene, die online identifiziert und bioanalytisch dem Auftreten von Viskoelastizität basierend auf der Freisetzung von Zelldebris in das Perfusat zugeordnet werden konnten. Damit gibt es nun eine realistische Messgröße als Grundlage für zukünftige Prozessautomatisierung und Qualitätskontrolle. Weiterhin wurden die etablierten Verfahren von biomechanischer und elektrophysiologischer Stimulation auf die Kultivierung von Ganzherz-Konstrukten übertragen und in “proof of principle“ Studien etabliert. Unter Dehnung des linken Ventrikels zeigte sich dabei in kurzen kontrollbasierten Modell-Kultivierungen eine deutliche Steigerung in der räumlichen Organisation und metabolischen Aktivität sowie in der Entwicklung von zellbiologischen Grundbausteinen myokardialer Funktionalität wie Myosin und Connexin 43 in neonatalen Kardiomyozyten. Zusätzlich zeigte die Stimulation über ein achtpoliges elektrisches Feld eine deutliche gesteigerte Intensität von Amplituden und Schlagraten gemessener spontaner elektrophysiologischer Aktivität sowie ebenso gesteigerte Anteile der myokardialen Markerproteine Myosin, Troponin T, Desmin und Connexin 43. Die Erkenntnisse aus diesen Studien liefern somit eine solide Basis und wichtige Ansatzpunkte für zukünftige Optimierungsprozesse.

Abstract

Cardiac diseases and subsequent injury to the heart belong to the major causes of mortality in the EU with a quota of more than 20 % [1]. Up to now, in many circumstances truly curative treatment options remain beyond of our abilities. But in the recent past, the approach of whole heart tissue engineering has raised hope by providing access to the complex architecture of native myocardial extracellular matrix for the by now very advanced and sophisticated field of myocardial regenerative medicine [2-4].

This work focuses on interface and transfer problems between scientific advance in whole heart tissue engineering and basic requirements for a potential pharmaco-industrial production of whole heart constructs (WHC) as medical devices. While current studies on the generation and processing WHC have already reported promising results, the consensus seems to aspire to one step optimization by trial and error [5-9]. Thereby preferably human sized scaffolds are repopulated preferably with cells of a prospective clinical relevance at maximal cell-densities and processed as long as technically possible under biophysical stimulation, which again is mostly designed as advanced as possible. In contrast, the central working hypothesis of this work is that neither the scientific advance and state of knowledge, nor the scientific-technical state of the art already complies with the demands of that high scientific level.

From the perspective of a procedural upstream, at first the black-box process of cell removal by decellularization had to be enlightened. For the first time, we resolved the dynamics and kinetics of biomass depletion and determined parameters and variables that enabled us to describe the decellularization as a decomposition process. Thereby discovered characteristics imply a certain independency from the biomass amount, but rather an increased susceptibility for individual organs with regards to mass transport limitations. Moreover we identified characteristic fluid dynamical phenomena and evaluated the underlying development of viscoelasticity in the perfusates as a quantitative measure for the release of cell-debris during perfusion based whole heart decellularization.

Furthermore we designed an open and integrative bioreactor system that transfers key principles of biophysical stimulation, that have been established in the field of myocardial tissue engineering, to the whole heart approach. By our concept of fully automated and controlled left ventricular stretching we found a clearly beneficial impact on cellular spatial alignment, metabolic activity and the development of myocardial functionality by increasing the specific contents of myosin heavychain and connexin 43 in control based short term model cultivations (CMC) with neonatal rodent cardiomyocytes. Moreover we adapted the concept of electrical field stimulation to the spatially highly organized WHC by an alternating 8-pole setting. Its application in the herein established CMC method could provoke significantly increased functional electrophysiological activity as measured by amplitudes in surface voltage recordings and as indicated by the rate of spontaneous beating activity. These findings could further be substantiated by western blot analyses showing increased ratios of myosin heavychain, cardiac troponin T, desmin and connexin 43.

Overall this work presents first cornerstones for a non-destructive monitoring and quality control of the decellularization process on the one hand and for further process optimization on the subsequent procedural flow of WHC generation and processing.

Content

1. Introduction

1.1. Background

In the field of regenerative medicine the concept of organ engineering raises hope to generate functional replacement tissue for damaged or diseased organs, at least in parts, and to a partial or minimally required level of functionality.

In case of the heart, such scientific endeavour still is an ambitious long-term objective, as due to the high complexity of native myocardium myocardial tissue engineering still is restricted to fundamental laboratory research. Notwithstanding, in recent years the possibility of decellularization of whole organs has established a promising path to deal with that complexity by the utilization of the naturally designed micro-architecture. In its biochemical and biophysical environmental characteristics the resulting whole organ scaffolds already contain and provide structures for parenchymal and interstitial revitalization for the generation of considerable holistic constructs.

Scince its first emergence by the pioneering work by Ott et al. in 2008 the whole-organ engineering approach established a novel and independent area of research [2]. Even though this field is still a young discipline, it is expected that it could dramatically enhance the perspectives of a curative therapy of end-organ failure in several clinical disciplines. And this potential outlook is even hoped for the near future to achieve clinical reality. So Prof. Stephen Badylak from the McGowan Institute for Regenerative Medicine at the University of Pittsburgh described a prognosis of five to seven years until he expected the first successfully implanted tissue engineered lungs or lobes of the liver already in 2013 [10].

Actually it was him again, who recently presented successfully reconstructed functional skeletal muscle tissue after transplantation of large volume decellularized muscle-patches in clinical studies [11]. Moreover, Prof. Doris Taylor from the Texas Heart Institute in Houston, Texas, the senior author of the mentioned pioneering work from 2008, presumes that in case of tissue engineered myocardium based on decellularized whole heart scaffolds, even imperfectly matured patches could be clinically applicable e.g. for underdeveloped hyperplasized hearts [10].

Of course this new path is not as unresistingly straight to go, as in the same it arises hope to overcome complex problems simply by *mother nature's* design. By the inherent high and even super-ordinate organization, whole organ scaffolds bring a new dimension that also has to be mastered in technical and scientific handling. Ultimately, this new dimension challenges it all, the preservative generation, the selective repopulation as well as the processing of resulting constructs and their analytical evaluation.

Regarding this, in the relative young field of whole organ tissue engineering, there are no established standard methods yet. As a matter of cause, special method development as well as adaption of common methods to the specific demands of the artificial whole heart constructs is involved in this research project as required working tools.

But to meet these challenges systematically in a coherent concept, it is important to stay focussed on the desired clinical application of the produced constructs. It has to be pointed out that in general the longterm-objective for the development of medical devices is to strive towards an FDA Approval (or equivalent in non-US-countries) for clinical trials. Of course this is far beyond the ambition of the present work, but nevertheless it becomes more and more topical. Recently teams of experienced and knowledgeable experts discussed and scripted detailed strategies for potential pre-clinical and clinical trials for both “conventional” tissue engineered myocardial patches as well as whole heart constructs [12-15].

1.2. Objectives

In this context, the most coherent concept to solve the given actual challenges in whole heart tissue engineering seems to be the incorporation into the logic of an industrial upstream procedure. Consequently, this thesis describes a multi-level approach to solve main interface- and transfer problems between scientific advance in whole heart tissue engineering and basic requirements for a potential pharmaco-industrial production of tissue engineered myocardium. More precisely the establishment of upstream approaches in 4 steps is attempted:

1) Verification of availability of suitable biologic raw-material.
2) Enabling of quality control and process automation for a preparative process-upstream.
3) Enabling automation for processing and cultivation methods for production processes.
4) Development and optimization of bioprocesses for the production.

From the procedural point of view, at the actual state of the art in science and technology the specific actual challenges in whole heart tissue engineering determine industrial barriers and technical hurdles that complicate or impede the proceeding to commercial provision of whole organ constructs in general as illustrated in figure 1.

Those technical complications usually arise at the junction of closely related thematic fields and areas of research. Here the first 2 steps are required to adapt the conventential procedures of the whole heart decellularization field to an efficient and controllable flux to further processing by repopulation and cultivation. The third step is essential to provide suitable processing equipment and methodology, which can be derived by the field of modern bioreactor technology. But prior to any processing, the basic concepts have to be transferred and translated from the established fundamentals of the Cardivascular Tissue Engineering field.

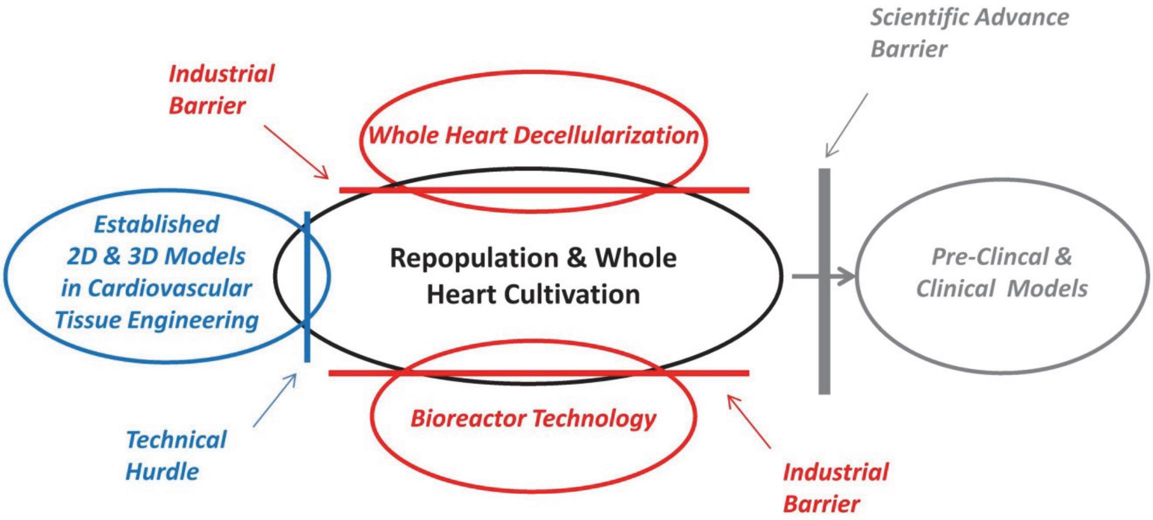

Fig.1: Thematic Diagram. Illustration of connected thematic fields representing the context of this thesis in a scheme. It describes the overall proceeding by overcoming technical hurdles and industrial barriers to work towards the systematic destination of whole heart constructs as a medical device.

1.3. Classification to the actual state of the art and available technology

In a nutshell the approach of whole organ tissue engineering is a sequential progression of scaffold preparation, repopulation and processing of the resulting construct. The technical backbone for this is mainly based on perfusion systems. Starting with the preparation of a whole organ scaffold, especially out of a whole heart, there are simply two basic requirements. First there has to be an easy adapter to access the donor organ´s vascular system, the coronary bed, and secondly a mechanism to perfuse it with reactants to remove cellular biomass.

At the current state of the art typical protocols represent a procedure of fix sequences of time-discrete perfusion steps [2, 7, 16-18] with or without additional physical treatment [16]. The degree of automation ranges between systems of controlled perfusion pressure [2, 17, 19] to steered protocols for whole organs [20]. Still there is a lack of non-destructive quality control and process-automation that barricades a commercial supply by pharmaco-industrial production. Most probably this is due to the black-box character of decellularization processes. So there is an urgent need for enlightenment by process-analytics that in turn have to be developed and adapted at first. Providing methods of resolution for this complex is **the first sub-aspect** of this thesis that highlights **Process Analytics and Process Automation for Whole Heart Decellularization**.

Pursuing this initial objective, **the first work,** that is incorporated in the entity of this study, entitled "*Mechanistics of Biomass Discharge During Whole-Heart Decellularization*" (under revision at Biomedical Materials), covers in depth analysis of the whole heart decellularization procedure. Therefore ovine hearts were decellularized by the application of a perfusion based protocol derived by modification of a previously established rodent heart decellularization method. It is based on the reflection of decellularization as a biomass-depletion process. Thereby a biomass-balancing was used to determine parameters describing benchmark data of the process, valuing then investigated dynamics and kinetics of decellularization comparatively. Characteristics, variances and limitations were investigated and complemented by developing courses of evolving viscoelasticity in the perfusate. Finally the identified dynamical and kinetical characteristics were fitted to a simple and general biomass-degression model to determine kinetical parameters and investigate limitations. The premised quality of acellularity was determined by common methods, e.g. DNA quantification, detection of residual proteins serving as myocardial markers by blotting techniques, and the evaluation of the relative collagen content. A graphical abstract of the study design is shown in figure 2.

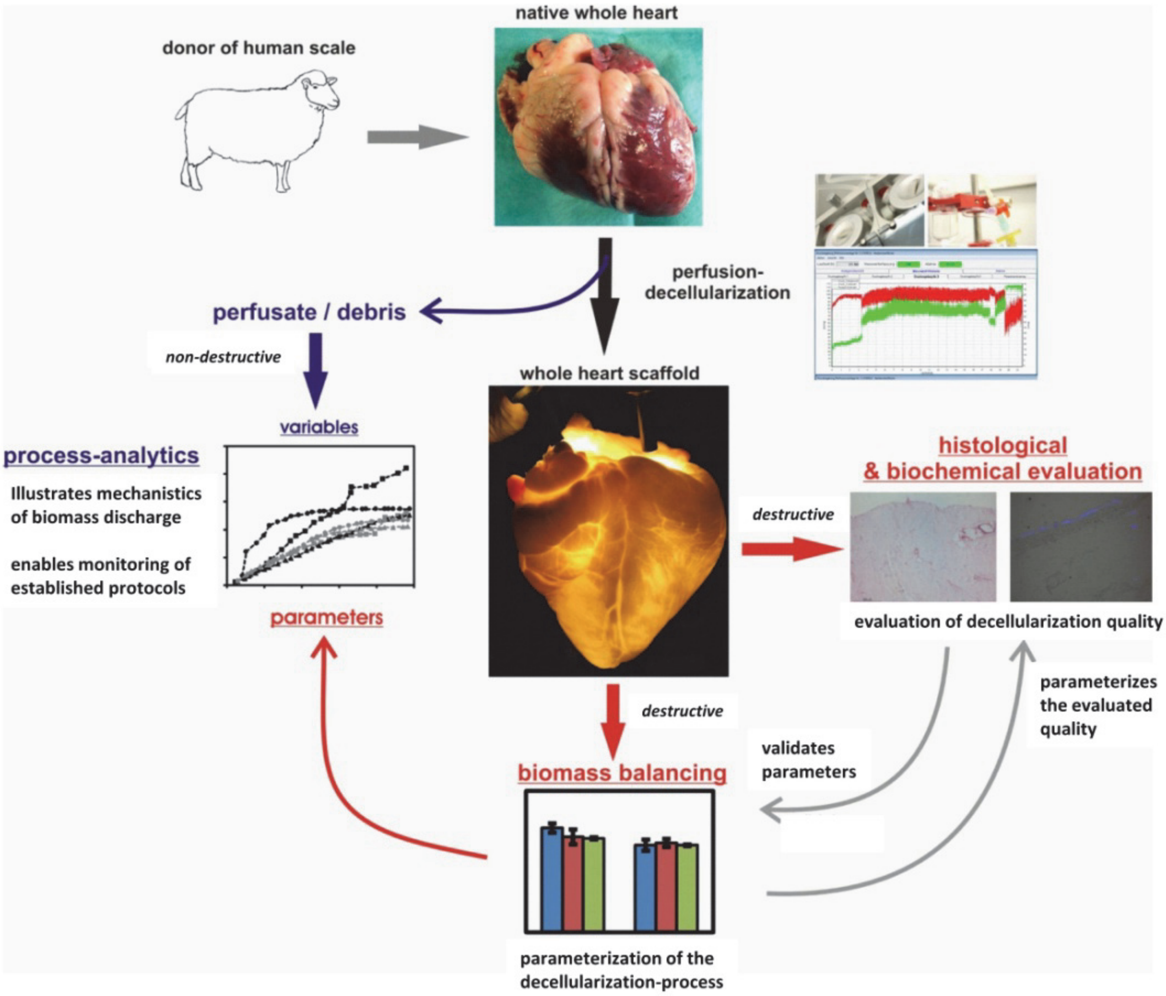

Fig. 2: Graphical abstract of the process analytical strategy. Native ovine hearts are decellularized by a standard perfusion protocol. Completeness and quality of the decellularization is evaluated by classical disruptive methods, which also resulted in validated benchmark data by biomass balancing. Thereby determined parameters characterize the process and become utilized as complement to variables of non-destructive process monitoring. The entire process can be described using these parameters and variables and specific dynamics can be determined. *(This figure was incorporated into the R1 version of the manuscript in 3.1)*

In addition to the demand of non-destructive quality control, another continuative aspect of the same project approach is to find quickly measurable variables that indicate ongoing biomass depletion and thereby enable monitoring and control of the process. In this regard, **the second work** entitled "*Rheology of perfusates and fluid dynamical effects during whole organ decellularization: A perspective to individualize decellularization protocols for single organs*" (Biofabrication. 2015 Sep 3;7(3):035008. doi: 10.1088/1758-5090/7/3/035008) describes observed fluid-dynamical phenomena during perfusion based whole heart decellularization which has been contrasted to biochemical and rheological measurements. The method of recording rheological flow curves of perfusate-samples, showing the course of viscosity-development as a function of the shearing rate, has then been investigated for its ability to detect debris and its composition by testing series of standards for DNA, protein and debris of varying organs. By the detection of specific characteristics this approach could be demonstrated as a fast and non-destructive analytical method capable for a process-accompanying quality control. Process characteristics could be detected online via the courses of the perfusion pressure and the actuating rotational speed of the perfusion pumps. These characteristics were then validated to be caused by debris-release and its fluid dynamical effects in the coronary system by the found protein and DNA contents as well as the evolving of viscoelasticity thereby.

To the best knowledge of the author, both works have dealt with the aspects of illumination and the procedural manageability of decellularization processes for the first time in literature.

On the consecutive part of processing repopulated constructs, perfusion systems turn to bioreactors that add functions for medium conditioning and stimulation. Up to date, bioreactors for the cultivation of whole heart constructs count a rather modest number [2, 6-9, 21-22] and usually are restricted to custom made unique copies that can hardly be commercially offered, what depicts another industrial barrier. Against that actual situation, a typical laboratory research project depending on limited third-party-financing would demand a flexible system that can be continuously adapted to the current level of scientific advance. In turn, such a system depends on integrative modularity, e.g. as it has been provided by Hülsmann et al. by the means of an integrative process-control-system [21-23].

In myocardial tissue engineering much of exciting research has been invested to find impacts and conditions to generate functionality out of immature origin-constructs in 2D and 3D models. Today the most meaningful impact on myocardial constructs can be recapped to biophysical stimulation by biomechanical stretching [24-25] and electrophysiological pacing [26-29].

Besides problems of initial generation, e.g. repopulation techniques, the main hurdles to transfer those proven principles to a complex whole heart construct is to adapt and deliver the stimulus. The previously evaluated mechanisms do not only have to operate in 3D, they have to adapt to the organ´s complex architecture, and moreover, they have yet to be adjustable and controllable. To overcome these hurdles, boundary surfaces, interfaces and transfer-mechanisms have to be designed, disturbances and tunable correcting values have to be identified and be embedded into the process control.

This is the **second sub-aspect** of this thesis. It represents a fundamental requirement for functional whole organ tissue engineering and may reveal the core of the interdisciplinary character of tissue engineering. In respect to the mentioned impacts to enhance myocardial maturation this ambition translates technically and practically **the third work**, entitled "*A novel customizable modular bioreactor system for whole-heart cultivation under controlled 3D biomechanical stimulation*" (J Artif Organs. 2013 Sep;16(3):294-304. doi: 10.1007/s10047-013-0705-5) that lays the groundwork by examining the required **Bioreactor Design for Biomechanical Stimulation of Whole Heart Constructs**.

Consistently and corresponding to the central circle of figure 1, illustrating the complex of “Repopulation and Cultivation”, the further objectives in the structuring of this study demand furthermore the development and establishment of a complex inter-coordinated workflow based on a tailored mechanical build-up and well adapted manual procedures. So this work is partitioned into two parts, actually to a non-accredited first part and fully accredited results. In the first part it describes the development of the bioreactor in its hardware as well as the integrative process control system and the fully-automated left ventricular stretching system as its key component. This part has been credited for the authors M.Sc. thesis and should not be validated in this dissertation.

The second part describes a proof of principle study using the control-based model cultivation (CMC) method that should be fully credited to this dissertation. Here decellularized whole hearts were repopulated by injection of C2C12 cells and cultivated under continuous left ventricular stretching using the presented bioreactor system. To evaluate the impact of this mechanical stimulation model, the formazan-based commercial WST-1 Assay (Roche) was adapted and modified, where a perfusion-based application with whole heart constructs was developed (exemplary lillustrated by figure 3).

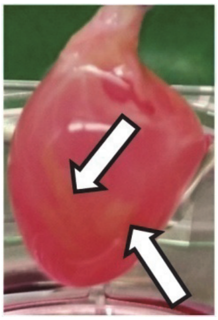

Fig. 3: Perfusion Based WST-1 Assay for Assessment of Metabolic Activity in Repopulated Whole Heart Construct. The scaffold appears in red caused by the phenol-red pH indicator of the perfused cell culture medium. The contrasted areas macroscopically illustrate injections sites that demonstrate metabolic activity of the repopulated cells by the chromatic formazan product as illustrated by the arrows.

Furthermore, a method was developed that combines the detection of the cell´s orientation angles and circularity distributions to the detection of fractions of oriented cells (FO) and the specific orientation density (O.D.) as exemplary illustrated by figure 4. Both parameters were introduced by this work and provide a tool to determine impacts to cellular spatial-orientation and alignment inside of whole heart constructs.

The concept of generating a whole heart construct with subsequent bioreactor cultivation using whole left ventricular stretching for biomechanical stimulation, the process accompanying evaluation of viability by repetitive WST-1 assay, as well as the terminal determination of O.D. can also be found as a protocol published in the Springer “Methods in Molecular Biology” series [23].

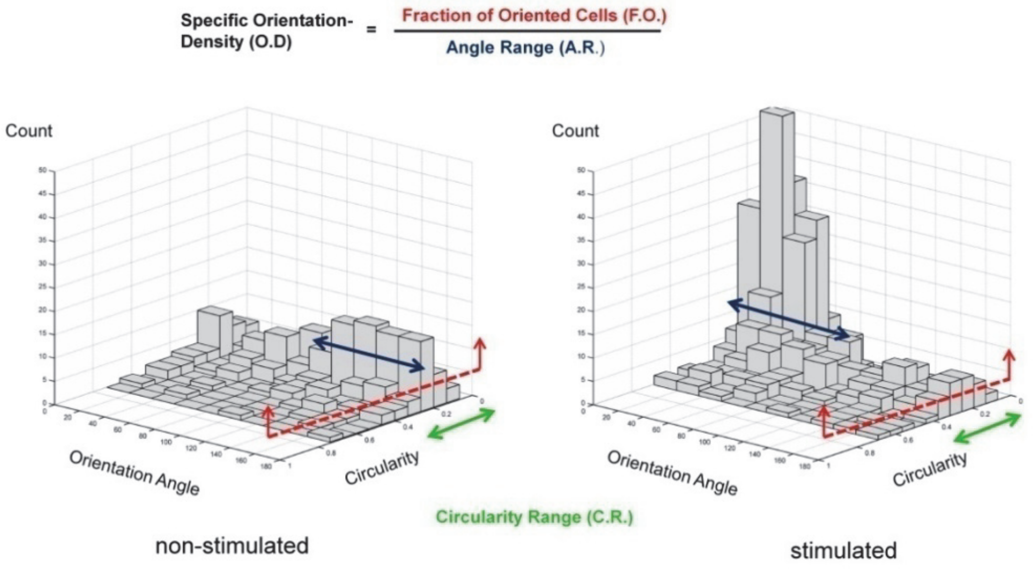

non-stimulated

stimulated

Fig. 4: 3D Distribution of evaluated circularities and orientation angles for nuclei in confocal microscopic digitalization of whole heart constructs after specific staining. Fractions of clearly oriented cell structures (FO) can be identifiedfor stimulated constructs vs. non-stimulated controls. The resulting specific orientation density can further be determined by relating the particular FO to its corresponding angle range (AR).

After overcoming main technical hurdles and industrial barriers, the first 3 levels are passed and by the fourth level, bioprocesses can be developed and optimized, representing the **third sub-aspect** reflecting a continuative **Bioprocess Design for Biomechanical Stimulation of Whole Heart Constructs**.

As already mentioned above, the number of bioreactors for the cultivation of whole heart constructs are quite modest, and consistently, so are the underlying processing strategies. Until today, reported stimulation modes are mostly based on electro-physiological current injection [2, 5-6]. However, while current work has resulted in interesting results and promising processing strategies using very advanced stimulation modes, the consensus seems to aspire to one step optimization by trial and error. Thereby preferably human sized scaffolds are repopulated preferential with cells of prospective clinical relevance at maximal cell-densities and processed as long as technically possible under biophysical stimulation, which again is experimentally designed as advanced as possible.

The **central working hypothesis** of this work is that neither the scientific advance and state of knowledge, nor the scientific-technical state of the art already complies with the demands of that high scientific level. From the procedural point of view there are essential tasks left unresolved beginning with the set of problems of repopulation by proliferative invasion vs. high-cell-density injection as one aspect for a suitable cell source, whereas the optimal cell source is also yet a matter of debate. Another non-enlightened factor is the mode of operation, effectiveness and effective propagation of biophysical stimulation in the complex whole heart architecture where essentially control-based studies are missing. Accordingly, in this thesis, a stepwise establishment of process development and optimization is pursued, beginning with the testing and verification of transferred biophysical stimulation in control-based short model-cultivations (CMC).

So as a direct continuation of the bioreactor design and the evaluation of a basic model-cultivation as outlined above, **the fourth work** entitled: "*The impact of left ventricular stretching in model cultivations with neonatal cardiomyocytes in a whole-heart bioreactor.*" (Biotechnol Bioeng. 2017 May;114(5):1107-1117. doi: 10.1002/bit.26241) deals with a suitable **Bioprocess Design for Biomechanical Stimulation of Whole Heart Constructs**. This work contains the central examination of the model and the process using neonatal cardiomyocytes in the real cardiac-like environment of decellularized whole heart scaffolds subjected to whole left-ventricular stretching. Essentially, this model holds the ability to develop functional myocardium, but may also suffer dedifferentiation both in dependency of the adequacy of cultivation and processing [23]. On this matter, the impact of biomechanical stimulation was first evaluated by a metabolic activity assay and orientation density determination using the afore-mentioned methods. Further these data were contrasted to a LIVE/DEAD Assay and complemented by real-time quantitative polymerase chain reaction (qRT-PCR) and western blotting of myocardial markers. Finally, the observed results were counter-checked by immuno-fluorescence (IF) staining of tissue sections of whole left ventricular walls and functionality was validated by electrophysiological multi-electrode-assay (MEA) recordings.

The investigation of 3D constructs, more precisely whole left ventricular walls, required the adaption of common IF protocols and of course a reconsideration of specific signals derived by MEA recording or confocal microscopy.

Also common methods like qRT-PCR and western blot analysis had to be assessed specifically and in a maybe uncommon manner due to the multiple control-based setting by evaluating stimulated vs. non-stimulated constructs and further matching to maturation vs. dedifferentiation. To meet these demands qRT-PCR (for connexin 43) and western blot analysis (for MHC) data were evaluated construct-sepcific as well as control-specific regarding native adult and neonatal myocardial tissue. The graphical abstract is shown in figure 5, which also illustrates this study on the journal´s homepage.

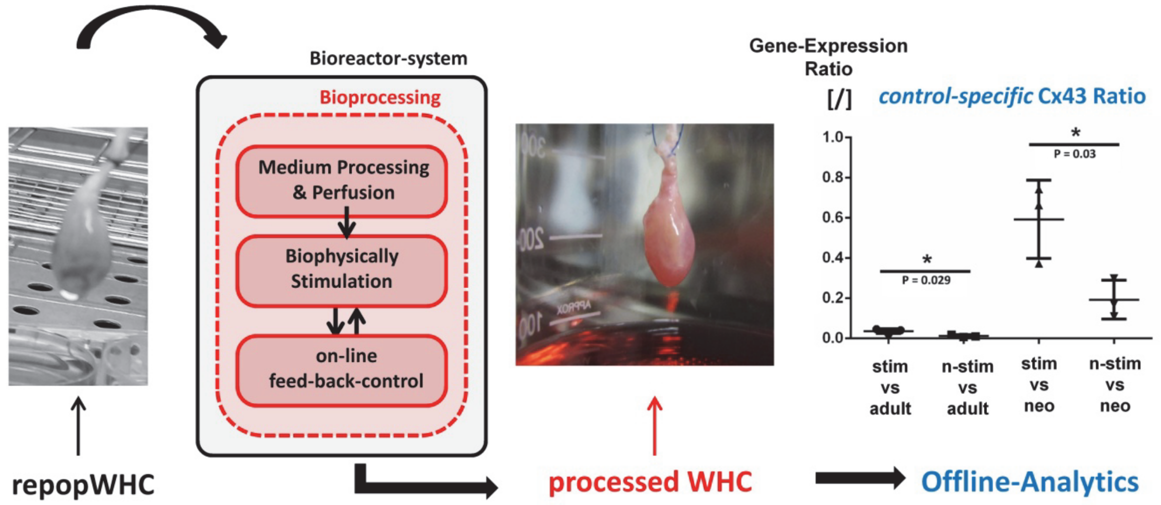

Fig. 5: Graphical Abstract of the Study. The shown sequence illustrates the processing and following exemplary investigation of the processed whole heart constructs (WHC) to investigate the impact of left-ventricular stretching to myocardial development in WHC.

In addition, building on the findings and the gained methodological expertise of the first four works as outlined above, the structuring of this thesis could be completed by a proof of principle study entitled “*Electrophysiological Stimulation of Whole Heart Constructs in a three-dimensional 8-pole Electrical Field*” concerning the required **Bioreactor Design for Electrophysiological Stimulation of Whole Heart Constructs**, that relates in equal measure to both, the **second** and the **third sub-aspect** of this thesis.

In addition to biomechanical stimulation by stretching, electrophysiological stimulation has been proven and established as a clearly beneficial impact to myocardial constructs before. In fact this has been incorporated into the whole heart TE concept from the beginning and today the application of current injection by immersion or surface-contact electrodes has shown promising results [2, 6].

However, the majority of published studies investigating electrophysiological stimulation of myocardial constructs have used electrical fields that yet have not been transferred to the whole heart approach [27-31]. This work shows a concept for electrophysiological stimulation in an 8-pole electrical field integrated into our bioreactor system as an alternative to the principle of direct current injection to the construct. Therefore the study was designed in a typical proof of principle concept that shows the buildup of an 8-pole field by voltage and current measurements. Moreover electrical voltage mapping in a MEA system have been performed for functional evaluation. In detail, spontaneous electrophysiological activity was at first evaluated qualitatively by recorded sequences of surface voltage and these data were further complemented by a more in-depth comparative signal sorting as well as direct contrasting assessment by the determination of mean voltage amplitudes and beating rates for stimulated constructs vs. non-stimulated controls. In addition to the investigation of spontaneous activity, impulse response testing complemented the functional electrophysiological evaluation and a contrasting counter check by classical western blot analysis of myocardial markers completed the study.

The herein established 8-pole setting in a processing chamber, representing the centerpiece of this study, is depicted in figure 6.

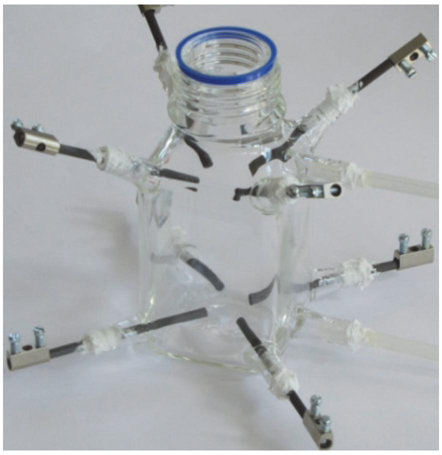

Fig. 6: Hardware Setup of an 8-pole Stimulation Processing Chamber. The perfusion and processing chamber for WHC is based on a square formed 250 ml flask. There are 6 mm olives added at all 8 edges to insert carbon rod electrodes sealed in by food-silicone. Two more olives are placed centric at the upper and above end of one planar side to connect tubes for the perfusion path and potential medium exchange. The perfused WHC is mounted in combination with the screw-cap and localizes centrally in between the electrodes.

1.4. Study contents

To put it briefly, the afore reflexed sub-aspects of this thesis aim at overcoming industrial barriers and technical hurdles as illustrated in figure 1 and finally at establishing transferred biophysical stimulation concepts in model cultivations as a prerequisite for further process optimization. An overview of the total study design of the structuring is illustrated in figure 7 that relates specific problems and approaches to the single sub-aspects and the related studies.

On the contrary, further process optimation, e.g. by prolonged cultivations, raised empiricism and thereby further developed processing strategies is excluded from consideration in this thesis as depicted in figure 7 as well.

Furthermore the complex and fundamental question of a suitable cell source of clinical relevancy cannot be processed or discussed in the context of this work, as it simply opposes the central working hypothesis and would go beyond the scope of this thesis. But indeed the strategic approach is targeted exactly towards this very important and absolutely crucial subject.

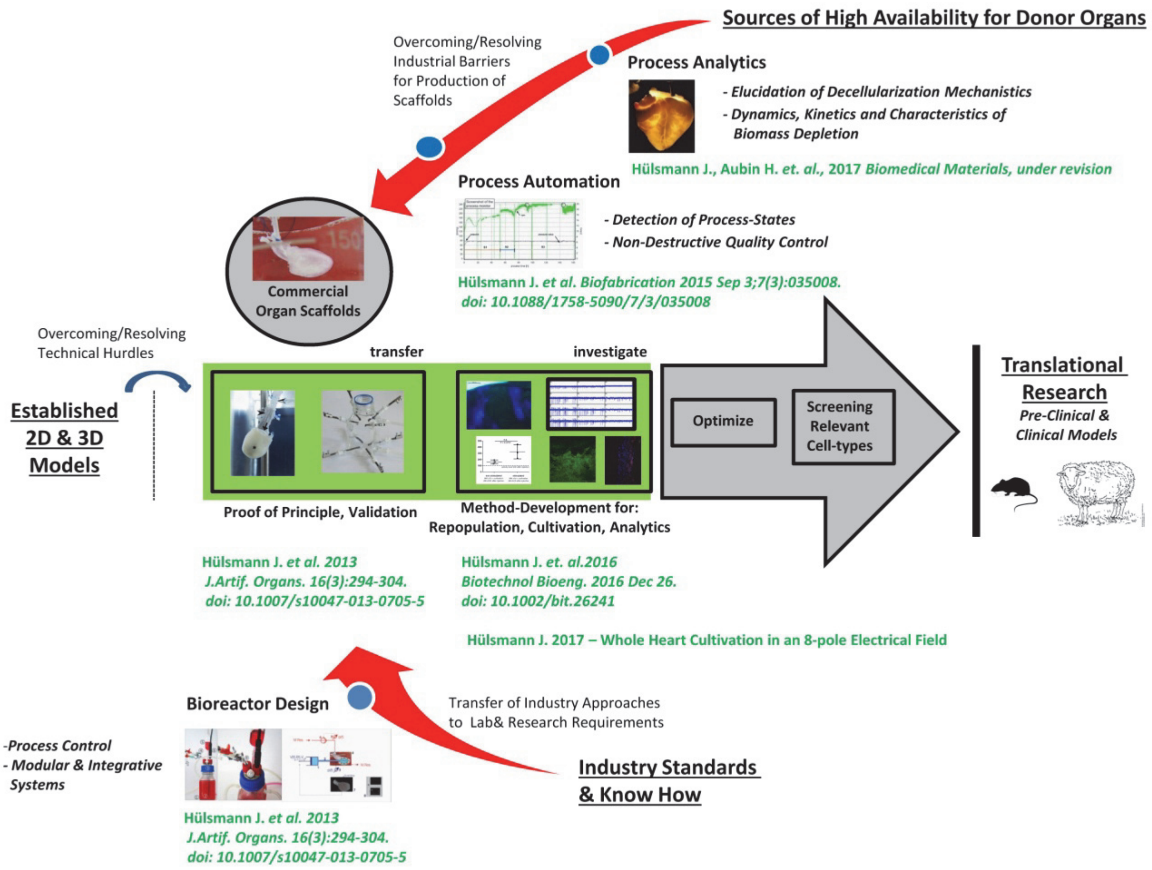

Fig. 7: Study Structure: In accordance to figure 1 industrial barriers are indicated in red and technical hurdles in blue. Here the corresponding methods aiding to overcome these limitations are illustrated by arrows and contrasted by the related works. The wide horizontal arrow in the middle illustrates the central circle of figure 1, showing the procedure of the third sub-aspect with its design to develop and optimize bioprocessing strategies. In green: achievements contributed by this work. In grey: potential continuative work.

Also all kinds of conceivable *in vivo* experiments e.g. regarding biocompatibility or integrability of the produced scaffolds or constructs are not integrated into the study, as this would be a contradiction to the central working hypothesis as well.

In this context, next to the applied parenchymal repopulation by injection seeding, an interstitial revitalization of the WHC is excluded from this work as well. Although a rebuild functional endothelium would be crucial prior to application for any replacement tissue that has to be integrated into blood circulation, we regard this aspect as a separate field of research that should be adopted by meaningful specialized studies.

In fact, the crux of this thesis is rather to close a scientific-technical gap, what enables to broaden and deepen the understanding and the molecular-biological knowledge in Regenerative Medicine by the provision of novel tools for the generation of whole heart constructs, their sophisticated physiological functional processing as well as bioanalytical methodology.

2. Brief review of the embedded studies

Overview

	Title	Personal Contribution	Journal	Impact Factor *(in 2016)*
1	**Mechanistics of Biomass Discharge During Whole-Heart Decellularization**	60 %	*under revision at* ***Biomedical Materials****;* *as for Oktober 2017*	(2.469)
2	**Rheology of perfusates and fluid dynamical effects during whole organ decellularization: A perspective to individualize decellularization protocols for single organs**	70 %	**Biofabrication** *fully accredited*	5.240
3	**A novel customizable modular bioreactor system for whole-heart cultivation under controlled 3D biomechanical stimulation**	70 %	**Journal of Artificial Organs** *in parts not accredited*[1]	1.350 (½ = 0.675)
4	**The Impact of Left Ventricular Stretching in Model Cultivations with Neonatal Cardiomyocytes in a Whole-Heart Bioreactor**	70 %	**Biotechnology and Bioengineering** *fully accredited*	4.481
			total IF:	**10.396** **+ (2.469)**

5	**Electrophysiological Stimulation of Whole Heart Constructs in an 8-pole Electrical Field**		*non-published data*

1: according to description in 1.3 page 14

Mechanistics of Biomass Discharge During Whole-Heart Decellularization.

(under revision at Biomedical Materials)

Author 1: Jörn Hülsmann, author 2: Hug Aubin, author 3: Fabian Oberle, author 4: Nicolas Schütterle, author 5: Shahbaz T. Bandesha, author 6: Makota Iijima , author 6: Artur Lichtenberg, author 8: Payam Akhyari.

	Author 1	Author 2	Author 3	Author 4	Author 5	Author 6	Author 7	Author 8
Conceptual design of the research approach, planning of investigation, study design	Construction and design of the basic concept, planning and design of study and experiments part 2: Process analytics.	Construction and design of the basic concept, planning and design of study and experiments part 1*: Classical evaluation of decellularization quality.						Consultancy at supplementation and complementation of the conceptual design.
Experimental work, data acquisition	Independent execution of experimental work and data acquisition Part 2. Consultancy and support of experimental work part 1*.	Consultancy and support of experimental work part 1* Support of experimental work Part 2.	Assistance and support of experimental work part 1*.	Assistance and support of experimental work part 1*.	Assistance and support of experimental work part 1*.	Assistance and support of experimental work part 2.		
Data Analysis, data interpretation	Analysis and interpretation of acquired data, presentation of the results part 2. Consultancy of data interpretation and –presentation part 1*.	Analysis and interpretation of acquired data, presentation of the results part 1*. Consultancy of data interpretation and –presentation Part 2.	Analysis and interpretation of acquired data, presentation of the results part 1*.	Analysis and interpretation of acquired data, presentation of the results part 1*.	Analysis and interpretation of acquired data, presentation of the results part 1*.			Discussion of data interpretation and –presentation.
Draft, phrasing and revision of the manuscript	Draft, preparing and final revision.	Critical revision, corresponding author.	Critical discussion.	Critical discussion.	Critical discussion.	Critical discussion.	Critical discussion.	Critical revision.

* *The content of part 1 is marked by green topics in the manuscript at the results chapter*

Rheology of perfusates and fluid dynamical effects during whole organ decellularization: A perspective to individualize decellularization protocols for single organs.

(Biofabrication, 2015. 7(3): p. 035008)

Author 1: Jörn Hülsmann, author 2: Hug Aubin, author 3: Shahbaz T. Bandesha, author 4: alexander Kranz, author 5: Volker R. Stoldt,
author 6: artur Lichtenberg , author 7: Payam Akhyari.

	Author 1	Author 2	Author 3	Author 4	Author 5	Author 6	Author 7
Conceptual design of the research approach, planning of investigation, study design.	Construction and design of the basic concept, planning and design of study and experiments.	Consultancy at supplementation and complementation of the conceptual design.					Consultancy at supplementation and complementation of the conceptual design.
Experimental work, data acquisition.	Independent execution of experimental work and data acquisition.		Assistance and support of experimental work.	Assistance and support of experimental work.			
Data analysis, data interpretation.	Analysis and interpretation of acquired data, presentation of the results.	Discussion of data interpretation and – presentation.	Discussion of data interpretation and – presentation.	Discussion of data interpretation and – presentation.			Discussion of data interpretation and – presentation.
Draft, phrasing and revision of the manuscript.	Draft, preparing and final revision, corresponding author.	Critical revision.	Critical discussion.	Critical discussion.	Critical discussion.	Critical discussion.	Critical revision.

A novel customizable modular bioreactor system for whole-heart cultivation under controlled 3D biomechanical stimulation.

(J Artif Organs. 2013 Sep;16(3):294-304.)

Author 1: Jörn Hülsmann, author 2: Hug Aubin, author 3: alexander Kranz, author 4: Erhardt Godehardt, author 5: Hiroshi Munakata, author 6: Hiroyuki Kamiya , author 7: Mareike Barth, author 8: Artur Lichtenberg, author 9: Payam Akhyari.

	Author 1	Author 2	Author 3	Author 4	Author 5	Author 6	Author 7	Author 8	Author 9
Conceptual design of the research approach, planning of investigation, study design.	Construction and design of the basic concept, planning and design of study and experiments.								Consultancy at supplementation and complemen-tation of the conceptual design.
Experimental work, data acquisition.	Independent execution of experimental work and data acquisition.		Support by preparative laboratory work at decellularization.	Assistance and support of experimental work.	Support by preparative laboratory work at decellularization.	Support by preparative laboratory work at decellularization.			
Data analysis, data-interpretation.	Analysis and interpretation of acquired data, presentation of the results.	Discussion of data-interpretation and presentation.	Discussion of data-interpretation and presentation.	Discussion of data-interpretationand presentation.			Critical revision of microscopic figures, discussion of data-interpretation and presentation.	Discussion of data-interpretation and presentation.	Discussion of data-interpretation and presentation.
Draft, phrasing and revision of the manuscript.	Draft, preparing and final revision.	Critical revision.	Critical discussion.	Critical discussion.	Critical discussion.	Critical discussion.	Critical discussion.	Critical discussion.	Critical revision, corresponding author.

The content of the non accredited part, according to description in chapter 1.3 page 14, is marked by blue topics in the manuscript.

The Impact of Left Ventricular Stretching in Model Cultivations with Neonatal Cardiomyocytes in a Whole-Heart Bioreactor.

(Biotechnol Bioeng. 2017 May;114(5):1107-1117.)

Author 1: Jörn Hülsmann, Author 2: Hug Aubin, Author 3: Alexander Wehrmann, Author 4: Artur Lichtenberg, Author 5: Payam Akhyari

	Author 1	**Author 2**	**Author 3**	**Author 4**	**Author 5**
Conceptual design of the research approach, planning of investigation, study design.	Construction and design of the basic concept, planning and design of study and experiments.	Consultancy at supplementation and complementation of the conceptual design.			Consultancy at supplementation and complementation of the conceptual design.
Experimental work, data acquisition.	Independent execution of experimental work and data acquisition.		Support by preparative laboratory work at decellularization.		
Data analysis, data interpretation.	Analysis and interpretation of acquired data, presentation of the results.	Discussion of data interpretation and presentation.	Discussion of data Interpretation and Presentation.	Discussion of data interpretation and presentation.	Discussion of data interpretation and presentation.
Draft, phrasing and revision of the manuscript.	Draft, preparing and final revision.	Critical revision, corresponding author.	Critical discussion.	Critical discussion.	Critical revision.

Electrophysiological Stimulation of Whole Heart Construct in an 8-pole Electrical Field.

These data are summarized and expressed to fluently integrate into the presentation form of the thesis. The presented results are not peer-reviewed or submitted for publication yet.

3. Results

3.1. Process Analytics for Decellularization of Whole Hearts

Mechanistics of Biomass Discharge During Whole-Heart Decellularization*

** pre-print version*

Jörn Hülsmann[1#], Hug Aubin[1#], Fabian Oberle[1], Nicolas Schütterle[1],ShahbazT. Bandesha[1], Makoto Iijima[2], Artur Lichtenberg[1*], Payam Akhyari[1]

[1]Department of Cardiovascular Surgery, Medical Faculty, Heinrich-Heine-University, Düsseldorf, Germany

[2] Department of Cardiovascular and Thoracic Surgery, Hokkaido University, Graduate school of Medicine, Sapporo, Japan

[#]both authors contributed equally

***Corresponding Author:**
Univ.-Prof. Dr. med. Artur Lichtenberg
Department of Cardiovascular Surgery
Heinrich-Heine-University Düsseldorf
Moorenstr. 5, 40225 Düsseldorf, Germany
Phone: 00492118118331
Fax: 00492118118333
eMail: artur.lichtenberg@med.uni-duesseldorf.de

Abstract

Whole-organ engineering - based on the functional repopulation of acellular whole-organ scaffolds derived from perfusion-based *in toto* decellularization of the specific organ system- is one of the most promising fields in tissue engineering. However, to date, we still have hardly any insights into the process of perfusion-based scaffold generation itself, with human-scale scaffolds usually obtained by adoption of small animal decellularization models, although those organs are of decreased biomass and potentially different biological characteristics. Therefore, in this study we analyzed perfusion-based human-scale whole-heart decellularization by evaluating and comparing the dynamics of biomass discharge and its kinetic characteristics during *in toto* decellularization of ovine and rodent hearts, while introducing a theoretical model of biomass depletion during perfusion-based whole-heart decellularization. Our results suggest highly varying process characteristics for the *in toto* decellularization of individual human-scale organs, such as protein discharge kinetics or time-dependent viscoelasticity of formed debris, despite seemingly consistent inter-sample decellularization efficacy, as evaluated by conventional disruptive analysis of obtained ECM scaffolds. Hence, the here exposed insights into the mechanistics of whole-heart decellularization as well as the introduced non-disruptive process accompanying tools may help to monitor and further optimize the decellularization process, especially with regards to human-scale scaffold production.

1. Introduction

The field of tissue engineering and regenerative medicine has tremendously progressed within the last 25 years [1]. Meanwhile, we have not only gained the expertise to recapitulate complex and physiological functional tissues in three-dimensional (3D) *in vitro* models, ranging from micro-scale platforms for pharmaceutical testing and disease modeling to human-size constructs for clinical applications, but by now we even strive towards the recreation of whole-organ systems[2]. Although the whole-organ engineering field is still a young discipline, it holds the promise to revolutionize the field of regenerative medicine as in many clinical disciplines curative therapy of end-organ failure depends on availability of donor organs.

Whole-organ engineering is usually based on acellular whole-organ scaffolds derived from perfusion-based *in toto* decellularization of the specific organ system [3-6]. This approach allows the generation of extracellular matrix (ECM)-based scaffolds with almost complete preservation of 3D architecture and microstructure, most notably including an intact and patent vasculature supplying the whole system [7]. Until today, thiskind of precision in maintaining biological fidelity to the prototype organ has been largely unmet by other means, such as synthetic 3D scaffold fabrication [8].

Since the pioneering work from Ott et al. in 2008, in which for the first time a decellularized whole-heart scaffold was successfully repopulated *in vitro* showing traces of physiologic organ function[9], much effort has been invested in optimizing repopulation techniques and evaluation of scaffold biocompatibility [10,11]. In the case of whole-heart engineering, we are now even approaching human-scale pre-clinical models, with the evaluation of decellularized human hearts as possible whole-heart grafts[12]and first heterotopic transplantations of human-sized decellularized and recellularized whole-hearts in large animal models[13].

Though, despite those intriguing advances, until today we still have hardly any insights into the process of perfusion-based whole-organ scaffold generation itself. Especially when it comes to the generation of human-scale scaffolds, decellularization protocols are often adopted from small animal models, although those organs are of decreased biomass and potentially different biological characteristics. Hence, in the literature a variety of different protocols can be found, with differing pre-treatments, decellularization agents and perfusion conditions. Further, scaffold quality is usually solely analyzed at the end of the process by disruptive analysis independently from the decellularization process itself [14]. However, to date, perfusion-based decellularization is still a black box with a substantial lack of understanding of its mechanistics and potential correlations to decellularization efficacy and scaffold quality. Therefore, in this study we analyzed the mechanistics of perfusion-based human-scale whole-heart decellularization by evaluating and comparing the dynamics of biomass discharge and its kinetic characteristics during *in toto* decellularization of ovine and rodent hearts, while introducing a theoretical model of biomass depletion during perfusion-based whole-heart decellularization.

2. Methods

All animal experiments were performed in accordance to §6 and §8 of the German animal welfare act of North-Rhine-Westphalia (TierSchG) as well as to the Guide for the Care and Use of laboratory animals published by the US National Institutes of Health (NIH Publication 85-23, revised 1996), and approved by the animal care committee of the Heinrich-Heine-University as well as local governmental authorities in North-Rhine-Westphalia, Germany (LANUV, German state office for nature, environment and consumer protection of NRW; reference number G/O89/2012).

2.1 Whole-heart decellularization

2.1.1 Detergent-based semi-automatic coronary perfusion

For this study, ovine and rodent hearts were decellularized *in toto* by detergent-based decellularization *via* coronary perfusion in a customized, semi-automated pressure controlled decellularization system, in order to ensure standardized decellularization conditions, as previously described [15,16]. Chemical decellularization was achieved by adaption of a simplified decellularization protocol for whole-heart decellularization, based on sodium dodecyl sulfate (SDS; Carl-Roth) and desoxycholic acid (DCA; Amresco) and followed by double distilled water and phosphate-buffered saline (PBS; Gibco) perfusion, as previously described[16]. In all cases, an excess of perfusate volume was chosen for decellularization (perfusate [mL] per wet organ biomass [mg]: > 33) in order to avoid potential saturation and biomass limitation effects.

However, depending on the subset of experiments, the applied perfusion protocol included closed or open loop perfusion, which was varied due to technical reasons in order to address specific questions (see respective sections for further clarification). All decellularized hearts were then stored in PBS supplemented with penicillin/streptomycin at 4°C before further processing.

2.1.2 Ovine donor hearts

For ovine whole-heart decellularization donor hearts from equal-weight lambs (3 months of age) were retrieved from a local slaughterhouse. Immediately after sacrifice of the animal, the heart was excised from the thorax, carefully dissected from surrounding pericardial and lung-tissue and then manually perfused with 500 ml heparinized (Heparin, Ratiopharm, Ulm, Germany) physiological saline solution (10.000 IU heparin per 1000 ml) blended with 10.000 IU streptokinase (Sigma-Aldrich, St. Louis, MO, USA) *via* direct cannulation of the coronary ostia, in order to free the coronary system from remaining blood and possible clots. Hearts were then stored at 4°C until further processing in the laboratory (time from explantation to decellularization or further processing < 180 min.). Only those hearts in which the coronary system could macroscopically be identified to be patent and functional by complete paling of the myocardium after saline perfusion, were selected for subsequent decellularization.

For perfusion-based whole-heart decellularization coronary ostia of ovine hearts were permanently cannulated with silicone coronary artery ostial cannulae (Medtronic, Mineapolis, MN, USA) secured with a purse-string-suture (Prolene 4-0, Ethicon, Somerville, NJ, USA) and serving as feed-inlet for the decellularization perfusate. After passing the coronary system, the perfusate was allowed to passively drain out of the heart into a reservoir, connected to the perfusion cycle and serving as perfusion outlet. Coronary perfusion pressure was maintained at 100 mmHg, automatically adapting the perfusion flow by the employed semi-automatic decellularization system, as previously described [15,16].

A total of 12 ovine hearts were decellularized *in toto* by 24 h perfusion with 0.75 m/v% SDS and 0.25 m/v% DCA in PBS followed by 1 h of double distilled water and subsequent PBS perfusion. Out of those 12 hearts, 6 hearts were perfused within a closed loop with 10 L of recirculating perfusate volume for each individual heart, while the other 6 hearts were perfused within an open loop without perfusate recirculation. Continuous and time-discrete collection of perfusate was performed during the decellularization process in order to enable direct as well as temporally resolved sampling.

2.1.3 Rodent donor hearts

For rodent whole-heart decellularization hearts of Wistar rats (male, 400 to 500 g) were explanted and decellularized *in toto* by standardized semi-automated pressure controlled retrograde aortic perfusion, as previously described [15]. In order to allow direct comparison to larger-scale ovine whole-heart decellularization a subset of 5 rodent hearts was decellularized following the identic protocol that was used for the ovine hearts, as described above.

2.1.4 Decellularization of minced ovine left ventricular tissue samples as an optimal non-perfusion-based decellularization model

In order to validate perfusion-based whole-heart decellularization on the basis of assumed optimal decellularization of myocardial tissue under non-limited mass transport conditions, standardized native tissue samples of the ovine left ventricular wall, lacking epicardial fat deposits, were manually minced to a homogenous mass and decellularized under dynamic detergent incubation, as previously described[17]. Briefly, 10 g of the minced tissue were placed into a 250 ml flask and incubated for 24 h in 200 ml of detergent solution (0.75 m/v% SDS and 0.25 m/v% DCA in PBS) followed by 1 h incubation in double distilled water under orbital shaking at 150 rpm (KS 15, Edmund Bühler GmbH, Hechingen).

2.2 Evaluation of decellularization efficacy

Efficacy of whole-heart decellularization was evaluated by macroscopic inspection, representative histological staining and biochemical analysis of respective standardized specimens.

2.2.1 Macroscopic inspection

For macroscopic inspection decellularized hearts were cut into cross-sections and visualized using a Canon EOS digital camera (Canon, Tokio, Japan). Decellularization efficacy was assumed to be satisfactory, when complete translucence of the tissue was achieved and no gross cellular myocardial tissue remnants were visible.

2.2.2 Histological staining

For histological evaluation of decellularization efficacy, standardized specimens of the left ventricle (LV) of native and decellularized ovine hearts were fixed in 4% phosphate buffered paraformaldehyde solution (Sigma Aldrich, St. Louis, MO, USA)and paraffin-embedded following standard protocols. Sections of 4.5 µm were stained with hematoxylin and eosin (H&E) or DAPI (Vector Laboratories Inc., Burlingame, CA, USA) according to standard protocols and then visualized using a transmission light microscope (DM 2000; Leica, Wetzlar, Germany).

2.2.3. Biochemical analysis

DNA analysis

For DNA analysis standardized tissue samples of the left ventricle (LV), the right ventricle (RV) and the septum (S) were dissected from native and decellularized ovine hearts, shock frozen in liquid nitrogen and processed using the DNeasy mini Kit (Qiagen, Hilden, Germany) according to the manufacturer's instructions for tissue samples (n=3, respectively). Briefly, DNA was isolated from the individual specimens by homogenizing the tissue specimens and passing the lysate through a DNA spin column, which selectively bound DNA. Afterward DNA could be eluted and concentration assessed by photometric absorption at 260 nm. Regional samples were pooled for each respective heart in order to gain a broad overview over the total DNA content of decellularized whole-hearts.

Collagenous to non-collagenous protein analysis

For a protein-based analysis of the decellularization efficacy, the ratio of collagenous to non-collagenous protein as an estimate of the proportion of extracellular matrix to cellular biomass was assessed for standardized tissue samples of LV, RV and S of native and decellularized ovine hearts (n=3, respectively), as previously described[23]. This colorimetric method is based on sirius red staining of fibrillar collagen and fast green staining of remaining non-collagenous protein. Briefly, cryo-embedded specimens were cut into 16-µm-thick sections and incubated for 10 min in sirius red (Abcam, Cambridge, UK, cat.nr.: ab150681) and fast green solution (Abcam, Cambridge, UK, cat.nr.: ab146267) (0.1% sirius red F3BA, 0.1% fast green in saturated picric acid solution). After elution of the dyes with methanol, relative content could be assessed by photometric absorption at 540nm (sirius red) and 605nm (fast green), as previously described [23].

Western blot analysis of residual cardiac actin and desmin

Western blot analysis of cardiac actin and desmin, as exemplarily markers for specific intracellular sarcomeric and cytoskeletal proteins, was carried out for standardized tissue samples of the LV, RV and S of native and decellularized ovine hearts, pooling regional samples analog to the DNA analysis. For protein isolation tissue samples were minced and incubated in 8M urea + 1 % SDS in an orbital shaker for 24 h. Then protein homogenates were separated on SDS-PAGE (Invitrogen) using the Laemmli method and the polypeptide bands were transferred to PVDF membranes (Invitrogen). Blots were probed with primary antibodies for cardiac actin (PROGEN Biotechnik GmbH, Heidelberg, Germany, cat.nr.: 65175) and desmin (Abcam, Cambridge, UK, cat.nr.: ab15200). Protein bands were visualized using WesternBright™ Quantum Western Blotting Detection System (Advansta, Menlo Park, CA, USA) following standard protocols. The membrane was digitalized using an EPI Chemi II Darkroom imaging system (UVP, Cambridge, UK)and densitometry analysis was carried out using ImageJ software (National Institutes of Health, Bethesda, MD, USA). For better comparison all values were normalized to the relative amount in the native myocardium.

2.3 Biomass balance analysis

In order to assess the amount of solid biomass that is discharged during whole-heart decellularization process a biomass balance analysis was performed for a series of native and decellularized ovine and rodent hearts (n=5, respectively).

2.3.1 Wet and dry biomass of heart samples

After assessing the wet biomass (WBM)for all samples under equal conditions using a micro scale (BP110S, Sartorius AG, Göttingen, Germany), the respective samples were then desiccated under exposure to 90° C for 72 h and weighed again to determine the dry biomass (DBM), following standard recommendations for discrimination between the water and solid mass content of myocardial tissue [18,24,25].Hereby, representative standard WBM and DBM values before ($\mathrm{WBM}_{\text{native-stand}}$; $\mathrm{DBM}_{\text{native-stand}}$) and after decellularization ($\mathrm{WBM}_{\text{decell-stand}}$; $\mathrm{DBM}_{\text{decell-stand}}$) could be assessed for each sample type.

2.3.2 Fat-independent dry biomass of native hearts

Prior mincing of the ovine native and decellularized hearts and additional 12 h incubation at 4° C after initial desiccation allowed to separate the gross soluble lipid fraction from the remaining DBM ($\mathrm{DBM}_{\text{fat-free}}$), as biomass denaturation under exposure to 90° C leads to lipid fluidization and phase separation upon subsequent cooling. This was especially relevant as native ovine hearts, as well as adult human hearts, usually include a large inherent fraction of epicardial fat that constitutes the largest part of the gross soluble lipid fraction of the DBM (Fat). Thereby, the DBM fractions including and excluding fat could be assessed individually for each native sample, as well as the total fat fraction of the DBM (Fat (DBM)^{-1}).

2.3.4 Estimation of solid biomass discharge during whole-heart decellularization

The difference in DBM before and after decellularization ($\Delta\mathrm{DBM}_{\text{process}} = \mathrm{DBM}_{\text{native}}–\mathrm{DBM}_{\text{decell}}$) for each individual sample determines the amount of relevant solid biomass discharged during the decellularization process. However, due to technical reasons, for each specific sample only the $\mathrm{WBM}_{\text{native}}$ prior to the decellularization process is available. Therefore, in order to be able to estimate the amount of solid biomass discharge for a particular heart, the $\mathrm{DBM}_{\text{native}}$ was approximated by using the respective $\mathrm{DBM}_{\text{native-stand}}/\mathrm{WBM}_{\text{native-stand}}$ ratio, as determined above, as point of reference. Hence, the $\Delta\mathrm{DBM}_{\text{process}}$ could be estimated for each particular sample using equation 1.

$$\Delta DBM = WBM_{native}(x) \cdot \frac{DBM_{native-stand}}{WBM_{native-stand}} - DBM_{decell}(x) \tag{1}$$

x = designator for particular sample

For ovine hearts, in order to merely approximate the amount of DBM discharged from the myocardial tissue, and therefore excluding the gross soluble lipid fraction originating from the epicardial fat, solely the fat-free DBM fraction ($DBM_{fat\text{-}free}$), as determined above, was used for ΔDBM approximation. Further, due to biological variability of organ size and corresponding variation in total biomass amount, ΔDBM of each individual heart was normalized to its respective WBM ($\Delta DBM\ (WBM)^{-1}$) to allow inter-sample comparability and thereby provide a standardized quality measure for the biomass discharge.

2.3.5 Validation of fat-independent determination of solid biomass discharge during ovine whole-heart decellularization

Standardized native and decellularized minced ovine left ventricular tissue samples (n=5, respectively), obtained via processing as described above and solely composed of myocardial tissue without epicardial fat, were further used to validate the above used estimation of fat-independent solid biomass discharge.Therefore, the respective WBM and DBM were assessed as described above and determined ΔDBM of the non-perfusion-based decellularization process was compared to the estimated fat-independent ΔDBM of the ovine whole-heart samples.

2.4 Protein discharge during whole-heart decellularization

2.4.1 Protein content of decellularization perfusates

Protein content of decellularization perfusates was measured by a detergent compatible protein assay (Bio-Rad™ protein assay, Bio-Rad Laboratories, Munich, Germany) according to the manufacturer's manual. Therefore, decellularization perfusates were collected at 1 h intervals continuously during the first 6-8 h of open loop perfusion (ovine n=6) and terminally after 24 h. Additionally, samples were also collected during closed loop perfusion (ovine and rodent, n=3, respectively). Protein concentration was measured in each of those samples. For the particular sampling intervals, the detected protein concentrations were used to calculate the therein discharged protein-mass by multiplication with the corresponding measured volume of the collected outflow during open loop perfusion, or with the total fluid-volume in the system in case of closed-loop perfusion, respectively.

By addition of the individual total perfusate protein contents during the respective decellularization intervals, the total protein discharge (P_{tot}) for one respective whole-heart decellularization cycle could be determined. The ratio of the discharged protein-mass to the calculated solid biomass discharge during whole-heart decellularization ($P_{tot}\ (\Delta DBM)^{-1}$) was used to determine the detectable protein fraction of the discharged solid biomass within the decellularization perfusates.

2.4.2 Protein discharge kinetics during whole-heart decellularization

Time-dependent accumulative and total protein discharge were used to plot the protein discharge dynamics and kinetics of individual whole-heart decellularization cycles, while allowing to estimate the specific discharge-rates. As due to biological variability both anatomical heart size and respective biomass content may vary, the ratio of time-dependent protein discharge was normalized to the WBM of the respective heart ($P_{tot}(t,x)\ (WBM(x))^{-1}$), revealing the general discharge dynamics, or the total discharged (washed out, WO) protein ($P_{tot}(t,x)\ (P_{tot\ WO}(x)^{-1})$). This allowed inter-sample comparison while directly depicting the overall specific decomposition-rate $q_{d/x}(t,x)$ that can be approximated by the slope according to equation 2.

$$q_{d/x}(t) = \frac{P_{tot}(t_2) - P_{tot}(t_1)}{P_{tot\,WO}(x) \cdot (t_2 - t_1)}\ [h^{-1}] \tag{2}$$

x = designator for particular sample
t = variable for perfusion-time [h]

2.4.3 Protein size-dependent discharge kinetics during whole-heart decellularization

In order to assess whether protein discharge during whole-heart decellularization varies depending on protein size, cumulative protein discharge of 7 consecutive standardized time-intervals during the first 10 h of an exemplary ovine whole-heart decellularization were subjected to quantitative SDS PAGE analysis using standard Laemmli method allowing to discriminate the total discharged protein into size (kDa)-dependent fractions. Therefore,10 µg protein per sample were loaded per lane to 12 % gels, which were run and processed using a BioRad Mini-Protean® Gel System subjected to quantitative fluorescent protein staining by BioRad Flamingo™ Fluorescent Gel Stain (BioRAD, Hercules, CA, USA) according to manufacturer's manual. Bands were detected and analyzed using an EPI Chemi II Darkroom imaging system (UVP, Cambridge, UK).For quantification of the protein-mass for the individual band, the particular intensities of the single bands were proportioned to the total signal of the corresponding lane, representing 10 µg protein each. Then for the bands of each particular molecular weight, the accumulative discharged protein mass was calculated and depicted combined with the temporal course for all protein-size-fractions.

2.5 Rheological assessment of discharged biomass during whole-heart decellularization

Standardized samples of decellularization perfusates were subjected to the evaluation of rheological flow curves, as described previously [17], using a MCR-rheometer (Anton Paar, Graz, Austria). Briefly, the viscosity of the samples was recorded as a function of the shearing rate (s) in a range of 1 to within the decellularization perfusates as well as changes of viscoelasticity can then be correlated to content of higher molecular biomass. The medial differential quotient of the viscosity (MDQ) was calculated as a measure for the degree of texture in the perfusate. The progression of the MDQ and the viscosity at a shearing rate of 1000 s^{-1} (Visc 1000) was then plotted for the course of the perfusion process and contrasted to the concentration of total protein in the samples (P_{tot}) and the accumulated protein discharge in order to reveal individual process characteristics.

2.6 A biomass depletion model for perfusion-based decellularization

A biomass depletion model for perfusion-based decellularization, based on a simple and commonly used model for microbiological growth [26], was used to match experimental data by numerical estimation. For detailed description of the model, parameter estimation and model matching please refer to the supplemental material (**suppl. data**). Briefly, the model is based on the debris formation rate ($q_{d/t}$), the maximal tissue-specific uptake rate ($q_{a/t\ max}$) and the monod-limitation constant for cellular tissue mass(k_{tc}) for the decellularization process. For model matching a numerical script was employed, matching the corresponding protein discharge functions to the simulated model-based course of protein discharge. This was based on minimizing the sum of a quality-functional J(x), comparing each datapoint of the normed instantaneous cumulative charged protein with the corresponding value of the simulated function.

2.7 Statistics

Data are presented as mean ± standard deviation for all measured and calculated values. For direct group comparisons, Student's t-tests were performed. Statistical significance was assumed for P-values lower than 0.05. Data analysis was realized using GraphPad Prism 6 (GraphPad Software, San Diego, CA).

3. Results

3.1 Up-scaling of whole-heart decellularization towards a human-scale model

3.1.1 Intoto decellularization of ovine hearts

In order to up-scale whole-heart decellularization towards a human-scale model, an already established and standardized detergent-based protocol for *in toto* decellularization of rodent hearts *via* coronary perfusion [15,16] was modified accordingly and applied to ovine hearts, which are characterized by larger size and increased biomass. Hereby, a consistently overall satisfactory macroscopic decellularization efficacy could be achieved in repetitive decellularization cycles, translating into homogenous tissue transluminescence free from detectable gross decellularization deficits (**Fig. 1A-C**.) This macroscopic quality could be reproduced continuously throughout the study, as demonstrated by standardized sample sections (**Fig. 1D-H**).

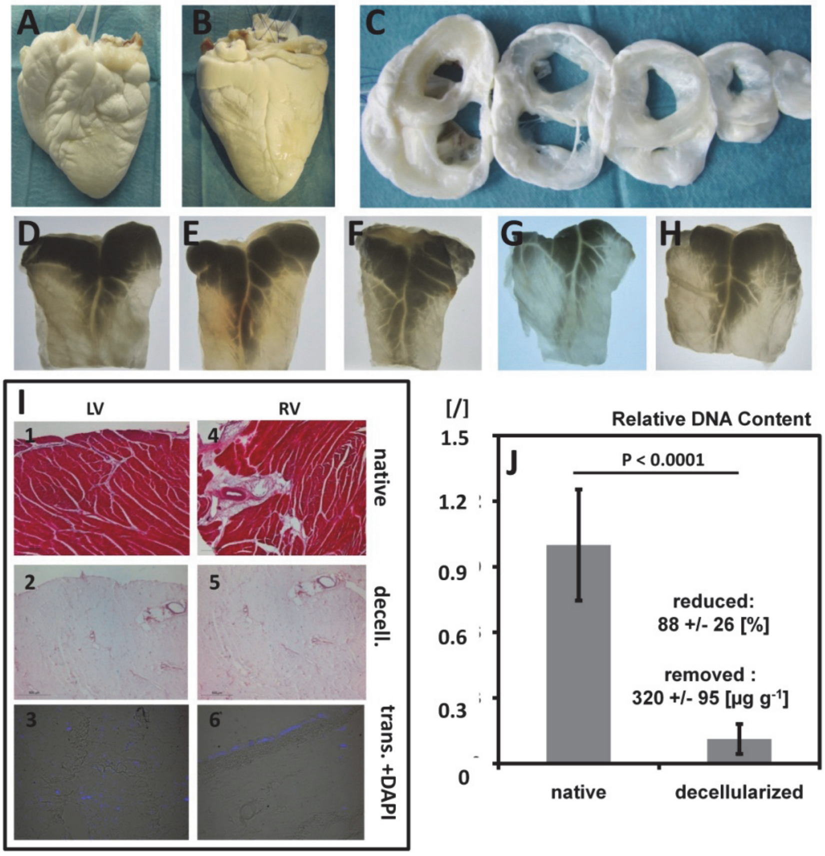

Fig. 1: Decellularization efficacy of human-scale *in toto* decellularized ovine whole-hearts I.A-C) Representative macroscopic images of perfusion-based decellularized ovine whole-hearts showing no gross decellularization deficit; (A) back view, (B) front view, (C) cross sections. **D-H)** Representative macroscopic images of standardized sections of *in toto* decellularized ovine hearts, demonstrating consistent homogeneous transparency. **I)** Representative images of HE (1-2,4-5) and DAPI (3,6) stained standardized sections of native (1,4) and *in toto* decellularized ovine hearts (2-3,5-6), showing removal of cell nuclei and cellular remnants, with however remaining DNA traces after whole-heart decellularization. Scale bar, 500 µm. **J)** Quantitative assessment of DNA tissue content in native and *in toto* decellularized ovine hearts normalized to the native control and plotted as relative fractions. Data presented as mean ± SD.

3.1.2 Validation of decellularization efficacy

Macroscopic decellularization efficacy of the employed decellularization protocol was further validated by histological analysis of decellularized tissue specimens, showing a largely cell free ECM with preserved matrix microarchitecture including patent myocardial vessels, as compared to non-decellularized native controls (**Fig. 1I)**. However, although no intact cell structures could be observed after the decellularization process, DNA remnants could still be identified within the dense collagenous matrix, as visualized by regional accumulation of hematoxilin and DAPI signal. This was concordant to the biochemical DNA analysis of the decellularized hearts, which showed a 88 ± 26 % reduction of DNA ($p<0.0001$) as compared to non-decellularized native controls, translating to a removal of 320 ± 95 µg DNA per g of native tissue (**Fig. 1J**). Further, regional analysis showed a high degree of cellular biomass elimination demonstrated by a statistically significant reversal of the ratio of collagenous to non-collagenous protein as compared to native non-decellularized controls (**Fig. 2**), with only7 ± 9 % of total non-collagenous protein remaining in the tissue after the decellularization process as compared to 96 ± 0.7 %of non-collagenous protein in the native myocardial tissue ($p<0.0001$) (**Fig. 2A**). Loco-regional analysis of the left ventricular wall, right ventricular wall and septum showed consistent values, with non-collagenous protein content before and after decellularization of95 ± 0.1 % vs. 15 ± 0.6 %, 95 ± 0.1 % vs. 2 ± 3.9 % and 96 ± 0.4 % vs. 7 ± 12.8 for the respective regions (**Fig. 2B**). This was further confirmed by specific Western blot analysis for remaining cardiac actin and desmin, indicating almost full removal of cardiac actin - as a marker for myocardial cellular protein - and only marginal detection of desmin - as a representative cell-ECM-junction protein - within the decellularized tissue samples as compared to native non-decellularized controls (**Fig. 2C-G)**.Densitometric analysis of the blot signals showed a quota to the corresponding signal of the native control of 10 ± 9 % for desmin ($p<000.1$) and 2.7 ± 1.4 % for desmin ($p<000.1$) and 2.7 ± 1.4 % for cardiac actin ($p<000.1$)(**Fig. 2G**).

3.2 Biomass discharge during whole-heart decellularization

3.2.1 Dry biomass loss

In toto decellularization of ovine and rodent hearts translated to a significant loss of biomass after the completion of the decellularization process, which is optically illustrated in **Fig. 3A-E**. Ovine hearts however, in contrast to rodent hearts, are usually characterized by a large inherent fraction of epicardial fat, which is also vascularized by the coronary vessel system and therefore might impact the perfusion-based decellularization process (**Fig.3A,C**). **Fig. 3B** illustrates the remaining fat-free DMB of a decellularized ovine heart after separation of the gross soluble lipid fraction, which can be compared to the DBM of decellularized heart left *in toto* in **Fig. 3A. Fig. 3D-E** illustrates the DBM before and after decellularization of standardized native ovine myocardial tissue samples, visualizing the loss of biomass during the decellularization process.

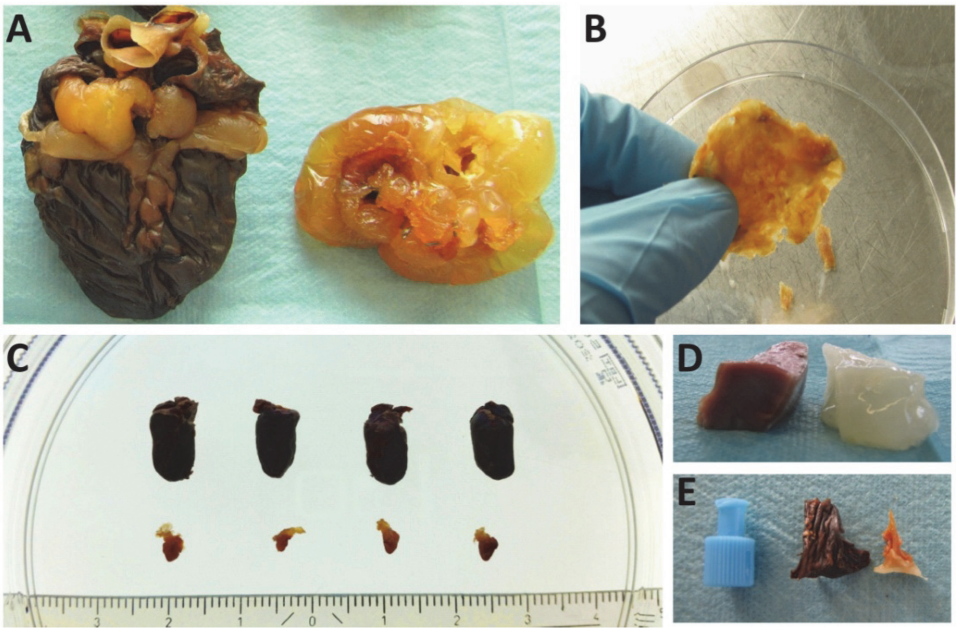

Fig. 2: Biomass discharge during ovine whole-heart decellularization I – macroscopic view. Representative macroscopic images of dry biomass (DBM) of native and perfusion-based *in toto* decellularized ovine hearts. **A**) Left: desiccated native ovine heart. Right: desiccated decellularized ovine heart. **B**) Total DBM of one complete ovine heart after *in toto* decellularization and separation of the gross soluble lipid fraction. **C)** Desiccated native (upper line) and *in toto* decellularized (lower line) rodent hearts. **D-E)** Wet and desiccated standardized ovine myocardial tissue samples before (left) and after non-perfusion-based decellularization (right).

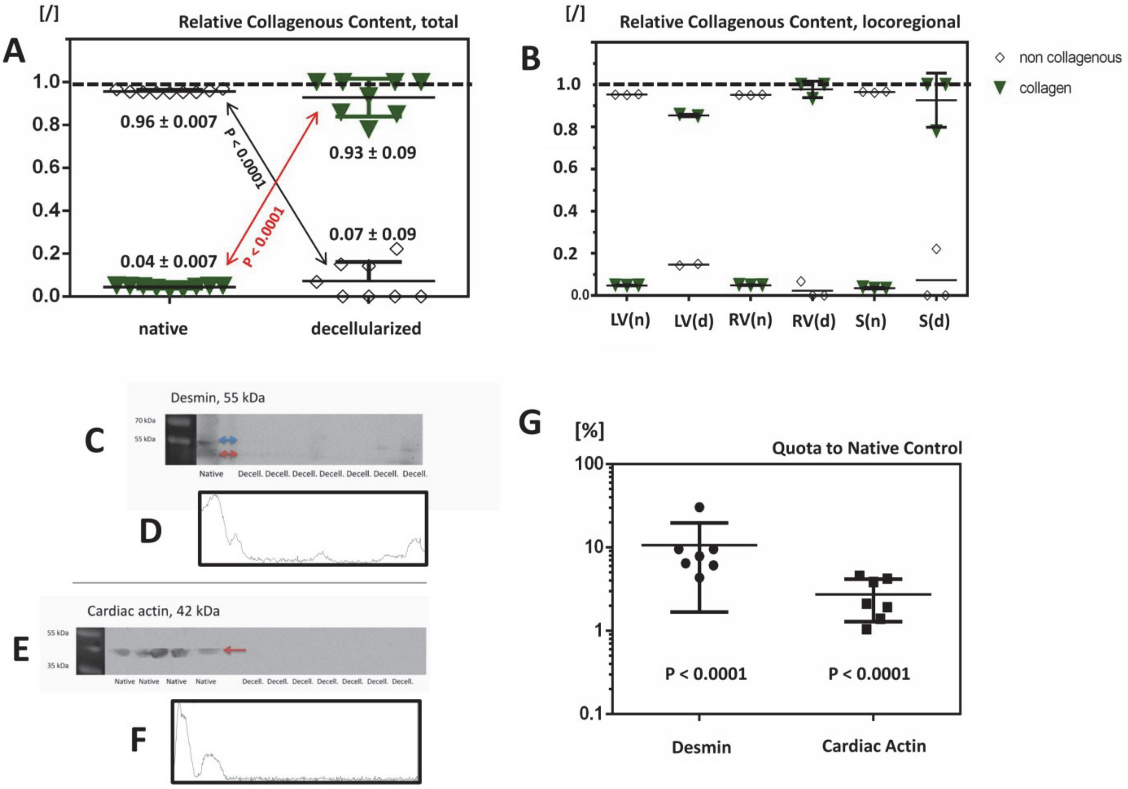

Fig. 3: Decellularization efficacy of human-scale *in toto* decellularized ovine whole-hearts II.A) Relative collagenous to non-collagenous protein content of ovine hearts before and after perfusion-based *in toto* decellularization, demonstrating a statistical significant reversal of the ratio after the decellularization process. **B)** Locoregional analysis of relative collagenous to non-collagenous protein content showing consistent values after the decellularization process, independent from the myocardial region. n, native; d, decellularized; LV, left ventricular; RV, right ventricular; S, septum. Data presented as mean ± SD. **C-F)** Representative Western blot signals and corresponding densitometric histograms for desmin and cardiac actin for *in toto* decellularized ovine hearts as compared to native controls, respectively. **G)** Semi-quantitative evaluation of the densitometric signals presented as quota to the signal of the native control (normalized to 100 %), revealing almost full removal of cardiac actin and only marginal detection of residual desmin. p<0.0001.

In quantitative analysis for decellularization of ovine whole-hearts of comparable donor animals mean DBM before and after decellularization was determined to be 49.8 ± 7 g vs.2.9 ± 1.6 g, respectively(P<0.0001); while for rodent heartsmean DBM before and after decellularization was determined to be 0.16 ± 0.02 g vs. 0.01 ± 0.002 g (P<0.0001), respectively (**Fig. 4A**). Therefore, the total amount of DBM that is discharged during the decellularization process from the myocardial tissue, excluding the gross soluble lipid fraction originating from the epicardial fat, was approximately94± 13 % of the native DBM for ovine hearts and 92 ± 21 % of the native DBM for rodent hearts. Under assumed optimal decellularization of myocardial tissue under non-limited mass transport conditions, the total amount of DBM that is discharged during the non-perfusion-based decellularization process of standardized minced native tissue samples of the ovine left ventricular wall was 92± 11 % of the native DBM, with 1.4 ± 0.4 g vs. 0.1 ± 0.07 g (P=0.0007) mean DBM before and after decellularization,respectively (**Fig. 4A**).

3.2.2 Impact of fat content on dry biomass

While in native rodent hearts the gross soluble lipid fraction of the DBM (Fat)is negligible, with the $DBM_{fat\text{-}free}$ equaling the total DBM of rodent hearts, in native ovine hearts it does constitute an important part of the total DBM, with the mass ratio of Fat to $DBM_{fat\text{-}free}$ equaling 0.31 ± 0.05(**Fig. 4B**). Therefore, in native ovine hearts the $DBM(WBM)^{-1}$ratio excluding fat is significantly lower than the $DBM(WBM)^{-1}$ratio including fat, with 22 ± 1 %vs. 27 ± 1 %, respectively (p=0.0009) (**Fig. 4B**). The discrepancy between those ratios could be validated independently by determination of 6.7 ± 1 % $Fat(WBM)^{-1}$ for native ovine hearts and 7.3 ± 0.1 %$Fat(WBM)^{-1}$for decellularized ovine hearts (**Fig. 4B**), demonstrating that the gross soluble lipid fraction of the DBM,which is constituted largely by the epicardial fat, does not become discharged during the decellularization process, thus making it a non-negligible factor in the process. This is validated, when DBM to WBM ratios of native ovine hearts are comparedto those of standardized minced native tissue samples of the ovine left ventricular wall or of rodent hearts, which are both free of large epicardial fat deposits. In all of the latter corresponding $DBM(WBM)^{-1}$ratios show quite similar values when the Fat of the ovine heart is neglected, with 22 ± 1 % vs. 20 ± 1.6 %vs. 19.9 ± 0.2 %, respectively (p>0.05) (**Fig. 4C**).

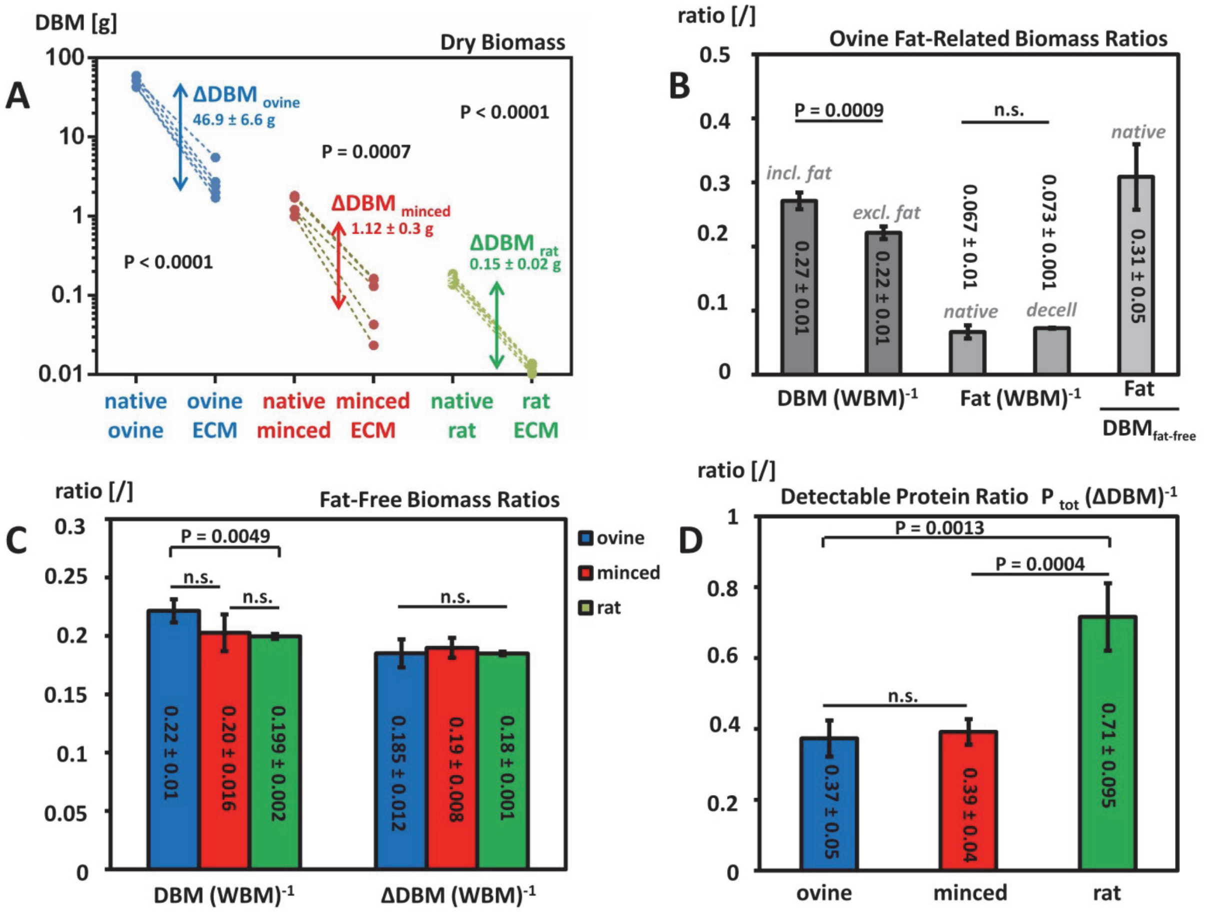

Fig. 4: Biomass discharge during ovine whole-heart decellularization II - parameters of biomass balancing. A) Dry biomass (DBM) of ovine (blue) and rodent (green) hearts as well as standardized ovine myocardial tissue samples (red) before and after decellularization, showing the total solid biomass discharge during the process (ΔDBM). For ovine hearts this illustrates the total amount of DBM that is discharged during the decellularization process from the myocardial tissue, excluding the gross soluble lipid fraction originating from the epicardial fat, which is not present in the other two sample types. **B)** Fat-dependent and -independent biomass ratios of ovine hearts, demonstrating the important gross soluble lipid fraction (Fat) of the total DBM after the decellularization process**.** DBM(WBM)$^{-1}$, illustrates the relation of DBM to WBM with and without Fat after the decellularization process. Fat(WBM)$^{-1}$, illustrates the relation of Fat to WBM before and after the decellularization process. Fat/DBM$_{\text{fat-free}}$, illustrates the mass ratio of Fat to fat-free DBM in native ovine hearts. **C)** Fat-free biomass ratios of initial DBM (native) and DBM discharge during the decellularization process (ΔDBM) normalized to their corresponding native WBM of ovine (blue) and rodent (green) hearts, as well as standardized ovine myocardial tissue samples (red), revealing comparable values for all samples. **D)** Detectable protein fraction of the discharged solid biomass during the decellularization process of ovine (blue) and rodent (green) hearts, as well as standardized ovine myocardial tissue samples (red), demonstrating a much lower detectable protein fraction for ovine as compared to rodent tissue.

3.2.3 Solid biomass discharge

Further, in above described experiments, a mean standardized biomass discharge per initial tissue weight [ΔDBM (WBM)$^{-1}$] of 18.5 ± 1.2 % was determined for ovine hearts and of 18 ± 0.1 % for rodent hearts when the gross soluble lipid fraction of the DBM is excluded from the calculation (**Fig. 4C**). Validation by non-perfusion-based decellularization of standardized minced ovine left ventricular tissue samples demonstrated a very similar ΔDBM (WBM^{-1}) ratio of 19 ± 0.8 % (**Fig. 4C**).Therefore, the applied decellularization processes led to a discharge of solid biomass that correlates to approximately about 18 % of the initial wet biomass for all analyzed organs or tissues.

3.2.4 Composition of biomass discharge

By additional determination of the cumulative total protein content of the decellularization perfusates (P$_{\text{tot}}$), the proportion of protein detected within the decellularization perfusate could be correlated to the discharged biomass for each individual heart (P$_{\text{tot}}$ (ΔDBM)$^{-1}$). Interestingly, the total protein amount detected within perfusates correlated to 71 ± 9.5 % of solid biomass discharge for rodent hearts, and only to37± 5 % of solid biomass discharge for ovine hearts (**Fig. 4D**). Validation by analysis of non-perfusion based decellularization of standardized minced ovine left ventricular tissue samples showed a very similar correlation of total protein amount detected within the respective decellularization solution of 39 ± 4 % of solid biomass discharge, as compared to the ovine whole-heart samples (**Fig. 4D**).

3.3 Protein discharge during whole-heart decellularization

3.3.1 Organ-dependentprotein discharge dynamics &kinetics

In order to evaluate biomass specific protein discharge kinetics of ovine whole-heart decellularization, time-dependent accumulative protein contents within the decellularization perfusates $P_{tot}(t)$of independent decellularization cycles were normalized to the WBM of the respective heart to account for biological biomass variance, and plotted against time (**Fig. 5A**).Hence, **Fig. 5A** depicts the progression and the dynamics of the protein discharge for six ovine hearts with comparable organ size, illustrating the respective decellularization process. For all analyzed hearts the total amount of discharged protein at the end of the decellularization process was found to lie within a defined range, bounded by the mean standardized detectable protein discharge within the decellularization perfusates per initial tissue weight [P_{tot} (ΔDBM WBM)$^{-1}$] on the lower margin, and the mean standardized solid biomass discharge per initial tissue weight [ΔDBM (WBM)$^{-1}$] on the upper margin. However, out of the six analyzed hearts only four lied within the mean P_{tot} (ΔDBM WBM)$^{-1}$ range, while one heart slightly exceeded that range and another heart almost reached the upper boundary. Interestingly, although decellularization efficacy of all analyzed hearts - as determined by above mentioned standard parameters including macroscopic inspection as well as histological and biochemical analysis – was comparable, the depicted curves of biomass specific protein discharge varied for each individual heart, ranging from saturated to more linear courses in varying degrees.

By normalizing the time-dependent accumulative protein contents within the decellularization perfusates $P_{tot}(t)$ to the total discharged protein wash out $P_{tot\ WO}(x)$, reaction rates in terms of protein elimination ($q_{d/t}$) could be established for each individual ovine whole-heart decellularization cycle, which varied between 0.04 h^{-1} and 0.1 h^{-1}, depending on the respective organ (**Fig. 5B**). This translates into an organ-dependent 2.5-fold difference in functional reactivity for the protein discharge process. Interestingly, three of the apparently slower discharging hearts showed a *de facto* linear progress, while the other three apparently faster discharging hearts revealed a non-linear kinetic in terms of a typical monod-limitation turnover. Further, an exemplary direct comparison of protein discharge kinetics of those ovine organs showing a non-linear kinetic with rodent organs during the first 10 h, under the same unlimited conditions and identical decellularization protocol, demonstrated nearly congruent courses independent from organ-size (**Fig. 5C**).

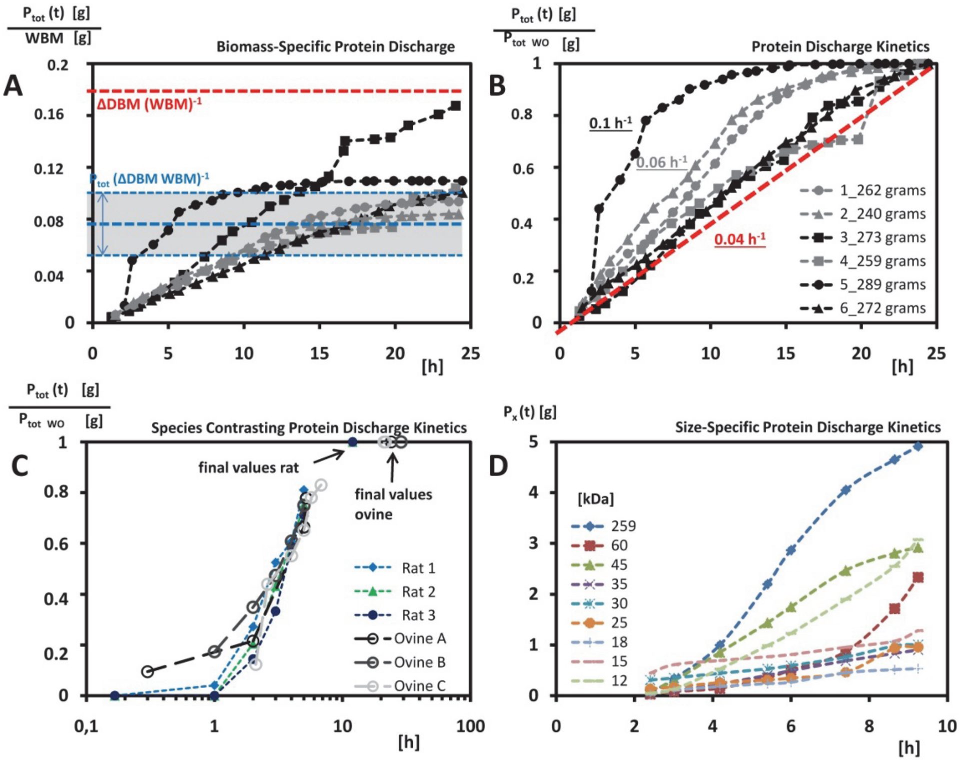

Fig. 5: Biomass discharge during ovine whole-heart decellularization III - discharge dynamics based on detected total-protein in perfusates. **A)** Cumulative discharged total protein P_{tot} (t) over time during ovine whole-heart decellularization normed to the WBM of the individual heart. Blue line /grey area, mean/range of standardized detectable protein discharge within the decellularization perfusates per initial tissue weight [P_{tot} (ΔDBM WBM)$^{-1}$]; red line, mean standardized solid biomass discharge per initial tissue weight [ΔDBM (WBM)$^{-1}$] **B)** Cumulative discharged total protein P_{tot} (t) over time during ovine whole-heart decellularization, normed to the total protein wash-out ($P_{tot\ WO}$) of the individual hearts, allowing the approximation of the debris formation rate ($q_{d/t}$). **C)** Normalized protein discharge kinetics (($P_{tot}(t)(P_{tot\ WO})^{-1}$) over time of the decellularization process of exemplary rodent and ovine hearts, demonstrating almost congruent courses for those particular hearts irrespective of donor species. **D)** Protein size-dependent discharge over time during ovine whole-heart decellularization, demonstrate diverging discharge dynamics depending on protein-size fractions.

3.3.2 Protein size-dependent discharge kinetics

In order to assess whether discharge of proteins during whole-heart decellularization varies depending onthe size of the respective protein, cumulative protein discharge during the first 10 h of ovine whole-heart decellularization was segmented into protein size fractions after defined intervals and plotted against time (**Fig. 5D**). Depicted exemplary protein size-dependent discharge kinetics demonstrate diverging discharge dynamics depending on protein-size fractions, with e.g. the 60 kDa protein fraction discharge strongly increasing towards the end, while the 45 kDa protein fraction presenting with an apparent saturation
at that point of time.

3.4 Rheological evaluation of discharged biomass during whole-heart decellularization

Perfusates derived from independent ovine whole-heart decellularization cycles were subjected to rheological evaluation in order to assess time-dependent viscosity and structure of the discharged biomass (**Fig. 6A-C**), as a non-disruptive process accompanying tool, as previously introduced [17]. Interestingly, process time until detectable viscosity in the perfusates re-approached the initial viscosity of the pure detergent solution during the decellularization process varied between individual decellularization cycles. As demonstrated in **Fig. 6** for three exemplarily decellularization cycles, in the first two decellularization cycles depicted in **Fig. 6A,D and 6B,E** viscosity in the perfusates could be detected up to 15-16 h within the decellularization process, while in the case of the third heart with decellularization cycle depicted in **Fig. 6C,F** already after 7 h there was no detectable viscosity in the perfusates anymore, despite identical decellularization protocols. As viscosity in the perfusates translates into large debris transportation, this finding further indicates individual process characteristics in terms of time-dependent biomass discharge during perfusion-based whole-heart decellularization.

3.5 Individual process characteristics during whole-heart decellularization

By plotting the corresponding medial differential quotient of the viscosity (MDQ) contrasted to the respective viscosity at a shearing rate of 1000 s^{-1}, the concentration of total protein, and the accumulated protein discharge over time, up to the point in which perfusate viscosity re-approached the initial viscosity of the pure detergent solution, organ-specific process characteristics for each individual decellularization process could be depicted (**Fig. 6D-F)**.Generally, the course of viscosity initially followed the course of protein discharge, but declined when protein discharge lost dynamics in terms of a decreasing discharge rate (decreasing slope of the protein discharge course). Simultaneously the MDQ increased with decreasing protein concentration within the decellularization perfusates, seemingly peaking at a point of increased protein discharge rate (steepest slope of protein discharge course) during the decellularization cycle. This pattern could be reproduced for three independent decellularization cycles, however with organ-specific dynamics and individual process characteristics.

3.6 Model matching to the introduced biomass depletion model for perfusion-based decellularization

In addition to the general considerations concerning the dynamics and kinetics of biomass discharge, experimental data was matched to the introduced model (please refer to **supplementary data** for detailed model description), determining the respective parameters by numerical estimation (**Fig.7**). The decellularization process of ovine hearts showing non-linear protein discharge kinetics during whole-heart decellularization could be well matched by the introduced model in contrast to the decellularization process of ovine hearts exhibiting a rather linear trend of discharge kinetics (**Fig. 7A).** As coherently assessed by the minimized sum of error-squares (quality functional J(x)) only the three hearts with non-linear protein discharge kinetics conformed to the applied model by revealing a satisfactory minimized divergence with values of < 0.1 (**Fig. 7B**). Two of those hearts as well as one heart with a mismatch of the experimentally observed data to the introduced model showed moderate to fast maximal tissue-specific uptake rates $q_{a/t\ max}$ ranging between 0.345 $h^{-1}$and 0.114 h^{-1}, while the other three hearts remained at lower rates of 0.074 h^{-1} to 0.088 h^{-1}. Further, matched decellularization processes exhibited a monod limitation, as demonstrated by calculated monod limitation constants (k_{tc}) > 0.1, while for decellularization processes not fitting the model respective monod limitation constant (k_{tc}) became negligible with <0.1 (**Fig. 7B)**.

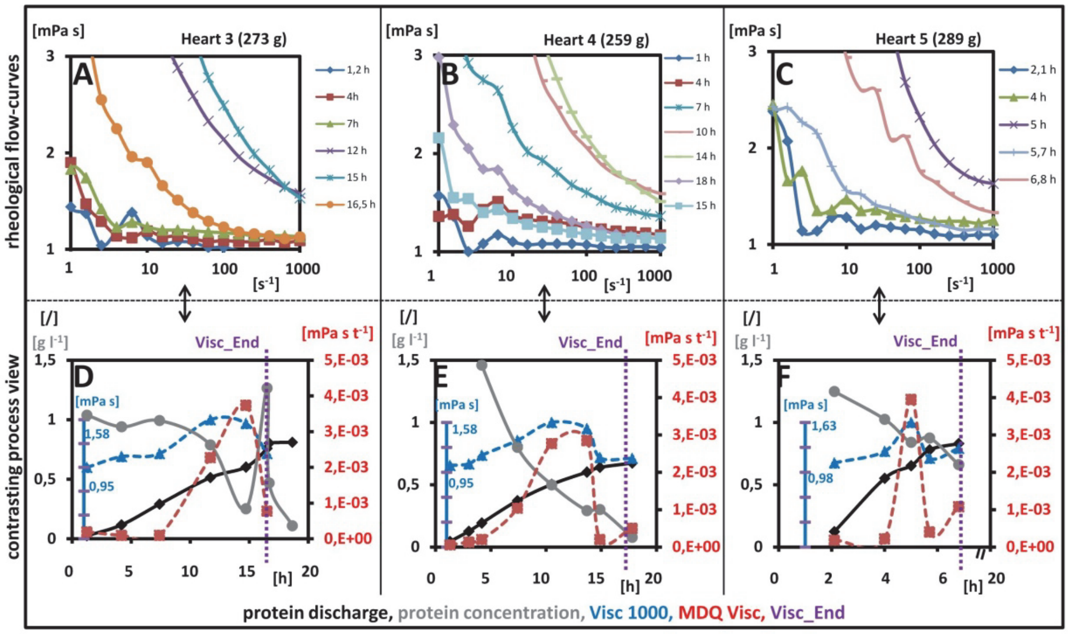

Fig. 6: **Rheological evaluation of perfusates during ovine whole-heat decellularization and individual process characteristics. A-C)** Rheological Flow Curves of decellularization perfusates of standardized time points during three independent ovine whole-heart decellularization cycles, depicting the measured viscosity as a function of the shearing rate and viscoelasticity changes during the process. **D-F)** Individual process characteristics for three independent ovine whole-heart decellularization cycles, depicted by plotting the corresponding medial differential quotient of the viscosity (MDQ Visc; red line) contrasted to the respective viscosity at a shearing rate of 1000 s^{-1} (Visc 1000; blue line), the concentration of total protein within the perfusate (protein concentration; grey line), and the accumulated protein discharge over time (protein discharge; black line), illustrating a general pattern with however organ-specific process characteristics for each individual decellularization. The process parameters are only depicted up to the point of the decellularization cycle in which perfusate viscosity approached the initial viscosity of the pure detergent solution, e.g. marking the end of detectable viscosity in the perfusates (Visc_End; purple).

Estimated Parameters for Biomass Discharge Model for Ovine Hearts 1-6

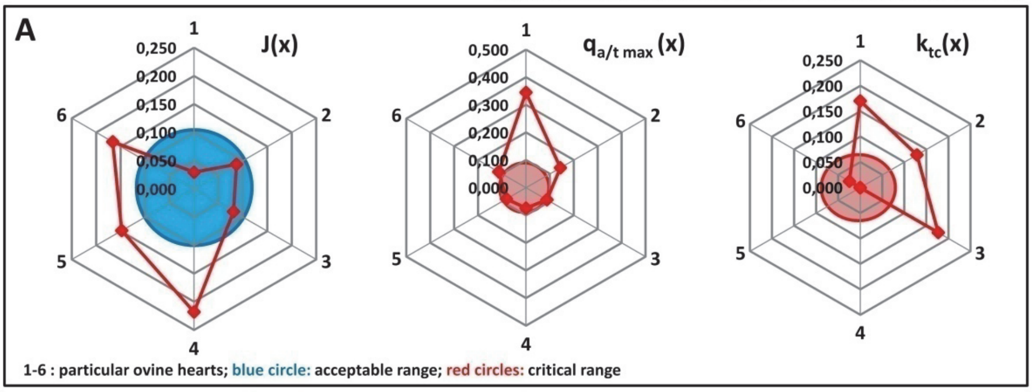

B

heart nr. = x	quality functional J(x) [/]	tissue-specific uptake rate $q_{a/t\ max}$ (x) [h^{-1}]	monod limitation constant k_{tc}(x) [/]
1	0.029	0.345	0.170
2	0.087	0.144	0.129
3	0.081	0.088	0.177
4	0.218	0.074	4.E-04
5	0.148	0.082	2.E-04
6	0.167	0.114	0.025

Fig. 7: Model matching and parameter estimation for the detected biomass discharge. Parameter estimation and model matching for six independent ovine whole-heart decellularization cycles, as computed by the matching algorithm. **A**) Model parameters displayed in net-plots to highlight the distribution while simultaneously illustrating areas of differing quality. J(x), quality functional representing the minimized sum of the error-squares (satisfactory matching<0.1); blue circle, area of satisfactory matching. $q_{a/t\ max}$ (x), tissue specific uptake rate indicating the accessibility of the biomass to decellularization agents; red circle, area of limited mass-transport. $\mathbf{k_{tc}}$. monod limitation constant; red area, area of limited mass-transport. **B**) Estimated parameters for each independent ovine whole-heart decellularization cycle. Blue, optimal matching with moderate to fast discharge kinetics and monod dynamics indicating unlimited mass-transport conditions; red, sub-optimal matching indicating mass-transport limitations.

4. Discussion

Here, we analyzed the mechanistics of perfusion-based human-scale whole-heart decellularization by evaluating and comparing the dynamics of biomass discharge and the characteristics of the involved kinetics during *in toto* decellularization of ovine and rodent hearts. Our results suggest highly varying process characteristics for the *in toto* decellularization of individual organs of human-scale biomass despite seemingly consistent inter-sample decellularization efficacy, as evaluated by conventional disruptive analysis of obtained ECM scaffolds.

As recently shown, *in toto* decellularization of human-scale organs is feasible by perfusion-based decellularization resulting in cell free ECM scaffolds with high biological fidelity [3-6]. In this study, - as has already been shown in the past - we could demonstrate that by adoption of a detergent-based decellularization protocol from a small animal model *in toto* decellularization of organs with larger size and increased biomass is possible, with consistent decellularization efficacy in terms of standard histological and biochemical analysis. However, the focus of the study was not the creation of an optimal decellularization protocol for human-scale organs, but rather gaining insights into the process itself and into potential disturbances by emerging physicochemical interactions and/or mass transport limitations due to the increased biomass of human-scale scaffolds.

By biomass analysis before and after the decellularization process, solid biomass discharge of rodent and ovine hearts during perfusion-based whole-heart decellularization was determined to consistently correlate to approximate 18 % of initial tissue weight of the particular organ. This was not only validated by non-perfusion-based decellularization of myocardial tissue, resulting in almost equal values of solid biomass discharge during assumed optimal decellularization, but it also very closely correlates to the proportion of cellular biomass within the myocardium, which was determined to be 18.9 % by independent tracer based and morphometric measurements by Aliev et al. [18]. Interestingly though, there was a large significant discrepancy between rodent and ovine hearts regarding the total protein amount that could be detected within the respective decellularization perfusates, amounting to 71% of the solid biomass discharge for rodent hearts, and to only 37% of the solid biomass discharge for ovine hearts. While the non-detected protein fraction within the respective perfusates may indeed be due to methodological limitations inherent to the applied analytical techniques, the large discrepancy between ovine and rodent organs in the detectable protein fraction may indicate a potential organ-specificity for the decellularization process. Here, biomass-dependent increase in concentration and size of debris fragments, crosslinking effects, vesicle-formation or other physicochemical effects as well as varying mass-transport conditions may play a fundamental role, hence potentially masking part of the protein fraction in the perfusates.

Individual biological characteristics of organs of different size are corroborated by the fact that ovine hearts have a significantly larger proportion of epicardial fat as compared to rodent hearts. In contrast to rodent hearts, in ovine hearts the gross soluble lipid fraction could be determined to constitute an important fraction of the DBM, with its proportion of about 30 % contrasted to the fat-free DBM. Thus, the epicardial fat should be considered a non-negligible factor in the decellularization process, especially with regards to human-scale organs.

Under ideal conditions, an excess in decellularization agents as compared to the organs biomass and optimal organ perfusion conditions should lead to a spatio-temporally balanced delivery of decellularization agents to the tissue as well as a homogenous biomass wash out from the organ, resulting in similar process characteristics independent from organ characteristics. However, as exemplified by the series of ovine hearts decellularized *in toto* under identical conditions and with consistent decellularization efficacy, biomass specific protein discharge varied for each individual organ with different discharge dynamics, - ranging from more saturated to more linear courses in varying degrees - as well as varying reaction rates resulting in up to 2.5-fold changes in functional reactivity.

Nonetheless, within all *in toto* decellularized hearts the total amount of discharged protein at the end of the decellularization process was found to lie within a defined range, bounded by the mean standardized detectable protein discharge within the decellularization perfusates per initial tissue weight [P_{tot} $(\Delta \text{DBM WBM})^{-1}$] on the lower margin, and the mean standardized solid biomass discharge per initial tissue weight [$\Delta \text{DBM } (\text{WBM})^{-1}$] on the upper margin.

Interestingly, as further shown in this study, under certain conditions and independent from the decellularization efficacy, protein discharge dynamics and kinetics during whole-heart decellularization of ovine hearts may closely mimic those of rodent hearts despite largely differing in their total biomass amount. Thus, this indicates certain organ- rather than size-dependent process characteristics within the same decellularization protocol and method. As rodent discharge dynamics superpose those of fast and apparently unlimited courses of ovine discharge curves almost congruently, this further implies a general independency from biomass, but rather a certain increasing susceptibility for limitations by increasing organ size.Assessment of time-dependent viscosity and structure of the discharged biomass and correlation to the corresponding protein discharge dynamics and kinetics depicted a general pattern of the perfusion-based whole-heart decellularization process. Intriguingly, after peaking of the MDQ the dynamic of protein discharge consistently decreases. Thereby, its decay apparently introduces the saturation of the overall protein discharge, which could be due to emerging of characteristic structural components, which in consequence may lead to specific physco-chemical interactions, potentially also masking the above discussed non-detectable protein fraction within the decellularization perfusates.

Indeed, size-dependent protein discharge kinetics observed in this study demonstrate diverging discharge dynamics depending on protein-size fractions. This indicates that the functional reactivity of the discharge process and its characteristics at different time points is a composition of differing dischargedynamics, potentially dominated by the most prevalent factor at the respective time point. The content of the instantaneously decomposed cellular biomass is expected to vary between cell membrane components, soluble cytoplasmatic macromolecules and fibrous components and others, depending on the stage of the decellularization process[19]. Accordingly, specific destabilization of target components at specific time points could be applied to optimize the overall functional reactivity of the discharge process, potentially accelerating the decellularization process as well as impacting ECM preservation quality.

Nonetheless, in our experiments each organ still displayed a very distinct organ-specific dynamic with individual process characteristics, potentially due to varying mass-transport conditions. In fact, process time until detectable viscosity in the perfusates re-approached the initial viscosity of the pure detergent solution varied between individual decellularization cycles. However, this may represent a critical turning point within the decellularization process, as it most probably indicates cessation of large debris transportation, potentially due to completion of the process or due to emerging biomass transportation limitations. Consequently, process accompanying rheological monitoring of decellularization perfusates [17] may be a powerful tool to control the decellularization process.

The introduced theoretical model of biomass depletion for perfusion-based decellularization and model matching of an initial series of ovine whole-heart decellularization cycles further visualized organ-specific individual process characteristics. Out of six independent ovine whole-heart decellularizations, only three with moderate to fast discharge kinetics and monod dynamics showed optimal model matching in terms of the quality functional J(x) indicating unlimited mass-transport conditions, while the remaining half showed a sub-optimal matching indicating mass-transport limitations.

Hence, the here revealed new insights into the mechanistics of whole-heart decellularization as well as the introduced process accompanying tools may help to monitor and to further optimize the decellularization process, which until now is usually solely validated at the end of the process by disruptive analysis of the resulting ECM scaffold. Although some efforts have already been made to implement non-disruptive analytical tools as process accompanying quality metrics for the decellularization process, such as investigation of fluid and flow dynamics of the decellularization perfusates [17,27] or CT scanning for the evaluation of DNA elimination[20], we still stand at the very beginning. However, deeper insight to the perfusion-based decellularization process may not only enable us to optimize the decellularization process and to economize resources, but it may also help in implementing process accompanying quality metrics. Further studies will have to show, whether this may also impact the quality of generated ECM scaffolds in terms of their clinical suitability, as matrix assessment by conventional means, - such as the methods exemplarily employed in this study - indicated comparable scaffold characteristics despite differing process characteristics. Though, it is to be expected that more powerful analytical tools focusing on ECM composition, such as proteonomics [21,22], may reveal process-dependent differences on a molecular level. Nevertheless, independently from the potential correlations to matrix quality, process monitoring and quality control tools will be a prerequisite not only for dealing with regulatory agencies, such as the food and drug administration (FDA), but also for industrial-based production of whole-organ human-scale grafts.

Nonetheless, as we are just starting to gain insights into the process of perfusion based whole-organ decellularization this study inevitably suffers from inherent limitations. Most importantly, although more comparable to rodent hearts in size and biomass, ovine hearts still differ from human hearts in their biological characteristics. As the use of human hearts is however restricted by their availability and due to ethical concerns, we have to rely on alternatives, bearing in mind that the obtained findings may not translate one to one to other species. In addition, due to methodicallimitations of the employed analytical tools, physicochemical interactions of decomposed biomass may have remained undetected, potentially masking certain biomass transport characteristics. Further, rheological analysis of fluid dynamics within the setting of perfusion-based decellularization still needs to be optimized, especially with regards to the sensitivity of the method and interpretation of the results. Hence, implemented process accompanying tools, as well as experimentally determined and estimated reference values need to be validated in larger series and independently from the decellularization protocol employed in this study. Similar validation is needed for the introduced theoretical model of biomass depletion for perfusion-based decellularization. Therefore, further studies are strongly warranted in order to implement universal quality metrics for perfusion-based whole-organ decellularization.

5. Conclusion

The results of this study suggest highly varying process characteristics for the *in toto* decellularization of individual human-scale organs, such as protein discharge kinetics or viscoelasticity of formed debris, despite seemingly consistent intersample decellularization efficacy, as evaluated by conventional disruptive analysis of obtained ECM scaffolds. Hence, the here exposed insights into the mechanistics of whole-heart decellularization as well as the introduced non-disruptive process accompanying tools may help to monitor and further optimize the decellularization process, especially with regards to human-scale scaffold production.

6. Acknowledgements

The authors acknowledge the Susanne Bunnenberg-Stiftungat the Düsseldorf Heart Center, as well as a personal stipend from the Schmeil-Stiftung (Heidelberg, Germany) to JörnHülsmann.

7. References

1. Mao, A. S. & Mooney, D. J. Regenerative medicine: Current therapies and future directions. *Proceedings of the National Academy of Sciences* **112,** 14452-14459 (2015).

2. Peloso, A., Dhal, A., Zambon, J. P., Li, P., *et al.*Current achievements and future perspectives in whole-organ bioengineering. *Stem cell research & therapy* **6,** 1 (2015).

3. Tapias, L. F. &Ott, H. C. Decellularized scaffolds as a platform for bioengineered organs. *Current opinion in organ transplantation* **19,** 145 (2014).

4. Arenas-Herrera, J. E., Ko, I. K., Atala, A. &Yoo, J. J. Decellularization for whole organ bioengineering. *Biomedical materials* **8,** 014106 (2013).

5. He, M. &Callanan, A. Comparison of methods for whole-organ decellularization in tissue engineering of bioartificial organs. *Tissue Eng Part B Rev* **19,** 194-208 (2013).

6. Badylak, S. F., Taylor, D. &Uygun, K. Whole-organ tissue engineering: decellularization and recellularization of three-dimensional matrix scaffolds. *Annual review of biomedical engineering* **13,** 27-53 (2011).

7. Aubin, H., Kranz, A., Hülsmann, J., Pinto, A., *et al.* A novel native derived coronary artery tissue-flap model. *Tissue Engineering Part C: Methods* **19,** 970-980 (2013).

8. Mandrycky, C., Wang, Z., Kim, K. & Kim, D. -H. 3D bioprinting for engineering complex tissues. *Biotechnology advances* **34,** 422-434 (2016).

9. Ott, H. C., Matthiesen, T. S., Goh, S. -K., Black, L. D., *et al.*Perfusion-decellularized matrix: using nature's platform to engineer a bioartificial heart. *Nature medicine* **14,** 213-221 (2008).

10. Scarritt, M. E., Pashos, N. C. &Bunnell, B. A. A review of cellularization strategies for tissue engineering of whole organs.*Frontiers in bioengineering and biotechnology* **3,** 43 (2015).

11. Moran, E. C., Dhal, A., Vyas, D., Lanas, A., *et al.*Whole-organ bioengineering: current tales of modern alchemy. *Translational Research* **163,** 259-267 (2014).

12. Sánchez, P. L., Fernández-Santos, M. E., Costanza, S., Climent, A. M., *et al.*Acellular human heart matrix: a critical step toward whole heart grafts. *Biomaterials* **61,** 279-289 (2015).

13. Kitahara, H.,Yagi, H., Tajima, K., Okamoto, K., *et al.*Heterotopic transplantation of a decellularized and recellularized whole porcine heart. *Interactive cardiovascular and thoracic surgery* **22,** 571-579 (2016).

14. Keane, T. J., Swinehart, I. T. &Badylak, S. F. Methods of tissue decellularization used for preparation of biologic scaffolds and in vivo relevance. *Methods* **84,** 25-34 (2015).

15. Akhyari, P., Aubin, H., Gwanmesia, P., Barth, M., *et al.* The quest for an optimized protocol for whole-heart decellularization: a comparison of three popular and a novel decellularization technique and their diverse effects on crucial extracellular matrix qualities. *Tissue Engineering Part C: Methods* 17, 915-926 (2011).

16. Aubin, H., Kranz, A., Hülsmann, J., Lichtenberg, A. &Akhyari, P. Decellularized whole heart for bioartificial heart. *Cellular Cardiomyoplasty: Methods and Protocols* 163-178 (2013).

17. Hülsmann, J., Aubin, H., Bandesha, S. T., Kranz, A., *et al.*Rheology of perfusates and fluid dynamical effects during whole organ decellularization: A perspective to individualize decellularization protocols for single organs. *Biofabrication***7,** 035008 (2015).

18. Aliev, M. K., Dos Santos, P., Hoerter, J. A., Soboll, S., *et al.* Water content and its intracellular distribution in intact and saline perfused rat hearts revisited. *Cardiovasc Res* **53,** 48-58 (2002).

19.Crapo, P. M., Gilbert, T. W. &Badylak, S. F. An overview of tissue and whole organ decellularization processes.*Biomaterials* **32,** 3233-3243 (2011).

20. Geerts, S., Ozer, S., Jaramillo, M., Yarmush, M. &Uygun, B. E. Non-destructive methods for monitoring cell removal during rat liver decellularization. *Tissue Engineering* (2016).

21. Li, Q., Uygun, B. E., Geerts, S., Ozer, S., *et al.*Proteomic analysis of naturally-sourced biological scaffolds. *Biomaterials* **75,** 37-46 (2016).

22. Calle, E. A., Hill, R. C., Leiby, K. L., Le, A. V., *et al.*Targeted proteomics effectively quantifies differences between native lung and detergent-decellularized lung extracellular matrices. *ActaBiomaterialia***46,** 91-100 (2016).

23. Joseph, J., Joseph, L., Shekhawat, N. S., Devi, S., *et al.*Hyperhomocysteinemia leads to pathological ventricular hypertrophy in normotensive rats. *American Journal of Physiology-Heart and Circulatory Physiology* **285,** H679-H686 (2003).

24. Clarke, N. E. & Mosher, R. E. The water and electrolyte content of the human heart in congestive heart failure with and without digitalization.*Circulation* **5,** 907-914 (1952).

25. Salisbury, P. F., Cross, C. E. &Rieben, P. A. Distensibility and water content of heart muscle before and after injury. *Circ Res* **8,** 788-793 (1960).

26. Luttmann, R., Bitzer, G. &Hartkopf, J. Development of control strategies for high cell density cultivations. *Mathematics and computers in simulation* **37,** 153-164 (1994).

27. Lee, P.F., Chau, E., Cabello, R., Yeh, A.T., et al. Inverted orientation improves decellularization of whole porcine hearts.*ActaBiomater* 49, 181-191 (2017).

8. Supplementary data

8.1 A biomass depletion model for perfusion-based decellularization

In principle, the process of decellularization describes a depletion of a defined amount of biomass that becomes decomposed into debris and is removed from a tissue or organ. According to the conservation of mass, the discharged biomass should equal the accumulated amount of debris. This exemplifies the inverse analogy to a microbiological growth curve in a standard batch process, where a defined amount of substrate becomes converted to biomass by mass-progression. The generally accepted model of mass progression to describe a microbiological batch process demands a spatio-temporal homogeneity which is provided technically by ideal stirring. In analogy, the perfusion-based decellularization process demands a spatio-temporal synchrony of mass transport *via* ideal perfusion of the tissue or organ. Due to this direct causality, the discharge dynamics and kinetics of the decellularization process can be used as an indirect measure for the underlying mass-transport conditions, representing fundamental quality metrics for the process itself. Hence, here we introduce a biomass depletion model for perfusion-based decellularization, based on a simple and commonly used model for microbiological growth [26].

8.2 Description of the model

8.2.1 Standard model for microbiological growth

Microbiological growth is generally described as a progression of cell-mass (m_{cell} (t)) by a cell specific growth rate ($q_{X/X}$ (t)), as expressed in equation M1.

$$\frac{dm_{cell}}{dt}(t) = m_{cell}(t)\cdot q_{x/x}(t) \qquad \text{(M1)}$$

m_{cell} = cell-mass [g]
$q_{x/x}$ = cell-specific growth rate [h^{-1}]
t = variable for process-time [h]

The growth dynamics of a standard batch process are mainly based on an initial phase of unlimited microbiological growth, where $q_{x/x}$ (t) is invariant and is usually described as μ_{max}. The general description for the cell-specific growth rate is expressed in equation M2 as the product of the specific uptake rate for a substrate ($q_{S/X}$(t)) and the yield of biomass that gets produced by metabolizing the substrate ($y_{X/S}$ (t)).

$$q_{x/x}(t) = y_{x/s}(t)\cdot q_{s/x}(t) \qquad \text{(M2)}$$

$y_{x/s}$ (t)= rate of substrate-specific cell-mass yield [g g^{-1}]
$q_{s/x}$ (t)= cell-specific substrate uptake rate [h^{-1}]

For unlimited growth $y_{x/s}$ and $q_{s/x}$ are expected to be maximal and thereby invariant, with $q_{s/x}$ (t) expressed as $q_{s/xmax.}$ After this unlimited phase, the growth rate becomes limited by decreasing availability of the corresponding substrate. To include substrate limitation to the model, a monod-kinetic, conforming to general Michaelis-Menten kinetics, is integrated into the model according to equation M3.

$$q_{s/x}(t) = q_{s/xmax}\cdot\frac{c_s\,(t)}{k_s\ + c_s(t)}\,(t) \qquad \text{(M3)}$$

c_s (t)= substrate concentration [g l^{-1}]
k_s= monod limitation constant

Exemplary plots for an ideal and a general microbiological growth curve in a batch process according to above equations are depicted in **fig S1 A-B**.

8.2.2 Biomass depletion model for perfusion-based decellularization

In order for a simplified depletion model for perfusion-based decellularization in analogy to microbiological growth, the biomass discharge was considered to be inversely derived from equation M1, as described in equation M4.

$$-\frac{dm_{tc}}{dt}(t) = m_{tc\,0} \cdot q_{d/x}\,(t) \qquad \text{(M4)}$$

m_{tc} = *cell-mass of the tissue [g]*
$q_{d/t}$ = *debris formation rate [h^{-1}]*
t = variable for process-time [h]

In M4, the cell specific growth rate was replaced by the debris formation rate. In close analogy to the general description for the cell-specific growth rate, as expressed in equation M2, the debris formation rate was assumed to be in direct dependency of a tissue-specific uptake rate and debris yield, as described in M5.

$$q_{d/t}(t) = y_{d/s} \cdot q_{a/t}\,(t) \qquad \text{(M5)}$$

$y_{d/t}$ = *tissue-specific debris yield [/]*
$q_{a/t}$ = *tissue-specific uptake rate for decellularization agents [h^{-1}]*

In M5, $q_{a/t}$ describes the accessibility of the specific tissue for the applied decellularization agent, e.g. ionic or an-ionic detergents. We consider $q_{a/t}$ to be highly variant, as the content of the instantaneous decomposed cellular biomass is expected to vary very clearly between e.g. cell membrane components, soluble cytoplasmatic macromolecules, fibrous components and others, while $y_{d/t}$ has to be invariant according to the conservation of mass between discharging biomass and accumulated debris. However, $q_{a/t}$ will reach a maximal value under unlimited conditions. In analogy to equation M3, a monod-kinetic is implemented into the equation to account for substrate-limitation, as shown in M6.

$$q_{a/t}(t) = q_{a/tmax} \cdot \frac{m_{tc}\,(t)}{k_{tc} + m_{tc}(t)}\,(t) \qquad \text{(M6)}$$

k_{tc}= *monod limitation constant for cellular tissue mass*

Exemplary plots for the biomass-discharge model in a batch process with little impact of substrate limitation as well as for an increased substrate according to above equations are depicted in **fig. S1 C-D**.

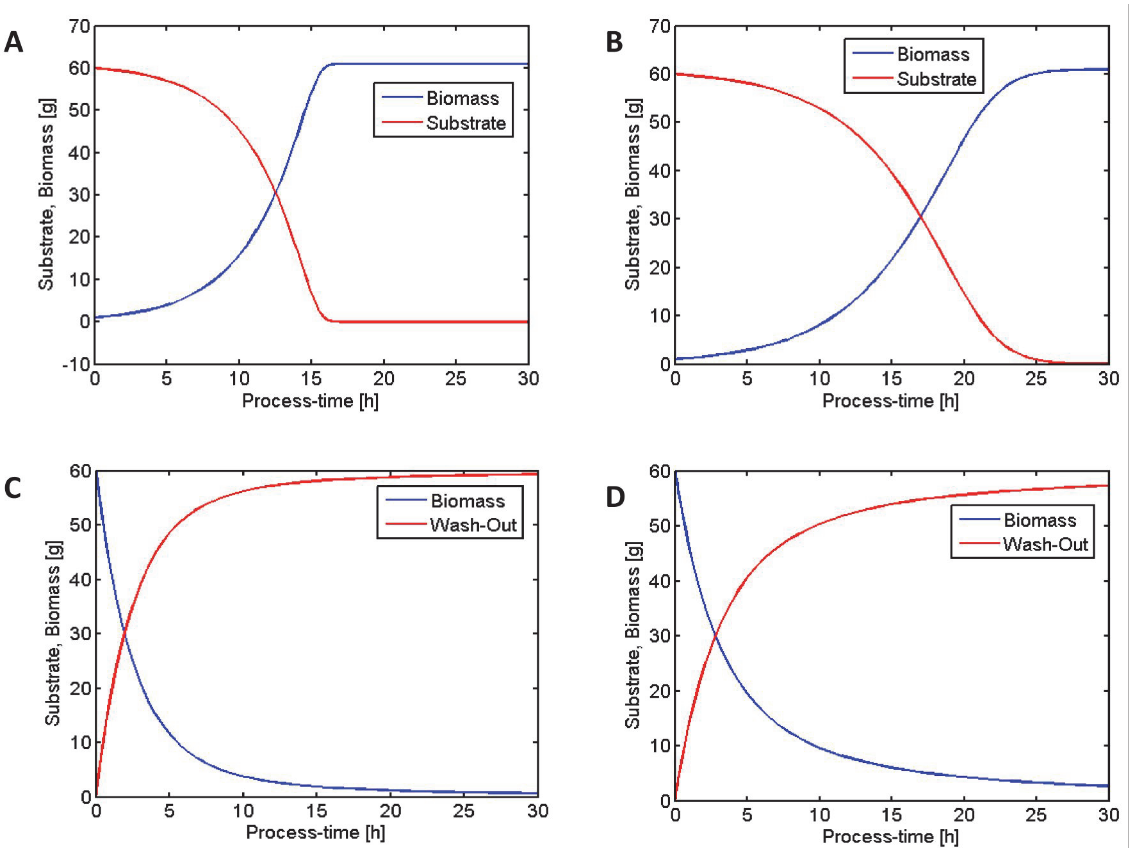

Fig. S1: A biomass depletion model for perfusion-based decellularization – Microbiological Growth Curve vs. Biomass Discharge in a Batch Process. Exemplary plots for microbiological growth and biomass discharge, with $y_{X/S} = 1$ and $y_{d/t} = 1$ and substrate and biomass pf 60 g, respectively. **A)** Plot of an ideal microbiological growth curve in a batch process. **B)** Plot of a general microbiological growth curve in a batch process impacted by substrate limitation according to the monod model. **C)** Plot of the biomass-discharge model in a batch process with little impact of substrate limitation ($k_{TC} = 5$). **D)** Plot of the biomass-discharge model in a batch process for an increased substrate limitation ($k_{TC} = 15$).

8.3 Parameter estimation

In order to match experimental data with the introduced model for biomass depletion for perfusion-based decellularization, according to above equations (M4 – M6), a numerical script was employed matching the corresponding protein discharge functions to the simulated model-based course of protein discharge. This was based on minimizing the sum of quality-functional J(x), comparing each datapoint of the normed instantaneous cumulative discharged protein with the corresponding value of the simulated function. Thereby, following parameters could be estimated for each individual heart: "*tissue-specific uptake rate for decellularization agents* $q_{a/t\ max}$" as well as *"monod limitation constant* k_{tc}". Variations from ideal discharge dynamics by limitations, which can be credited to low $q_{a/t\ max}$ indicate a sub-optimal accessibility by low perfusion quality. If k_{tc} vanishes simultaneously, this may indicate a drastic deceleration of mass transport kinetics, so that the effect of decreasing substrate or biomass gets negligible. Exemplary plots of those estimations, - by inverting protein-accumulation to biomass discharge by $-y_{d/t} = 1$ - contrasting the simulated protein discharge vs. respective experimentally measured data are illustrated in **fig. S2**.

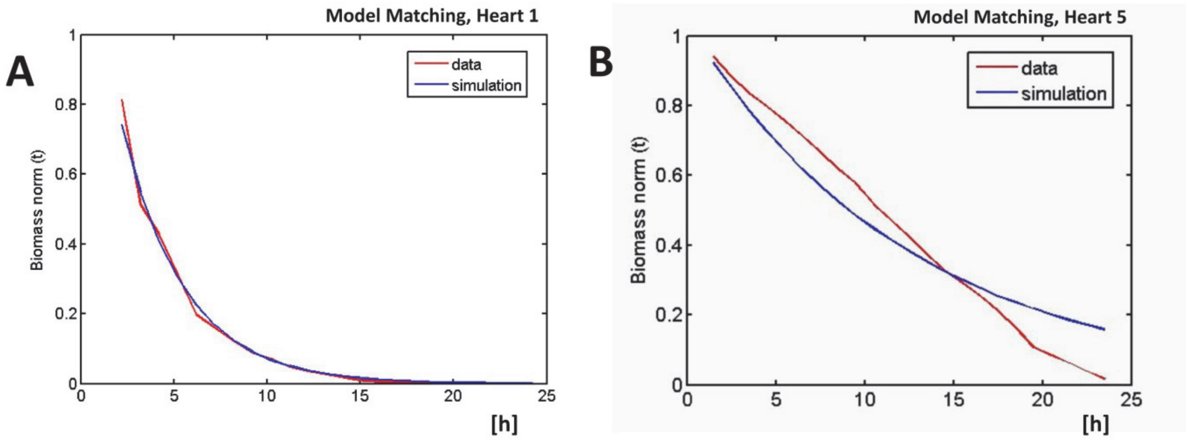

Fig. S2: Model matching and parameter estimation for the detected biomass discharge. **A)** Exemplary pattern of one in toto decellularized ovine heart (heart 1) with congruent matching to the model. **B**) Exemplary pattern of one in toto decellularized ovine heart (heart 5) with a clear mismatch to the model by an almost linear and very slow discharge course, apparently lacking any substrate limitation but revealing a clearly decreased discharge rate.

8.4 Virtual comprehensive biomass decomposition

In order to complement the protein-based discharge dynamics for organs of different biomass, experimentally measured solid biomass before and after decellularization was used to further determine biomass discharge dynamics. Therefore, mean DBM values at different time points of the decellularization process were plotted against the duration of the decellularization process. Hereby, the minimal total biomass-discharge rate of the decellularization process can be deduced from the slope of the plotted curve. A simple comprehensive regression can be employed *via* temporal parallel transition of the associated value-pairs of native and decellularized DBM for ovine and rodent hearts as well as for minced ovine left ventricular myocardial tissue samples. Employed regression enables a direct assessment of the general decellularization dynamics for individual pairs, as demonstrated in **fig. S3**.

The temporal transition of the associated pairs of DBM before and after decellularization of ovine and rodent hearts, as well as standardized minced ovine left ventricular tissue samples plotted on a logarithmic scale, reveal a linear alignment of the slopes over the whole range of biomass. Thereby, a simple exponential regression could be performed leading to a coefficient of determination (R^2) of 0.992 (**Fig. S3A**). Displayed on a linear scale, the exponential regression line for biomass discharge fits all respective values of each DBM pair, thus illustrating virtual comprehensive biomass decomposition, without variations despite differing biomass ranges (**Fig. S3B**). The exponential regression can be expressed as a function (DBM(t)) with a discharge rate (q_x) of approx 0.1 h^{-1} per initial DBM of 44.6 g (eS3).

$$DBM(t) = DBMe^{-q_x t} \tag{eS3}$$

x = designator for particular hearts, organs
t = variable for perfusion-time [h]

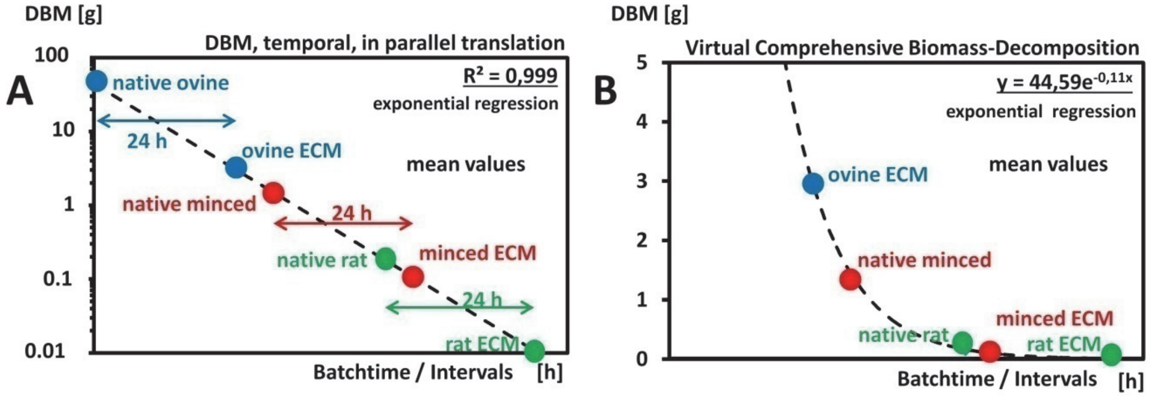

Fig. S3: Biomass-comparative discharge dynamics & kinetics. A) Dry biomass (DBM) of ovine (blue) and rodent (green) hearts as well as standardized ovine myocardial tissue samples (red) before and after decellularization in temporal intervals according to the duration of the decellularization process, logistic scale. By temporal parallel transition a simple comprehensive regression could be applied, fitting all datapoints ((R^2) of 0.992). **B**) Dry biomass (DBM) of ovine (blue) and rodent (green) hearts as well as standardized ovine myocardial tissue samples (red) before and after decellularization in temporal intervals according to the duration of the decellularization process, linear scale; showing a virtual comprehensive biomass decomposition course equal for all ranges of biomass represented.

3.2. Process Automation for Decellularization of Whole Hearts

Rheology of perfusates and fluid dynamical effects during whole organ decellularization: A perspective to individualize decellularization protocols for single organs*

Jörn Hülsmann[1], Hug Aubin[1], Shahbaz T Bandesha[1], Alexander Kranz[1], Volker R Stoldt[2], Artur Lichtenberg[1,3] and Payam Akhyari[1]

[1.] Research Group for Experimental Surgery, Department of Cardiovascular Surgery, Medical Faculty, Heinrich Heine University Dusseldorf, Dusseldorf, Germany
[2.] Institute of Hemostasis and Transfusion Medicine and Biological Medical Research Center, Medical Faculty, Heinrich Heine University Dusseldorf, Dusseldorf, Germany

3 Author to whom any correspondence should be addressed

E-mail: Joern.Huelsmann@med.uni-duesseldorf.de, Hug.Aubin@med.uni-duesseldorf.de, Shahbaztareq.Bandesha@med.uni-duesseldorf.de,Alexander.Kranz@med.uni-duesseldorf.de,Volker.Stoldt@uni-duesseldorf.de,Artur.Lichtenberg@med.uni-duesseldorf.de andPayam.Akhyari@med.uni-duesseldorf.de

Keywords: Rheology, decellularization, viscosity, shear stress, individualization
Supplementary material for this article is available online

Abstract

The approach of whole organ decellularization is rapidly becoming more widespread within the tissue engineering community. Today it is well known that the effects of decellularization protocols may vary with the particular type of treated tissue. However, there are no methods known to individualize decellularization protocols while automatically ensuring a standard level of quality to minimize adverse effects on the resulting extracellular matrix. Here we follow this idea by introducing two novel components into the current practice. First, a non-invasive method for online monitoring of resulting fluid dynamical characteristics of the coronary system is demonstrated for application during theperfusion decellularization of whole hearts. Second, the observation of the underlying rheological characteristics of the perfusates is employed to detect ongoing progress and maturation of the decellularization process. Measured data were contrasted to the respective release of specific cellular components. We demonstrate rheological measurements to be capable of detecting cellular debris along with a discriminative capture of DNA and protein ratios. We demonstrate that this perfusate biomass is well correlated to the biomass loss in the extracellular matrix produced by decellularization. The appearance of biomass components in the perfusates could specifically reflect the appearance of fluid dynamical characteristics that we monitored during the decellularization process. As rheologicalmeasuring of perfusate samples can be done within minutes, without any time-consuming preparation steps, we predict this to be a promising novel analytic strategy to control decellularization protocols, in time, by the actual conditions of the processed organ.

1. Introduction

During the last 4–5 years, the principle of 'whole organ tissue engineering' has become popular, as previously unmet levels of functionality have become achievable for extracellular matrix (ECM) employed for engi-neered tissues and organs, such as bioartificial liver and lung [1, 2]. So far, the most successful reports in this field have employed decellularized whole organs as an organotypic scaffold to achieve highly functional engineered tissues, as demonstrated in one of the pioneering studies by Ott et al in 2008 [3]. As a matter of consequence, perfusion systems are used as chemical reactors (e.g., for decellularization) and as bioreactors (e.g., during re-population and cultivation) to process whole organs [4, 5]. Furthermore, decellularization techniques have earned an increasing level of attention in parallel with their technical advancement

[6–8], as it has become evident that they may be well-adapted to applications on different tissue types and organs [9].

More importantly, the use of different principles of decellularization offers the unique possibility of systematic manipulation with regards to major characteristics of the resulting ECM scaffold [10, 11]. However, up to now, there are no methods known for the individualization of currently applied protocols in order to tailor them according to the specific demands of single organs. This would be of great importance to minimize adverse effects of a given protocol and the included reagents on the ECM, e.g., degradation or extensive loss of ECM components. Therefore, an ade-quate process-accompanying monitoring of the trea-ted organ would represent a desirable basic prerequisite for an ideal decellularization process. Moreover, it appears useful to acknowledge the bio-processing character of organ decellularization. Fol-lowing this theoretical consideration, the procedure of tissue decellularization is defined by the decomposi-tion rate of cellular biomass that has to be transported out of the depth of the organ by diffusion into and out of the vascular system. This cellular biomass consists mainly of (a) proteins, (b) lipids, (c) carbohydrates, and (d) nuclear acids in differing amounts and propor-tions. While in solution, each component exhibits dif-ferent physical characteristics with a more or less strong impact on the flow characteristics of the perfu-sate within the organs vasculature, which is mirrored by the rheological characteristics of the decellulariza-tion solution or perfusate. Hence, observing these changes in the physical characteristics of the perfusate and the resulting fluid dynamical impacts while per-fusing the capillary system may provide novel insights into the biomass decomposition, corresponding to the maturation of the process of decellularization of whole organs.

Though physical effects of cellular biomolecules have been investigated in the past, changes in the rheological characteristics and resulting effects to fluid dynamical characteristics never gained much interest in the literature. This may be partly due to the sparseness of events with a strong release of cellular biomole-cules common to the situation of whole organ decellularization by perfusion. Here, we aim to identify these effects to fluid dynamical characteristics that occur during the course of whole organ decellularization. As a first step, we have focused on the DNA and protein components of the biomass. The chromoso-mal DNA is a large molecule, which we suspect to have an observable fluid dynamical impact even in the marginal concentrations present during common decellularization processes. This may be expected particularly for released DNA in the presence of detergents that may further disturb the integrity of DNA-histone architecture. On the other hand, pro-teins may gain a fluid dynamical impact caused by their relatively high cellular concentration.

In the presented work, we introduce a specific method for the rheological evaluation of the perfusate as a very fast and sensitive analytical method that can be performed as a repetitive and non-destructive pro-cedure accompanying the ongoing decellularization. The resulting data demonstrate the value of this method for a refinement of decellularization proce-dures and suggest its implementation into future stu-dies, particularly into perfusion-based whole organ decellularization methods.

2. Materials and methods

2.1. Perfusion decellularization

Donor hearts (n= 10) of male Wistar rats weighing 220 to 270 grams were decellularized using a simplified detergent-based protocol that has been previously described and extensively characterized [4]. In brief, a software-governed closed-loop perfusion circuit with a regulated perfusion pressure of 70 mmHg was used to subject the hearts to a coronary perfusion-based decellularization. Perfusion pressures, pump speed values, pH, and temperature were monitored online and stored by the software. Hearts were mounted in a 250 ml flask and bathed therein in a solution-reservoir of 250 ml volume. From here, the perfusion circuit is fed by the upper level of the flask and the perfusate flows back into the reservoir directly by draining fromthe bathed heart.

Six hearts were used for rheological testing and the evaluation of biomass decomposition in whole single perfusates of each step according to figure 1. Therefore, the perfusate solutions were sampled in a discrete pattern throughout the decellularization procedure by taking a sample of the perfusate in 12 h intervals at the end of every perfusion step of the protocol, according to figure 1. Nomenclature of the samples is introduced in figure 1. Out of these, three hearts were used for quantitative analysis of DNA content and other three hearts were subjected to histological evaluation. For another four hearts, the perfusate batches of the first step of the protocol were sampled to determine a temporal resolution of the perfusates' changes in viscosity and protein content during the decellularization process. Six more hearts were decellularized according to figure1aswell, but differed by a clearly shortened period of detergent perfusion of 12 h versus the original 48 h. Out of these, three hearts were used for quantitative analysis of DNA content, while the other three hearts were subjected to histological evaluation.

2.2. Model decellularization of different organs (heart, lung, liver, kidney)

To investigate tissue-specific characteristics of decellularization debris, we decellularized tissue samples of ovine heart, lung, liver, and kidney. To maximize unlimited conditions for the tissue decomposition, we used 50 grams each of finely minced tissue in 250 ml

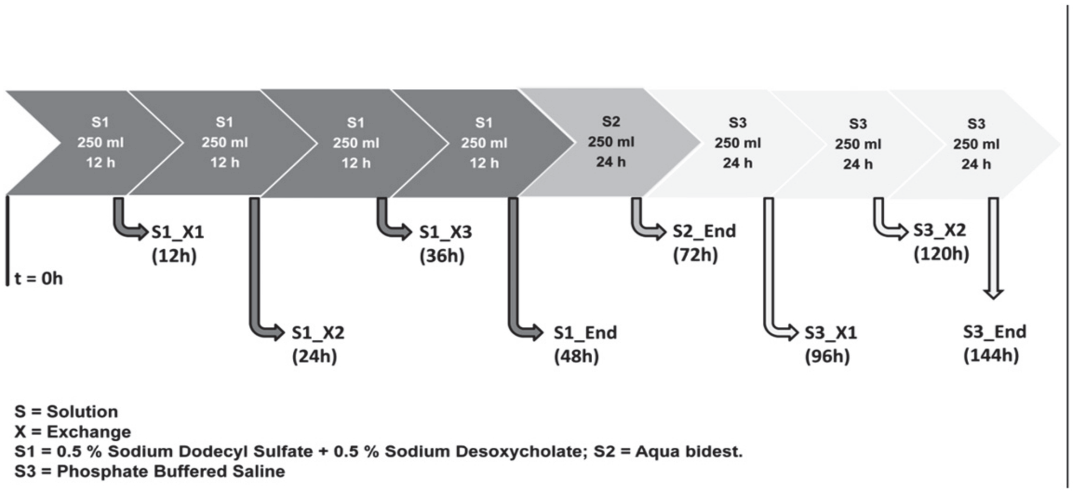

Figure 1. Flow chart of the decellularization protocol and sampling operation timetable. Single arrowheads symbolize single batch-wise perfusion intervals. The durations of each interval and the respective perfusion solution are denoted. The lower arrows symbolize the time point of sample withdrawal of the perfusate at the end of each single interval. The glossary of the samples is indicated by the order of the used solutions and the number of exchanges done. S, solution; X, exchange; SDS/DCA, detergent-based solution containing SDS and sodium desoxycholate (DCA); aqua bidest; double-distilled water; phosphate buffered saline (PBS)

detergent solution S1 that was used for the perfusion decellularization of the hearts as well. These preparations were shaken in square-formed 250 ml flasks. The decellularization solution was collected and exchanged after 12 and 24 h. Samples of these solu-tions were subjected to measurement of dry biomass and rheological measurement after being matched to samples containing equal amounts of biomass.

2.3. Measurement of dry biomass

To measure the average dry biomass of native and decellularized hearts, whole hearts (n= 4) were decellularized according to steps given in section 2.1 and transferred to micro test tubes of 2 ml volume. Decellularized and native hearts were dried in a drying chamber at 75 °C for three days. Subsequently, the weight of the dry biomass was measured.

The dry biomass of decellularization perfusates was measured by drying 2 ml of the perfusate exactly the same way. These samples were additionally blanked versus the dry mass of 2 ml of the according decellularization solution.

2.4. Protein quantification

The total protein content of the perfusate samples was determined using the Bio-Rad™ detergent compatible protein assay (Bio-Rad Laboratories, Munich, Germany) according to the manufacturer's manual, using bovine serum albumin (BSA) as standard protein dissolved in each solution of the protocol.

Additionally, for further validation of the methodology, we performed a complementary sodium dodecyl sulfate (SDS) PAGE of the perfusate samples using a 12% polyacrylamide gel according to the Laemmli method [12]. In brief, samples were diluted1:1 with the two-fold concentrated Laemmli buffer. In the case of the perfusate solutions, no further protein extraction was needed, as these already contained solubilized proteins.

For quantitative detection, we used the sensitive Bio-Rad Flamingo® Fluorescent Gel stain (Bio-Rad Laboratories) according to the manufacturer's man-ual. Gel documentation was performed using a UVP Epi chemi II Darkroom with UV transillumination and a UVP PCO CCD camera in combination with the LabWorks software (UVP Laboratory, Upland, CA, USA) for visualization and densitometric analysis of the bands.

2.5. DNA quantification

For quantitative determination of the DNA content of the perfusate samples, ethidium bromide (0.2 $\mu g\ ml^{-1}$) was directly added to the solution and fluores-cence was measured at its 620 nm peak with an excitation at 540 nm using a SynergyHT fluorescence plate reader (Biotek Instruments, Bad Friedrichshall, Germany). We used standards prepared of herring sperm DNA (Promega, Madison, USA) in a range from 0.2 to 10 $\mu g\ ml^{-1}$ dissolved in pure water.

The DNA content of native (n= 3) and decel-lularized rat hearts (n= 3 for the regular and the shor-tened protocol) was investigated by the application of the com-mercially available DNeasy Mini Kit® by Quiagen (Hilden, Germany) according to the manual for tissue samples.

2.6. Setting up myocardial debris standard

To set up a biomass standard of equal biomolecular composition like the decellularization debris of whole hearts, we precipitated and re-dissolved myocardialdebris, which was produced as described in section 2.2. Whole debris was precipitated by adding 0.1 M sodium acetate and the two-fold volume of cold ethanol and was centrifuged at 4000 rpm in 50 ml Falcons. Pellets were washed two times with 70% ethanol and re-dissolved in the detergent-based decel-lularization solution 1 (0.5% SDS + 0.5% sodium desoxycholate). The content of dry biomass was measured as described in section 2.3.

2.7. Rheological evaluation

Rheological evaluation of the perfusate samples was performed using a HAAKE MARS rheometer (Thermo Scientific, Karlsruhe, Germany) with a cone60 mm in diameter and an angle of 1° in combination with the manufacturer's RheoWin software. We chose to observe the viscosity (η) and the shearing stress (τ) in double logarithmic flow curves with a shear rate (g) range of 0 to 1000 rounds per second. Therefore, the shear rate initially increased, rested for 5 s at the maximum speed, and then decreased the reverse way to zero. By this wide shearing range, the potentially characteristic rheological patterns that are specific for several biomolecules should be exposed, and those should also bear the real shearing conditions of the coronary flow during perfusion decellularization in one single dialogue. Perfusates were sampled as described in section 2.1and figure 1.

Standard solutions of DNA and protein were used to obtain references for each perfusate solution of the protocol. In the case of DNA, standards of herring sperm DNA in a range from 0.2 to 10 μg ml^{-1} were employed (see section 2.5). For the standard protein solution, we used solutions of 1 to 50 mg ml^{-1} BSA dissolved in decellularization solution 1 (0.5% SDS + 0.5% sodium desoxycholate; see section 2.4) and water, respectively. An additional 0.3 μg ml^{-1} of pre-fragmented DNA (approximately 2000 bp frag-ments) was added to a standard solution of 10 mg ml^{-1} BSA dissolved in water to observe a potential summation of characteristics and their distinctness. In order to observe the sensitivity for myocardial debris, standards as described in Section 2.6were measured in range from 0.3 and 10 mg ml^{-1} dry biomass (DBM). Potential tissue specificity of the rheological flow curves were evaluated by measuring the perfusates described in section 2.2that were set to a content of 20 mg ml^{-1} DBM. Furthermore, valvular interstitial cells were dispersed in the decellularization solution 1, allowed to lyse by incubation for 30 min, and were subjected to rheological evaluation in a serial dilution.

2.8. Histology

Whole decellularized hearts were fixed in 4% neutral buffered paraformaldehyde for 2 h and subsequently cry-embedded in KP-CryoCompound– Klinipath (Duiven, Netherlands) and sections of 4.5μmthickness were used for histological evaluation.

Hematoxylin and eosin staining (H&E) was used for evaluation of microscopic tissue morphology and the absence of cellular remnants.

2.9. Statistical analysis

Values are expressed as mean ± standard deviation. To determine significant differences in quantitative analytics of the perfusates (DNA and protein content), we applied a multicomparison analysis of variance (ANOVA). To determine the significance in thedifference between the evaluated dry mass of native and decellularized hearts, we applied an unpaired two-tailed t-test. Differences were considered as statistically significant for $p < 0.05$.

2.10. Ethics statement

Donor heart explantation was carried out according to §6 and §8 of the German animal welfare act of North-Rhine-Westphalia (TierSchG) and authorized by the LANUV (Landesamt für Natur, Umwelt und Verbraucherschutz NRW; the German state office for nature, environment, and consumer protection of North-Rhine-Westphalia).

3. Results

3.1. Pressure profile during perfusion decellularization

For perfusion decellularization processes using feedback control for the perfusion pressure, we observed perfusion-pressure profiles that appear to be characteristic for each decellularization step (figure 2). For the detergent-based step (SDS/desoxycholic acid (DCA)), a broad-based peak of the revolution speed ofthe pump (RS-P) was observed while the perfusion pressure crept towards the set point. At the declining side of the peak, it exhibited a highly negative slope of the RS-P while keeping the perfusion pressure constant. This pattern endured for a period of about 10 h, which may indicate an increasing viscosity of the perfusate by disposal of debris. After the perfusion solution of this step (S1, SDS/DCA) was exchanged for the first time, and the trend of the RS-P inverted. There was a continuous increase of the RS-P during all following exchanges of the first perfusion solution (S1, SDS/DCA) while the perfusion pressure remained constant. Switching the perfusion solution to the second solution (S2, aqua bidest) resulted in a rapid increase of the actuating RS-P, which howeverdecreased in the following over time. In the following step of the protocol, the third solution (S3, PBS) was applied. As a consequence, the RS-P actuated con-tinuously by increasing until it reached the maximum adjustment, where it rested until the decellularization process was finished.

3.2. Dry biomass

We evaluated a drastic loss of mass of the hearts after decellularization (figure 3(a)). This is visualized by a

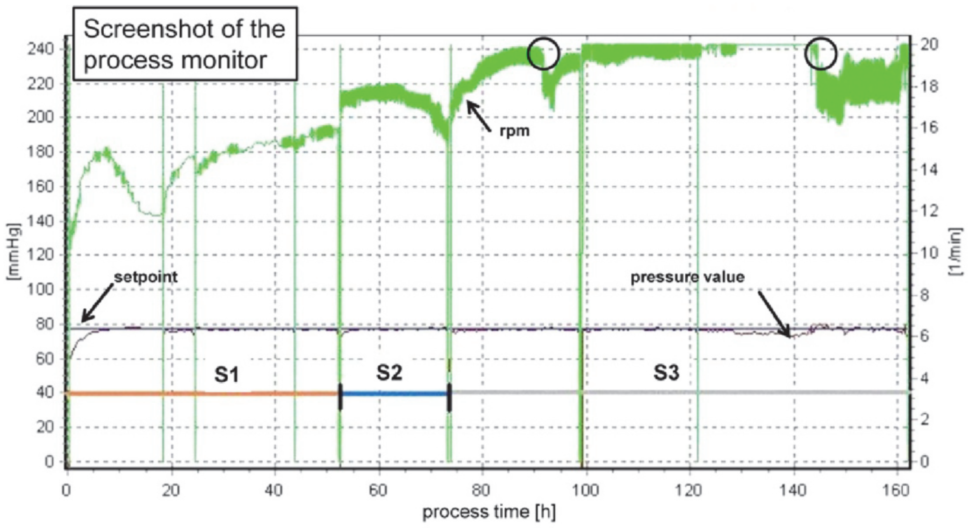

Figure 2. Exemplary course of perfusion pressure and the actuating RS-P. The courses of the value of perfusion pressure (expressed in mmHg, purple line) and the actuating RS-P (rounds per minute, green line) as well as the fix setpoint for the perfusion pressure (black line) are marked with black arrows. The single steps of the protocol are indicated by the bars and the denotation of the used solutions (S1, solution 1; S2, solution 2; S3, solution 3). The feedback control system keeps the perfusion pressure in the range of the setpointwith a very good quality of control (80 mmHg). The black circles mark the events and time points when the pumps occlusion and the regulator parameters were adjusted because the actuating variable reached its maximum range.

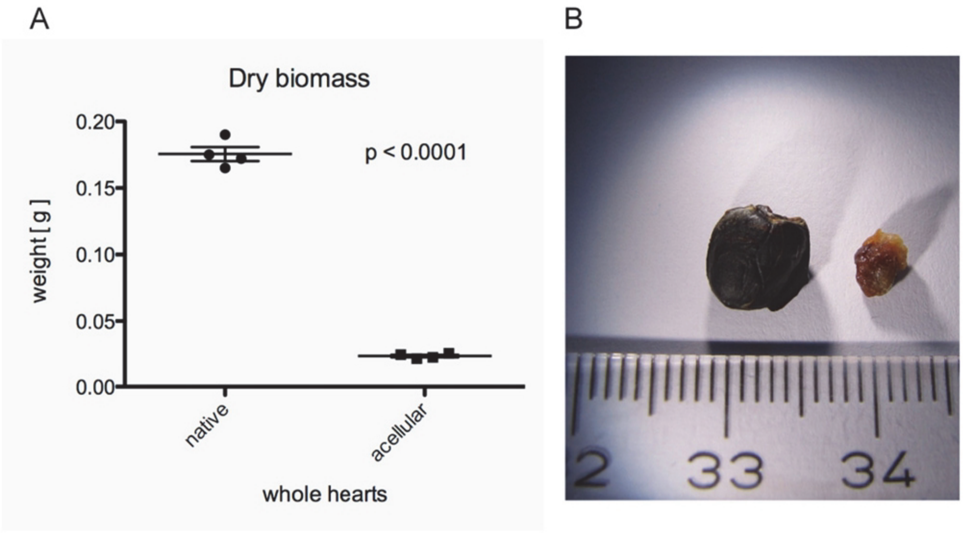

Figure 3. Dry biomass of native versus acellular rat hearts. (a) Mass of the weighted dried native and acellular hearts ($n = 4$ for each group), $p < 0.0001$. (b) Representative images of dried native and decellularized hearts demonstrate the remarkable reduction in the volume of the remaining dried ECM in contrast to the whole native heart.

substantial shrinking of the dried decellularized heart, as depicted in figure 3(b). The wet weight of the hearts was approximately 1 g (data not shown). Our data show that native hearts of rats of comparable body weight (250–270 g) had a dry weight of about 176 ± 10.5 mg, which was reduced to an average of 23 ± 1.9 mg after complete decellularization ($p < 0.0001$). Accordingly, the remaining ECM repre-sents about 16% of the whole dry biomass of the native heart. The average discharged biomass is found to be in the range of about 150 mg per heart for the examined six hearts.

3.3. Amount of total protein

Quantitative analysis demonstrated that only in the perfusate of the very first step of the decellularization measurable total protein content was detectable. Interestingly, we observed an average amount of about 150 mg total protein in the perfusate of the first six hearts (figure 4), which directly correlates to the total loss of biomass after complete decellularization (see section 2.4). Additional high sensitive fluorescent staining of the separated protein bands by means of SDS PAGE showed that protein bands could be detected mainly in the perfusate of the first perfusion

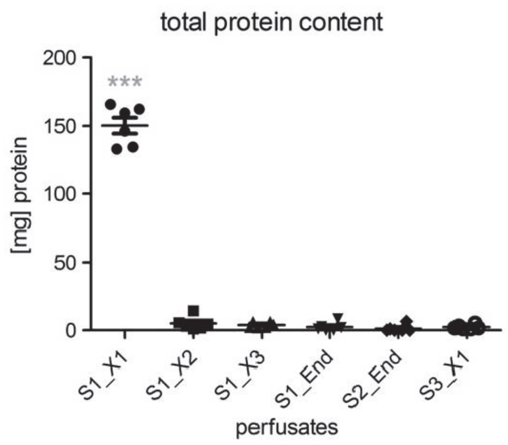

Figure 4. Chart of the total protein amount in the perfusates. Samples of perfusates were obtained at the end of every perfusion interval (while exchanging the perfusion solution) during the decellularization of whole hearts (n= 6). Abbreviations and sampling operation timetable are according to figure1.Significant protein content was only detected in theperfusates of the first and the second perfusion interval of the first step (SDS/DCA). The underlying measured data of allfollowing samples are close to zero, according to the applied methods. ***$p< 0.001$ for perfusate S1_X1 versus all other perfusates.

interval of the first step. Figure 5(a) depicts results of this analysis, where bands of different intensity could be separated in the range of 15 to 250 kDa. Bands at the lower end of the separation range could also be detected, indicating the presence of peptides with a molecular weight of less than 15 kDa as well. Furthermore, the absence of detectable protein bands in all following perfusion intervals and processing steps is demonstrated by a surface plot of the density of the band intensities. The applied methodology of staining and documentation results in a detection sensitivity of less than 0.25 ng protein per band, as indicated by the manufacturer's manual.

We further analyzed the temporal resolution of the protein decomposition during the progress of decellularization. Figure 5(b) shows the temporal resolution for perfusates in the first step of the pro-tocol for four sample hearts at different time points. The dynamic protein decomposition demonstrates an exponential character during the first 5 h. After 12 h at the end of the first perfusion step, total the amount of the washed-out proteins correlates with the above-mentioned decrease in dry biomass. We compared protein wash-out efficacy of the first 5 h to the total protein content in the perfusates after 12 h. The respective results indicate that protein decomposition shows a declining character, while the total amount of washed-out proteins approx-imates a saturation level after 12 h at the end of the first perfusion step. This course is also reflected bythe development of the hearts optical transparency, that can be observed macroscopically at figure 6

3.4. DNA quantification

As depicted in figure 6, fluorescence intensity measurement calibrated by chromosomal DNA standards revealed small amounts of DNA in the range of 0.2 μg ml^{-1} in the first perfusion interval of the first step. In contrast, relatively high amounts of DNA in the range of about 0.9 μg ml^{-1} were detected in the steps involving a perfusion with aqua bidest. When the average additive DNA discharge was calculated, the total amount of DNA eliminated by the applied protocol reached up to 340 μg (table 1), whereas on average, a DNA discharge of 298 ± 34.6 μg per heart was achieved in the perfusion step with water.

The total content of DNA of native rat hearts, shown in figure 7(a), was determined to be 685 ± 80 μg on average per heart, while the average total DNA content of all perfusates was determined to be approximately 325 ± 23 μg. Hearts that were decellularized by the regular protocol, as depicted in figure1,showed a remaining DNA content of12 ± 2.8 μg in contrast to 20.6 ± 5 μg DNA for hearts that were subjected to the protocol of only 12 h detergent perfusion, as shown in figure 7(b).

3.5. Rheological evaluation

The flow curves of the pure solutions S1, S2, and S3 shown in figure 8(a) demonstrate almost congruent reversible characteristics that start with a short range of quasi-dilatant behavior at very low shear rates before they turn over to its typical pattern of a Newtonian fluid. The areas I, II, and III that are marked by dashed lines define the regions of low (I), medium (II), and high shear stress (III) at which the viscosity positively differs from solutions without any containing biomolecular structures.

The DNA standards shown in figure 8(b) start at quite high viscosities of 10 mPas for the 1 μg ml^{-1} standard and 6 mPas for the 10 μg ml^{-1} standard. In region I, both standards present a shear thinning char-acter but the ten-fold lower concentrated standard holds this character in region II too, while the higher standard already turned over to a Newtonian character in congruence with the water control. In region II, both standards show a Newtonian character in con-gruence with the water control and holds it reversibly while running the shear rate back down to zero.

The protein standards that were dissolved in water shown in figure 8(c) reveal a general shear thinning character in regions I and II that turns over to a quasi-Newtonian character in region III at slightly increased viscosities compared to the water control. While running the shear rate back down, they show again a shear thinning character in region II; but at decreased viscosities, it turns over to a quasi-Newtonian character in region I. The flow curves are shifted down to lower viscosities by decreasing the protein concentration. The 0.6 mg ml^{-1} standard starts at a relative high viscosity of 14 mPas. Protein standards dissolved in S1

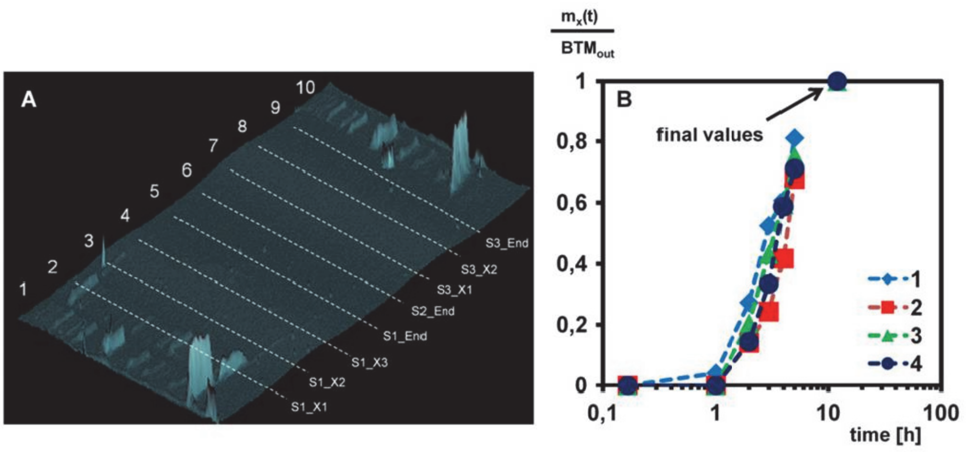

Figure 5. (a) Protein content of the perfusates as determined by SDS PAGE. Protein bands were stained with Bio-Rad™Flamingo pink. Presented is a surface plot of the band intensities. Lines represent the perfusate samples: (1)& 10) Ladder (10–250 kDa); the absence of protein bands in lines 4–9 supports the findings demonstrated in figure 4. (b) Time course of cumulatively discharged total protein m_x(t) in [g] standardized to the absolute discharged protein BTM out in [g]. It can be observed that the discharge of total protein seems to reveal an exponential character that reaches a saturation limited by the total cellular protein content of the hearts. (b) Rheological flow curves while perfusion step one (S1_X1). Series of flow curves of the corresponding samples show that detectable evolution of viscosity may not be observed before 4–5 h of perfusion. Colored points display the starting point of each flow curve.

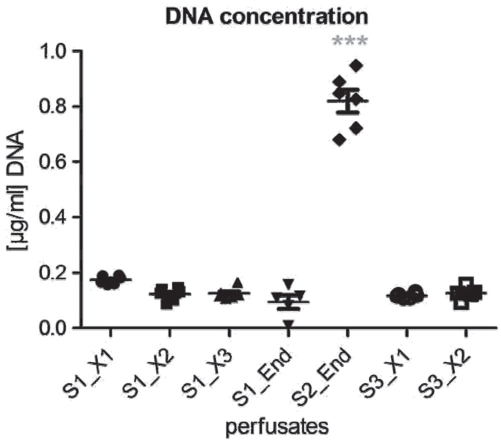

Figure 6. DNA concentration in perfusates derived at different stages of the decellularization. Samples of perfusates were obtained at the end of every perfusion interval during the decellularization of whole hearts (n= 6) and DNA concentration was measured (triplet measurements). DNA was washed out almost solely during perfusion with H_2O (solution 2, S2). Corresponding total DNA amounts arepresented in table 1. Abbreviations and sampling operation timetable are according to figure 1. ***p< 0.001 for S2_End versus other perfusates.

Table 1. Calculated DNA amounts in perfusates. Measured concentrations of DNA are projected to the volume of each perfusate and displayed as total DNA amount. Perfusate S1_X1 values range at the lower border of calibration, whereas all following perfusates of solutions S1 and S3 were below the detection level. However, the largest DNA amount was found in the aqua bidest perfusate (S2_End), where the vast majority of DNA removal took place.Abbreviations and sampling operation timetable are according to figure1.

Total DNA amount [µg]						
n	1	2	3	4	5	6
S1_X1	50.1	57.3	54.6	48.3	56.7	47.4
S1_X2	0	0	0	0	0	0
S1_X3	0	0	0	0	0	0
S1_End	0	0	0	0	0	0
S2_End	248.1	284.7	254.4	216.6	267	204
S3_X1	0	0	0	0	0	0
S3_End	0	0	0	0	0	0
total	298.2	342	309	264.9	323.7	251.4

reveal that shear thinning character in region I only at very high concentrations like 50 mg ml-1as shown in figure8(c). Five-fold reduction of the protein concentration demonstrates a similar Newtonian character of the flow curve only at slightly increased viscosities in comparison to the S1 control. Both standards hold the same Newtonian character while running the shear rate back down. Here the highest standard of 50 mg ml^{-1} shows a maximal viscosity of 4 mPas.

Cell debris of valvular interslital cells (VIC) cells reveals a completely reversible shear thinning character at all regions at equal maximal viscosities at the start and ending points of the flow curves, as shown in figure9(a). Overall, the flow curves are shifted to lowerviscosities by lowering the concentration.

The same pattern can be observed in figure 9(b) for serial dilutions of re-dissolved myocardial debris. Here the flow curves are slightly shifted upwards to higher viscosities while running the shear rate back down.

In figure 9(c), the comparative flow curves of decellularization debris of different organs show all the same shear thinning character in region I, which turn over to a quasi-Newtonian character in regions II and II almost congruent for lung, liver, and kidney, while the flow curve of the heart is clearly shifted upwards to higher viscosities. All flow curves show a quasi-Newtonian pattern while running the shear rate back down. Figure 9(d) shows the flow curves of decel-lularization debris of the same processed tissues as those depicted in figure 9(c) but after another 12 h of

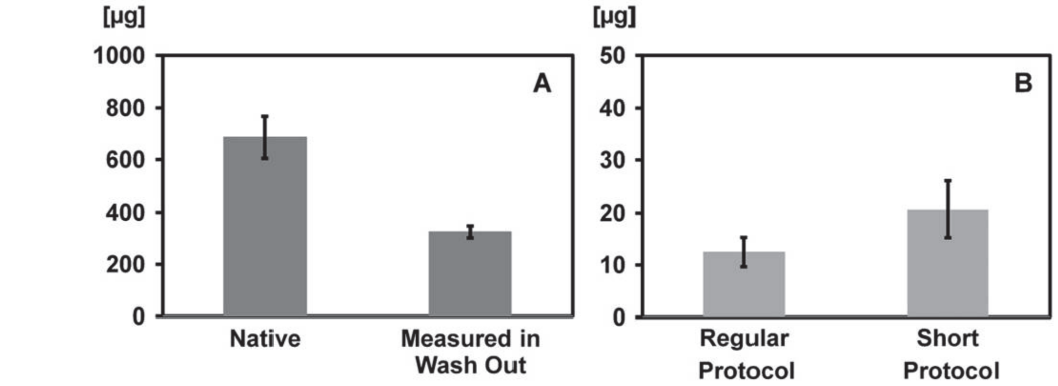

Figure 7. DNA contents in native and decellularized hearts and cumulative measured DNA wash-out. (a) The DNA content of native rat hearts versus the cumulative registered DNA wash-out in decellularization perfusates. There is a clear difference between the expected amount of DNA in the unprocessed organ and the measured DNA wash-out in the perfusates at which both values had to be calculated by different analytical methods. DNA content was measured by absorption at 280 nm for native hearts, while the wash-out was evaluated by ethidium bromide–based fluorescence reading. (b) The DNA content of decellularized hearts. The remaining DNA content of hearts that were decellularized with the regular protocol of 48 h detergent perfusion is contrasted to the content of hearts that were decellularized by the shortened protocol of 12 h detergent perfusion.

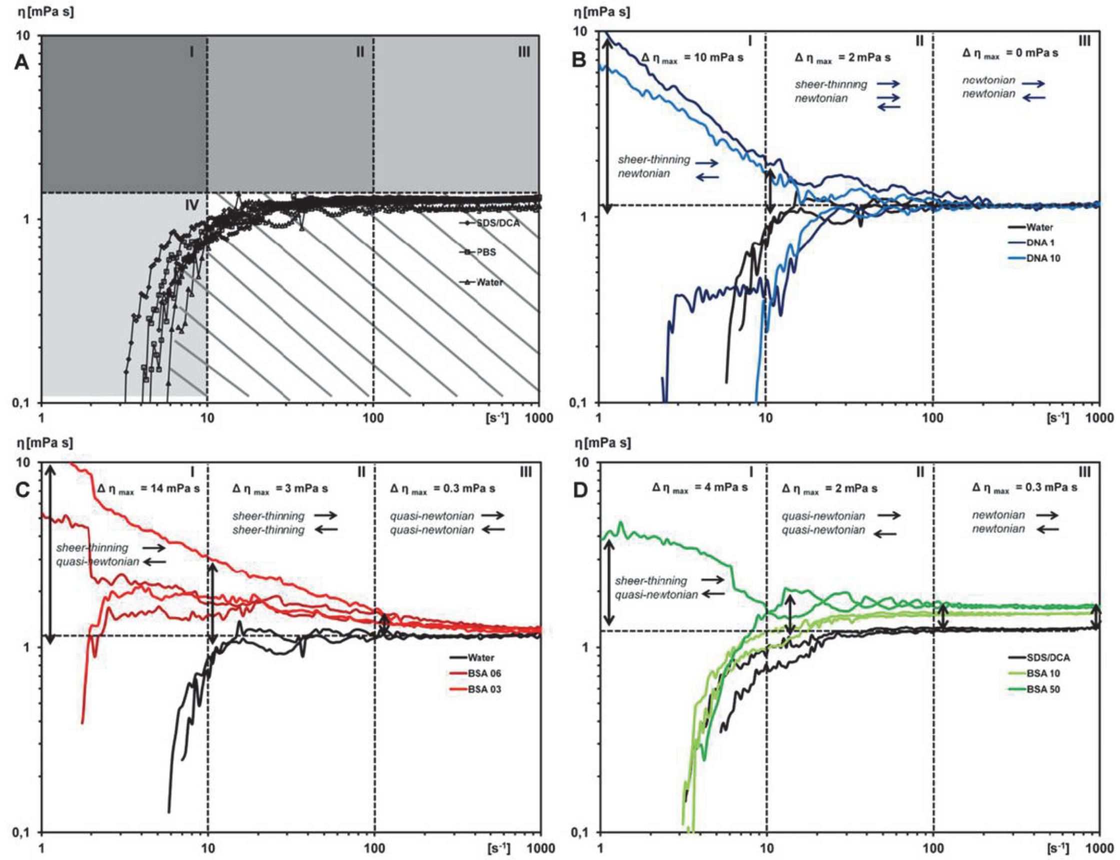

Figure 8. Flow curves of standards and (a) decellularization solutions are depicted as controls. The grey fields highlight the areas where signals should indicate the content of added molecular structures. Regions I, II, and III classify regions of low, medium, and high shear stress. (b) DNA standards dissolved in water. Concentrations are stated in μg ml^{-1}. (c) BSA standards dissolved in water. Concentrations are stated in mg ml^{-1}. (d) BSA standards dissolved in S1. Concentrations are stated in mg ml^{-1}.

processing with fresh S1. In comparison to the patterns in figure 9(c), the flow curve of the heart stays almost the same but it turns into a shear thinning character in region I while running the shear rate back down. The patterns of the flow curves of the liver and the kidney switch to a similar pattern and are shifted up to similar viscosities in region II, while the flow curve of the kidney additionally converts to a clear reversible shear thinning character throughout regions II and III and ends in a similar viscosity at the maximal shear rate, like that depicted in figure 9(c). The pattern of the lungs almost does not get altered

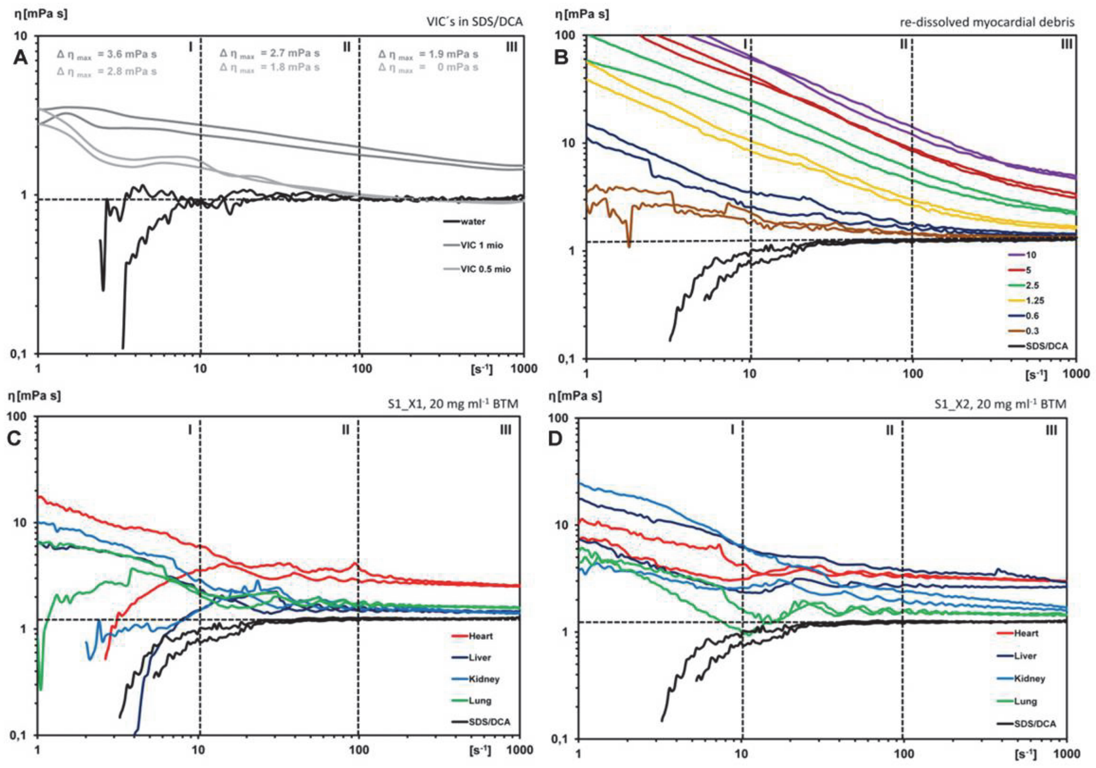

Figure 9. Flow curves of different types of debris. (a) Valvular interstitial cells processed in S1. Concentrations are stated in cells ml^{-1}. (b) re-dissolved myocardial debris. Concentrations are stated in mg ml^{-1}. (c) Decellularization solutions of different organs sampledfrom S1_X1. Concentrations are set to 20 mg ml^{-1}. (d) Decellularization solutions of different organs sampled from S1_X2. Concentrations are set to 20 mg ml^{-1}.

but it turns into a shear thinning character in region I while turning the shear rate back down.The flow curve of a combined standard of 10 mg ml^{-1} BSA in water with 0.3 mg ml^{-1} fragmented DNA is contrasted to its components in figure 10(a). The DNA standard reveals a quasi-Newtonian character over all regions with an increased viscosity in compar-ison to the water control. The combined standard shows a similar pattern to the BSA standard but with a slightly increased viscosity in region III, where it reaches similar viscosities like the DNA standards. In region I, it turns over to a shear thinning character while running the shear rate back down in contrast to both components, which reveals a quasi-Newtonian character.Figure 10(b) shows testing of the temporally higher sampled perfusates of the first decellularization step. The flow curves of the first 5 h of perfusion can only be distinguished from the S1 control in region I by shifting leftwards and with a slight increase of visc-osity. For the 12 h sample, the flow curves show a com-plete shear thinning character over all regions ending in a maximal viscosity of 15 mPas while turning the shear rate back down.

After determining the rheological characteristics of all different standards, we subjected samples of the actual decellularization perfusates to identical testing, shown in figures 10(c) and (d). When the firstperfusate solution was subjected to rheological testing, we observed that the flow curves represent a pattern that equals the reversed pattern of DNA standards combined with the shift to higher viscosities, as observed in protein standards, as shown in figures 8(b) and (c), and the shear thinning character that could be observed for debris in figures 9(a) and (b). The viscos-ity values and pattern while running down the shear rate is similar to the 1 million cell ml-1 VIC standard as shown in figure 9(a) and the myocardial debris as shown in figures 9(c) and (d). The pattern of the water perfusates shown in figure 10(d) exhibits exactly the same pattern as the DNA standards shown in figure8(b), but starting at approximately two-foldhigher viscosities in region I.The sensitivity of the rheological measurement to detect the different tested kinds of biomass in the dif-ferent decellularization solutions is summarized in figure11.Here the concentrations of the lowest testedsamples are contrasted to determined or calculated concentration of analytes that can be expected in the perfusates.

3.6. Histological evaluation

H&E staining of whole heart sections, given in figure13,shows that detergent perfusion for 48 h (a) and (b) left less nucleic acid, as indicated by the blue arrows than there could be detected after 12 h (c) and

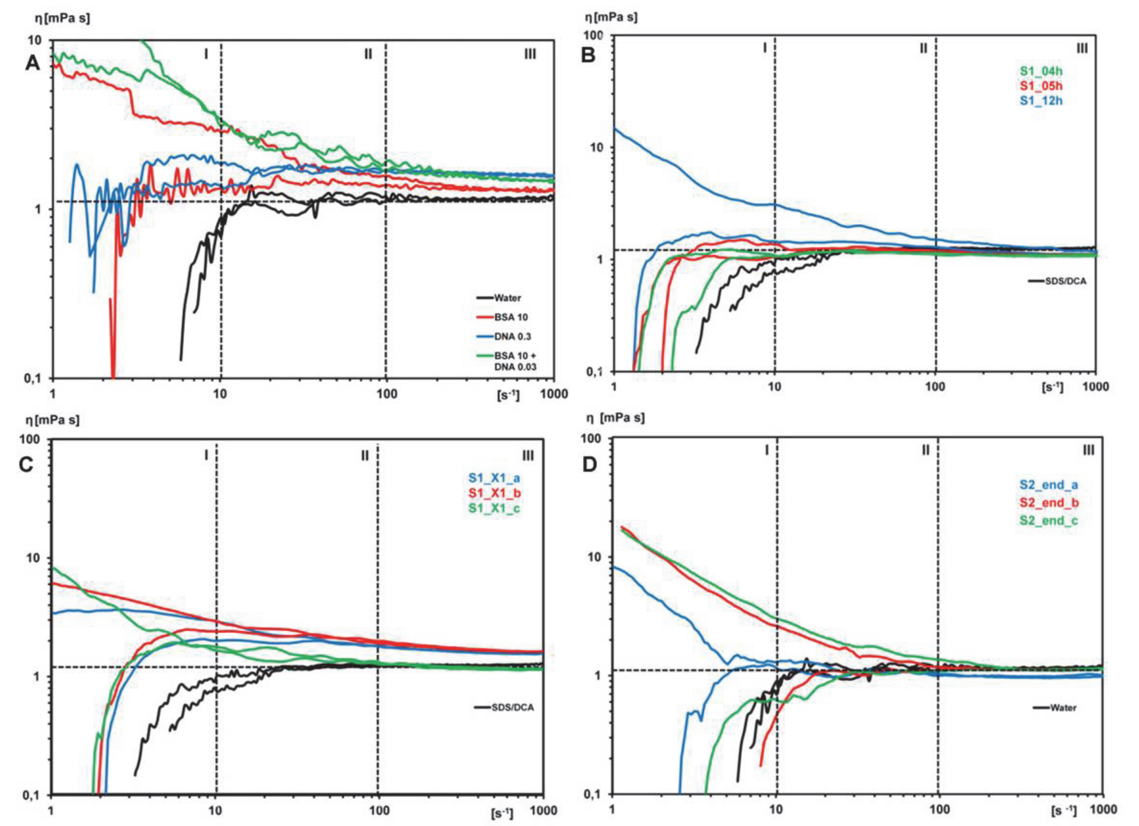

Figure 10. Flow curves of combined standards and decellularization perfusates. (a) Combined DNA and BSA standards dissolved in water. Concentrations are stated in mg ml^{-1}. (b) Perfusate samples from S1_X1 in a time-dependent series of sampling. (c) Perfusate samples from S1_X1 for a series of different hearts. (d) Perfusate samples from S2_End for a series of different hearts.

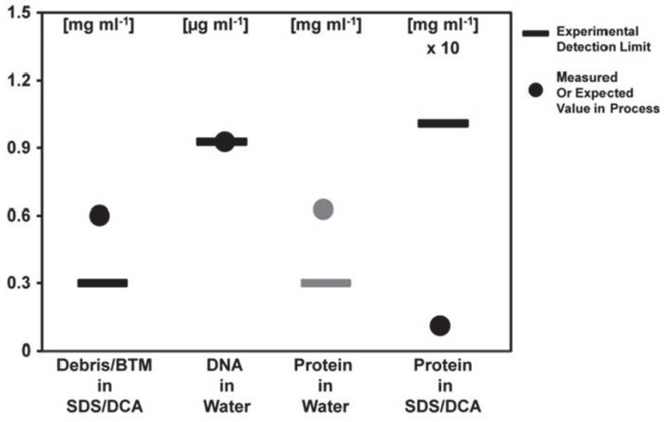

Figure 11. Approximated detection limit of the applied rheological measurements for different biomolecular structures.

(d). In turn, all sections are absent of cellular remnants.The red arrows indicate regions of fine structured microarchitecture that is shown to be clearly decreased after 48 h of detergent perfusion.

4. Discussion

In the present work, we sought to detect the biomass released by decellularization of whole organs in the decellularization perfusates in near real-time as a measure of quality assurance and as a base for novel process-guiding strategies.

Thereby we integrated rheological measurements of decellularization perfu-sates as a low-cost and non-invasive method for online process control. By observing and following the profiles of perfusion pressure and the actuating RS-P of the peristaltic pumps during the process of perfu-sion decellularization, we recovered certain character-istic patterns for different protocols. Based on these considerations, we developed the idea of using these phenomena to characterize, detect, and monitor phases and conditions of the decellularization process,

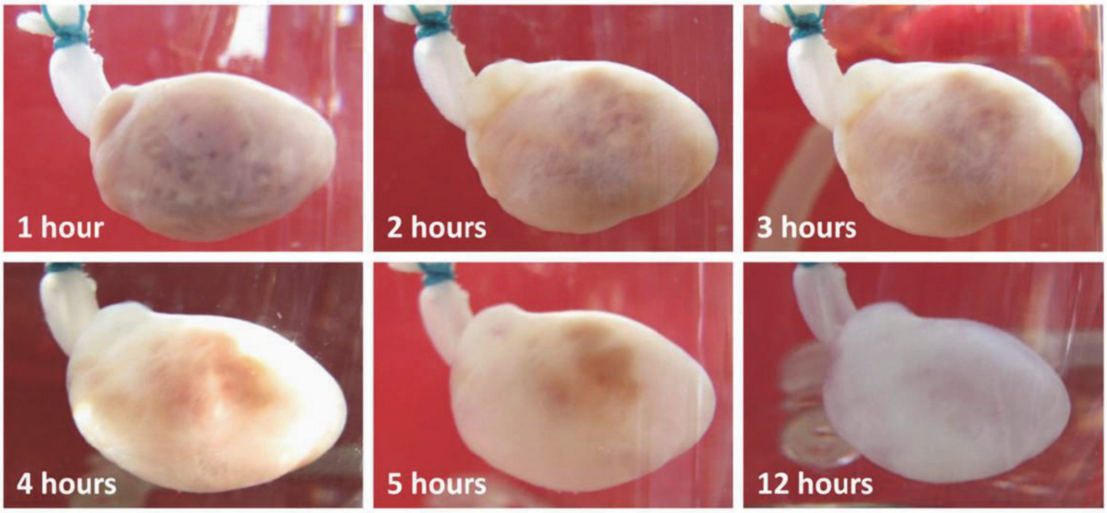

Figure 12. Time-discrete sequence of close-up views of an exemplary perfused rat heart during decellularization.

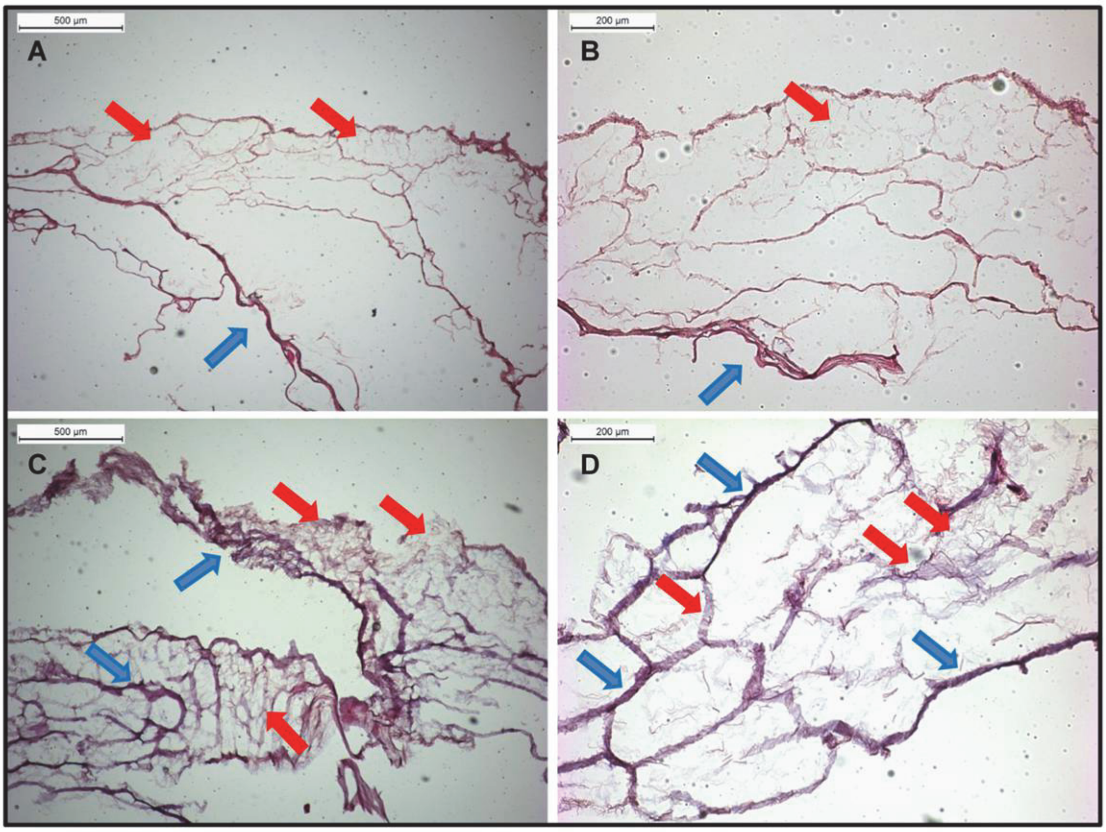

Figure 13. H&E staining of histological cryosections of decellularized hearts. (a) and (b) representative sections of hearts that were decellularized including 48 h of detergent perfusion. (c) and (d) Representative sections of hearts that were decellularized including only 12 h of detergent perfusion. Blue arrows indicate remnants of nucleic acid smear. Red arrows indicate regions of recognizable fine structured microarchitecture. It can be observed that collagen structures reveal distinct fine structures for (c) and (d), while (a) and (b) show clearly affected structures. Blue nucleic acid smear can be observed in (c) and (d) but it is almost completely eliminated in (a) and (b). No structures of cellular remnants can be observed.

all with the aim of automation and better control over the process in the future. Here, we have focused on a popular and well-characterized protocol, as it resembles a relatively short procedure, yet resulting in a good organ decellularization suitable for further applications [4]. However, the applied protocol serves merely as a subject for the proof of concept. With respect to the value of the analytic step using rheological measurements, the particular decellularization protocol plays a minor role and may be exchanged in favor of other protocols in other experimental settings.

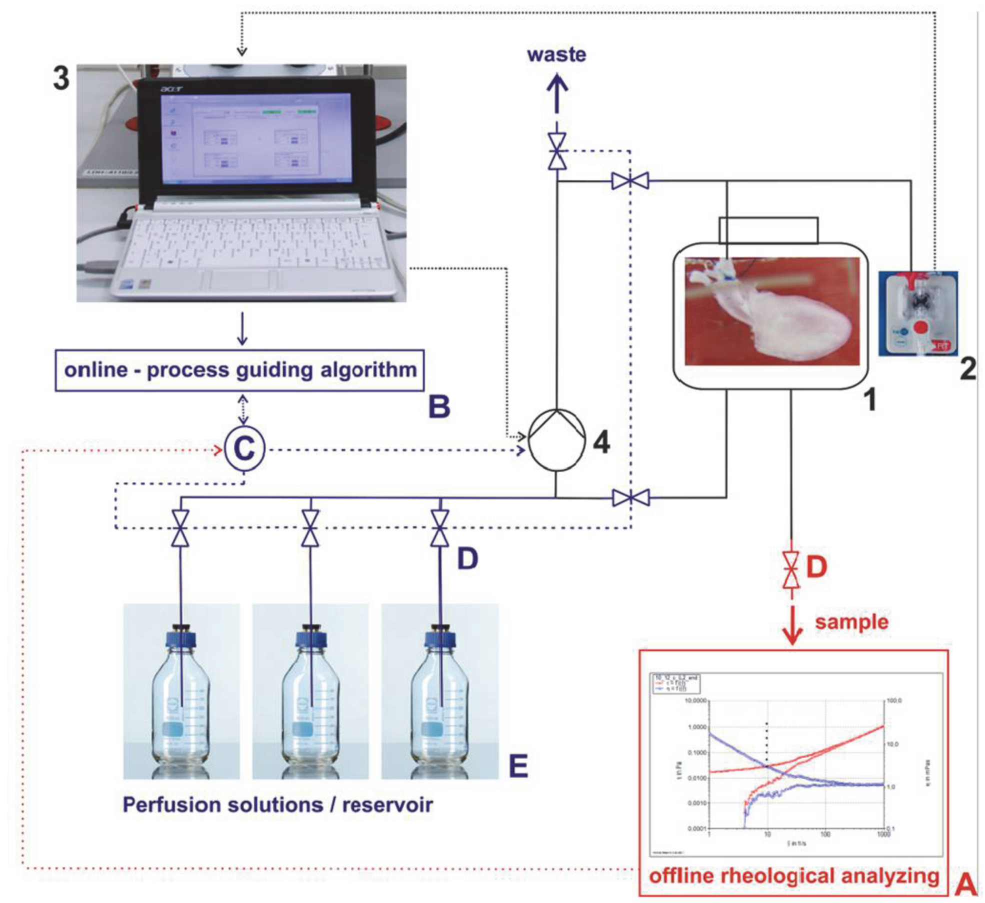

Figure 14. Perspective integration of online detection of characteristic fluid dynamical events or alternatively manual rheological measurements for individualization of whole organ decellularization. A software-controlled perfusion circuit is improved by adding either information of an online process-guiding algorithm (see online supplementary material passage 2) or the results of rheological measurements to the process control principle. This algorithm screens the perfusion control data for characteristic events based on effects to fluid dynamical characteristics caused by potentially altering rheological activity of the perfusate (see figure 2)(blue). As an alternative, process-accompanying rheological measurements enable the detection of characteristic process stages to adapt the process-guiding strategy to individual organs (red). The pressure-controlled perfusion circuit is drafted in black, as adopted from previous work [4]. (1) Organ perfusion chamber; (2) perfusion pressure transducer; (3) computer hardware running the custom engineered control software; (4) actuating peristaltic perfusion pump. (a) Rheological characterization of a fresh perfusate sample; (b) algorithm for a stepwise analysis of the progress of decellularization; (c) digital out converter and interface to the valves, governing the inflow of different solutions to the perfusion circuit (d); and (e) reservoirs containing single perfusion solutions, volume renewal and feeding of the perfusion system is organized by draining the needed volume from here.

To our best knowledge, this is the first approach to use detectable alternations of the perfusate in its physi-cal properties to assess the ongoing progress of decellularization. In this respect, we hypothesize that the observed decreasing actuation of the RS-P in combination with constant perfusion pressure can only be the consequence of an increasing viscosity of the perfusate. We observed this event for the first detergent perfusing step as well as for perfusing water following detergent perfusion. In turn, increasing RS-P could be due to either decreasing viscosity or decreasing coronary vascular resistance. The latter instance seems to be likely for the second and following detergent perfusion intervals, because the cellular mass, which regulates the vascular tone, is probably being extracted at this stage of the decellularization process. In contrast, a decrease in the viscosity may be the major event leading to a similar change of RS-P at the later stage after switching the perfusion solution to PBS when no more manipulation of the vascular system would be expected. In fact, we were able to prove this hypothesis by perfusate analysis and comparative measurement of rheological characteristics of perfusates probed at these two time points (S1_X2 versus S3_X1/2) while comparing them to rheological characteristics of stan-dard DNA and protein solutions. We highlight this effect separately in the online supplemental data in passage 1 and figure S1.

By monitoring and detecting the anticipated fluid dynamical events during the whole organ perfusion for decellularization purposes via the perfusion pres-sure and RS-P profiles, their implementation in the feedback control may become feasible. Thus, protocol adaptations to single organs may be facilitated and potential negative residence times of agents may be reduced or minimized. Furthermore, this is the first approach to analyze the perfusate and to monitor the discharge of biomass in a non-invasive manner. For this purpose, the dry biomass balance of native versus decellularized hearts was generated to demonstrate that the bulk part of biomass is taken out, while only about 16% of the native dry biomass remains, repre-senting the preserved ECM. The average discharge of total biomass is nearly equal to the detected average total protein content in the perfusate. Considering the residual inaccuracy of current protocols for total pro-tein determination due to protein-to-protein var-iances, and further considering the fact that all other constituent parts of the cellular biomass, e.g., lipids and carbohydrates, are of minor ratio, these results support the plausibility of the herein presented approach. Roughly all of the proteins washed out of the heart are collectively found in the perfusate solu-tion at the end of the first perfusion interval of the first step (S1_X1). This finding was fostered when a sensi-tive fluorescence staining of SDS PAGE analysis of the perfusate of all perfusion intervals of all steps of the protocol was applied. Further, the visual clearance of the perfused hearts during decellularization corre-sponds approximately to the dynamic presented in figure5(b) and seems to be completed within the firstperfusion interval of the protocol, as shown in figure12.

In excess of the total protein discharge, we eval-uated the discharge of DNA, the cellular molecule with presumably the highest impact on potential effects to fluid dynamical characteristics [13], during the decellularization process. According to our initial hypothesis, dissolving the decruited chromosomal DNA out of the processed hearts during the perfusion step with pure water would lead to the characteristic decrease of the actuating RS-P, which is typically observed at the time of changing the perfusion solution from the detergent solution to water. We further hypothesized that such an accentuated removal of DNA would be accessible to our rheometry-based approach and hence this method may serve as a non-invasive detec-tion system for the extend of DNA wash-out in future process-guiding strategies. To prove this, we had to detect and quantify the assumed DNA content on the one hand and prove its impact to fluid dynamical characteristics as suggested by the rheological mea-surement of the perfusate on the other hand. The for-mer held the difficulty to detect and quantify very small concentrations of DNA comparative for all steps of the protocol. Unfortunately, almost all common methods were inapplicable because of strong dis-turbances caused by detergents, as used in the first decellularization solution. Hence, we chose to quan-tify DNA via specific fluorescence determination after the intercalation of ethidium bromide, a process that is not disturbed by detergents. Our method was success-ful to detect and quantify DNA concentrations down to the lowest standard of 0.2 μg ml^{-1}. Using this method, we found that out-taken DNA in fact was located almost entirely in perfusate no. 2 (pure water) and another, yet by a far lower amount in the first perfusion interval of the first step. Interestingly, the presented measurement was capable of presenting a DNA concentration profile in the different perfusates that differs remarkably from the occurrence of dissolved proteins at the same time points. Moreover, an association between these observed phenomena and the online-recorded RS-P was noted. In addition, the results of this method were in line with findings of the rheological measurements.

For rheological measurements, our experimental evaluation is based on sensing and analyzing the cone´s torsion moment while shearing the samples. This methodology involves the application of a wide range of shearing rates, while characteristics due to different physical impacts are recorded. That way, a short range of quasi-dilatant behavior can be observed for water, before it turns over to its typical pattern of a Newtonian fluid. To simplify the evaluation, we describe this pattern in region I as quasi-Newtonian because this characteristic of the experimental setting dis-appears for real non-Newtonian fluids, due to their much stronger correspondening internal forces.

By recording flow curves of protein and DNA standards as well as combined protein and DNA standards, cell-debris, and decellularization solutions of different organs, we could identify several similarities and discriminations between the observed patterns. All in all, the highest viscosities could be observed in region I at low shear rates. The perfusate samples shown in figure12(c) and (d) reveal robust detectable viscosities-mainly in region I. This indicates that this might be a region of relevant shear rates that may appear inside of the heart's coronary vascularity while whole organ decellularization underlies the observed events in the profile of the RS-P. The highest sensitivity could be observed for DNA standards dissolved in water, which show the same pattern as the samples of the water perfusates S2_End. Though the same pattern can also be observed for protein dissolved in water, as shown in figure8(c), and combined standards of protein and-nucleic acid of low molecular range, as shown in figure12(a), we have found DNA but no significantprotein content in these perfusates. So, the rheological flow curve alone can indicate the content of biomole-cular structures but not definitely indicate the compo-sition. The pattern of the perfusates in the first perfusion step shown in figure 12(c) seems to be quite unique: the course of viscosity while running up the shear rate show similarities to those of high protein concentrations dissolved in the same solution S1, but reveal also a shear thinning character mostly in region II, which indicates the content of higher-molecular structures. While running the shear rate back down, it reveals a shear thinning character as it can be observed protein, DNA, and debris as well. This might indicate the release of biomolecular structures out of the debris induced by the shearing stress. A roughly similar pat-tern can be observed for the re-dissolved myocardial debris, where the viscosities increase while running the shear rate back down.

The rheological flow curves of the same samples show that the evolution of viscosity may not be detec-ted before 4–5 h of perfusion. This indicates, on one hand, that the sensitivity of this method is somehow related to the size of the perfused organ (and the over-all quantity of the biomass). On the other hand, with respect to the observed patterns, it seems that the discharged biomass of the earlier hours does either not contain detectable amounts of DNA or the crude debris is not destabilized enough to set it free by shearing. However, this finding is in line with the considerations made with respect to the pressure and RS-P profiles during decellularization. The above-described declining side of the initial RS-P peak occurs after 5–6 h of perfusion. While the peak exhibits a highly negative slope, perfusion pressure remains constant. This is directly compatible to the hypothesis, that such phenomenon can only be the consequence of an increasing viscosity of the perfusate.

The investigation of potential rheological tissue specificity of decellularization perfusates of different organs, as shown in figures 11(c) and (d) indicates that different cellular compositions result in different rheological patterns that vary time-dependently on the ongoing decellularization process. On one hand, this underscores the assumption that the type of protein composition may be mirrored by the flow curve, as the main differences between the different tissues are due to the protein machinery of their cells. On the other hand, the process of decellularization and potential differences in the formation of debris could be conceivable as well.

For practical interest, rheological measurements of small volume perfusate samples (1 ml) as described here can be performed directly without any preparations with a minimal time expenditure of only a few minutes. Interestingly, we found a very similar statement in the literature by Klotz et al, where the viscoelasticity measurement was concluded as a quick and easy measurement for the presence and size of DNA molecules in Escherichia coli lysates. The authors speculated in 1972 that this method may serve as a predictive tool for future applications [15]. Ultimately, our inferential prospect to the near future will be to adapt our findings into automation algorithms and procedures in order to put the advertised individuali-zation option into effect, as illustrated in figure 14and the online supplemental data passage 2 and figure S2.

Finally, we transferred our findings to a shortened protocol of only 12 h of detergent (S1) perfusion to investigate if the decellularization process was already completed after we could not identify biomass outtake online or in the perfusates afterwards. The comparative evaluation of H&E stained samples confirmed impressively that the microarchitecture could be prevented intact in contrast to the 48 h detergent perfusion, where the microarchitecture was clearly affected. Meanwhile there were no observable cellular remnants for both conditions; the 12 h detergent perfusion protocol left more remaining DNA-smear stuck at the collagen scaffold. Nevertheless, the overall remaining DNA content in these hearts was only slightly increased by trend and they still reveal a sufficient DNA reduction by decellularization. However, undissolved DNA remnants in the matrix are not directly interacting with the complex of sensing and online monitoring but they indicate the demand for it in terms of bioprocessing strategies a fortiori.

There are some limitations to the presented method. This approach is limited to the general method of decellularization, which is represented sim-ply by the releasing and elution of cellular compo-nents. An additional enzymatic digestion of cellular components, particularly a digestion of DNA and pro-teins, would deplete the effects that are employed in this approach. This would have an impact on the visc-osity evolution during decellularization, and therefore would necessitate an increase of the detection sensitiv-ity. However, on the other hand, the presented approach may overcome the requirement of enzy-matic steps of certain decellularization protocols by introducing an increased control over the elution pro-cess, possibly omitting the necessity of applying harsh enzymatic steps. Furthermore, our approach is greatly affected by the dissolving or repelling capacities of the single solution solvents with respect to the different cellular components. So the solvents have to be adjus-ted to the process-guiding strategy to avoid limited or uncontrolled solvation of DNA and proteins. Finally, a systematic integration of this method for the guidance of a given decellularization process warrants a thor-ough mixture of the perfusate during the process and a well standardized procedure for probe sampling, in order to avoid system inherent variances in the perfu-sate samples.

5. Conclusion

The focus of this work was to investigate the detectability of biomass in decellularization perfusates to enable automation, customization, and online quality control of the decellularization process, leading to tailored decellularization concepts for single organs. For the first time, this study was able to demonstrate the impact of biomass discharge during decellularization with respect to the viscosity of the perfusate and the variables of pressure controlled perfusion-based decellularization. This could enable us to individualize decellularization protocols to single organs, avoiding or minimizing potentially negative residence time of diverse molecules in the processed organ. A substantial versatility of this approach is indicated by the possibility of adapting this method to a variety of decellularization protocols and respective target organs.

Further, the fluid dynamical effects mirrored by its underlying rheological changes in the perfusate may be registered by a fast and direct rheological measurement method that may as well be integrated as an alternative non-invasive, accompanying tool into the overall decellularization process, as illustrated in figure14aswell.

Acknowledgments

The authors thank Karlheinz Preuss and engineo GmbH (Kelkheim, Germany) for excellent technical support in the continuous improvement and engineering of the software and hardware of the organ perfusion system. This work is funded by institutional grants from the Dept. of Cardiovascular Surgery, the Medical Faculty of Heinrich Heine University, and by the Susanne Bunnenberg Stiftung at Düsseldorf Heart Center to Artur Lichtenberg. The authors also acknowledge a stipend from Schmeil-Stiftung (Heidelberg, Germany) to Jörn Hülsmann.

References

[1] Sullivan D C et al 2012 Decellularization methods ofporcine kidneys for whole organ engineering using a high-throughput system Biomaterials337756–64
[2] Song J J and Ott H C 2011 Organ engineering based ondecellularized matrix scaffolds Trends Mol. Med.17424–32
[3] Ott H C et al 2008 Perfusion-decellularized matrix: usingnature’s platform to engineer a bioartificial heart Nat. Med.14213–21
[4] Aubin H et al 2012 Decellularized whole heart for bioartificial heart ed J Walker Methods in Molecular Biology. CellularCardiomyoplasty (New York: Springer)
[5] Hülsmann J et al A novel customizable modular bioreactorsystem for whole-heart cultivation under controlled 3D biomechanical stimulation. J. Artificial. Organs.16294–304
[6] Badylak S F, Taylor D and Uygun K 2011 Whole-organ tissueengineering: decellularization and recellularization of three-dimensional matrix scaffolds Annu. Rev. Biomed. Eng.1327–53
[7] Gillies A R et al 2011 Method for decellularizing skeletal musclewithout detergents or proteolytic enzymes Tissue Eng. Part CMethods 17383–9
[8] Shamis Y et al 2011 Organ-specific scaffolds for in vitro expansion, differentiation, and organization of primary lung cells Tissue Eng. Part C Methods17861–70
[9] Hülsmann J et al 2012 Transplantation material bovinepericardium: biomechanical and immunogenic characteristics after decellularization versus glutaraldehyde-fixing Xenotransplantation 19286–97
[10] Witzenburg C et al 2012 Mechanical changes in the rat rightventricle with decellularization J. Biomech.45842–9
[11] Akhyari P et al 2011 The quest for an optimized protocol forwhole-heart decellularization: a comparison of three popular and a novel decellularization technique and their diverse effects on crucial extracellular matrix qualities Tissue Eng PartC Methods 17915–26
[12] Laemmli U K 1970 Cleavage of structural proteins during theassembly of the head of bacteriophage T4 Nature227680–5
[13] Ross P D and Scruggs R L 1968 Viscosity study of DNA. II. Theeffect of simple salt concentration on the viscosity of high molecular weight DNA and application of viscometry to the study of DNA isolated from T4 and T5 bacteriophage mutants Biopolymers 61005–18
[14] Mason T G, Dohple A and Wirtz D 1998 Linear viscoelasticmoduli of concentrated DNA solutions Macromol.313600–3
[15] Musti R et al 1995 Viscoelastic properties of entangled DNAsolutions Competes Rendues de l’Académie des Sciences Serie II 320 599–605
[16] Klotz L C and Zimm B H 1972 Size of DNA determined byviscoelastic measurements: results on bacteriophages, Bacillus subtilis and Escherichia coli J. Mol. Biol. 72779–800

3.3. Bioreactor Design for Biomechanical Stimulation of Whole Heart Constructs

J Artif Organs
DOI 10.1007/s10047-013-0705-5

ORIGINAL ARTICLE

A novel customizable modular bioreactor system for whole-heart cultivation under controlled 3D biomechanical stimulation*

Jörn Hülsmann   Hug Aubin   Alexander Kranz   Erhardt Godehardt
Hiroshi Munakata   Hiroyuki Kamiya   Mareike Barth   Artur Lichtenberg
Payam Akhyari

Received: 16 September 2012 / Accepted: 17 March 2013
The Japanese Society for Artificial Organs 2013

* The permission to re-use this article within this dissertation was granted by the Japanese Society for Artificial Organs

Abstract In the last decade, cardiovascular tissue engineering has made great progress developing new strategies for regenerative medicine applications. However, while tissue engineered heart valves are already entering the clinical routine, tissue engineered myocardial substitutes are still restrained to experimental approaches. In contrast to the heart valves, tissue engineered myocardium cannot be repopulated in vivo because of its biological complexity, requiring elaborate cultivation conditions ex vivo. Although new promising approaches—like the whole-heart decellularization concept—have entered the myocardial tissue engineering field, bioreactor technology needed for the generation of functional myocardial tissue still lags behind in the sense of user-friendly, flexible and low cost systems. Here, we present a novel customizable modular bioreactor system that can be used for whole-heart cultivation. Out of a commercially obtainable original equipment manufacturer platform we constructed a modular bioreactor system specifically aimed at the cultivation of decellularized whole-hearts through perfusion and controlled 3D biomechanical stimulation with a simple but highly flexible operation platform based on LabVIEW . The modular setup not only allows a wide range of variance regarding medium conditioning under controlled 3D myocardial stretching but can also easily be upgraded for e.g. electrophysiological monitoring or stimulation, allowing for a tailor-made low-cost myocardial bioreactor system.

Keywords: Tissue engineering bioreactors, Whole organ tissue engineering, Biomechanical stimulation, 3D stretching, Process control system

Electronic supplementary material The online version of this article (doi:10.1007/s10047-013-0705-5) contains supplementary material, which is available to authorized users.

J. Hülsmann H. Aubin A. Kranz E. Godehardt H. Munakata H. Kamiya M. Barth A. Lichtenberg
P. Akhyari
Research Group for Experimental Surgery, Department of Cardiovascular Surgery, Medical Faculty, Heinrich Heine University Medical School, Duesseldorf University Hospital, Moorenstr. 5, 40225 Duesseldorf, Germany
e-mail: joern.huelsmann@med.uni-duesseldorf.de

P. Akhyari
e-mail: payam.akhyari@med.uni-duesseldorf.de

H. Munakata
Division of Cardiovascular Surgery, Department of Surgery, Kobe University Graduate School of Medicine, Kobe, Japan

Introduction

In the last decade, the emerging field of cardiovascular tissue engineering has made great progress designing and developing new strategies for regenerative medicine applications. One of the key ventures of the field is the creation of bioartificial cardiovascular tissue in order to support the diseased heart. The in vitro creation and the study of functional tissue engineered constructs, however, requires complex culture conditions ex vivo, in analogy to the natural environment during the in vivo development. The application of bioreactor systems has therefore gained increasing interest. For instance, bioreactors allowing cyclic perfusion have promoted the in vitro engineering and study of bioartificial heart valves forged from decell-ularized matrices and appropriate cell populations in the past [1]. Although such tissue engineered heart valves are now starting to enter clinical evaluation [2], mostly fol-lowing an in vitro repopulation approach omitting the need for bioreactor cultivation [3], such a development would not have been possible without the prior thorough ex vivo study of such valves in artificial environments mimicking natural conditions with high fidelity.

In contrast, tissue engineered myocardial substitutes are still restrained to experimental approaches [4]. Until today, it did not seem possible to generate a functional myocardial substitute solely by the in vivo application of biomaterials or cells, respectively. In contrast to the heart valves, the great biological complexity of the native myocardium demands the ex vivo consolidation of biomaterials and cells altogether with adequate biophysical stimulation using appropriate bioprocessing strategies. Therefore, in vitro cultivation of artificial myocardium requires elab-orate stimulation, in form of biomechanical or electro-physiological stimuli, in order to maturate cells and ECM scaffolds into functional myocardium. For instance, active biomechanical stimulation, e.g., by in vitro stretching of the cultures has been demonstrated as effective supporting the in vitro tissue remodeling by guiding cellular orienta-tion and elongation, which directly relates to the natural function [5–9]. Also, the stimulation of cell–matrix inter-actions in terms of a spatial guiding of matrix remodeling was observed in those studies. Coherently, appropriate mechanical cues stimulate cell differentiation, e.g., as it was indicated by the Connexin 43 expression.

Nonetheless, bioreactor technology needed for the in vitro generation of functional myocardial tissue still lags behind in the area of user-friendly and low-cost systems. Suitable bioreactor systems should be flexible, modularly conceived, highly instrumentable, and continuously expandable and upgradeable. Furthermore, promising new approaches in myocardial tissue engineering, like the whole-heart decellularization concept [10], which allows the creation of acellular heart scaffolds preserving the basic anatomy as well as critical extracellular (ECM) charac-teristics of the native heart [11], make it necessary to develop new bioreactor systems and cultivation strategies adapted to the new emerging developments, such as the so called whole-organ tissue engineering. The latter term refers to the sequential process consisting of decellular-ization, reseeding and cultivation of 3D cultures based on whole organs [12].

However, to our knowledge, there are no previous reports describing a bioreactor system specifically designed for whole-heart cultivation. Here, we present a novel cus-tomizable modular bioreactor system, specifically aimed at the cultivation of such decellularized whole-hearts through coronary perfusion and controlled three-dimensional (3D) biomechanical stimulation with a simple but highly flexible operation platform based on LabVIEW . The modular setup not only allows a wide range of variance regarding medium conditioning under controlled 3D myocardial stretching, but can also easily be upgraded for, e.g., electrophysiological monitoring or stimulation allowing for a tailor-made low-cost myocardial bioreactor system.

Materials and methods

Decellularized whole-hearts

As a 3D whole-organ scaffold we used decellularized rat hearts obtained from male Wistar rats weighing 350–450 g. Donor hearts were decellularized using a simplified deter-gent-based protocol [13]. Using this decellularization technique, the coronary system remains intact as previously shown [11, 13], resembling the basic prerequisite for the whole organ TE approach [12]. Moreover, this way an anatomic basis for the adaptation of any bioreactor and bioprocessing technique is provided.

Whole-heart bioreactor

The bioreactor system is based on the combination of a software-based process control system and a hardware concept consisting of hardware for automation as well as processing hardware for the single specific functions. The latter is described individually in the following single sub chapters. For automation hardware we used a combination of ADAM 4017 analog input and ADAM 4024 analog output modules (Advantech, Irvine, USA) for the com-munication with sensors and actors of medium condition-ing within a RS 485 serial network. This RS 485 network is coupled by a normal serial port to a standard PC via an ADAM 4520 RS 232/RS 485 converter (Advantech, Irvine, USA). In the case of the pressure signal applied for the biomechanical stimulation, a fast data acquisition is war-ranted. Therefore, the respective device is integrated directly by an Advantech USB 4716 module (Advantech, Irvine, USA). Overall all analog devices can easily be incorporated by 2 pole wire leads to each module. Modbus-based devices can be connected as well, as the modules are entirely Modbus compatible. Finally, we created a single LabVIEW code to function as software based PCS, con-trolling the complete system. For more details, refer to the online data supplement a including an overview of the hardware system in figure S1.

Biomechanical stimulation

Biomechanical stimulation of the decellularized whole-hearts was carried out through controlled 3D leftventricular stretching. Therefore, we used an inflatable latex bal-loon that can be inserted into the left ventricle. The balloon is mounted and sealed with food-silicone Ottoseal S27

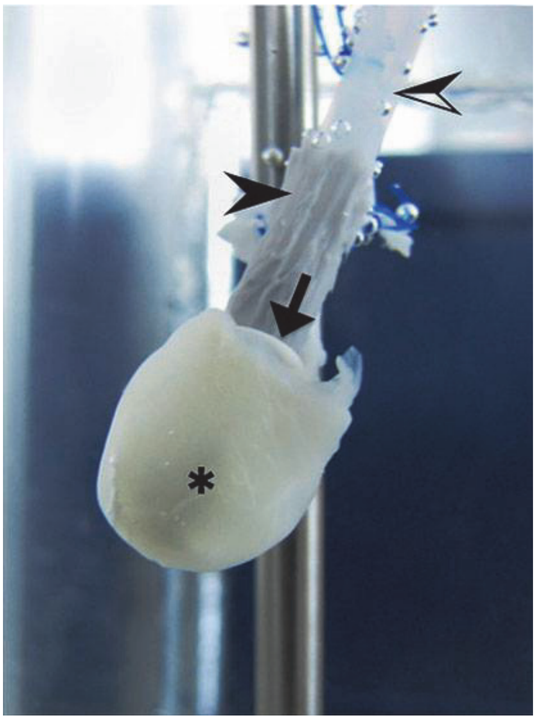

Fig. 1 Close-up view of a decellularized rat heart mounted into the processing chamber. Asterisk ventricular part of the decellularized heart, black arrow upper end of the balloon inserted into the left ventricle via the mitral valve, filled arrow head sealing coat of the pressure pipe, half-filled arrow head pressure pipe (duroplastic tube)

(Hermann Otto GmbH, Fridolfing, Germany) onto a non-expandable polytetrafluorethylene-tube (Fig. 1). We used PBS supplemented with penicillin, streptomycin (300 U/ml and 300 lg/ml, respectively) and amphotericin (7.5 lg/ml) as an incompressible fluid to vary the volume and transfer pressure-energy. A Sera-RS 204.1 membrane pump (Sey-bert & Rahier GmbH ? Co. Betriebs-KG, Immenhausen, Germany) was used to pulsate controllable volume-strokes at controllable frequencies into the system. The static fill-ing volume of the balloon is actuated by a Tecan Cavro - XLP-6000 syringe pump (Tecan Group Ltd., Ma¨nnedorf, Switzerland). The pressure inside of the system is con-trolled by a highly resolving Jumo d-Trans p30 pressure sensor (Jumo, Fulda, Germany).

Surface scanning of stimulated hearts

For surface scanning of the stretched whole heart constructs, we used a special installation based on the DAVID Laser scanner (DAVID Vision Systems, Koblenz, Ger-many). A schematic flow chart of the process is depicted in Fig. 2, where the biomechanical stimulation and the sur-face scanning are marked in blue. Figure 3illustrates a surface scanned heart again as a detail picture. On-line scanning of these constructs during cultivation necessitates a processing-vessel featured with a port for optic availability. According to this approach, a 250 ml four-cornered Schott Duran flask for medium-perfusion is modified by replacing the walls with thin planar fused silica discs (Fig. 4).

Controlled perfusion

For the perfusion cycle we used a hardware setup composed of a Smith Logical invasive pressure transducer (Smith Medical, Ashford, UK) and a simple Spetec MP 12 OEM peristaltic pump (Spetec, Erding, Germany), alto-gether with a silicone tubing system and bubble trap directly prior to the mounting cannula connected to the bioreactor processing chamber (Fig. 4, element nr. 4).

Medium conditioning

For the medium reservation and conditioning we used a hardware setup of a double-jacket stirrer vessel with a minimal operational volume of 300 ml (Braun Biotech, Melsungen, Germany), equipped with a Mettler Toledo 405-DPAS-SC-K8S/200 pH Sensor (Mettler Toledo, Greifensee, Switzerland), an optical modbus pO_2 Sensor Hamilton Visiferm DO^{TM} (Hamilton Bonaduz AG, Bonaduz, Switzerland), and a pt-100 temperature sensor (Braun Biotech, Melsungen, Germany). It was further featured by a disk-type stirrer (Braun Biotech), a sparging ring (Braun Biotech, Melsungen, Germany) for gassing and uptake tubes for supplementing, exchanging and pumping the medium into a circuit with the processing chamber actuated by Spetec MP 12 OEM peristaltic pumps. For gas mixing we build a gas mixing unit composed of three Bu¨rkert El Flow mass flow controller for air/$O_{2,}$ CO_2 and N_2 (Bu¨rkert, Ingelfingen, Germany). Medium may be pooled and con-ditioned in the central vessel. The pH and pO_2 values were controlled independently by a central gas mixing algorithm that was specifically created for the purpose of this study. For more details please refer to the online data supplement b.1 including the figures S2–S4, giving explicit information about the control methods.

Proof of concept

To prove and validate the concept of the whole-heart bioreactor, decellularized hearts were repopulated with a murine myoblast cell-line (C2C12) and cultivated under prolonged stimulation inside the bioreactor system under standard culture conditions. As a proof of concept test trials including three different cultures under stimulated condi-tions and corresponding three static cultivations as controls were performed. Therefore, preseeded whole-heart scaf-folds were cultivated for 96 h, with or without continuous

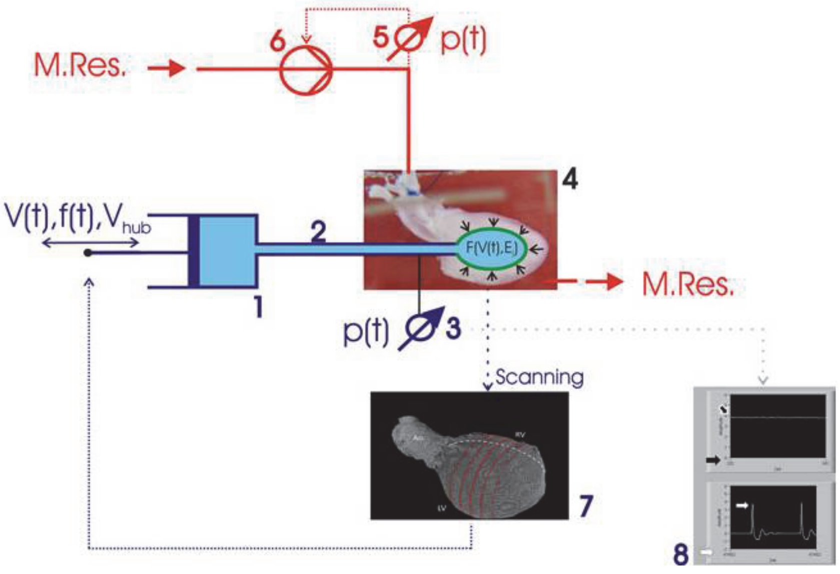

Fig. 2 Draft of the bioreactor systems functions. 1 Pump system. The movable cock indicates the composition of a membrane and a syringe pump. So the volume V(t) is adjustable as well as the bursting of the system with volume-pulses of controllable stroke volume $V_{hub}(t)$ and frequency f(t). 2 Unexpandable PTFE tubes conducting the expand-ing-fluid. 3 Pressure transducer to observe the pressure signal of the 3D stretching device fluid. 4 Perfused and stimulated, re-populated decellularized rat heart. The inflatable stretching balloon is inserted to the left ventricle. The aorta is cannulated for perfusion of the coronaries. The transmural pressure inside of the balloon is a function of the filling-volume as well as the elasticity and the form of the ventricle. 5 Pressure transducer for the perfusion pressure inside of the silicone tubing system. 6 Peristaltic pump. Herewith the perfusion pressure is actuated by the volume flow. 7 Vertex-net as achieved by laser scanning of the surface of a re-populated, perfused and processed whole heart in the bioreactor system. Ao Cannulated aortic root, LV left ventricle, RV right ventricle. Red rows give an impression of differing operation states resulting in differing degrees of stretching. 8 Screenshot of the PCS visualizing flow charts of the stimulation pressure signal (lower) and of the determined pressure amplitude (upper). White arrow indicates the actual pressure ampli-tudes; white arrow with black edge indicates the axis of abscissa, that is scaled to the cycles of the process control system (several pressure peaks are incorporated to one single cycle); black arrow indicates the axis of abscissa of the amplitude control course that is scaled in minutes of process time; black arrow with the white edge shows the line of the amplitude of pressure.

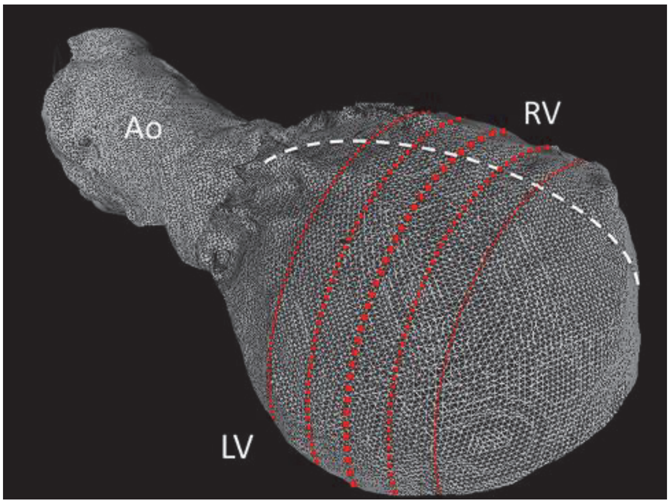

Fig. 3 Surface scanned processed rat heart. Detail-picture of subitem 7 of Fig. 2. The heart is displayed by a vertex-net as achieved by laser scanning of the surface of a re-populated, perfused and processed whole heart in the bioreactor system. Ao Cannulated aortic root, LV left ventricle, RV right ventricle. Red rows give an impression of differing operation states resulting in differing degrees of stretching

application of biomechanical stimulation, respectively. In the stimulated group, the biomechanical conditioning resulting in a stretching of 10 % longitudinal elongation of the myocardial ECM as determined at the epicardial sur-face. Biomechanical stimulation was initiated after an ini-tial 24-h culture period the preseeded hearts. The online data supplement b.2 including figure S5 gives additional information about the relating volume to pressure relations, that were used for setting up the control algorithm. The online data supplements b.3 and c including the figures S5 and S6 further illustrate the chosen setpoints and combined control strategies of the experiments.

Cell culture and seeding

C2C12, a murine myoblast cell line with the capability to form myotubes was used, as this resembles a straightforward and widely used cell culture system for proof of principle experimental set-ups. Cells were cultured in growth medium composed of low-glucose I-glutamax DMEM supplemented with antibiotics and 10 % FCS. Prior to seeding, decellularized hearts were perfused with 5 ml of 100 % FCS followed by a 2 h incubation at 37 LC for preloading of the hearts ECM with growth factors. We expect the latter factors to be retained by the matrix

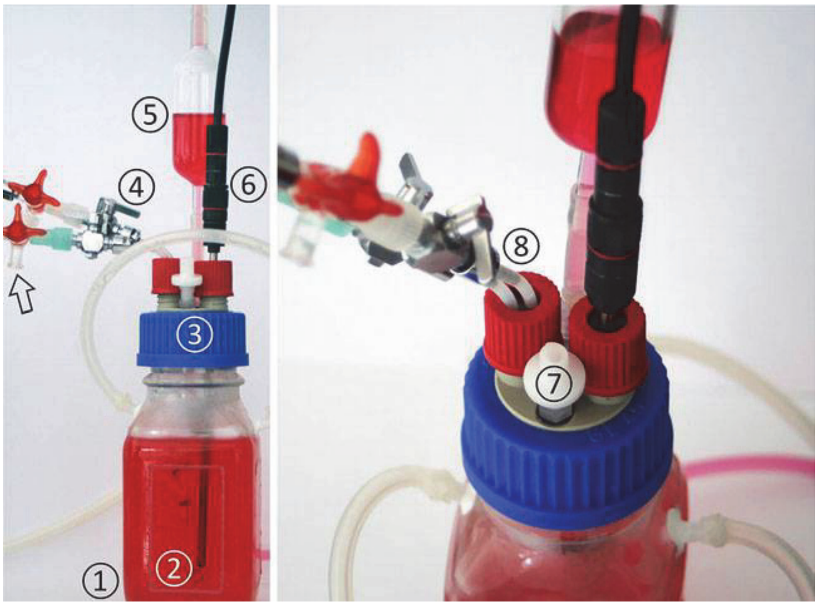

Fig. 4 Lateral view of the culture chamber. Based on a commercially available reagent bottle, a custom-made and application-adopted culture chamber was constructed. 1 250 ml flask; 2 thin planar glass panel for optical accessibility and high precision optical analysis; 3 modified GL 45 2-Port lid; 4 cut-off cocks of the pressure pipes; 5 bubble trap; 6 pt-100 temperature sensor; 7 filter-equipped (0.2 lm) connection for pressure compensation; 8 pressure pipes for balloon expansion

preserved GAGs, as this has been demonstrated by previous work [11]. Cells were then injected with a density of 1 9 10^6 cells per ml into the left ventricular wall (LVW). Injections were apportioned into 10 segments of 0.1 ml suspension that were evenly spread over the LVW. Pre-seeded hearts were cultivated for 24 h before initiation of the stretch regimen.

WST-1 cell proliferation assay

Prior to initiation of 3D stretching and after 3 days of cultivation under 3D mechanical stimulation, whole hearts were analyzed for cellular viability using the WST-1 pro-liferation reagent (Roche Diagnostics GmbH, Mannheim, Germany, REF: 05015944001). Working solutions of 5 ml per heart were prepared using growth medium and directly perfused into the whole hearts. After 1 h of incubation (37 LC, 5 % CO_2) 1 ml medium was perfused into each heart to wash out the assay product and the perfusate was analyzed according to the manufacturers manual.

Confocal microscopy

Nucleic acids of the Whole heart constructs were stained by perfusion with acridine orange staining reagent (Thermo Scientific, Waltham, Massachusetts, USA) at 0.1 mg/ml according to the manufacturers manual. The LVW were then dissected and F-Actin staining was performed by incubating the LVW-flaps in 2 U phalloidin/rhodamine conjugate (Invitrogen, Carlsbad, California, USA, cat.nr. A12379) for 20 min at 37 LC and 5 % CO_2. The stained flaps were then directly analyzed by confocal microscopy using a Zeiss LSM 700 microscope (Carl Zeiss AG, Oberkochen, Germany).

Cellular alignment

To quantify the alignment of the seeded cells we analyzed the circularity and the spatial orientation angle of the nuclei based on images obtained by confocal microscopy. Therefore we used image J image processing software (NIH, USA). We used the data to generate the distributions of the circularity factor and the observed orientation angles, following in principle previously published meth-odology [14, 15] and described in the online data supple-ment e. Further we determined the fractions of cells, which were clearly aligned in a common angle range (AR) and a common circularity range (CR). Clearly outstanding frac-tions, that differed at least twofold from the bulk fractions with colliding corresponding AR's, were summed up and defined as the fraction of oriented cell (FO). We chose the quotient of the FO with its corresponding total AR as a specific characteristic, that we called specific orientation density (OD) to evaluate the extent of alignment of the cells inside of the stimulated vs. nonstimulated constructs.

Statistics

To determine differences in quantitative analysis of the WST-1 assay of mechanically stimulated vs. non stimulated hearts with n = 3 each, we applied an F test of the equality of variances. Data are presented as relative chan-ges to the viability measures at 24 h. To investigate sig-nificant differences in the calculated extent of alignment of the cells inside of the stimulated vs. nonstimulated constructs, we applied an unpaired two-tailed t test. Differences were considered as statistically significant for $P < 0.05$.

Results

Whole-heart bioreactor

In toto decellularized whole-hearts were successfully used for the development of an automation process embedded in a bioreactor that specifically aims at the cultivation and stimulation of repopulated whole-hearts. This concept was demonstrated to be able to cultivate and process repopu-lated decellularized rat hearts in a batch wise operation mode. As a secondary positive finding, no major problems associated with contamination were encountered.

The conceptual design of the whole-heart bioreactor is modular (Fig. 4) so that we were able to successfully integrate and independently regulate medium perfusion, medium conditioning and biomechanical stimulation, as described beneath. Additionally, the modular design allows a stepwise up-date of additional components such as electrophysiological monitoring or stimulation.

Biomechanical stimulation

In order to stimulate and/or differentiate cells seeded into the decellularized whole-heart scaffold, we used a system of an inflatable balloon to induce controlled 3D ventricular stretching of the left ventricle of the whole-heart in com-bination with an 3D optical observation of surface stretching, that was custom-engineered specifically for the purpose of these experiments (see Figs. 2nr.7, 3). For a truly 3D stretching of a 3D matrix, the construction of a super-ordinate spatial design (the ventricle) allowing a simultaneous 3D transmission of power as well as volume feeding with an incompressible fluid medium perfusion, altogether with a flexible boundary surface to the matrix (ECM) is required. Therefore, the controlled inflation of the balloon induced an expansion of the endoventricular cavity, resulting in stretching of the ECM matrix by increasing the stress level within the LV wall. In order to control and regulate mechanical stimulation the balloon's intrinsic static pressure that increases with every inflation was measured. Additionally, the extent of 3D stretching was monitored by laser scanning of the surface in a time-discrete manner and acquired data were correlated with the transmural pressure signal of the expanding system using LabVIEW . A graphical presentation of the surface scan-ning in the form of a vertices-net is displayed by Fig. 2. The ventricle stretching could be selectively induced at frequencies ranging from 0 to 2.5 Hertz and at a magnitude of twice of the average volume of the non-stretched left ventricle with minimal variability, even after prolonged stimulation.

Perfusion

Once mounted inside the bioreactor chamber decellularized whole-hearts were perfused with conditioned media via coronary perfusion through retrograde aortic perfusion with the perfusion path starting at the coronary ostium at the aortic root following coronary arteries, draining via coro-nary veins to the coronary sinus and finally into the right atrial cavity. Perfusate remained sterile even after long-term perfusion. The standard working volume of medium for one heart was 500 ml. However, this working volume can be reduced or easily adjusted by replacing perfusion vessels of differing capacity. Coronary perfusion pressure remained constant at the preset pressure with minimal variability even after long-term perfusion. Therefore, the presented system allows for controlled perfusion pressure technically feasible in the range from 0 to 400 mmHg, adapting to the cultivation needs and physical character-istics of the present vascular network. For instance it is possible to subsequently increase perfusion pressure over cultivation time, giving cells time to adhere to the ECM.

Medium conditioning

The presented whole-heart bioreactor allows for high var-iance and accurateness in medium conditioning. Through a novel combined pH and pO_2 control concept by an expanded gas mixing algorithm based on proportional-integral and derivative (PID) feedback control and further expanded with internal computational models, pH, pO_2 and temperature can be regulated independently from each other, providing the experimental freedom to cover the full ranges of the special capacities of the media capacity. All controlled process variables (pH, pO_2, T) of the medium could be kept within the setpoint range with a minimal variability even after long-term perfusion. Moreover, the dynamic control system allows for short-term changes in the pre-set settings. This way, a temporary alteration of crucial experimental conditions is feasible, e.g., a selective induction of hypoxia during the cultivation period. For more details please refer to the online data supplement c.

Proof of concept

To proof the concept of a whole-heart bioreactor for the cultivation and prolonged stimulation of repopulated decellularized whole-hearts, the latter scaffolds were preseeded with murine myoblasts (C2C12) through multiple injections and subsequently cultivated under stimulated conditions inside the presented bioreactor. The preseeded whole-heart scaffolds were cultivated for 96 h, respectively with and without continuous application of biomechanical stimulation resulting in a stretching of 10 % longitudinal elongation at the epicardial surface. The pH value was constantly arranged to 7.4, the pO_2 value was constantly kept under 100 % air saturation (what equals 220 mbar in total). Coronary perfusion pressure was continuously monitored and controlled at a setpoint of 70 mmHg.

Using the introduced system, all of the targeted variables were successfully controlled and maintained at the preset setpoint with minimal variability over time. During the culture period, following parameters were continuously monitored and resulting data stored by the bioreactor sys-tem: pH, pO_2, temperature, perfusion pressure and pressure amplitude in the PTFE tubing system while volume stroking corresponding to the amount of ventricular stretching. During our initial test trials, no bacterial con-tamination of the medium nor a significant coronary per-fusion leakage or ventricular tear occurred. We observed a significant increase of cellular viability after the additional 72 h of cultivation of the preseeded scaffolds of 18 ± 6 % for mechanically stimulated hearts, in contrast to 164 ± 92 % for nonstimulated hearts (p \ 0.01; Fig. 5). Confocal microscopy analysis after the cultivation periods showed an increase in cellular 3D spatial orientation with elongated cell bodies and nuclei forming aligned cellular networks inside the matrix for the mechanically stimulated hearts in comparison to the nonstimulated hearts. Never-theless, cells in nonstimulated hearts also showed a general cellular orientation. However, despite the expected spatial alignment of the cells along the ECM-fibers of the native myocardial matrix in both groups, in the controls less elongated cell bodies and nuclei with a lower spatial ori-entation level was observed, as demonstrated representa-tive in Fig. 6. Rows I and II illustrates the presence of a certain degree of orientation in nonstimulated hearts, which markedly increases after the application of 3D stretching to the left ventricle. In rows III and IV this trend becomes more clarified, as it seems that the cells in nonstimulated group orient themselves along the matrix fibers. In the stimulated hearts a higher arrangement amongst the cells can be observed. Rows V and VI show the cells in a higher magnification where it can be observed, that in stimulated hearts the cells present themselves more outspread with a more pronounced orientation of the cytoplasm, while the location of the cytoplasm signals in nonstimulated hearts present a lower arrangement. The online data supplement d including the figure S7 and the movie M1 offer additional 3D visual impressions of the cell populations inside of the ECM.

By additional image processing of the pictures shown in Fig. 6, we quantified the alignment of the depicted cells by analyzing the circularity and the orientation angle of their nuclei. The results are listed in Table 1. Details of the applied image processing and the underlying processed images are presented in the online data supplement e and the according supplemental figure S8.

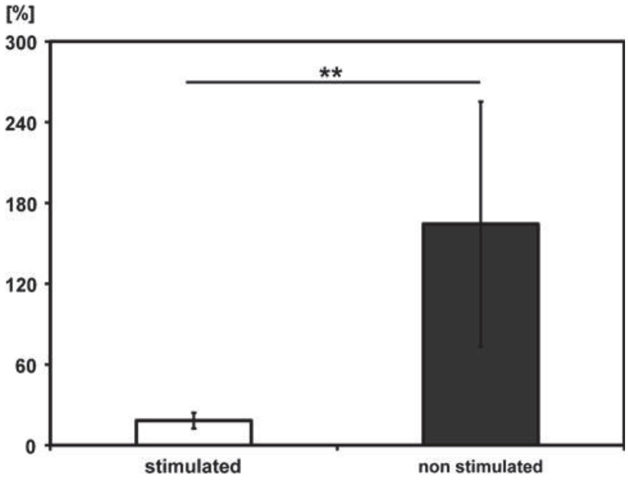

Fig. 5 Increase of cellular metabolism after cultivation by WST-1 cell proliferation reagent. Cellular metabolism was measured by perfusion application of 1/3 concentrated WST-1 cell proliferation reagent assay. The assay was applied before the initiation of the mechanical stimulation (24 h after seeding) and after finishing the process (96 h after seeding) both for stimulated and non stimulated hearts. The diagram depicts the percentage of augmentation of measured cellular metabolism after 96 h of cultivation relative to the activity after 24 h of cultivation. The calculated percentaged increase of metabolism is depicted in bars representing the arithmetic average with error bars representing the standard deviation. Two stars represent p \ 0.01 for control vs. stimulated group

Both stimulated and non stimulated constructs showed explicit FOs, while the FOs of the stimulated group tended to result in higher percentages of all detected cells (ca. 44 ± 4 vs. 34 ± 5 %). Nuclei of both groups showed a predominantly ellipsoidal shape with a circularity factor between mostly 0.05 and 0.25. In contrast to the nonsti-mulated group, the FOs of the stimulated group were dis-tributed onto clearly smaller AR's, what results in a significantly increased extend of alignment, as it is indi-cated by the ODs, shown in Fig. 7. The underlying com-plete distributions of the circularity and the calculated angles are presented in figure S9 in the online data sup-plement f.

The results of the colorimetric viability assay in conjunction with the microscopic results on cell alignment collectively confirm an effective treatment as exerted by the 3D-biomechanical stimulation in the resented proof-of-concept experiments. In summary, the performed test trials indicated that the cultivation and stimulation processes using the presented whole-heart bioreactor are not only operational but also highly reproducible and that such a bioreactor is ready to be used for the repopulation of decellularized whole-hearts, proving the concept of a functional whole-heart bioreactor.

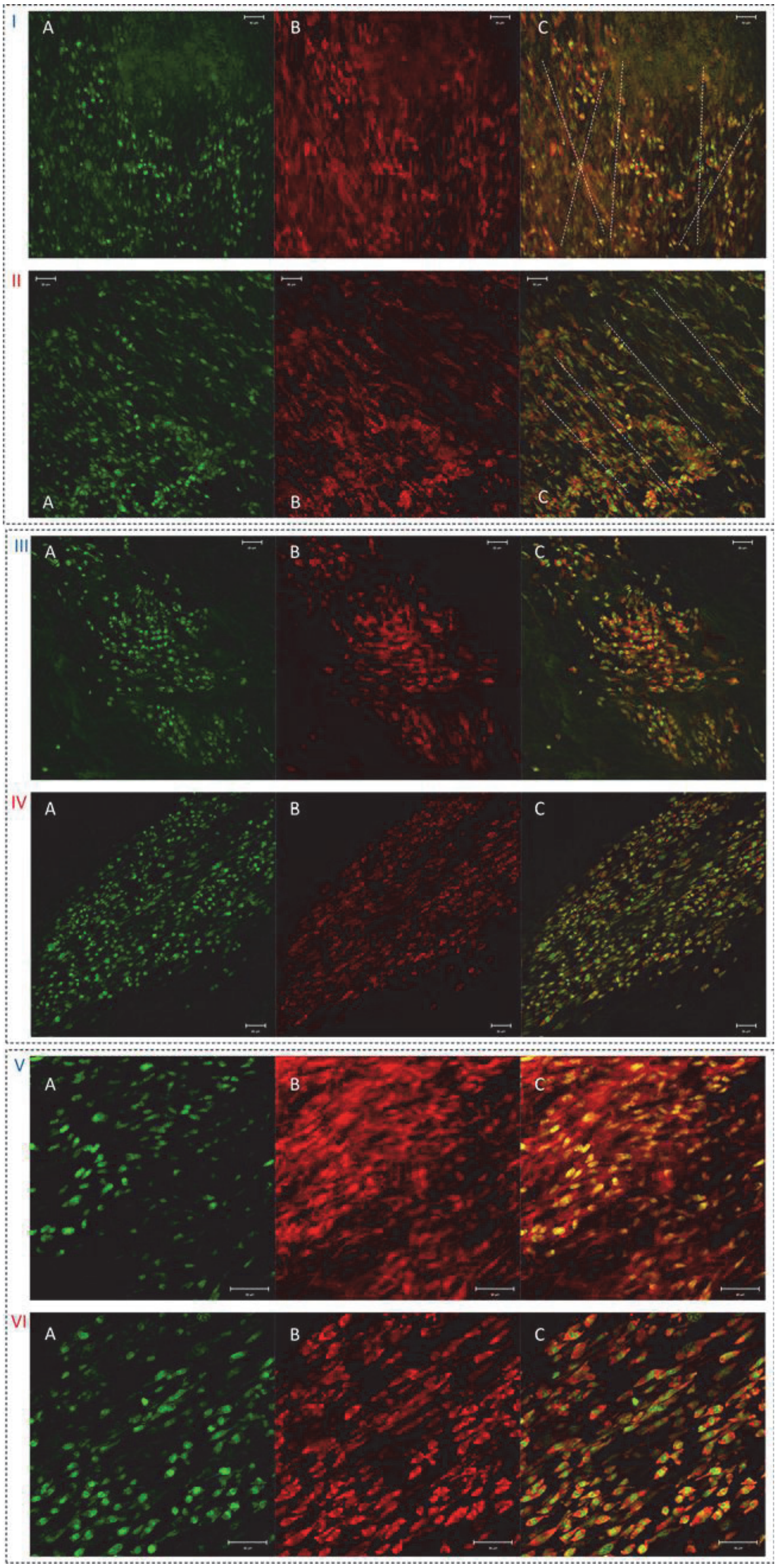

Fig. 6 Confocal microscopic visual analysis of cellular orientation and arrangement of the cultivated cells inside of the hearts ECM. Representative images of repopulated hearts with C2C12-myoblast, demonstrate viable cellular networks with aligned cells. While in nonstimulated hearts cellular orientation can be observed along ECM fibers following the anisotropy of the matrix, mechanically stimulated hearts show a higher 3D spatial orientation with more elongated cell bodies and nuclei. Nuclei and cytoplasmatic nuclear acids are presented in green by acridine orange staining, while the cytoskeleton is presented in red by F-Actin staining. Representative pictures of nonstimulated and stimulated hearts are depicted in paired columns marked by the dashed rectangles. Nonstimulated hearts: marked blue (I, III and V); mechanically stimulated hearts: marked red (II, IV and VI). Rows A, B and C show the acridine orange, the F-actin and the merged signals respectively. White dotted rows in row I and II indicate the different preferred orientational axis of the pictured cells in the different layers. Bars 50 lm

Table 1 Quantification of alignment by image processing of Fig. 6. The table lists the determined parameters of cellular alignment that were identified for the listed pictures of fig. 6

	FO [%]	AR [1L]	OD [%/1L]	CR
Fig. 6IA (non stimulated)	31.89	53–144	0.35	0.05–0.42
Fig. 6IIA (stimulated)	48.50	107–161	0.90	0.06–0.25
Fig. 6IIIA (non stimulated)	30.63	107–178	0.43	0.12–0.26
Fig. 6IVA (stimulated)	41.22	0.7–54	0.77	0.07–0.25
Fig. 6VA (non stimulated)	40.69	0.34–89.72	0.46	0.05–0.24
Fig. 6VIA (stimulated)	41.33	18–53	1.18	0.06–0.18

FO Fraction of clearly oriented cells, AR angle range of the con-cerning FO, OD specific orientation density, CR circularity range of the concerning FO

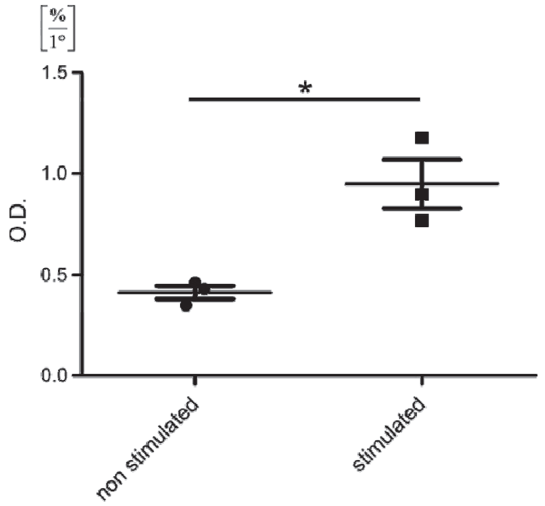

Fig. 7 Specific orientation density (OD) of cells inside of stimulated vs. nonstimulated constructs. OD representing the ratio between the fraction of clearly oriented cells (FO) and angle range of the concerning FO (AR) is depicted for the stimulated vs. the nonstimu-lated constructs, demonstrating a significantly greater alignment for the stimulated group (p = 0.0128)

Discussion

The processing of whole organ tissue engineered constructs via ex vivo cultivation using bioreactors systems seems to be the most promising and logical consequence to proceed in the field of whole-organ tissue engineering, as the com-plexity of the processing strategies will increase in parallel with the experience. Starting with modified Langendorff perfusion systems in the early beginning by Ott and colleagues [10], an increasing interest and activity has risen in this scientific field. For example, today commercial biore-actors are available that allow for the stimulated cultivation of whole lungs by applying an integrated air ventilation to mimic the biophysical (mechanical) stimulation effected by breathing [16]. Nonetheless, bioreactor technology still lags behind in the sense of user-friendly, flexible and low-cost systems that can be easily adapted to the upcoming needs of the tissue engineering society.

Here, we present the first bioreactor system capable of cultivating decellularized whole-hearts under 3D biomechanical stimulation. The main advantage of the presented bioreactor system, e.g., in comparison to already known modified Langendorff systems [10, 17], lies in its modular and integrative character that was realized by programming a complete PCS in LabVIEW . This way, any changes to the system may be done without the commercial depen-dency on a given manufacturer design.

Doubtless we are not the first using LabVIEW to control stimulation devices for tissue engineered applications. A review of contemporary literature reveals a frequent use of LabVIEW, particularly in reports dealing with myocardial tissue engineering, where steering of electric field stimulation of myocardial tissue engineered constructs is needed [18]. However, to our best knowledge the pre-sented work the first approach involving LabVIEW as a complete PCS providing fully integrated control of the bioprocess. This allows us to easily integrate any further stimulation devices or other features into the same system at any time. The existing system could for instance be upgraded for electrophysiological monitoring or stimula-tion depending on the actual needs varying with culture and stimulation conditions as well as target cell populations.

In a state of the art bioreactor system common process parameters like pH and pO_2 values should be arranged independently from each other while being highly variable. For instance, it has been shown that experimentally induced hypoxia may increase the proliferative capacity of myogenic cells [19], this being just one example of why process parameters need to be of high variability. Here, we successfully applied a central control algorithm that regu-lates different gas elements in an independent manner via variable gas mixing, allowing for independent and selective control of the process parameters. In contrast, a comparable effect could not be achieved by applying fix gas mixtures together with membrane oxygenators, as it has been the common practice in Langendorff systems [10, 17].

By engineering the introduced 3D stretching device together with the direct incorporation of its full data processing and control into the unique PCS, the application of controlled 3D mechanical stimulation of a decellularized whole-heart was demonstrated for the first time. Today it is well known that biomechanical stimulation by stretching the constructs can lead to an intensive enhancement of spatial orientation and organization and moreover to phe-notypic hypertrophy and inducible contractility of myo-genic constructs, e.g., reported by Eschenhagen and colleagues [6, 20]. Numerous previous reports have dem-onstrated the mechanical stimulation of 3D constructs, providing a considerable amount of evidence for the role of biomechanical stimulation. However, those previous reports still lack a super ordinate spatial design, e.g., present in a complete ventricle. Hence, in most cases the gross direction of the effective stimulation remained in 2D. In contrast, this work describes an approach to stretch reseeded decellularized whole hearts as a first step at the very beginning of a process refinement in this field. The only other contrastable system and approach yet published, has used a roughly similar 3D stretching device to stretch isotropic hydrogel-based constructs with a high initial density of neonatal rat-myocardial cells [21].

To our best knowledge, today the employment of a commercial system of comparable analog complexity and variability would involve immense cost expenditure. As indicated by inquiring quotes of common providers, these can easily exceed 100.000 Euro. In contrast, we present a tailor-made low-cost solution introducing a modular myo-cardial bioreactor system with full up-date capacity adap-ted to the needs of whole-heart cultivation. To prove the concept and functionality of our modular bioreactor for whole-heart cultivation, whole-hearts were repopularized by injecting cells into the free left ventricular wall as previously described by Ott and colleagues in 2008 [10]. The repopulation of the matrix proved to be successful as cellular viability measures increased over the time of cultivation in stimulated and nonstimulated repopulated hearts. Additionally, visualization of seeded cells after 96 h of culture revealed large cell networks with elongated cytoskeletons throughout the matrix, indicating viable and active cells. Cellular viability demonstrated a larger increase in the nonstimulated hearts in contrast to the mechanically stimulated hearts. There are a number of possible explana-tions for this observation. The observed differences may be due to a cell differentiation process induced by the mechanical stimulus which has been demonstrated to have a negative impact on the proliferation activity along with an altered metabolism of the cells. This assumption would be assisted by the increased cellular orientation and arrange-ment of the C2C12 cells inside of the matrix and the clearly elongated cell bodies and nuclei [5–8, 21]. Of course a profound explanation of this phenomenon would require more detailed analysis of differentiation and proliferation markers. Another explanation could be stress or damage to the cells by potential local overexpansion as optimal stimulation parameters inside of the left ventricle have yet to be investigated and determined in detail. This will demand extensive analysis series involving powerful analytic instruments as the 3D anisotropic ECM of the native myo-cardium is expected to undergo a complex deformation during each stimulation cycle. This will turn the task of precise definition of the local forces and elongation levels to a experimental challenge. In the presented proof-of-concept experiments we chose to set the surface elongation at the region of interest (LVW) to 10 %, which was confirmed by optical surface mapping.

By combined staining of nuclei and cytoplasmatic nucleic acids (acridine orange) together with cytoskeleton staining (phalloidin) we observed in confocal microscopy that the cells arranged themselves into a general orientation inside of the ECM and at a much lower degree even in nonstimulated hearts. Furthermore, we could confirm this graphical impression by the evaluation of the fractions of clearly oriented cells (FOs) and their specific orientation densities (OD’s). Both were increased for the stimulated group, which represents a further proof for the biological response to the applied biomechanical stimulation. Inter-estingly, we could find a significance for the more stringent ODs even in the rather small groups that were included in this proof-of-concept study. Since cellular orientation seemed to follow the orientation of the matrix fibers and varied with the anisotropy of the matrix, we believe this to be most probably due to the intrinsic orientation of the ECM structure, as we already observed in similar studies in the past [11]. Likewise, this finding accompanies the idea of utilizing the preserved microstructure of decellularized organs in the whole organ TE approach.

The degree of orientation and spatial arrangement as well as cell elongation was markedly increased in the mechanically stimulated hearts. This phenomenon was already reported for 2D and thin 3D cultures under uni- and bidirectional mechanical stimulation [5–8, 21]. For the first time, we could successfully transfer that interaction to a real 3D model of mechanical stimulation involving an anisotropic three-dimensional ECM in a superior spatial design (the left ventricle). In following studies these interactions should be quantified and investigated in a more differentiated pattern, e.g. including the anisotropic orien-tation of matrix fibers.

Collectively, our exemplary cultivation experiments demonstrate that repopulation of decellularized whole-hearts using the presented bioreactor system is generally feasible. Furthermore, we implemented the well-known benefit of mechanical stimulation of myocardial constructs into the novel concept of whole heart tissue engineering. Moreover, the perspective to develop reasonable process guiding strat-egies is provided, allowing for adequate molecular biological and biochemical analysis of the cultured constructs.

However, the determination of an adequate cell population and the evaluation of different re-population strategies, the most appropriate cultivation parameters and the most effective stimulation conditions are out of the main focus of this work and remain to be determined in upcoming studies. Future work that most likely will involve the use of clinically relevant stem or progenitor cell populations will have to elucidate the optimal range and the appropriate time line for mechanical stretch as an in vitro tool for myocardial tissue engineering.

Conclusion

Following the needs of the recent advances in cardiac tissue engineering by the introduction of the whole-organ tissue engineering approach, we developed a novel bioreactor system for whole-heart tissue engineering. This modular bioreactor system allows the in toto cultivation and processing of whole-hearts after decellularization and in vitro pre-seeding under the continuous application of 3D biomechanical stimulation. For every particular component of the system a rather simple solution was developed to result in a final bioreactor that can be constructed without the need for large financial expenses for commercial hardware or analyzing-software. Furthermore, this system can be easily adapted to the progress of ongoing projects and expanded in any order. This way it can grow with the state of the art in science. Additionally, to our best knowledge, this is the first bioreactor system that allows biomechanical stimulation through defined and controlled 3D stretching of the heart ventricle.

Acknowledgments The authors are thankful to Antonio Pinto and Anja Vervoorts for the fruitful discussions and valuable comments throughout the progress of the project. Our very special thanks is due to Mrs. Susanne Bunnenberg for her generous donation that made our project possible in first place. The technical assistance of Gisela Mu¨ller and Martina Stuff is highly appreciated.

References

1. Lichtenberg A, Tudorache I, Cebotari S, et al. Preclinical testing of tissue-engineered heart valves re-endothelialized under simu-lated physiological conditions. Circulation. 2006;114:I559–65. doi:10.1161/CIRCULATIONAHA.105.001206.
2. Cebotari S, Tudorache I, Ciubotaru A, et al. Use of fresh decellularized allografts for pulmonary valve replacement may reduce the reoperation rate in children and young adults: early report. Circulation. 2011;124:S115–23. doi:10.1161/CIRCULATIONAHA.110.012161.
3. Akhyari P, Kamiya H, Gwanmesia P, et al. In vivo functional performance and structural maturation of decellularised allogenic aortic valves in the subcoronary position. Eur J Cardiothorac Surg. 2010;38:539–46. doi:10.1016/j.ejcts.2010.03.024
4. Chiu LLY, Iyer RK, Reis LA, et al. Cardiac tissue engineering: current state and perspectives. Front Biosci. 2012;17:1533–50.
5. Akhyari P, Fedak PWM, Weisel RD, et al. Mechanical stretch regimen enhances the formation of bioengineered autologous cardiac muscle grafts. Circulation. 2002;106:I137–42.
6. Eschenhagen T, Zimmermann WH. Engineering myocardial tissue. Circ Res. 2005;97:1220–31. doi:10.1161/01.RES.0000196562.73231.7d.
7. Kensah G, Gruh I, Viering J, et al. A novel miniaturized multi-modal bioreactor for continuous in situ assessment of bioartificial cardiac tissue during stimulation and maturation. Tissue Eng Part C Methods. 2011;17:463–73. doi:10.1089/ten.TEC.2010.0405.
8. Zhang T, Wan LQ, Xiong Z, et al. Channelled scaffolds for engineering myocardium with mechanical stimulation. J Tissue Eng Regen Med. 2011;. doi:10.1002/term.481.
9. Au HTH, Cheng I, Chowdhury MF, et al. Interactive effects of surface topography and pulsatile electrical field stimulation on orientation and elongation of fibroblasts and cardiomyocytes. Biomaterials. 2007;28:4277–93. doi:10.1016/j.biomaterials.2007.06.001.
10. Ott HC, Matthiesen TS, Goh S, et al. Perfusion-decellularized matrix: using nature's platform to engineer a bioartificial heart. Nat Med. 2008;14:213–21. doi:10.1038/nm1684.
11. Akhyari P, Aubin H, Gwanmesia P, et al. The quest for an optimized protocol for whole-heart decellularization: a compari-son of three popular and a novel decellularization technique and their diverse effects on crucial extracellular matrix qualities. Tissue Eng Part C Methods. 2011;17:915–26. doi:10.1089/ten.TEC.2011.0210.
12. Badylak SF, Taylor D, Uygun K. Whole-organ tissue engineer-ing: decellularization and recellularization of three-dimensional matrix scaffolds. Annu Rev Biomed Eng. 2011;13:27–53. doi: 10.1146/annurev-bioeng-071910-124743.
13. Aubin H, Kranz A, Hülsmann A, Lichtenberg A, Akhyari A. Decellularized whole heart for bioartificial heart. In: Kao RL, editor. Cellular cardiomyoplasty: methods and protocols. In: Walker J, editor. Methods in molecular biology. Humana Press, a part of Springer Science ? Business Media (in press).
14. Aubin H, Nichol JW, Hutson CB, et al. Directed 3D cell align-ment and elongation in microengineered hydrogels. Biomaterials. 2010;31:6941–51. doi:10.1016/j.biomaterials.2010.05.056.
15. Xu F, Beyazoglu T, Hefner E, et al. Automated and adaptable quantification of cellular alignment from microscopic images for tissue engineering applications. Tissue Eng Part C Methods. 2011;17:641–9. doi:10.1089/ten.TEC.2011.0038.
16. Song JJ, Ott HC. Bioartificial lung engineering. Am J Transpl. 2012;12:283–8. doi:10.1111/j.1600-6143.2011.03808.x.
17. Schmitz-Spanke S, Seyfried E, Schwanke U, et al. Das isolierte Kaninchenherz: ein Vergleich zwischen fu¨nf Varianten (The isolated rabbit heart: comparison between five different modifi-cations). Herz. 2002;27:803–13. doi:10.1007/s00059-002-2419-y.
18. Tandon N, Cannizzaro C, Chao PG, et al. Electrical stimulation systems for cardiac tissue engineering. Nat Protoc. 2009;4: 155–73. doi:10.1038/nprot.2008.183.
19. Koning M, Werker PMN, van Luyn MJA, et al. Hypoxia pro-motes proliferation of human myogenic satellite cells: a potential benefactor in tissue engineering of skeletal muscle. Tissue Eng Part A. 2011;17:1747–58. doi:10.1089/ten.tea.2010.0624.
20. Fink C, Ergu¨n S, Kralisch D, et al. Chronic stretch of engineered heart tissue induces hypertrophy and functional improvement. FASEB J. 2000;14:669–79.
21. Gonen-Wadmany M, Gepstein L, Seliktar D. Controlling the cel-lular organization of tissue-engineered cardiac constructs. Ann N Y Acad Sci. 2004;1015:299–311. doi:10.1196/annals.1302.025.

3.4. Bioprocess Design for Biomechanical Stimulation of Whole Heart Constructs

ORIGNAL ARTICLE

Biotechnology and Bioengineering

The Impact of Left Ventricular Stretching in Model Cultivations With Neonatal Cardiomyocytes in a Whole-Heart Bioreactor*

Jörn Hülsmann,Hug Aubin, Alexander Wehrmann, Artur Lichtenberg, Payam Akhyari

Medical Faculty, Research Group for Experimental Surgery, Department of Cardiovascular Surgery, Heinrich Heine University, Moorenstr. 5, Duesseldorf, North Rhine-Westphalia, Germany 40225; telephone: þ49-211-81-18331; fax: þ49-211-81-18333;

e-mail: hug.aubin@med.uni-duesseldorf.de

ABSTRACT: Here, we investigate the impact of integrated three-dimensional (3D) left ventricular (LV) stretching on myocardial maturation in a whole-heart bioreactor setting. Therefore, decellularized rat hearts were selectively repopulated with rodent neonatal cardiomyocytes (5 10^6 cells per heart) and cultured over 5 days. Continuous medium perfusion was maintained through the coronary artery system in a customized whole-heart bioreactor system with or without integrated biomechanical stimulation of LV. 3D repopulation effectiveness and cellular vitality were evaluated by repetitive metabolic WST-1 assays and 3D confocal microscopy analysis through fluorescent staining, also assessing cellular organization. Moreover, specific myocardial vitality was verified by detecting spontaneous electrophysiological activity using a multielectrode assay. Western blot analysis of cardiac myosin heavychain (MHC) and quantitative RT-PCR for Connexin 43 was used to analyze cardiomyocyte maturation. Decellularized whole-heart constructs repopulated with neonatal cardiomyocytes (repopWHC) showed vital 3D cell populations throughout the repopulation sites within the LV with a significant increase in metabolic activity (326 113% for stimulated constructs vs. 162 32% for non-stimulated controls after 96 h of continuous cultivation as compared to their state 24 h after injection, directly prior to bioreactor cultivation). Further, bioreactor cultivation under integrated mechanical LV stimulation not only led to a higher degree of cellular organization and an increased MHC content, but also to a significant increase of Cx43 gene expression resulting in a regain of 60 19% of native neonatal hearts expression level in contrast to 20 9% for non-stimulated controls (P¼ 0.03). Therefore, our study suggests that the integration of LV stretching into whole-heart bioreactor cultivation may enhance cardiac maturation not only by promoting cellular organization but also through adaptive protein and gene expression with particular implications for the formation of the conductive apparatus. Further, this study emphasizes the importance of suitable bioprocessing strategies within sophisticated bioreactor systems as tools for customized stimulation and cultivation of tissue engineered tissues and organs.

Biotechnol. Bioeng. 2017;114: 1107–1117. 2016 Wiley Periodicals, Inc.

KEYWORDS: whole-heart bioreactor; bioprocessing systems;myocardial tissue engineering; biomechanical stimualtion; left-ventricular strechting

Introduction

Whole-organ engineering is a rapidly evolving research field, which is gaining increased attention in the tissue engineering community, as it holds the potential to revolutionize regenerative medicine. However, for now, we still lack standardization of customized and integrated bioprocessing strategies within sophisticated bioreactor systems, which are needed to generate functional and clinically relevant tissue, engineered tissues, and organs. In most application settings, the respective required tools such as integrative modular bioreactor systems with suitable and customizable process control systems still need to be developed.

In the case of myocardial tissue engineering some progress has been achieved in the generation of tissue engineered constructs for functional myocardial support or partial replacement (Masuda and Shimizu, 2016; Tandon et al., 2009; Zimmermann, 2001). However, these promising results have yet not led to clinical applicability. Here, the whole-heart tissue engineering approach (Ott et al., 2008) may offer some advantages over previous 2D or 3D strategies, as it may enable the ex vivo generation of functional and mature native-like myocardial tissue in a standardized setting.

However, at the current state of science and technology of functional whole-heart tissue engineering, it remains yet a major challenge for a whole-heart bioreactor system to transfer and unify proven and established concepts of myocardial tissue engineering

Conflict of interest: None.
Correspondence to: H. Aubin
Contract grant sponsor: Department of Cardiovascular Surgery Contract grant sponsor: Heinrich-Heine-University
Contract grant sponsor: Susanne Bunnenberg-Stiftung Contract grant sponsor: Schmeil Stiftung
Received 3 June 2016; Revision received 15 December 2016; Accepted 18 December 2016

DOI 10.1002/bit.26241

into a holistic cultivation approach (Hülsmann et al., 2013). This means not only to promote the adaptive capacity of the donor cells together with the whole-heart scaffold to develop into functional myocardial tissue. Moreover, such a concept would have to be able to control and steer the entire process, for example with respect to cardiomyocyte organization, hypertrophy, electrical coupling, and formation of a contractile apparatus. Therefore, in this study, we have applied short-term model-cultivations of decellularized whole-heart constructs repopulated neonatal cardiomyocytes (repopWHC) within an integrative cultivation approach, in order to promote cardiac cell maturation along with the implementation of screening tools for myocardial tissue development into a modular and integrative whole-heart bioreactor system.

Methods

Ethics Statement

All animal experiments were carried out according to §6 and §8 of the German animal welfare act of North-Rhine-Westphalia (TierSchG) and authorized by the respective authority LANUV (Landesamt für Natur, Umwelt, und Verbraucherschutz NRW; the German state office for nature, environment, and consumer protection of North-Rhine-Westphalia).

Whole-Heart Scaffolds

Whole-heart scaffolds were produced by semi-automatic detergent-perfusion-based decellularization of donor hearts from male Wistar rats (400–500 g) at regulated perfusion pressure of 70 mmHg in order to ensure standardized decellularization quality, as previously described. (Akhyari et al., 2011; Aubin et al., 2013). That way, a series of standardized whole-heart scaffolds with an intact coronary system and myocardial microachitecture could be generated as a basic fundament for all whole-heart cultivations.

Neonatal Cardiomyocyte Isolation and Culture

Rodent neonatal cardiomyocytes were isolated following standard protocols (Hülsmann et al., 2015). Briefly, freshly gained hearts of 1–3 days old Wistar rats got minced and incubated in 400 Units per mL collagenase II (Thermo Fisher Scientific, Waltham, cat.nr.: 17101015) together with 0.05% trypsine (Thermo Fisher Scientific, Waltham, cat.nr.: 15090046) dissolved in DMEM (Thermo Fisher Scientific, Waltham, cat.nr.: 10567014). The basal third of the donor hearts was removed to obtain ventricular myocardial tissue. After mincing the ventricular myocardial mass was then incubated with an initial step of 5 min followed by four further incubations of 25 min, respectively. After each incubation, the resulting superna-tant was resuspended in one volume of cold cell culture medium composed of DMEM (Thermo Fisher Scientific, Waltham, cat.nr.: 10567014) supplemented with 10 Vol% fetal calf serum (Sigma– Aldrich, Munich, Germany, prod.nr.: 7542). After each digestion cycle, the remaining tissue fragments were resuspended in fresh enzyme solution. While the cell harvest obtained from the first incubation of 5 min is discarded, the four following fractions are centrifuged at 300 g for pooled resuspended cell harvest is pre-plated for 45 min. The non-attached cardiomyocyte-enriched cell suspension is further processed by another centrifugation step and resuspended in cell culture medium. After counting the final cardiomyocyte harvest using trypan blue staining (VWR, Radnor, Pennsylvania, cat.nr.: 97063-702) cells are directly used for repopulation experiments. For calculation of cell concentration, only the fraction of apparently large cells, were counted, while small cells were not considered. The ratio of large cells (representing cardiomyocytes) to small cells was determined to be greater than 80% for each suspension used for repopulation in this study.

Neonatal Cardiomyocyte Repopulation

One millilitre of neonatal cardiomyocyte cell suspension at a concentration of 5 10^6 cells per mL was injected into the ECM portioned into 0.1 mL increments scattered onto the area of the left ventricular (LV) wall using a needle of 0.4 mm in diameter. After seeding of neonatal cardiomyocytes, the repopulated decellularized whole-heart constructs (repopWHC) were incubated in a 6 well-plate with 10 mL cell culture medium for 24 h at 5% CO_2 and 37 C in a standard cell culture incubator (HERAcell 240i, Thermo Scientific, Waltham) to allow cellular adherence prior to further cultivation in the bioreactor. For comparative investigation of biomechanically stimulated constructs versus non-stimulated controls, pairs of repopWHC were repopulated by cells derived from the identical cell-pool and harvested from one single isolation.

Repopulated Whole-Heart Cultivation and Biomechanical Stimulation

After 24 h of incubation in 6-well-plates repopWHC were mounted into a customized modular bioreactor system and processed as previously described (Hülsmann et al., 2013, 2015). Briefly, each repopWHC is connected to an indepently running software-controlled coronary perfusion path via the pre-cannulated aorta. Coronary perfusion pressure was controlled at asetpoint of 70 mmHg for biomechanical stimulation each repopWHC is connected to an independently controlled stimulation unit based on an inflatable latex balloon (Radnoti LCC, California, —Size 4 or 5) that is inserted into LV chamber. Controlled inflation of the balloon is provided via a system consisting of a syringe pump (Tecan XLP 600, Tecan, Männedorf, Switzerland) for volume control, a membrane pump for controlled volume stroking (Sera RS 204.1– 1.2e Diaphragm Pump [Seybert und Rahier, Immenhausen, Germany] and a fast responding jumo p dTrans pressure transducer (Jumo, Fulda, Germany) to observe the pressure amplitude while stretching the LV. All perfusion paths and stimulation units are connected to an integrative process control system and thereby combined to a unified system as described previously (Hülsmann et al., 2013). Cultivation of repopWHC is performed under controlled coronary perfusion of cell culture medium for 96 h. Biomechanical stimulation was set to 10% longitudinal elongation of the construct at a frequency of 1 Hz.A total of 26 repopWHC were generated, of which 18 served in the frame of pre-experiments to validate the function and stability of the system and the applied assays. Eight repopWHC underwent pair wise cultivation with or without continuous biomechanical stimulation by LV stretching for direct comparison.

Metabolic Activity Assay

To assess the metabolic activity of repopWHC, we adapted the WST-1 proliferation agent[1] protocol (Roche Diagnostics GmbH, Mannheim, Germany, REF: 05015944001) to the whole-heart perfusion concept in order to allow repetitive measurements for direct comparison, as previously described (Hülsmann et al., 2013, 2015). Briefly, we prepared working solutions by diluting the WST-1 reagent in cell culture medium. Each repopWHC was perfused with 5 mL. After 1 h of incubation at 37 C and 5% CO_2 the assay product was washed out by perfusion of further 1 mL of pure cell culture medium. The perfusate was collected and absorption was measured at 440 nm. For relative assessment of metabolic activity decellularized but not-repopulated whole-heart scaffolds served as controls. Standard reagent concentra-tion was reduced to one fourth to ensure the repeatability on single repopWHC without assay-related impairment of vitality. The constructs were subjected to the assay repetitively immediately prior to mounting into the bioreactor and after 96 h of cultivation, respectively. Increase or decrease of metabolic activity after bioreactor cultivation was calculated and presented as a relative value expressed in percentage of the initial readout of freshly repopulated WHC (24 h after cell-injection) that was set to 100%. A total of n¼ 6 repopWHC representing three pairs, were subjected to metabolic activity assay.

Live/Dead Assay (Confocal Microscopy)

To provide a qualitative insight into the proportion of living versus dead cells in repopWHC prior to the bioreactor cultivation (24 h after repopulation) and subsequently (after additional 96 h of cultivation in the bioreactor) LV wall segments of repopWHC were dissected and subjected to calcein and ethidium homodimer staining to investigate cell survival and to estimate potential proliferation. Therefore, LV walls of repopWHC were dissected and subjected to calcein and ethidium homodimer staining (LIVE/DEAD[1] Vitality/Cytotoxicity Kit for mammalian cells; Thermo Fischer, Waltham, cat.nr: L3224) according to the manufacturers manual, incubating freshly separated LV wall in 250 mL staining solution at 37 C and 5% CO_2 for 30 min. Subsequently, stained LV wall specimens were analyzed by confocal microscopy using a Zeiss LSM 700 microscope (Carl Zeiss AG, Oberkochen, Germany) generating large area z-stacks in order to enable a broad insight to the spatial distribution of calcein versus ethidium signals. Quantitative analysis was performed by determining the fractions of calcein and ethidium signals using ImageJ (NIH). For Live/Dead assay four indepen-dent pairs of repopWHC were generated and subjected pair wise to bioreactor cultivation under stimulation versus non-stimulated control. Another set of four repopWHC were generated and subjected to analysis 24 h after repopulation. For each repopWHC three different injection sites were analyzed.

Evaluation of Myocardial Electrophysiological Activity

Local electrophysiological activity was scanned and recorded by applying whole repopWHC to a 2D 60EcoMEA-Glass Multielectrode Array (Multi Channel Systems MCS GmbH, Reutlingen, Germany). Data were monitored and recorded using systems belonging software MC_Rack— Version 4.5.16 field. N¼ 3 non-stimulated repopWHC were subjected to electrophysiological activity measur-ing directly after 96 h of bioreactor cultivation. Neonatal cardiomyocytes derived of the same isolation (cell-pool) were seeded on glas discs and cultivated in parallel to serve as controls. For electrophysiological voltage mapping dissected left ventricular walls of cultivated repopWHC and seeded glas discs were placed directly onto the 2D glass MEA. Therefore, the experimental setup is represented by a sandwich overlay of the constructs or galsdiscs on the MEA. Therefore, the contact is much weaker as compared to cells that were directly seeded on the MEA surface, but there is still an electrical connection via the thin liquid film of cell culture medium wetting the constructs and the glas discs surface.

Evaluation of Cellular Organization

To quantify cellular organization inside cultivated repopWHC, confocal images of the calcein AM stained repopWHC, that were prepared for Live/Dead assay (2.7) were subjected to graphical analysis of the circularity (C) and the spatial orientation angle (O), allowing a quantitative assessment of cellular alignment as previously described (Hülsmann et al., 2013, 2015). Briefly, histograms were generated to demonstrate the distribution of C and O. Clearly oriented cell fractions with colliding corresponding angle ranges can be summed up and defined as the fraction of oriented cell (FO). The FO was then normalized to its corresponding angle-range to calculate the specific orientation density (O.D.). In accordance to 2.7, a total n¼ 4 pairs of stimulated constructs versus corresponding non-stimulated controls as well as n¼ 4 repopWHC 24 h after injection, were subjected to the evaluation of their cellular OD. For each repopWHC three different injection sites were analyzed.

Evaluation of Gene Expression

RNA was prepared from four pairs of stimulated versus control repopWHC using the RNeasy Mini Kit (Quiagen, Hilden, Germany) according to the manufacturer's manual. N¼ 8 repopWHC, representing four pairs of stimulated versus unstimulated constructs were subjected to RNA isolation Entire repopWHC were snap-frozen in liquid nitrogen and pestled into powder. Powdered tissue samples were suspended in lysis buffer and further processed follwoing the manufacturer's protocol for tissue samples. RNA quality was analyzed by chip and one pair of constructs was omitted from further analysis due to low RNA quality, resulting in n ¼ 3 pairs subjected to qPCR. Isolated RNA was subjected to cDNA synthesis using the QuantiTect Reverse Transcription Kit (Quiagen, Hilden, Germany) according to the manufacturer's manual using a real-time cycler (StepOne Plus, Applied Biosystems, Foster City). The synthesized cDNA was subjected to real-time-polymerase chain reaction (qRT-PCR) to assess the expression levels of connexin 43 (Cx 43) relative

Table I. qRT-PCR primers for beta 2 microglobulin and connexin 43.

	Gene	NCBI reference sequence	Forward primer	Reverse primer
Gap junction protein, alpha 1 (connexin 43)	Gja1	NM_012567.2	GGTGTCCTTGGTGTCTCTCG	TTCTTCCCTTCACGCGATCC
Beta 2 microglobulin	B2m	NM_012512.2	ACTGAATTCACACCCACCGA	TACATGTCTCGGTCCCAGGT

to b2 microglobulin as housekeeping gene. Used primers were selected from the National Center for Biotechnology Information (NCBI) database (Table I). Recorded values were processed and analyzed using the DDCT method, representing relative increase or decrease of expression levels directly by the evaluation of the ratios between stretched samples and their corresponding non-stretched controls.

Western Blot

Loading and washing elutes produced by RNA isolation (see Evaluation of Gene Expression) were collected and processed according to the method described by Morse et al. (2006) in order to recover the protein fraction. Thereby, obtained protein pellets were re-dissolved in 8 M Urea supplemented with 1% SDS and analyzed using the Biorad DC Protein Assay according to the manufacturer's manual. SDS PAGE was performed with 10 mg protein per lane following the Laemmli method using 10% and 12% gels (Laemmli, 1970). Gels were subjected to Western blotting.

Western blot transfer was performed using a Bio-Rad Mini-Trans-Blot-Cell (Bio-Rad, Munich, Germany) onto polyvinylidene fluoride (PVDF) membranes. For immunodetection an antibodyagainst cardiac myosin heavy chain (MHC) (Abcam, Cambridge, UK, cat.nr.: ab50967) was used in combination with an Alexa 488 conjugated secondary antibody (Invitrogen, Carlsbad, CA, cat.nr.: A11029). For reference, total protein content was stained using Flamingo^{TM}fluorescent gel stain (Bio-Rad, Hercules, CS) according to the manufacturer's manual but applied to the membrane. The membrane was digitalized using an Amersham Imager 600 (GE Healthcare, Little Chalfont, UK). Densitometric analyses were performed using ImageQuant TL software (GE Healthcare, Little Chalfont, UK). Thereby for each detected band the computed integrated optical density units (IOD) were normalized to the protein signal of the corresponding lane. Relative increase or decrease of signals is represented directly by evaluation of the ratios

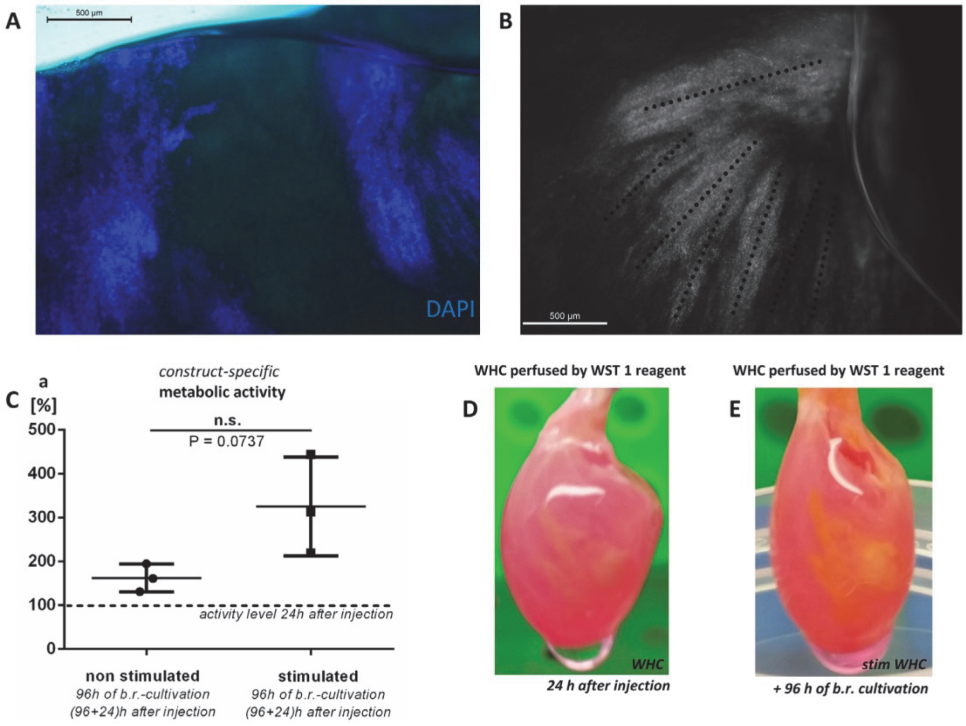

Figure 1.Repopulation and metabolic activity. (A) DAPI stained LVW of repopWHC. Spatially widespread DAPI signal (blue) indicates injected cells with a high depth ofinfiltration into the matrix cavity. (B) Differential spatial spreading of injected cells in the LVW of repopWHC. Image from a representative DAPI stained cross section has been converted to grayscale to highlight the spatial distribution of the cells. Dashed lines illustrate the main axes of different clustered strands. (C) The diagram depicts the gain of measured absorbance of the applied WST-1 stain after 96 h of bioreactor cultivation relative to the initial activity as measured 24 h after injection for stimulated versus non-stimulated constructs. (D and E) Repopulated and metabolic active areas become macroscopically visible after staining by WST-1 reagent.

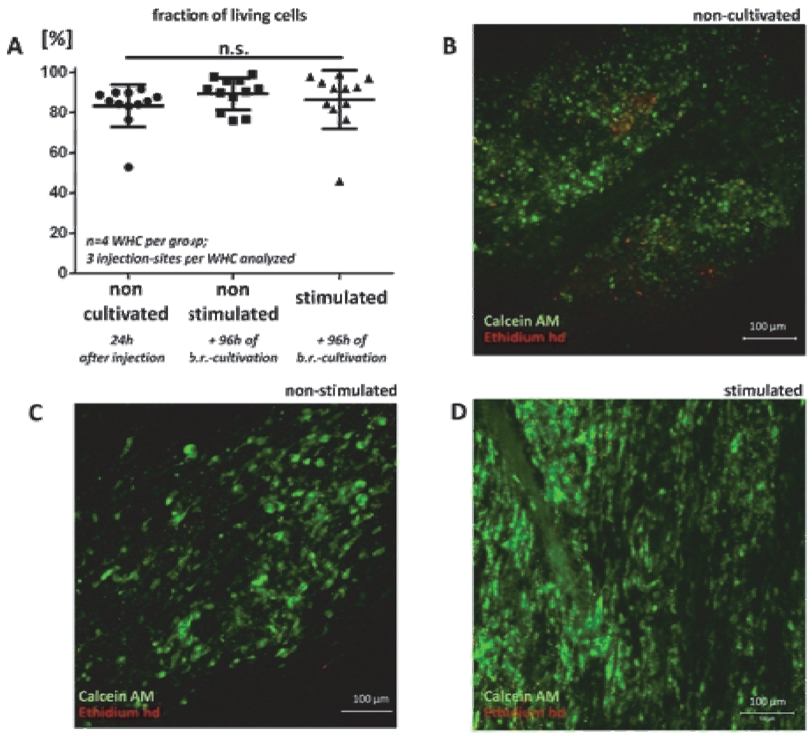

Figure 2.Cellular vitality of repopWHC. (A) Quantitative evaluation of the fractions of living and dead cells. At 24 h after injection living cells account for 83.3 10.4%, of all cells,with an increase to 89.3 8% and 86.5 15% after additional 96 h of static cultivation (non-stimulated) or cultivation with biomechanical stimulation of the left ventricle (stimulated), respectively. High cell vitality showing vast infiltration of the ECM. (B–D): Representative confocal images of LIVE/DEAD staining of LV specimens of repopWHC after 24 h of repopulation (B), and after additional 96 h of bioreactor cultivation under static conditions (C), or under LV biomechanical stimulation (D), respectively. Green, vital cells; red, non-vital cells.

between stretched samples and their corresponding non-stretched controls. A total of four pairs of stimulated versus unstimulated constructs were subjected to Western blotting.

Immuno-Fluorescence (IF) Staining

Repopulated and cultivated constructs were stained using primary antibodies (AB) against cardiac (MHC; Abcam Cambridge, UK, cat. nr.: ab50967) and connexin 43 (Cx43; Sigma–Aldrich, St. Louis, cat. nr.:C 6219). For detection, we used secondary AB conjugated with Alexa Flour 546 or 488 (Invitrogen, Carlsbad, cat.nr.: A11030 and A11070), respectively. Therefore, repopWHC were fixed in 4% paraformaldehyde and 10 % sucrose buffered in phosphate buffered saline (PBS) for 2 h and subsequently washed for another 2 h in PBS. Repopulated left ventricular walls (LVW) were dissected and permeabilized in 0.2% triton x 100 for 20 min on ice. Afterwards, LVW were blocked in 5% PBS buffered fetal calf serum þ2% bovine serum albumin (BSA) for 1 h at room temperature. Primary antibodies were added and incubated over night at 4 C at dilutions of 1:500 for both Cx43 and MHC in blocking buffer. Subsequently, LVW were washed three times for 5–10 min in blocking solution before fluorescence conjugated secondary antibodies were added and incubated for 1 h at dilutions of 1:500 for both secondary AB in blocking buffer at room temperature. After another washing sequence (3 times for 10 min in PBS) stained LVW were examined using a fluorescence microscope system (Leica DM 200; Leica Microsystems, Wetzlar, Germany) or a confocal microscope system (Zeiss LSM 700; Carl Zeiss AG, Oberkochen, Germany). For additional DAPI staining, IF stained LVW were incubated in Vectashield Antifade Mounting Medium with DAPI over night at 4 C (Vector Laboratories Inc., Burlingame, CA).

Statistics

Data are presented as mean standard deviation for all measured and calculated values. For direct group comparisons, Student's t-tests were performed. Statistical significance was assumed for P-values lower than 0.05. Data analysis was realized using GraphPad Prism 6 (GraphPad Software, San Diego, CA).

Results

Neonatal Cardiomyocyte Repopulation of Whole-Heart Scaffolds

Successful repopulation of LV of decellularized whole-heart scaffolds with rodent neonatal cardiomyocytes was visually confirmed by DAPI staining of cultivated repopWHC (Fig. 1A). The allocation of nuclei in the matrix illustrates a clear and wide spatial spreading of the injected cells (Fig. 1A). It further can be

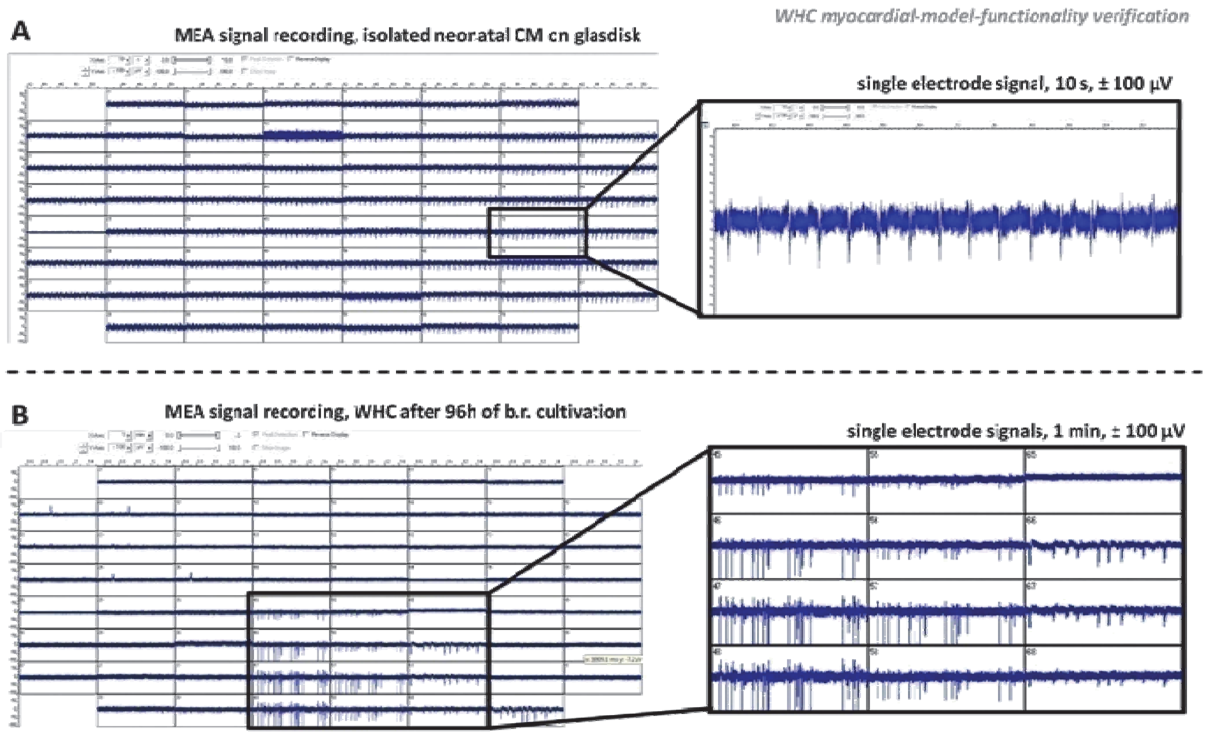

Figure 3.Myocardial functionality of the repopWHC model. (A) Electrophysiological voltage mapping of isolated neonatal cardiomyocytes as control in a multielectrode array(MEA) set-up. Isolated neonatal cardiomyocytes were seeded on glasdiscs and put onto a 2D glass MEA. (B) Electrophysiological voltage mapping of cultivated repopWHC using the same experimental set-up. The presence of functional, electrophysiologal active cardiomyocytes can be detected by patterns of spontaneous frequent activity.

observed that these cell structures populate distinct adjacent compartments of the ECM and thereby invade the scaffold's microarchitechture. (Fig. 1B).

Metabolic Activity, Cell Vitality, Myocardial Functionality, and Cellular Organization of Neonatal Cardiomyocyte Repopulated Whole-Heart Constructs

Metabolic Activity of repopWHC

Repetitive WST-1 assay demonstrated, an increase of 162 32% in metabolic activity of repopWHC after 5 days of cultivation as compared to their initial activity measured 24 h after injection. (Fig. 1C). For stimulated repopWHC there was a further trend to increased metabolic activity to a level of 326 113% (P¼ 0.737). The colorimetric emergence of the WST-1 product inside the ECM was even macroscopically visible on selective areas of the LV suggesting densely repopulated areas (Fig. 1D and E).

Cellular Vitality of repopWHC

Live/dead staining of repopWHC with calcein and ethidium homodimer, and subsequent 3D confocal microscopy analysis 24 h after repopulation showed vast infiltration of the ECM with cells, evenly distributed and at high cell density throughout the whole thickness of the respective LV wall (Fig. 2). Although, a high cell vitality could be observed with a fraction of 83.3 ± 10.4 % at vast large scale calcein-stained cell clusters continuously organized throughout the ECM (Fig. 2B), there were also non-vital, ethidium-stained cells visible, either isolated between the vital cell fractions, or in non-vital cell clusters (Fig. 2B). After bioreactor cultivation, this value was not significantly altered as compared to pre-cultivation values, neither for biomechanically stimulated constructs nor for non-stimulated controls (86.5 15% vs. 89.3 8% living cells in stimulated vs. non-stimulated cultures, respectively, P> 0.5). Moreover, all cultures revealed similar distributions of living versus dead cells.

Specific Myocardial Functionality of the repopWHC Model

Local electrophysiological activity was indicated by surface potentials obtained from repopWHC by 2D MEA field. The signals show spontaneous frequent patterns in similarity to signals obtained from 2D monolayers of isolated neonatal cardiomyocytes, which served as control. The signals are regionally conducting over a small area as sensed by adjacent electrodes. Using this experimental set-up, detected signal-amplitudes reached values of up to about 100 mV, thereby regionally clearly exceeding the amplitudes of the control, that reveals constantly a value of about 40 mV (Fig. 3).

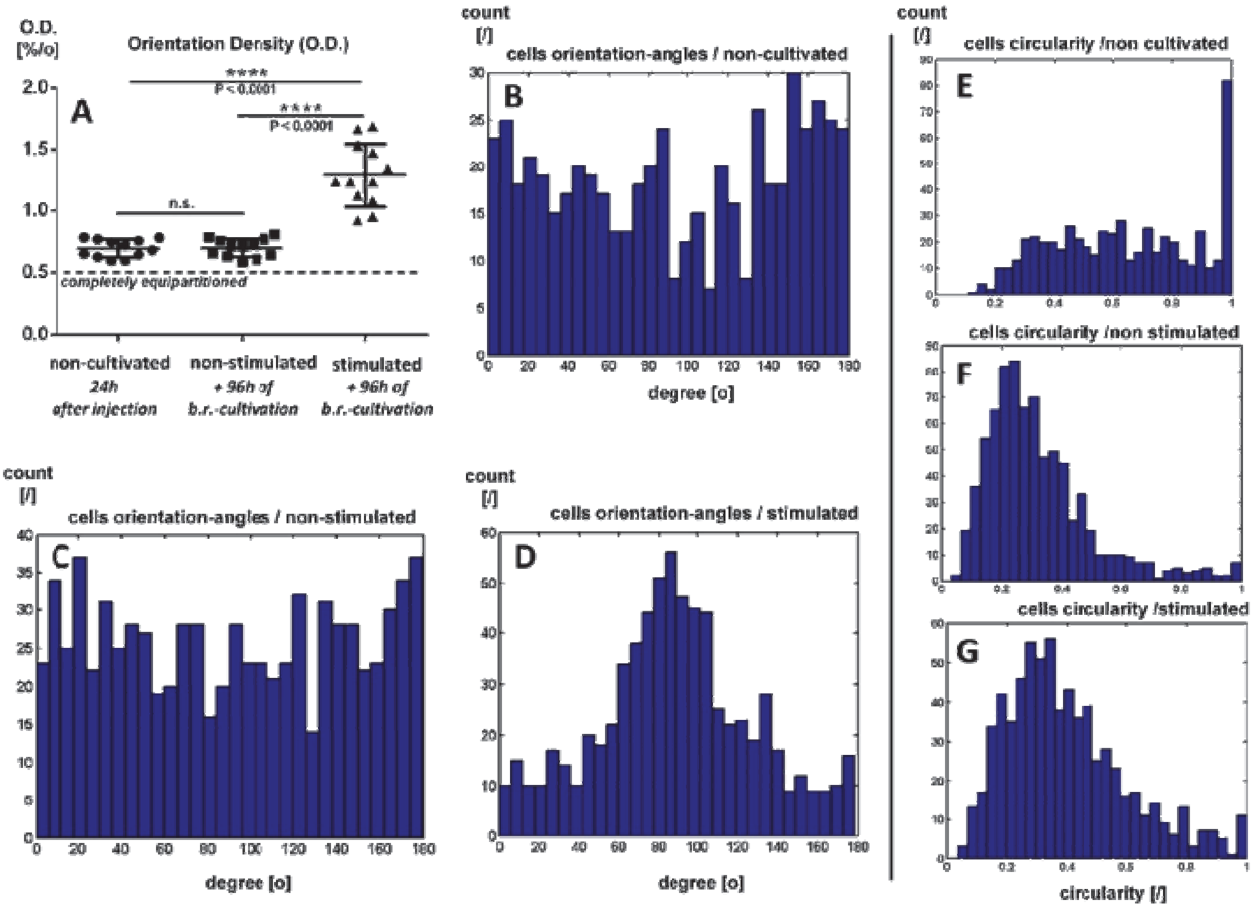

Figure 4.Cellular organization of repopWHC. (A) Orientation density (OD) of living cells inside was calculated for freshly repopulated WHC in contrast to repopWHC after 96 h ofcultivation under biomechanical stimulation versus non-stimulated (static) controls. (B–D) Histograms demonstrate the distribution of measured angles of orientation of cells in freshly repopopulated WHC (B), and in repopWHC cultivated under control conditions (C) versus stimulated conditions (D). (E–G) Histograms demonstrate the distribution of measured circularity of cells in freshly repopoulated WHC (E), and in repopWHC cultivated under control conditions (F) versus stimulated conditions (G).

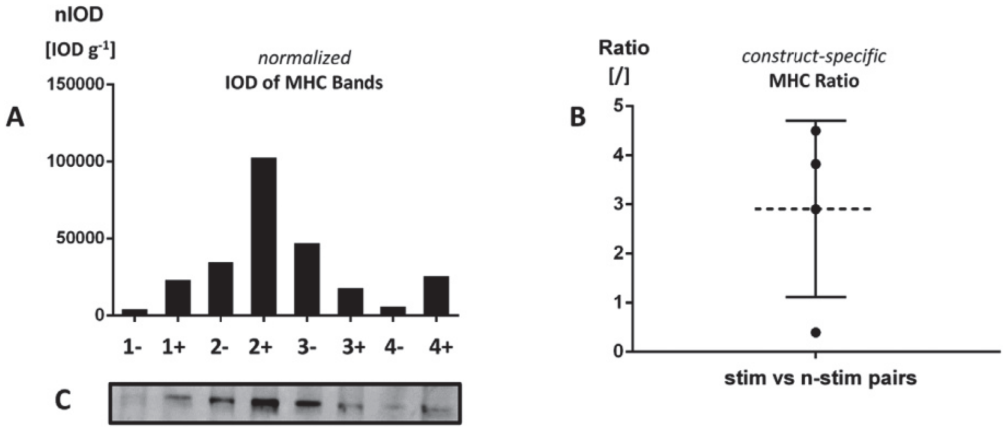

Figure 5. Densitometric evaluation cardiac myosin heavychain (MHC) blot signals: (A) The diagram shows the relative MHC signal intensity in normalized IOD [IOD g^{1}] of the WHCs. Levels 1–4 identifies the different pairs, while (+) indicates the stretched repopWHC, and (-) the non-stretched control of each pair. (B) The diagram shows the total protein signal intensity of the 223 kDa protein band, what represents the molecular weight of MHC. (C) Depiction of the corresponding MHC-blot-bands.

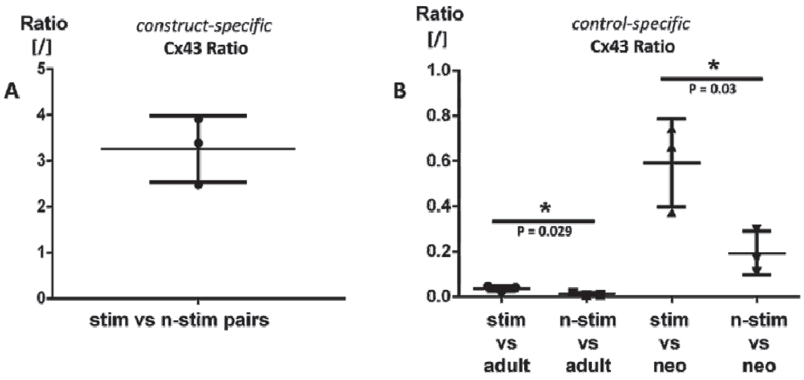

Figure 6. Selective gene expression of repopWHC. (A) Relative expression level of connexin 43: Pair wise comparison of Cx43 expression for stretched repopWHC versus non-stretched control. For all pairs the stretched repopWHC exhibit at least a 2.5-fold increased Connexin 43 expression with an average of more than 3. (B) Ratio of Connexin 43 expression in contrast to adult and neonatal native controls: Ration of Cx43 expression in repopWHC with or without biomechanical stimulation and with respect to adult and neonatal native controls.

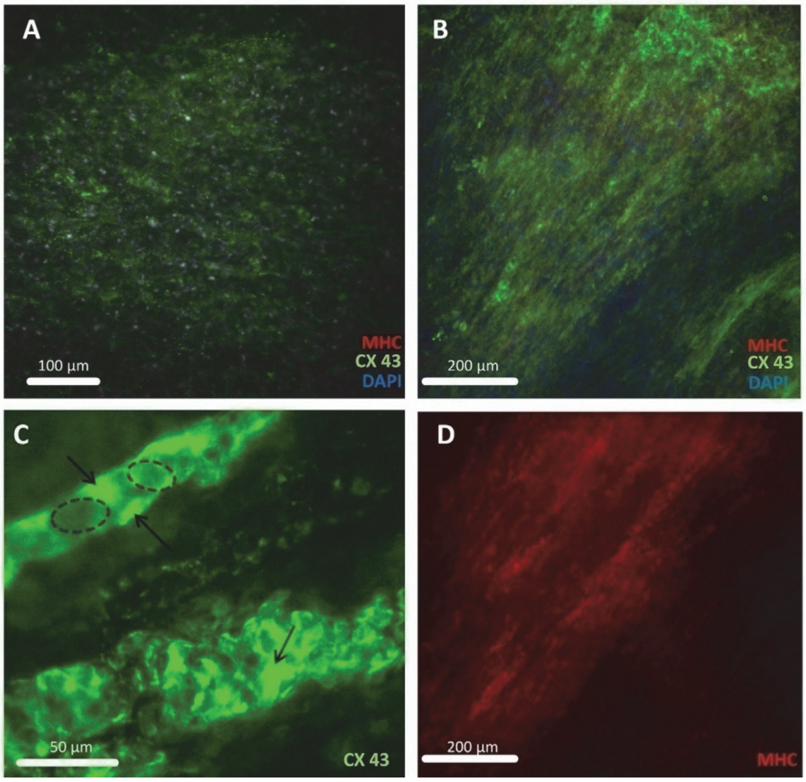

Figure 7. Immunodetection of Cx43 and MHC in repopWHC. Fluorescence microscopic image of immune stained whole left ventricular walls. (A) Non-stimulated repopWHC.Cx43 signals appear in a grainy pattern located in spots, surrounding cell bodies. (B) Stimulated repopWHC. Here, the Cx43 signals appear more intense and more densely distributed all over the repopulated area. The signal arrangement further displays the patterns of oriented strands that get superposed by DAPI stained nucleic structures. (C) Stimulated repopWHC at higher magnification. Cx43 signals appear as a conjunctive interstice (indexed by black arrows) between cell bodies, that can be distinguished by the shadow-nuclei (indexed by blue dashed circles), (D) Single image of the 546 nm channel corresponding to the overlay in B showing the isolated MHC signal for stimulated repopWHC. The MHC signal is present in the Cx43 positive areas, when compared to B.

Cellular Organization of repopWHC

After 96 h of cultivation in the bioreactor system, non-stimulated repopWHC showed a non-altered degree of organization as compared to constructs 24 h after repopulation with a O.D. of 0.7 0.07 [%/] in contrast to 0.69 0.07 [%/]. For biomechanically stimulated constructs the degree of organization revealed to be significantly increased to an O.D. of 1.28 0.26 [%/] (P< 0.0001) (Fig. 4A). While, in non-cultivated (24 h after repopulation) and non-stimulated controls the underlying confocal analysis of cellular orientation angles revealed an almost equal distribution, biomechanically stimulated repopWHC showed concentrated histograms with recognizable FOs (Fig. 4B–D). Concerning the cellular circularity freshly populated and non-cultivated constructs showed mostly equally distributed histo-grams revealing a spike of completely rounded cells at a circularity of one (Fig. 4E). In contrast, both stimulated constructs and non-stimulated controls showed a high concentration of elongated cells at circularities ranging from 0.2–0.4 (Fig. 4F and G).

Protein Characteristics of Neonatal Cardiomyocyte Repopulated Whole-Heart Constructs

Cardiac Myosin Heavy Chain

Western blot analysis revealed the presence of cardiac MHC in 3 out of 4 repopulated pairs of repopWHC after 96 h of cultivation in the bioreactor system. Direct comparison of MHC IOD values of stretched versus non-stretched repopWHC pairs, demonstrated a noticeable increase of MHC in 3 out of the 4 pairs (Fig. 5A and C). While those 3 pairs exhibited ratios of 2.9, 3.8, and 4.5 indicating an increase of up to 450% for the stimulated repopWHC, the fourth pair showed a ratio of only about 0.39, indicating that the MHC content was about 60% less in the stretched repopWHC as compared to its direct non-stretched control.

Selective Gene Expression of Neonatal Cardiomyocyte Repopulated Whole-Heart Constructs

Expression of Connexin 43

Gene expression analysis revealed a significant increase of connexin 43 (Cx43) expression in repopWHC cultivated under continuous biomechanical stimulation in the bioreactor system, as compared to non-stimulated controls. In direct comparison of stretched versus non-stretched repopWHC pairs a mean 3.3 0.7 -fold increase of Cx43 expression was observed, as a response to LV stretching during the bioreactor cultivation (Fig. 6A).

Contrasted to native neonatal myocardium as control, Cx43 expression of repopWHC cultivated under continuous biomechani-cal stimulation in the bioreactor system compared to about 60% of Cx43 expression of rodent neonatal myocardium, while non-stretched controls demonstrated only 20% of the native expression levels (0.59 0.19 vs. 0.19 0.09 of Cx43 gene expression of native neonatal rat hearts, P¼ 0.03). However, when compared to Cx43 expression levels observed in rodent native adult myocardium all repopWHC remained at yet negligible gene expression levels (Fig. 6B)

Immunofluorescent Detection of Cx43 and MHC in repopWHC

Cx43 signals occur grainy and located bordering to the cellular bodies, but rather equally distributed than highly organized in non-stimulated constructs after 96 h of bioreactor cultivation (Fig. 7A). For stimulated constructs, the signals appear denser and regionally highly concentrated (Fig. 7B). At higher magnitudes cells appear fractionated and moderately organized in strands. The Cx-43 signals appear as a conjunctive interstice in between the cell bodies (Fig. 7C). The MHC signal was too low to be visualized in the whole LVW of the non-stimulated constructs (Fig. 7A) but it could be detected in the stimulated specimens (Fig. 7B and D). Both MHC and CX43 signals appeared as oriented in strands that superpose the location of DAPI signals.

Discussion

After introducing the concept of integrated 3D LV stretching in a customized whole-bioreactor system in the recent past (Hülsmann et al., 2013, 2015), we now sought to evaluate the impact of such a system on myocardial maturation within an integrative cultivation approach and using a cardiac cell source. For this purpose, we analyzed short-term model-cultivations of decellularized whole-heart constructs repopWHC.

Neonatal cardiomyocytes may probably not present an ideal cell type for the generation of clinically relevant engineered myocardial tissues due to a variety of reasons, including availability and proliferation capacity. And yet, neonatal rat cardiomyocytes are still widely used for fundamental research in the context of myocardial tissue engineering (Lux et al., 2016; Noguchi et al., 2016), as they are pre-destinated to mature to adult myocardial cells in vivo. Due to the high complexity of functional myocardium and the implications thereof for whole-heart tissue engineering, innovative cultivation strategies need to transfer and unify both proven and established concepts of myocardial tissue engineering into a holistic cultivation approach in vitro. Thus, neonatal cardiomyocytes are an appropriate choice for the optimization of bioprocessing strategies within the whole-heart engineering approach, as they may mature to functional myocardium under optimal environmental conditions, but can also dedifferentiate if cultivation setting and processing is inadequate (Hülsmann et al., 2015).

The findings of this study demonstrate that neonatal cardiomyocytes can successfully be cultivated within 3D whole-heart scaffolds with completeness and quality of decellularization demonstrated in previous work (Akhyari et al., 2011; Aubin et al., 2013). Here, the employed repopulation technique led to viable, connected, and widespread cell aggregations within the ECM of the whole heart scaffolds, apparently adopting the microarchitecture of the scaffolds and resembling its conserved spatial patterns of myocardial cords after in vitro cultivation. Multielectrode mapping of voltage-signals further showed that the whole heart scaffolds preserved the electrophysiological activity of cardiomyocytes and thereby gained fundamental myocardial functionality after repopulation and subsequent cultivation. Thereby, the presented constructs fulfill the basic requirements of a biological model system to investigate the impact of various biophysical stimulation and bioprocessing techniques. More importantly however, our findings suggest that the maturation process of neonatalcardiomyocytes into functional myocardium may be identified and controlled following an integrative cultivation approach, for example by implementation of integrated LV stretching as a key biomechanical stimulus. Here, the previously reported effects of 3D biomechanical stimulation on cellular organization in whole-heart constructs could be reproduced using a neonatal cardiomyocyte cell source (Hülsmann et al., 2013). Indeed, the metabolic activity could be markedly increased by biomechanical stimulation. Interestingly, in comparison to previous data reported for C2C12 cells, the non-stimulated controls develop a gain in metabolic activity of similar dimensions, while for the stimulated constructs the trend is contradictive between neonatal cardiomyocytes and C2C12 cells (Hülsmann et al., 2013). In this study, additional Live/Dead assay showed no alteration in the relation of vital to dead cells neither after 96 h of non-stimulated cultivation in contrast to freshly repopulated WHC, nor in comparison between stimulated constructs and their corresponding non-stimulated controls. Although it cannot be excluded that the increase in metabolic activity could have been caused by proliferation of non-cardiomyocytes, the higher level of spatial organization of the cardiomyocytes cultivated under mechanical stimulation may still indicate an increased level of cellular activity as compared to the non-stimulated controls.

Therefore, the obtained results widely confirm the suitability of the integrative 3D LV stretching approach, which by now has also been adopted by others and integrated into larger scale whole-heart bioreactors (Guyette et al., 2016). However, —as demonstrated in this study—specific myocardial tissue remodeling in repopWHC was not only enhanced by promoting cellular organization but also through adaptive modulation of protein and gene expression. Western blot analysis showed increased MHC signals in 3 out of 4 directly compared stretched versus non-stretched repopWHC pairs. Overall this results in a threefold gain in developing MHC, as a key-marker for functional sarcomeric proteins, by the impact of biomechanical stimulation.

Remarkably, the observed gene expression pattern of repopWHC showed that 3D LV stretching might also have particular implications for the conductive apparatus of neonatal cardiomyo-cytes cultivated within whole-heart scaffolds. Consistent to the functional assessment, significantly increased Cx43 gene expression in stretched repopWHC may translate into structural tissue integrity and functionality. On the histological level, immuno-staining of whole left ventricular walls confirmed these findings favoring biomechanically stimulated constructs. For non-stimu-lated constructs the Cx43 signals seemed to be grainy and rather distributed bordering the cells. In contrast MHC signals were too weak to be detected. However, in stimulated constructs Cx43 signals appeared more densely and organized as a conjunctive interstice in between the cells and clear MHC signals were detected (Fig. 7C). Conforming to the findings derived by calcein AM staining, MHC, and Cx 43 signals were oriented in strands and closely localized to DAPI signals. In general, it should be taken into account, that IF staining of the whole left ventricular wall represents a relatively coarse method for additional cross-check and confirmation of our previous findings, than as a precise histological evaluation.

Especially concerning intracellular sarcomeric proteins, such as MHC, the permeabilization, and diffusion conditions would have to be optimized for more precise evaluations.

As in previous studies with bioreactor assisted stretching of neonatal cardiomyocytes repopulated in hydrogels, an impact of mechanical stimulation on Cx43 expression has remained inconsistent. A stimulation effect on Cx43 has proven not-detectable on collagen-I- and matrigel-based hydrogels (Kensah et al., 2011), while in fibrin-based hydrogels an increased expression has been shown (Salazar et al., 2015). Beyond these results from constructs based on artificial scaffold systems, the native-like environment of a whole-heart scaffold may represent an additional trigger that may potentially be amplified by the additional 3D stretching. In the current experimental setting and in contrast to previously published results in hydrogel scaffolds, the complex macro- and micro-architecture of native ECM may warrant a more variant and anisotropic mechanical stimulation to the cells.

These results, although promising in terms of promoting myocardial tissue remodeling within an integrative cultivation approach, still illustrate the need for optimization of the bioprocessing concept. Furthermore, development and implementation of screening tools for myocardial tissue remodeling as a part of integrative bioreactor systems represent urgent challenges in order to guide whole-heart tissue engineering towards clinically more relevant stages. Therefore, this is only a first step, as further studies are warranted in order to gain more insights into engineered myocardial tissue development and their integration into holistic whole-heart cultivation concepts.

Conclusion

This study illustrates the impact on myocardial maturation of 3D LV stretching within a customized whole-heart bioreactor system employing an integrative cultivation approach by analyzing short-term model-cultivations of decellularized whole-heart constructs repopulated with neonatal cardiomyocytes. The results of this study suggest that following such an integrative cultivation approach cardiac maturation can be enhanced not only by promoting cellular organization but also through adaptive modulation of protein and gene expression with particular implications for the formation of the conductive apparatus. Further, this study emphasizes the importance to optimize bioprocessing strategies within sophisti-cated bioreactor systems as tools for customized stimulation and cultivation of tissue engineered tissues and organs.

This work is funded by institutional grants from the Department of Cardiovascular Surgery, Medical Faculty of the Heinrich-Heine-University, and by the Susanne Bunnenberg-Stiftung at the Düsseldorf Heart Center. The authors also acknowledge a stipend from Schmeil-Stiftung (Heidelberg, Germany) to Jörn Hülsmann.

References

Akhyari P, Aubin H, Gwanmesia P, Barth M, Hoffmann S, Huelsmann J, Preuss K, Lichtenberg A. 2011. The quest for an optimized protocol for whole-heart decellularization: A comparison of three popular and a novel decellularization technique and their diverse effects on crucial extracellular matrix qualities. Tissue Eng Part C Methods 17(9):915–926.

Aubin H, Kranz A, Hülsmann J, Lichtenberg A, Akhyari P. 2013. Decellularized whole heart for bioartificial heart. In: Dr. John Walker, Race L. Kao, editors. Cellular Cardiomyoplasty: Methods and Protocols, Methods in Molecular Biology. New York, NY: Springer Science + Business Media.

Guyette JP, Charest J, Mills RW, Jank B, Moser PT, Gilpin SE, Gershlak JR, Okamoto T, Gonzalez G, Milan DJ, Gaudette GR, Ott HC. 2016. Bioengineering human myocardium on native extracellular matrix. Circ Res 118(1):56–72.

Hülsmann J, Aubin H, Kranz A, Godehardt E, Munakata H, Kamiya H, Barth M, Lichtenberg A, Akhyari P. 2013. A novel customizable modular bioreactor system for whole-heart cultivation under controlled 3D biomechanical stimulation. J Artif Organs 16(3):294–304.

Hülsmann J, Aubin H, Wehrmann A, Jenke A, Lichtenberg A, Akhyari P. 2015. Whole-Heart construct cultivation under 3D mechanical stimulation of the left ventricle. Methods in molecular biology. Totowa, NJ: Humana Press.

Kensah G, Gruh I, Viering J, Schumann H, Dahlmann J, Meyer H, Skvorc D, B€ar A, Akhyari P, Heisterkamp A, Haverich A, Martin U. 2011. A novel miniaturized multimodal bioreactor for continuous in situ assessment of bioartificial cardiac tissue during stimulation and maturation. Tissue Eng Part C Methods 17(4):463–473.

Laemmli UK. 1970. Cleavage of structural proteins during the assembly of the head of bacteriophage T4. Nature 227(5259):680–685.

Lux M, Andree B, Horvath T, Nosko A, Manikowski D, Hilfiker-Kleiner D, Haverich A, Hilfiker A. 2016. In vitro maturation of large-scale cardiac patches based on a perfusable starter matrix by cyclic mechanical stimulation. Acta Biomater 30:177–187.

Masuda S, Shimizu T. 2016. Three-dimensional cardiac tissue fabrication based on cell sheet technology. Adv Drug Deliv Rev 96:103–109.

Morse S, Shaw G, Larner S. 2006. Concurrent mRNA and protein extraction from the same experimental sample using a commercially available column-based RNA preparation kit. Biotechniques 40(1):54–58.

Noguchi R, Nakayama K, Itoh M, Kamohara K, Furukawa K, Oyama J, Node K, Morita S. 2016. Development of a three-dimensional pre-vascularized scaffold-free contractile cardiac patch for treating heart disease. J Heart Lung Transplant 35(1):137–145.

Ott HC, Matthiesen TS, Goh S, Black LD, Kren SM, Netoff TI, Taylor DA. 2008. Perfusion-decellularized matrix: Using nature's platform to engineer a bioartificial heart. Nat Med 14(2):213–221.

Salazar BH, Cashion AT, Dennis RG, Birla RK. 2015. Development of a cyclic strain bioreactor for mechanical enhancement and assessment of bioengineered myocardial constructs. Cardiovasc Eng Technol 6(4):533–545.

Tandon N, Cannizzaro C, Chao PG, Maidhof R, Marsano A, Au HTH, Radisic M, Vunjak-Novakovic G. 2009. Electrical stimulation systems for cardiac tissue engineering. Nat Protoc 4(2):155–173.

Zimmermann W. 2001. Tissue engineering of a differentiated cardiac muscle construct. Circ Res 90(2):223–230.

3.5. Bioreactor Design for Electrophysiological Stimulation of Whole Heart Constructs

Electrophysiological Stimulation of Whole Heart Constructs in an 8-pole Electrical Field*

** pre-print version*

Introduction: This study demonstrates the impact of three-dimensional electrophysiological stimulation of tissue engineered whole heart constructs (WHC) in a self-developed eight-pole electrical field stimulation system on short model cultivations with neonatal rat cardiomyocytes (CM).

Methods: WHC were generated by repopulation of decellularized rat hearts with neonatal CM and subjected to perfusion based cultivation with or without the subjection to biophysicalstimulation for 96 h. Spontaneous electrophysiological (EP) activity of the processed WHC was analyzed by qualitative evaluation of multielectrode assay (MEA) signal sequences,descriptive comparative spike sorting, and direct contrasting assessment in simple numerical quantities complemented by impulse response tests after phasing out spontaneous EP activity. Following the observation of a strong reduction ofvoltage signals by dECM, the active principle was determined and used to estimate the spectrum of source signals to recorded values by calculative elimination. Western blotting of key myocardial markers was employed to substantiate the functional EP evaluation by classic biochemical analysis.

Results: We observed stable spontaneous EP activity showing clear R and S, but predominantly rS patterns, for both stimulated WHC and non-stimulated controls. By the impact of stimulation mean voltage amplitudes and beating frequencies could be significantly increased. The active principle of signal reduction in dECM could be shown to follow a nonlinear damping function with good accuracy, illustrating that recorded signals of moderate voltage amplitudes can also represent far-field measurements of strong signals that are emitted in distant depths of the ECM while small amplitudes are limited to actually represent also rather weak source-signals. After phasing out spontaneous activity, both stimulated WHC and non-stimulated controls could be excited again to emit immediate impulse responses. The observedbeneficial impact of 8-pole field stimulation to functional EP activity could finally be validated on the biochemical level by showing increased ratios for myosin heavy chain, cardiac tropnin T, desmin and connexin 43 for stimulated WHC by Western blot analysis.

Conclusion: Although electrophysiological stimulation has been incorporated into whole heart TE concept from the very beginning, this study presents for the first time a concept for the transfer of electrical field stimulation to the whole heart tissue engineering approach. Furthermore to the best knowledge of the author, this is the first control-based study showing a comparative investigation of electrophysiological stimulation of whole heart constructs.

1) Introduction

In the field of whole organ engineering and especially for whole heart constructs (WHC) at the actual state of the art one of many challenges still is to overcome technical obstacles to transfer processing and stimulation concepts that gained acceptance in 2D and 3D myocardial models [1, 2]. By its pioneering work, Ott and colleagues have shown the fundamental corner-stones presented by a bioreactor system to provide perfusion-culture of the WHC and a biophysical stimulation concept providing organ-typical physiological effects [3]. For biophysical simulation of WHC the application of current injection by directly inserted or contacted electrodes has shown promising results [3, 4]. Additional to this, we were able to show the impact of whole left ventricular stretching as another key-stimulus in the recent past [2, 5, 6]. Simultaneously we believe that biophysical stimulation and processing of WHC should be incorporated in a modular and integrative process control system to enable the development and optimization of holistic WHC cultivation strategies and presented this in an adaptive bioreactor system [1, 6]. Here we show a concept for electrical field stimulation for the whole heart approach as an alternative electrical stimulation principle to the direct current injection to the construct applied in our bioreactor system. Today electrical field stimulation is a proven and established concept in myocardial tissue engineering that has been applied to various combinations of cell-scaffold constructions [7-12]. Here we picked up recommended parameters and arranged this in a three-dimensional 8-pole electrical field surrounding and permeating the WHC in the bioreactor [11].

2) Methods

2.1) Whole Heart Scaffolds

Whole rat hearts were subjected to semi-automatic detergent-perfusion-based decellularization at a regulated perfusion pressure of 70 mmHg as previously described [13, 14]. Thereby donor hearts from male Wistar rats (400–500 g) were used to produce whole heart scaffolds in a standardized series.

2.2) Cell Culture and Repopulation of WHC

Neonatal cardiomyocytes were isolated using the two-day Worthington Protocol. Therefore freshly gained hearts of 1–3 days old Wistar rats were initially prepared by removing the basal third of the donor hearts and quartering of the separated ventricular myocardial tissue. The cut pieces were then incubated in trypsine-blend (Thermo Fisher Scientific, Waltham, MA, USA, cat.nr.: 27250-018) at 1:250 dilution in HBSS (Thermo Fisher Scientific, Waltham, MA, USA, cat.nr.: 14170-138), in a 50 ml falcon over night at 4°C under continuous rolling at 20 rpm using a tube roller (Starlab, Hamburg, Germany). The next day the pre-digested pieces were washed in HBSS for 5 min at room temperature before subjection to a fractionated incubation in collagenase II (Worthington Biochemical Corp., Lakewood, NJ, USA, KN: X5C7962) at 125 U/ml diluted in HBSS. Therefore the heart quarters were incubated 4 times for 15 min each at 37°C using 10 ml of collagenase II solution. After each incubation cycle, the preparation was filtered using 100 µm cell strainer (Corning, New York, USA, cat.nr.: #352360) and the liquid-phase was collected in 10 ml of cold cell culture medium, what is composed by DMEM (Thermo Fisher Scientific, Waltham, cat.nr.: 10567014) supplemented with 10 Vol% fetal calf serum (Sigma– Aldrich, München, Germany, prod.nr.: 7542) and antiobiotics. Subsequently all fractions were centrifuged at 300 g for 6 min to pellet the isolated cells. The pellets were resuspended and pooled for depletion of fibroblasts by pre-plating incubation in 30 ml of cell culture medium for 45 min at 37°C using a T175 cell culture flask in a CO_2 Incubator (HERAcell 240i, Thermo Scientific, Waltham). For harvesting the resulting cardiomyocyte-enriched cell population, the suspension was then further subjected to another centrifugation step followed by resuspending of the pellet in fresh in cell culture medium. For calculation of the yielded cell number the harvest was counted using trypan blue staining (VWR, Radnor, Pennsylvania, cat. nr.: 97063-702). Thereby only contrastable large cells were counted, while small cells were recorded but not considered. Only preparations resulting in a ratio of large cells (representing cardiomyocytes) to small cells of greater than 80% were used for repopulation.

Whole Heart Constructs (WHC) were then prepared as previously described [2, 5]. Briefly, a volume of 1 ml cell-suspension was injected to each whole heart scaffold at a concentration of 5 10^6 cells per ml in 0.1 ml increments portioned to 10 injection-sites in the area of the left ventricular wall (LVW) using a needle of 0.4 mm in diameter. Thereby generated WHC were pre-incubated by insertion into a 6 well-plate with 10 ml cell culture medium for 24 h at 5% CO_2 and 37 °C prior to cultivation and processing in the bioreactor. To enable a comparative evaluation of stimulated vs. non-stimulated WHC, whole heart scaffolds were repopulated pairwise or in triplets (depending on the yielded cell-count) using cells derived from an identical cell-pool and harvested by one single isolation,

2.3) Electrical Field Stimulation

2.3.1) Processing Chamber

To deliver electric tension to the WHC-processing zone, we modified a square formed 250 ml flask by adding 6 mm olives added at all 8 edges. By these olives we inserted carbon rods of 3 mm diameter and sealed the channels with food silicone (Ottoseal S27, Hermann Otto GmbH, Fridolfing, Germany). The circular heads of the rods inside this processing flask span a cube with eight poles and a edge-length of about 2.6 cm surrounding the WHC (when mounted into the flask). The opposite ends of the rods outside of the flask are equipped with clamps to connect to the stimulation system (STG4002, Multi Channel Systems MCS GmbH, Reutlingen, Germany). For the connection to the perfusion system of the bioreactor as previously described and potential medium exchange, the flasks screw thread was chosen to GL45 and two more olives are placed centric at the upper and above end of one planar side [6].

2.3.2) Stimulation concept

To establish a three dimensional electrical field, each carbon rod was connected to an electric potential delivered by the stimulator. The distribution of potentials was arranged so that each positive pole was neighbored by negative poles side by side both in horizontal and vertical direction and faced to another positive pole on the opposite side. Electrical stimulation was set to 8V, resulting in 3 V/cm in between the carbon electrodes, in pulses of 5 ms duration followed by 328 ms of constantly 0 mV resulting in a frequency of 3 Hz programmed by the stimulators belonging software (MC Stimulus, Multi Channel Systems MCS GmbH, Reutlingen, Germany). By the application of these settings, we complied with the recommendations by Tandon et. al, that has been established for field stimulation of myocardial constructs before [11]. Electrical Field Stimulation was applied continuously for 96h while perfusion culture of the WHC in the bioreactor.

2.4) WHC cultivation

Subsequently to 24h of incubation in the 6-well-plate for ensuring sufficient adherence of the injected cells, the WHC were mounted into the modular bioreactor system as previously described [2, 5, 6]. Here particular processing chambers for electrical field stimulation as well as processing chambers without any biophysical stimulation devices were chosen and connected each to an indepently operating software-controlled perfusion path. Repopulated and pre-incubated WHC were then simply screwed in for coronary perfusion via the pre-cannulated aorta. Coronary perfusion was then initiated and controlled at a setpoint of 70 mmHg before electrical field stimulation was coupled in as well. Cultivation was performed for 96h for WHC under stimulation and corresponding controls without stimulation in parallel. For this study a total of 12 WHC were generated and cultivated. Thereof 6 WHC were repopulated as triplets whereof two WHC per triplet were subjected to stimulation while the third served as unstimulated control. The other 6 WHC were repopulated as duplets, due to lower yielded cell-count, and cultivated pairwise under stimulation vs. non-stimulated control.

2.5) Evaluation of Electrophysiological Activity

To detect and record local spontaneous electrophysiological activity of cultivated WHC, the repopulated left ventricular walls (LVW) were dissected and subjected to electrophysiological voltage mapping via a 2D Multielectrode Array (60EcoMEA-Glass Multielectrode Array) using the systems belonging software MC Rack (Multichannel Systems MCS GmbH, Reutlingen, Germany). Therefore dissected LVW were placed directly onto the 2D glass MEA by the epicardial surface. By this setup the electrical connection to the electrodes is given by a thin bridging film of cell culture medium that lowers the signal intensity. So electrophysiological measuring of

WHC by this setup represents a special case of voltage mapping that cannot be compared to cells that were seeded directly on MEA surfaces.

2.6) Analysis of Electrophysiological Activity

2.6.1) Spontaneous EP

The 2D MEA recordings, measured as described in 2.5, were further analyzed by the spike sorter tool of the MC Rack software to straighten out the signals by detecting and sorting varying action potentials. Action potentials were detected by thresholds set to 50, 100, 300, 500, 1000 and 3000 µV while the respective corresponding frequency or beating rate was calculated by the continuously detected spike intervals. Noisy background and artificial signals were filtered by elimination of all signals that did not exceed the 4-fold standard deviation of the measured signal. Samples of n=3 patches each for stimulated WHC as well as non-stimulated controls were recorded over a sequence of 2 minutes. Data of 3 electrodes per sequence were collected and subjected to Spike Sorter Analysis, resulting in a total of three biological and nine technical samples (n´s) for both stimulated WHC and non-stimulated controls. Comparative evaluation of the sorted signals was realized by plotting the amplitudes vs. their corresponding frequencies and vice versa contrasting for stimulated WHC and non-stimulated controls. Additional to qualitative analysis of the recorded signal sequences and the descriptive comparative spike sorting evaluation, a direct contrasting assessment of both groups in a simple numerical quantity was complemented. Therefore the entirety of all collected spikes per group were pooled and compared in their arithmetic mean and standard deviation of the amplitudes and beating rates.

2.6.2) Estimation of EP amplitude damping in dECM.

Electrophysiological voltage signals, that were detected on the surface of LVW as described in 2.4 are originated by cell structures that were injected into the LVW of whole heart scaffolds. As it has been reported previously these united cell structures are located in varying depths of the ECM relative to the epicardial surface [5]. Thereby the signals recorded at the epicardial surface represent a totality of signals that maybe originated at varying distances and overlay at the distinct locations of the recording electrodes. To estimate the potential error of measurement by differently reduced signal-intensities we measured the maximal reduction of voltage signals by passing the whole depth of LVW in sandwich constructions. To observe signal-reduction throughout the thickness of the LVW sandwich constructs of were recorded in an arrangement of a decellularized LVW patch placed on the 2D MEA and a freshly excised neonatal rat heart placed on the LVW patch. Subsequently the LVW patch was removed to record the same hearts signals without any reduction by decellularized ECM (dECM). That way two sequences of MEA voltage-readings were recorded per heart and sandwich construct while using n=3 hearts and n=3 decellularized LVW patches. So n=6 paired sets of amplitudes were measured herein after referred as **a** for theamplitude of native hearts and**b**for the corresponding amplitude of the sandwich construct (reduced signal). To observe potential principles of reduction as a function of the amplitudes magnitudes, the measured values were pairwiese sorted by the magnitude and logarithmized. The resulting patterns were subjected to a simple analysis of similarity.

2.6.3) EP by stimulation response

Stimulation response characteristics were tested by the direct application of short sequences of stimulation impulses using the same setup as described in 2.5. For recording electrophysiological stimulation response patterns, LVW were phased out of spontaneous activity before the stimulation sequences were applied. For stimulation 4 pulses of 8 mV in 5 sec intervals were applied by copper cables directly contacted to the LVW using the stimulation system as described in 2.3.

2.7) Western Blotting

For protein isolation each LVW of cultivated WHC were inserted into a 1.5 ml micro-test-tube and incubated in 200 µl 4M urea + 1 % SDS in an orbital shaker for 12 h at room temperature. Subsequently the pre-incubated LVW were pestled without distraction of the supernatant and incubated for another 6 h using the same preparation before the supernatant was harvested. Prior to separation and specific detection, thereby isolated protein samples were subjected to quantitative protein analysis using the Biorad DC Protein Assay according to the manufacturer’s manual. SDS PAGE was then performed for 10 µg protein per lane following the Laemmli method using 10% and 12% gels [15]. Western blot transfer was performed using a Bio-Rad Mini-Trans-Blot-Cell (Bio-Rad, Munich, Germany) onto polyvinylidene fluoride (PVDF) membranes following the manufacturers manual. For immunodetection antibodies against cardiac myosin heavy chain (MHC) (Abcam, Cambridge, UK, cat.nr.: ab50967), cardiac Troponin T (cTnT) (Abcam, Cambridge, UK, cat.nr.: ab8295), desmin (Des) (Abcam, Cambridge, UK, cat.nr.: ab15200) and connexin 43 (Cx43) (Signma-Aldrich, St. Luis, MO, USA, cat.nr.: C 6219) were used in combination with Alexa 488 conjugated goat-anti-mouse and Alexa 546 conjugated goat-anti-rabbit secondary antibody antibodies against (Invitrogen, Carlsbad, CA, cat.nr.: A11029), (Invitrogen, Carlsbad, CA, cat.nr.: A11010). Primary antibody dilutions were adjusted to 1:500 for MHC and cTnT, 1:1000 for Des and 1:100 for Cx43 in tris-buffered saline including 0.05 % tween (TBS-T) supplemented by 5% skim milk powder (blocking buffer). Both secondary antibodies were used in 1:1000 dilution in blocking buffer. Membranes were incubated over night at 4°C for primary antibody binding and for 1h at room temperature for the conjugation of secondary antibodies after two washing steps of 5 min each using TBS-T. For reference, total protein content was stained using Flamingo™ fluorescent gel stain (Bio-Rad, Hercules, CS) according to the manufacturer's manual but applied to the membrane. The membranes were digitalized using an Amersham Imager 600 (GE Healthcare, Little Chalfont, UK). Densitometric analyses were performed using ImageQuant TL software (GE Healthcare, Little Chalfont, UK). Thereby for each detected band the computed integrated optical density units (IOD) were normalized to the protein signal of the corresponding lane. Relative increase or decrease of signals is represented directly by evaluation of the ratios between stimulated samples and their corresponding non-stretched controls. All generated and cultivated WHC were finally subjected to Western blotting resulting in n=7 pairs of stimulated WHC vs. non-stimulated controls.

2.8) Statistical Analysis

Comparative data are presented as mean standard deviation. For direct group comparisons, Student's t-tests were performed. Ratios were subjected to one-sample t-test with an expected value of one. Statistical significance was assumed for P-values lower than 0.05. Data analysis was realized using GraphPad Prism 6 (GraphPad Software, San Diego, CA).

3) Results

3.1) Establishment of an 8-pole Electrical Field

Measuring the resulting current in x,y and z direction provoked by the application of 3, 5 and 8V electrical tension to the carbon electrodes as shown in figure 1A connected and operated in an alternating pattern as illustrated in figure 1B,C led to the courses as shown in figure 1D,E. The diagrams show the resulting current in mA at the ordinate, that could establish over the duration of 1, 5, 10, 50, 100 and 200 ms of applied alternating voltage.

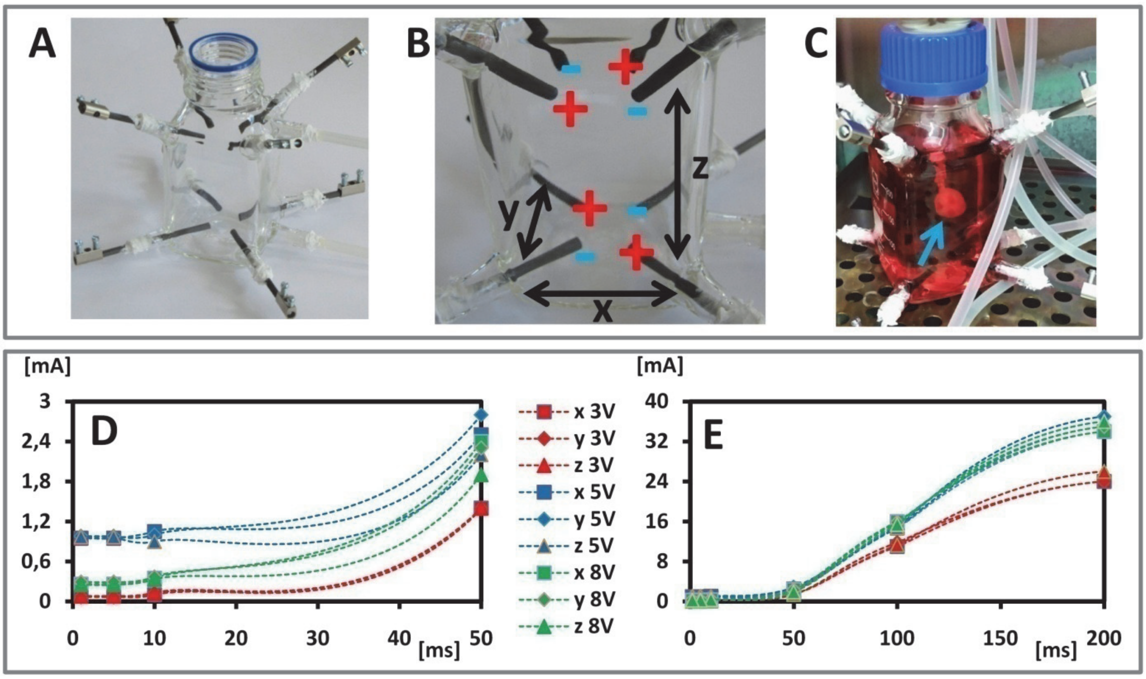

Figure 1: Processing Chamber and Electrical Field. **A:** Perfusion and processing chamber for WHC based on a square formed 250 ml flask. There are 6 mm olives added at all 8 edges to insert carbon rod electrodes. Two more olives are placed centric at the upper and above end of one planar side to connect tubes for the perfusion path and potential medium exchange. **B:** Depiction of the 8 pole electrical field, spanned by the carbon rod electrodes. **C:** Perfusion and stimulation installation at work placed inside a CO_2 Incubator. The blue arrows points at the mounted and processed repopulated WHC. **D:** Measured resulting current under applied field stimulation as shown in B. The current was measured in x, y and z direction (as shown in B) in warm cell culture medium (37°C) resulting to applied alternating voltage with pulse durations of 1 to 50 ms. **E:** same diagram as D but shown for pulse durations of 1 to 200 ms.

Data show, that the resulting current develops equally in x,y and z direction for all applied electrical tensions. In figure 2A,B, the bars and numerical values illustrate the arithmetic mean values and standard deviation of the particular oriented current flows for a validation of the graphical impression in figure 1. The data reveal a stable establishment of a three-dimensional electrical field for the whole range of pulse durations of 1 to 200 milliseconds and applied feeding voltages of 3 to 8 Volts. The small standard deviations of the means, varying only in the range from 2 to 12 percent, demonstrate an evenly establishment of current in the particular orientations x, y and z.

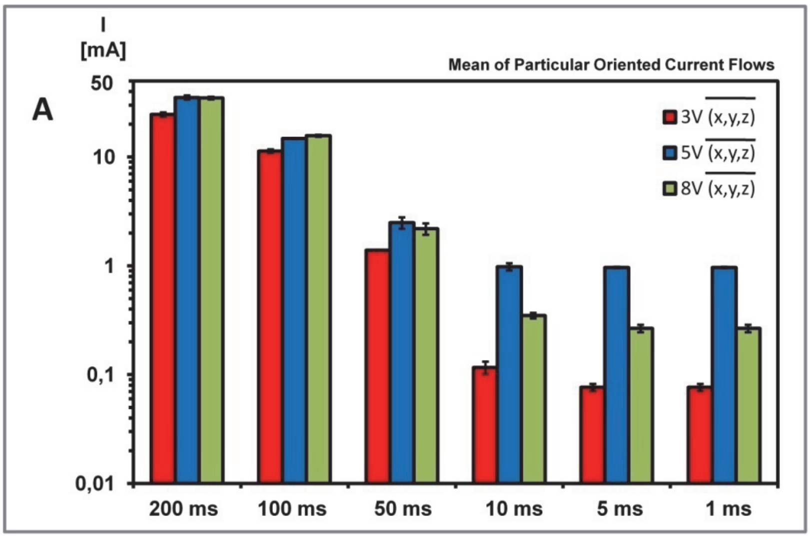

B

Underlying Numerical Values

	200 ms	100 ms	50 ms	10 ms	5 ms	1 ms
	Resulting Current I [mA] - $\overline{(x,y,z)}$					
3 V	24.67 ± 1.15	11.37 ± 0.4	1.40 ± 0.01	0.12 ± 0.02	0.08 ± 0.01	0.08 ± 0.01
5 V	35.33 ± 1.53	14.83 ± 0.15	2.50 ± 0.3	0.98 ± 0.08	0.97 ± 0.02	0.97 ± 0.02
8 V	35 ± 1	15.73 ± 0.31	2.20 ± 0.26	0.35 ± 0.02	0.27 ± 0.02	0.27 ± 0.02

Figure 2: Combining the Particular Oriented Current Flows in Arithmetic Mean Values. A: Bar Plot of the resulting current flow provoked by alternating voltage at 3, 5 and 8 V for pulse durations of 1 to 200 ms. The particular oriented current flows in x, y and z direction are combined into one arithmetic mean value complemented by its standard deviation to illustrate the spatial uniformity of the current establishment in the three-dimensional eight-pole setting.

Figure 2 A and the data in figure 2B further shows that at high frequencies of alternating voltage, the higher feeding voltage of 8V results in smaller measured resulting current of 0.35 ± 0.02 mA at 10 ms and 0.27 ± 0.02 mA at 1 to 5 ms as compared to 0.98 ± 0.08 mA at 10 ms and 0.97 ± 0.02 mA at 1 to 5 ms for 5 V. This way, the observed phenomenon indicates an emerging inertia effect, reducing the effective technical current flow.

3.2)Spontaneous Electrophysiological Activity of Cultivated WHC

Straight qualitative evaluation of MEA recordings of WHC that have been cultivated under field-stimulation show sequences of mostly chaotic and irregular but clearly detectable and strong spontaneous electrophysiological activity showing spikes ranging from about 200 µV up to 4000 µV and frequently complete action potentials, as shown in figure 3A. Less frequently also sequences of more regular signal patterns can be observed showing progressions of distinctive R and S spikes in a certain similarity to ECG patterns while reaching amplitudes of up to 4000 µV as shown in figure 3B. More frequently the recorded patterns appear more chaotic and seemingly superposed by signal series of R spikes and predominantly typical rS patterns of varying intensities as shown in figure 3C, showing mostly amplitudes of up to 200µV intermitted by signals ranging from about 400 µV up to isolated 600 µV peaks. In contrast, figure 3 D,E shows MEA recordings of non-stimulated WHC, that reveal signal-patterns of similar chaotic arrangement but at clearly smaller intensities, showing amplitudes varying in the range of about 100 µV and less frequently up to 300 µV.

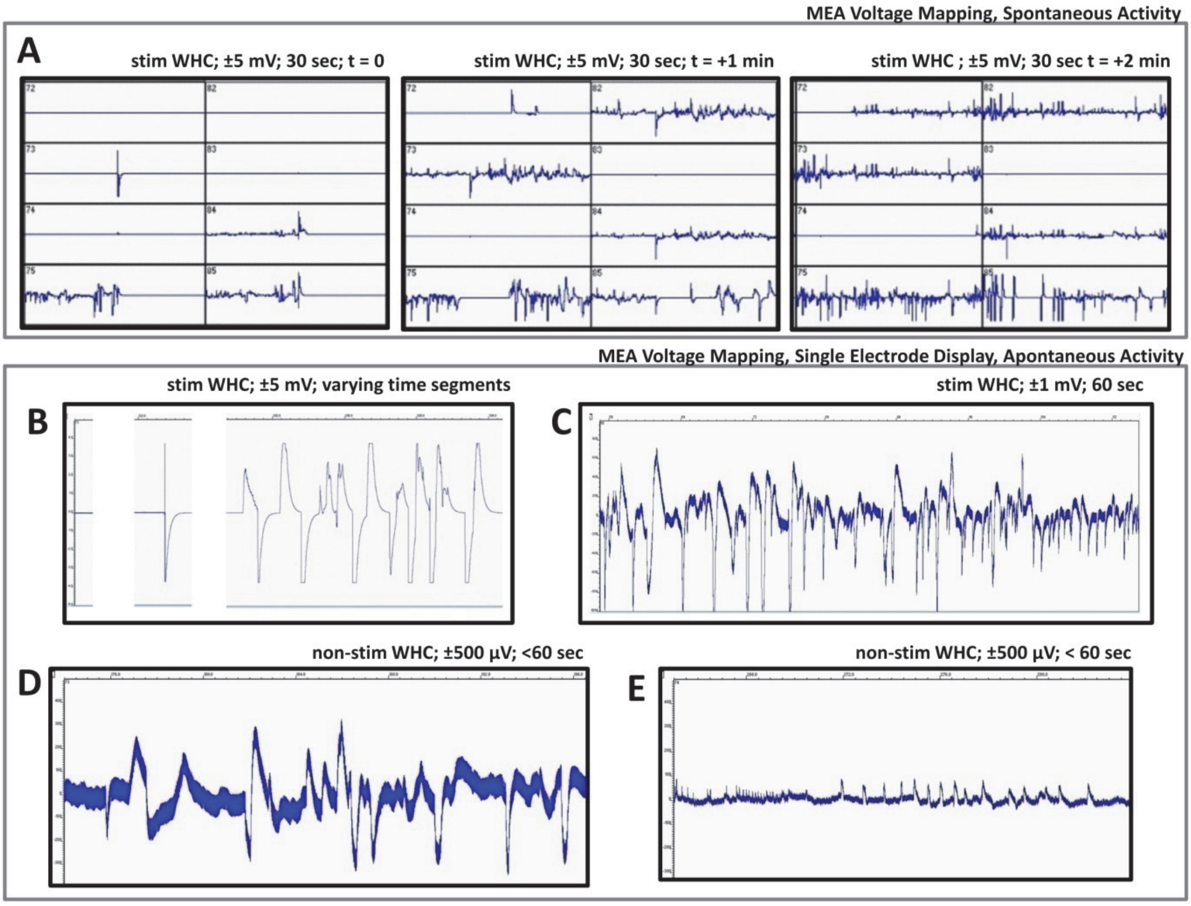

Figure 3: MEA voltage recordings of stim vs. non-stim WHC LVW patches showing spontaneous activity. **A:** Sequence of a recording of a stim WHC at intervals of about 1 minute. Each electrode shows data represented in a range of 60 sec at ±5 mV. **B:** Display of single electrode signals at varying time segments showing first a clear action potential and later on a sequence of a moderately orderly sequence of R and S spikes at an amplitude of 4 mV for a stim WHC. **C:** A chaotic and potentially superposed signal sequence as typically observed in WHC here shown for a stim WHC at a range of ±1 mV. **D:** Signal sequence as shown in B & C butfor a non-stim WHC at a range of ±500 µV. **E:** Signal sequence as shown in D showing amplitudes of only ±100 µV.

3.2.1) Quantitative Evaluation of Spontaneous Electrophysiological Activity

MEA recordings were filtered and analyzed using the Spike-Sorter tool to equalize and sort chaotic signal patterns. The resulting data of grouped pairs of voltage amplitudes and corresponding frequencies are represented in figure 4 A, B. For the non-stimulated constructs (illustrated in blue) the peaks are distributed in groups of up to 50, 100 and 300 µV but predominantly in the 100 µV group while the frequencies bundle in the range of 60 to 120 bpm respectively at 1.36 ± 0.3, 2.05 ± 1.3 and 2.25 ± 0.58 Hz. Signals of the stimulated constructs (illustrated in red) are distributed at generally higher amplitudes classified in 300, 500, 1000 and +3000 µV. The frequencies for the 300 and 500 µV groups bundle at clearly increased values of about 180 to 240 bpm respectively at 3.2 ± 1.16 and 2.99 ± 0.55 Hz. Peaks of the 3000 and 5000 µV groups appear more rarely at 1.443 ± 1.3 Hz for the 3000 µV group and only 0.07 ± 0.05 for the 5000 µV group.

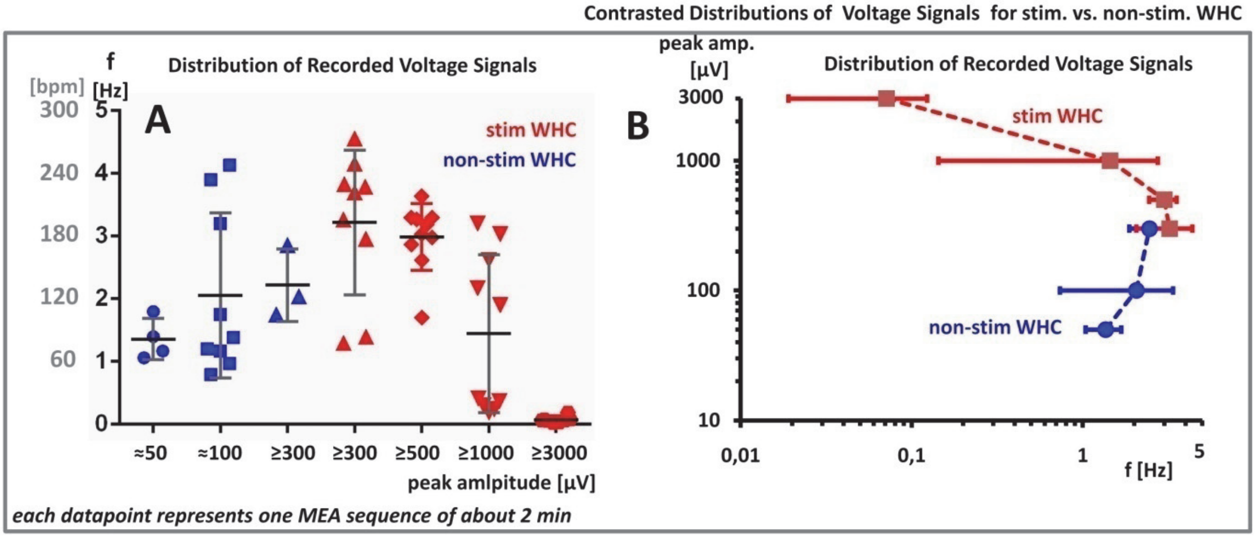

Figure 4: Sorting of action potentials in MEA recordings. **A:** Contrasting juxtaposition of detected action potentials for stim vs. non-stim WHC displayed in groups of detected amplitudes combined with their corresponding frequencies (beating rates) shown at the ordinate. **B:** Same diagram as C but presented in mean values and standard deviations. Axes are switched to show the frequencies at the abscissa and the voltage amplitudes at the ordinate in double logarithmic depiction.

While figure 4A focuses more on the observable illustration of the frequency distributions for the stepped amplitude ranges, figure 4B clearly demonstrates the growing disparity of amplitude ranges at frequencies near 1 Hz (60 bpm) that decreases slightly by increasing frequencies and closes finally by an overlapping of the 300 µV group at about 2 to 3 Hz, while the stimulated group exceeds the overlapping frequency band clearly by reaching frequencies of more than 4 Hz.

Further figure 5 shows the integration of all spikes per group into its arithmetic mean values. For the non-stimulated WHC an average amplitude of 172 ± 55 µV could be determined out of 702 detected spikes while for stimulated WHC this value was significantly increased to 533 ± 262 µV out of 926 detected spikes (P<0.0001) as it is depicted in figure 5A. The mean beating rates are illustrated in figure 5B, showing 2.52 ± 1.27 Hz for stim WHC vs. 1.92 ± 1.08 Hz for non-stim WHC that is also significantly increased for the stimulated group (P<0.0001).

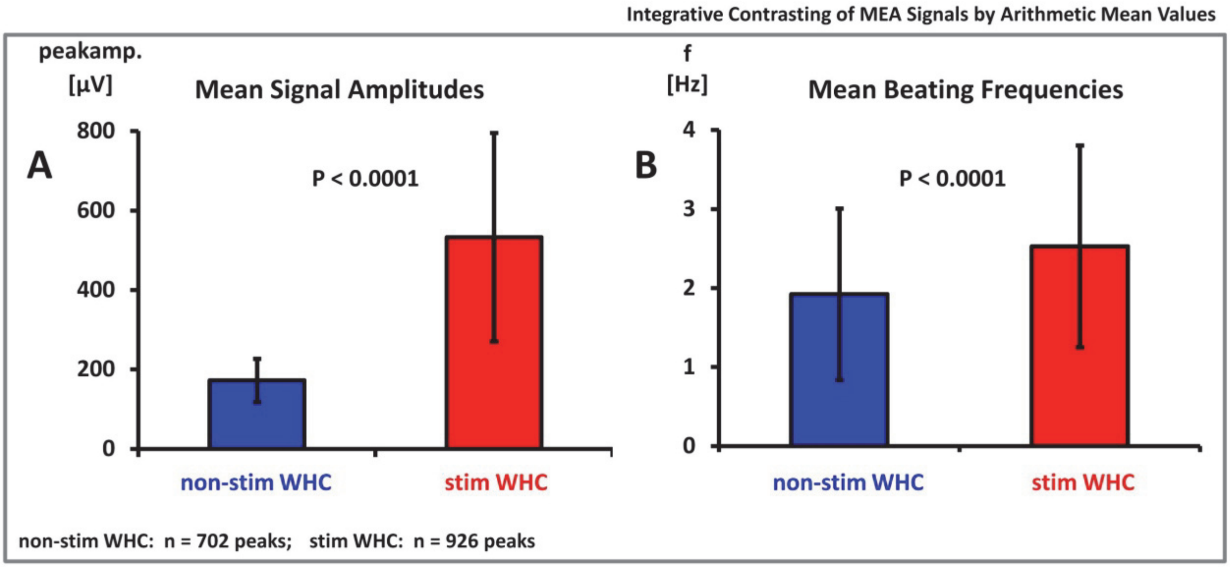

Figure 5: Contrasting Juxtaposition of Mean Signal Amplitudes and Frequencies for stim vs. non-stim WHC. The totality of all detected voltage signals by the spike sorter is compared by their arithmetic mean value and standard deviation for stim WHC in contrast to non-stim controls. **A:** Both stim WHC and non-stim controls show detectable spontaneous electrophysiological activity at mean values of 533 ± 262 µV (stim WHC) vs. 172 ± 55 µV (non-stim WHC) that is significantly increased for the stimulated group (P<0.0001). **B:** The mean beating frequencies for all detected signals are shown with 2.52 ± 1.27 Hz (stim WHC) vs. 1.92 ± 1.08 Hz (non-stim WHC) that is significantly increased for the stimulated group (P<0.0001).

3.2.2) Voltage Damping in dECM

After finding chaotic and potentially superposed signal patterns by MEA recording, it seemed likely and logic to investigate the impact of voltage reduction to near- and far-field recordings. In comparison to direct measurements of the source by neonatal hearts (figure 6A1), MEA recordings of sandwich constructions of dECM patches with beared on electrophysiologcal sources (neonatal hearts) revealed strongly decreased signals after passing the depth of the patch (figure 6A2). The illustration by a pairwise lineup of the directly measured source signals (blue) and the corresponding reduced signals of the sandwich construct (green) is shown in figure 6B. By this delineation it can be metered explicitly, that by trend stronger signals undergo a higher reduction, what implies rather a non-linear active principle by damping than a simple linear signal-decreasing by distance. Consequentially by pairwise plotting of the source-signals (blue) and the corresponding damped signals (green) logarithmized and ordered by the amplitudes of the particular source signal, figure 6C reveals that in logarithmic space the course of the source-signals (blue) can be approximated by a simple factorial shifting of the damped signals (green). For the amplitude of the source signals = **a** and the corresponding amplitude of the sandwich construct = **b**, basic factorial fitting resulted in damping parameters as expressed in equations 1 to 4

$$\mathbf{a} = (01.28 \pm 0.08)\mathbf{b} \qquad \text{eq. 1}$$
$$\mathbf{b} = (0.28 \pm 0.05)\mathbf{a} \qquad \text{eq. 2}$$
$$(-\mathbf{a}) = (01.28 \pm 0.13)(-\mathbf{b}) \qquad \text{eq. 3}$$
$$(-\mathbf{b}) = (01.28 \pm 0.08)(-\mathbf{a}) \qquad \text{eq. 4}$$

in logarithmic space, showing consistent parameters for both positive and negative signals. After de-logarithmation, the approximated active principle reveals its non-linear character by the expression in equations 5 and 6

$$\mathbf{a}_{\mathbf{max}} = e^{(01.28 \pm 0.08)\ln(\mathbf{b})} \qquad \text{eq. 5}$$
$$-\mathbf{a}_{\mathbf{max}} = e^{(01.28 \pm 0.13)\ln(|-\mathbf{b}|)} \qquad \text{eq. 6}$$

reflecting the general description of voltage damping but valid only for the whole depth of the used dECM patches derived by the left ventricular wall of decellularized rat hearts. So **a** have to be considered as the maximal conceivable source signal $\mathbf{a}_{\mathbf{max}}$ that can be estimated by the potentially damped measured value **b**.

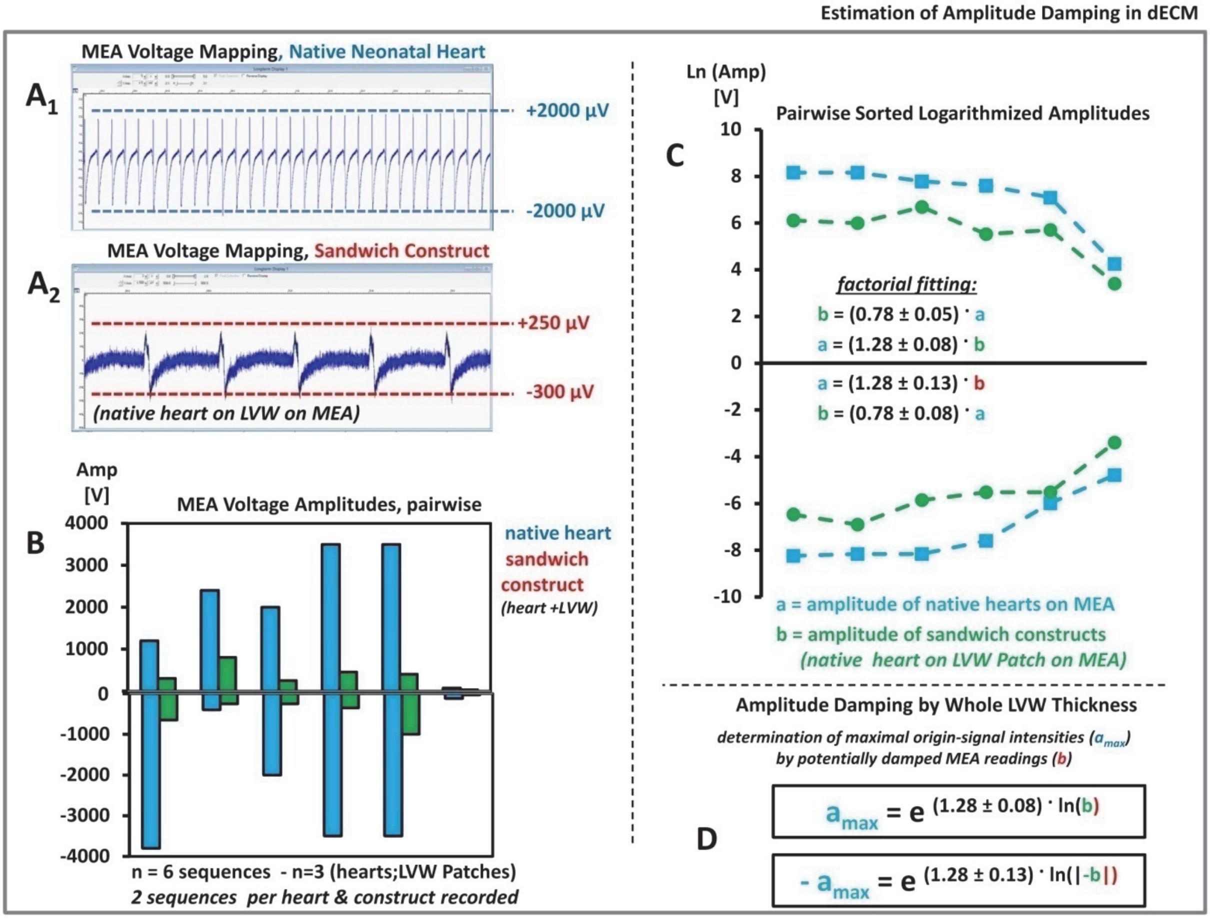

Figure 6: Estimation of amplitude damping in dECM. **A**: MEA recordings of native neonatal hearts and sandwich constructs of the respective neonatal heart placed directly on a LVW patch of a decellularized heart. To observe signal-damping througout the thickness of the LVW patch sandwich constructs were recorded first before the respective native heart was measured subsequently. **B:** Diagram showing the mean measured amplitude pairwise for single native hearts (pale blue) and the corresponding sandwich constructs (green). N=3 hearts were measured at varying time points after excision. **C:** Pairwise amplitudes as shown in B sorted (pairwise) and logarithmized. The contrasting of the patterns for native hearts vs. sandwich constructs show an apparently factorial shift. So a function for the amplitude damping could be approximated by a simple factorial fitting (in logarithmized space). **D:** Antilogarithmized functions allow to determine the maximal origin-intensities $\boldsymbol{a_{max}}$using the directly measured but potentially damped signals **b.** This estimation assumes the maximal potential distance of the signals origin and the MEA surface by the whole thickness of a LVW in a WHC.

After applying this description of eq. 5 and 6 to the MEA recordings of the stimulated WHC and the non-stimulated controls shown in 3.2.1 and figure 4 B, the distributions of the measured signals (conforming respectively **b(stim WHC)** and**b**(**non-stim WHC**) can be contrasted to the distribution of the approximated maximal conceivable source signals $\mathbf{a_{max}}$(**stim WHC**) and $\mathbf{a_{max}}$(**non-stim WHC**). Thereby the area between the courses of $\mathbf{a_{max}}$(x) and **b**(x) describe the span of conceivable source-signal intensities inside layers of varying depths inside of the repopulated WHC patches. Figure 7 illustrates roughly a cigar-stub shaped area for the stimulated WHC ranging from 1 to 7 mV at a beating frequency of 1.4 Hz to a span of 300 to 2800 µV at 3.2 Hz that further spreads out widely for the strong signals measured at low beating frequency to an overall funnel-shaped form. For the non stimulated controls the approximation of **a_{max}**(**non-stim WHC**) forms also a funnel-shaped area, but horizontally inverted in comparison to the stim-WHC and according to the lower **b**(**non-stim WHC**) values, at lower amplitudes. While the directly measured amplitudes show an overlapping only at 300 µV, a small triangular cross-section can be observed for the estimated amplitude-spans.

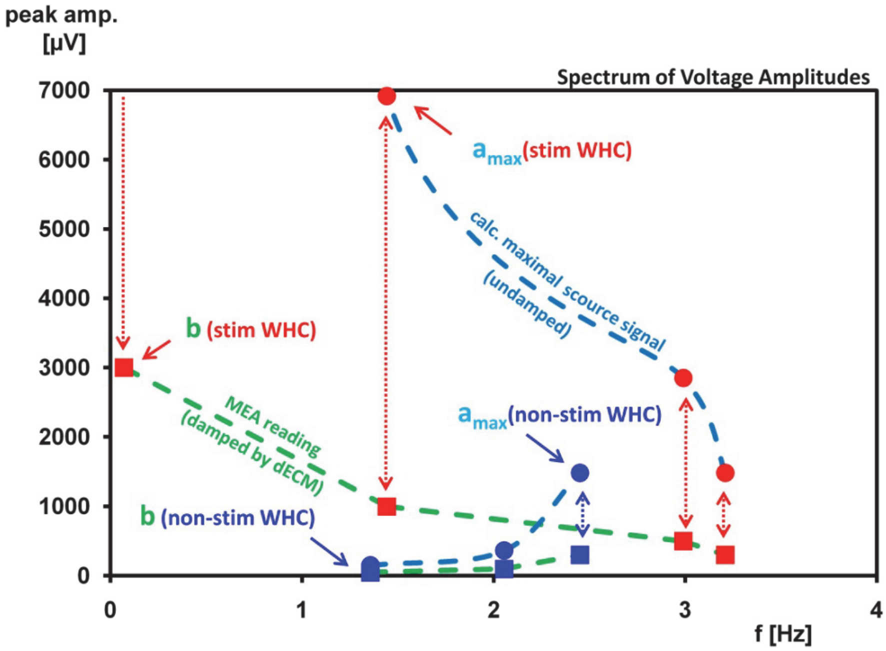

Figure 7: Spectrum of Voltage Amplitudes by Elimination of Potential Damping by dECM. Green dashed lines illustrate the distribution of measured voltage signals in equivalence to figure 4B for stimulated WHC (red boxes) and non stimulated controls (blue boxes) representing the potentially damped measuring values **b.** Blue dashed lines indicate the corresponding determined maximal source signal by elimination of the damping by dECM as described in fig 6D. Red circles display the calculated maximal source signal intensity **a_{max}** for stimulated WHC while the blue circles show **a_{max}** for non stimulated controls. The dotted lines show the spectrum of potential source signal intensities by varying depths of the emitting cell-clusters inside the repopulated dECM.

The funnel-shape characteristic illustrates graphically that recorded signals of moderate intensities can also represent far-field measurements of strong signals that are emitted in distant layers to the recording surface of the MEA. Small intensities are limited to actually represent also rather weak source-signals due to the exponential character of the active principle of damping, what is further reflected by the small intersection of the spectra for stimulated WHC in comparison to non-stimulated controls at the lower border. On the other hand, strong recorded signals, near to the physiological range, lead to exaggerated calculated values, so that a cut-off at physiological signal intensities seems reasonable and necessary to separate a certain margin, where damping gets unlikely.

3.2.3) Impulse Response Recording

As a second straight qualitative electrophysiological characteristic, we evaluated the ability of the WHC to respond to electrical stimulation impulses after the declining of spontaneous activity. Figure 8 shows exemplary the MEA recording of stimulated and non-stimulated WHC that were subjected to a series of 4 stimulation impulses at 8V in a 10 sec interval. Both stimulated WHC and non-stimulated controls show impulse-responses by immediately following depolarisations. For both groups the amplitude intensities are conform to the afore described observations by qualitative evaluation of spontaneous activity.

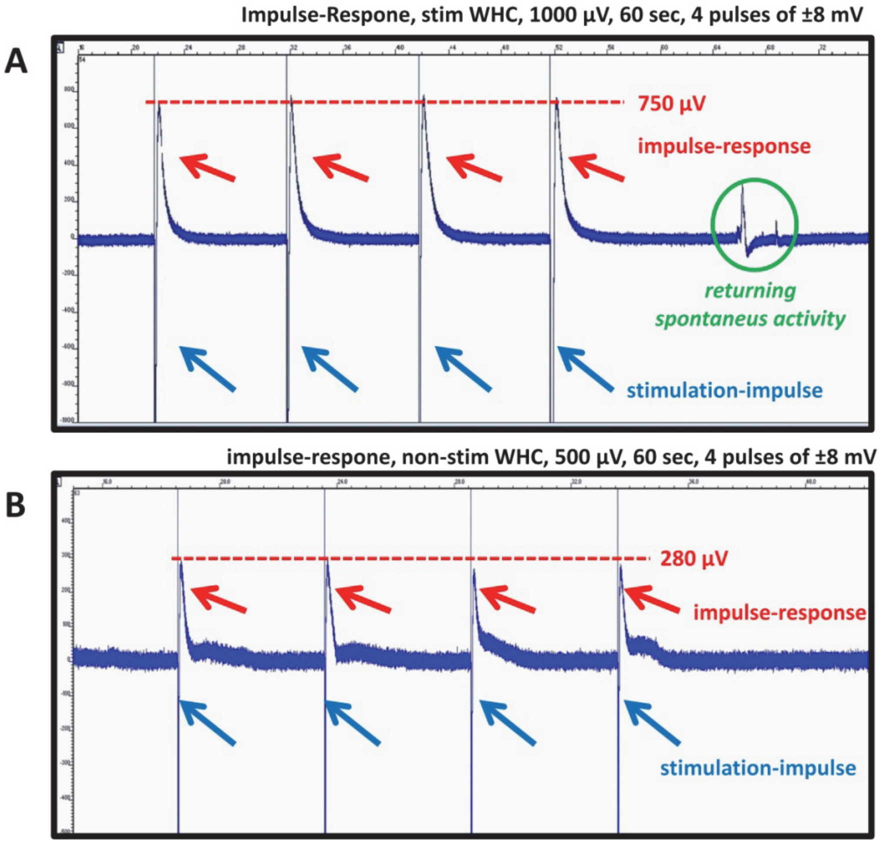

Figure 8: Detection of impulse-responses after declining of spontaneous activity. Sequences of 4 pulses of ±8 mV were applied directly on the MEA to LVW Patches of stim and non-stim WHC. Blue arrows mark the stimulation impulses. Red arrows mark the measured impulse-responses. **A:** stim WHC. The green circle marks a spot of returning spontaneous activity subsequently to a stimulation sequence. **B:** non-stim WHC.

3.3) Bioanalytical Evaluation

To substantiate observed impacts of 3D electrophysilogical stimulation concept to the myocardial development of WHC, western blotting of myocardial key proteins was performed. The examined proteins can be classified to functional sarcomeric markers by Myosin Heavychain (MHC) and cardiac Troponin T (cTnT) one the one hand in group I and more structural markers with Desmin (Des) as well as Connexin 43 (Cx43) for structural functionality in group II. The detected and normalized marker bands are displayed as ratios representing the relation of the particular normalized marker signals of stimulated WHC to the corresponding non-stimulated control in associated pairs per ratio. Thereby ratios of bigger than one describe an increased marker contend in simulated WHC, while ratios declining the value of one indicate a decreased contend. As shown in figure 9A, the investigated markers show consistently predominantly ratios of bigger than one with mean values of 1.9 ± 1.1 for MHC (P=0.081), 2.7 ± 1.4 for cTnT (P=0.032) in group I and 2.1 ± 1.7 for Des (P=0.130) as well as 3.4 ± 3.3 for Cx43 (P=0.097) in group II. But statistically significant distinction from an expected value of one could only be shown for cTnT. Within the groups the single pairs of stim vs. non-stim WHC show overall higher ratios for cTnT as compared to MHC with 4 of 6 pairs in group one (one pair was dropped out due to missing cTnT signals) (P=0.127). In group II 5 out of 7 pairs show higher ratios for Cx43 as compared to Des (P=0.056). Statistically for both groups no significant distinction could be found.

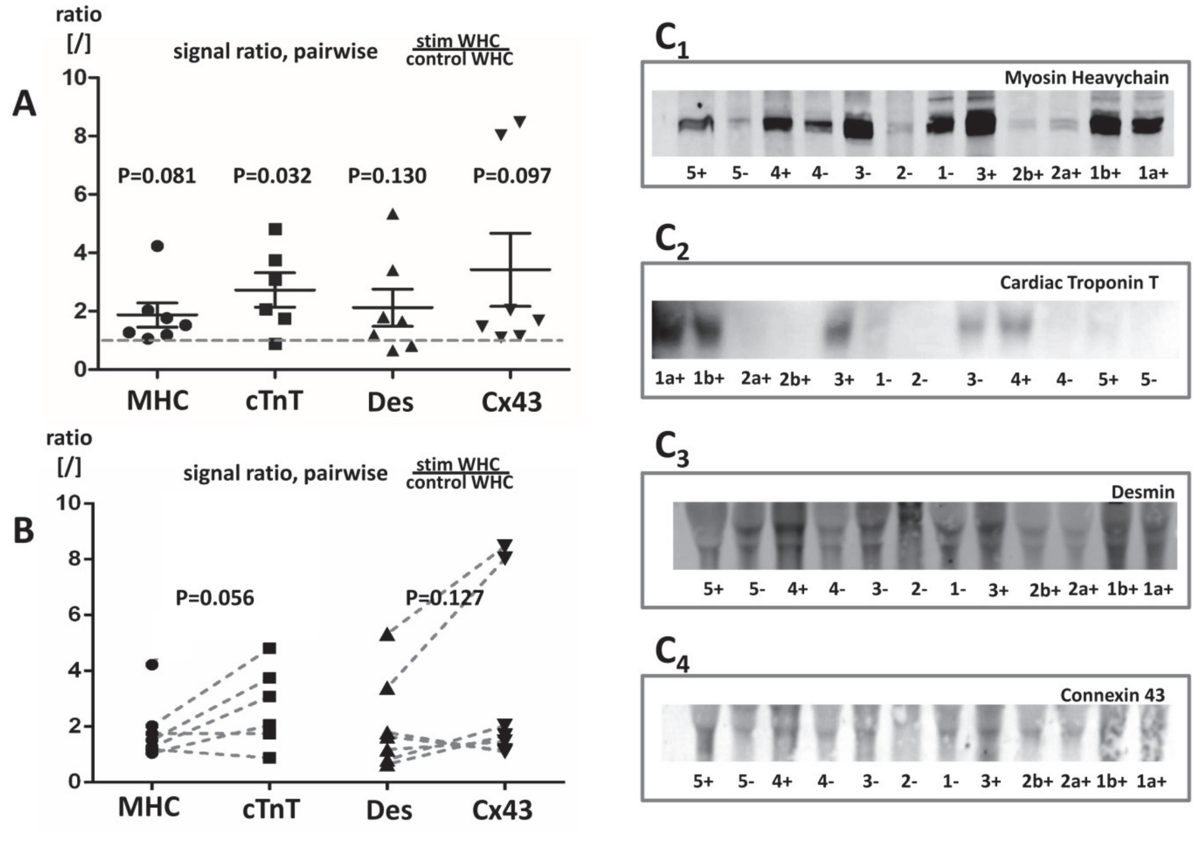

Figure 9: Western Blotting of cardiac Myosin Heavychain (MHC), cardiac Troponin T (cTnT), Desmin (Des) and Connexin 43 (Cx43) for stim vs. non-stim WHC. Each datapoint represents the ratio of measured signal intensities for one stim WHC referred to its corresponding non-stim control. **A:** Ratios

for MHC, cTnT, Des and Cx43 diagrammed side by side. Ratios of bigger than one indicate a higher content of the detected protein in stim WHC as compared to its corresponding non-stim control. **B:** same diagram as shown in A but demonstrating connected identical pairs for comparative evaluation of the markers. 4 of 6 pairs show a further increase of cTnT ratios contrasted to MHC. Equally to this 5 of 7 pairs show a further increase of Cx43 ratios as compared to Des.

4) Discussion

The purpose of this work was to critically investigate the successful transfer of electrical field stimulation to the cultivation of whole heart constructs as a proof of principle. Thereby this study represents the consequential continuation of our general ambition to transfer and unify proven and established concepts of myocardial tissue engineering into a holistic cultivation approach. As we belief and have stated previously, this still remains a major challenge at the current state of the art of science and technology in the field of whole organ tissue engineering [2, 5].

A lot of meaningful research emerged in the past regarding electrophysiological stimulation of myocardial constructs and established concepts are available by literature providing well founded information for scientific applications and technical realization [7-12]. So we were able to pick up already optimized basic principles like stimulation parameters and electrode material [11, 12]. However, the principle of an eight-pole field is a completely new self-development that delivers new options for complex three-dimensional stimulation of whole heart constructs. First trial runs of this stimulation system revealed a stable spatial establishment of the conceived three-dimensional electrical field, that delivers an evenly propagation of current in the particular orientations x, y and z. Interestingly, for high feeding voltage of 8V an emerging inertia effect could be observed for high frequencies of alternating voltage, that reduces the effective technical current flow as compared to a smaller feeding voltage of 5V. Actually this is a favored effect for electrical field stimulation where the constructs should not be penetrated by technically delivered charges, but of course the underlying measurements are also affected by the measuring instrument inertia.

Regarding the biological model, fundamental efficacy of repopulation and suitability of the WHC for myocardial development has been shown by previous work as well as the completeness and quality of decellularization for the used whole heart scaffolds [5, 13, 14]. In line with the mentioned previous work, here we hold on the concept of short-term model-cultivations of the WHC to identify fundamental impacts of biophysical stimulation. Primarily the investigation of spontaneous electrophysiological activity by MEA recordings of whole left ventricles seemed obvious to demonstrate potential effects to myocardial functionality. A first qualitative assessment of the recorded sequences stimulated WHC revealed sequences of quite regular signal patterns showing progressions that outline series of distinctive R and S spikes in a certain similarity to ECG patterns while reaching amplitudes in the range from about 200 µV up to 4000 µV. But more frequently the recorded patterns appear chaotic and seemingly superposed by signal series of R spikes and predominantly rS patterns of varying intensities. In contrast the non-stimulated controls revealed signal-patterns of similar chaotic arrangement but at clearly smaller intensities.

Actually continuative specific comparative quantitative analysis of MEA signals for whole heart constructs is a novel challenge that comprises technical and methodological hurdles for itself. So the development of a methodological approach for the evaluation of MEA recordings was involved in this proof of principle project as a required working tool as well. Thereby straightening out the recorded signal sequences by detecting and sorting varying action potentials into a distribution of stepped amplitude ranges and corresponding frequencies enabled more in depth insights. While non-stimulated WHC exhibit a maximum frequency for amplitudes in range of 100 to 300 µV at a mean of about 2 Hz that decreases by decreasing amplitude ranges, stimulated WHC show a generally inverse pattern reaching a maximum frequency at a mean of about 3 Hz for amplitudes in range of 300 to 500 µV at a clearly higher frequency range, that decreases by increasing amplitude ranges, that further exceeds the amplitude range of non-stimulated controls roughly by a whole power of 10. A direct contrasting by the arithmetic mean of all amplitudes that could be recorded for stimulated WHC vs. non-stimulated controls provided a simple numerical quantity that validated the qualitative impression by a clearly significant increased mean amplitude for stimulated WHC.

In an isolated analysis of the beating frequencies, 75 % of measured sequences bundle at frequencies of 1 to 2 Hz for the non-stimulated WHC. In contrast stimulated WHC exhibit a bunch of 50 % of the amplitudes with magnitudes of up to 3000 µV exceeding 3 Hz, 33 % in the range of 2 to 3 Hz and 17 % below of that. Strong signals of more than 3000 µV arise at frequencies of less than 1 Hz. This illuminates a clear shifting up of the beating rates by the impact of stimulation that further shows to be significant for the integration of all signals into an arithmetic mean value.

Comparative reference data in literature, that are based on utilizing neonatal rat cardiomyocytes in decellularized whole rat hearts, report mean amplitudes of 250 ± 100 µV for recorded RS patterns of electrophysiological stimulated bioartificial heart constructs and maximal spontaneous beating rates of 118 ± 6 bpm = 1.97 Hz [4]. So in direct comparison to the cited current injection principle, our 8-pole field stimulation concept could roughly double the mean voltage amplitude and increase the beating rate by 20 %, though this apparently seems to rather adapt to the stimulation frequency of 3 Hz. Interestingly the same effect was observed and reported for beating rates of electrically stimulated fibrin based constructs [7]. Other Whole Heart Studies either do not stimulate [16] or actually apply electrical stimulation, but use barely comparable cell-models and scaffolds [9]. The pioneering work by Ott et. al., still seems to set the gold standard by exemplary showing depolarisations with amplitudes of 10 mV [3]. But indeed it should not be ignored, that we also have observed sequences showing quite regular signal patterns of clear R and S signals with amplitudes of at least about 4 mV as shown in figure 4B. However those sequences are rather rarely scattered in the recordings, which admittedly show more frequently more chaotic signal sequences of lesser intensities.

Those typical chaotic patterns of spontaneous EP activity led to the assumption of potentially superposed near- and far-field recordings that are emitted by cell structures of varying locations of the ECM relative to the epicardial surface. Hence, the investigation of the interaction of decellularized ECM with pervading electrophysiological emission uncovered a strong damping impact to voltage signals. Consequently we determined the active principle and used it to estimate the spectrum of source signals to recorded values by calculative elimination as a supplemental tool for the interpretation of the observed signals. Enough interestingly the found funnel-shape characteristic for the span between potentially damped recorded signals and the calculative source signals illustrates graphically that measured signals of moderate intensities can also represent far-field measurements of strong signals that are emitted in distant layers to the MEA electrodes. On the contrary, small intensities are limited to actually represent also rather weak source-signals due to the exponential character of the active principle of damping. On the other hand this calculative tool holds the limitation that strong measured values, that already reveal intensities near to the physiological range, lead to exaggerated calculated values. Consequently a cut-off at physiological voltage ranges seemed reasonable and necessary to separate a certain margin, where damping got unlikely and a near-field recording appears more plausible. Finally, after phasing out spontaneous electrophysiological activity, both stimulated WHC and non-stimulated controls could further be stimulated again to emit stable electrophysiological impulse-responses to short sequences of voltage pacing. Both exhibited immediate depolarizations at amplitudes roughly conforming the afore observed voltage ranges for spontaneous activity.

In summary both qualitative and quantitative electrophysiological evaluation of cultivated WHC revealed a strong beneficial impact by the applied 8-pole field stimulation. In addition these functional findings could further be substantiated and validated generally by classical biochemical investigation of the cultivated WHC. Western blotting of myocardial key markers revealed apparently a clearly predominant count of pairs showing recognizable increased ratios for stimulated WHC for MHC, cTnT, Des as well as Cx43. Beyond of that, there are scattered ratios that show more than threefold contends of MHC, cTnT and Des and even up to eightfold contends of Cx43 for stimulated WHC in contrast to non-stimulated controls. However statistically significant distinction from a neutral expected value of one by one-sample t-test evaluation could only be found for cTnT. But this apparent discrepancy in observed causality and statistical validation is provoked by precisely these scattered high ratios, which results in high standard deviations. If the particular two highest ratios, that represent the strongest impact by stimulation, are not considered, the values turn to P=0.048 for Cx43 and P=0.026 for MHC showing statistically significant increased contends for stimulated WHC. So ultimately the beneficial impact of the 8-pole electrical field stimulation to functional myocardial development of the WHC as revealed by the investigated key markers remains plausible. For a continuative interpretation it should be considered that though MHC makes the predominant protein-mass in myocardium, the mol-ratio of cTnT in thin filaments and MHC in thick filaments represents a direct functional coupling. This can be reviewed additionally simply by the observation of paired ratios for MHC and cTnT, especially because this way a comparison of relative variations can be investigated, instead of absolute quantities. This way 4 out of 6 identical pairs, representing 66 % of the cultivated WHC exhibit a further increase of the cTnT ratio by the impact of stimulation as compared to the MHC ratios in group I thus showing a certain consistency in potential functionality. Admittedly, this principle cannot be transferred directly to group II with Des and Cx43,but nevertheless the consistency of increasing or decreasing for these structural and both functional and structural-functionality markers can be investigated this way as well. Interestingly the same trends continues similarly in group II showing a further increase of the Cx43 ratio for 57 % of cultivated WHC as compared to the Des ratio. But crucial for this observation is of course mainly the identifiable consistency of increasing myocardial key markers for stimulated WHC in contrast and exclusion from a potential chaotic distribution of increasing and decreasing markers.

So returning to the stated purpose of this study, by the described short model cultivations under the application of electrical 8-pole field stimulation we could show a successful transfer of the established electrical field stimulation concept to the whole heart tissue engineering approach.

5) Conclusion

Although electrophysiological stimulation has been incorporated into whole heart TE concept from the very beginning and today the application of current injection by directly inserted or contacted electrodes has shown promising results, for the first time we present a concept for the transfer of electrical field stimulation to the whole heart tissue engineering approach [3, 4, 9]. Furthermore to the best knowledge of the author, this is the first control-based study showing a comparative investigation of electrophysiological whole heart construct stimulation. The presented principle of an alternating eight-pole field is a completely new self-development that delivers new options for complex three-dimensional stimulation of whole heart constructs. By the integration into short model cultivations our concept could be proven to deliver clearly beneficial effects to myocardial development and thereby holds up with the standards that have already long been known for electrical stimulation of myocardial constructs.

References

1. E. J. Suuronen & M. Ruel (eds.). *Biomaterials for Cardiac Regeneration* (Springer International Publishing, Cham, 2015); Chapter 7. Aubin H., Hülsmann J., Pinto A., et. al., Whole-Heart Tissue Engineering: Use of Three-Dimensional Matrix Scaffolds.

2. Hülsmann, J. *et al.* Whole-Heart Construct Cultivation Under 3D Mechanical Stimulation of the Left Ventricle. *Methods in molecular biology (Clifton, N.J.)* **1502,** 181–194 (2016).

3. Ott, H. C. *et al.* Perfusion-decellularized matrix. Using nature's platform to engineer a bioartificial heart. *Nature medicine* **14,** 213–221 (2008).

4. Tao, Z.-W. *et al.* Establishing the Framework for Fabrication of a Bioartificial Heart. *ASAIO journal (American Society for Artificial Internal Organs : 1992)* **61,** 429–436 (2015).

5. Hülsmann, J., Aubin, H., Wehrmann, A., Lichtenberg, A. & Akhyari, P. The impact of left ventricular stretching in model cultivations with neonatal cardiomyocytes in a whole-heart bioreactor. *Biotechnology and bioengineering* **114,** 1107–1117 (2017).

6. Hülsmann, J. *et al.* A novel customizable modular bioreactor system for whole-heart cultivation under controlled 3D biomechanical stimulation. *Journal of artificial organs : the official journal of the Japanese Society for Artificial Organs* **16,** 294–304 (2013).

7. Mohamed, M. A., Islas, J. F., Schwartz, R. J. & Birla, R. K. Electrical Stimulation of Artificial Heart Muscle. A look into the electrophysiological and genetic implications. *ASAIO journal (American Society for Artificial Internal Organs : 1992)* (2016).

8. Edelmann, J.-C. *et al.* A Bioreactor to Apply Multimodal Physical Stimuli to Cultured Cells. *Methods in molecular biology (Clifton, N.J.)* **1502,** 21–33 (2016).

9. Guyette, J. P. *et al.* Bioengineering Human Myocardium on Native Extracellular Matrix. *Circulation research* **118,** 56–72 (2016).

10. Miklas, J. W. *et al.* Bioreactor for modulation of cardiac microtissue phenotype by combined static stretch and electrical stimulation. *Biofabrication* **6,** 24113 (2014).

11. Tandon, N. *et al.* Optimization of electrical stimulation parameters for cardiac tissue engineering. *Journal of tissue engineering and regenerative medicine* **5,** e115-25 (2011).

12. Tandon, N. *et al.* Electrical stimulation systems for cardiac tissue engineering. *Nature protocols* **4,** 155–173 (2009).

13. Aubin, H., Kranz, A., Hulsmann, J., Lichtenberg, A. & Akhyari, P. Decellularized whole heart for bioartificial heart. *Methods in molecular biology (Clifton, N.J.)* **1036,** 163–178 (2013).

14. Akhyari, P. *et al.* The quest for an optimized protocol for whole-heart decellularization: a comparison of three popular and a novel decellularization technique and their diverse effects on crucial extracellular matrix qualities. *Tissue engineering. Part C, Methods* **17,** 915–926 (2011).

15. Laemmli, U. K. Cleavage of structural proteins during the assembly of the head of bacteriophage T4. *Nature* **227,** 680–685 (1970).

16. Yasui, H. *et al.* Excitation propagation in three-dimensional engineered hearts using decellularized extracellular matrix. *Biomaterials* **35,** 7839–7850 (2014).

4. Discussion

4.1. Process Analytics and Process Automation for Whole Heart Decellularization

The decellularization of tissues and organs itself still represents a black-box procedure and the process of cell removal has remained inaccessible for analytical monitoring up to now. But certainly the state of completeness of disintegration and transport of cellular components would be of special interest for each single processed organ, once they are produced for medical application. Even if a particular protocol is proven as sufficient and applicable with high statistical significance, sporadic outliers would lead to devastating consequences if the produced device causes relevant immune responses *in vivo* in the clinical setting.

By crude biomass balancing analysis of native and decellularized hearts, for the first time a simple and basic system was introduced to characterize decellularization processes based on fundamental SI units. Likewise we presented process-analytical techniques to elucidate both parameters to characterize the efficacy of cell removal and variables to describe the ongoing mass-transport and elution of debris for the first time as well. Thereby we could determine the dynamics of biomass depletion during whole heart decellularization and estimate kinetical parameters to describe the decellularization process. Consequently we provided a first non-disruptive tool for quality control.

Furthermore and also for the first time, a simple and general model was introduced that enables to describe and numeralize decellularization procedures as biomass depletion processes based essentially on a debris formation rate, a tissue-specific uptake rate for decellularization agents and the tissue-specific debris yield. This could be a first cornerstone that enables computer based simulations of deeper matter.

The conventional wisdom concerning whole organ decellularization is that the efficacy and the application patterns of particular protocols depend on the organ-size and have to be adapted and scaled up to clinically relevant models [32-36]. In direct contrast to that, our results imply a certain independency from the biomass amount, but rather an increased susceptibility for individual organ characteristics with regards to mass transport limitations. By normalized biomass discharge courses, we observed in general a fast initial debris formation followed by a stage of apparent substrate-limitation indicating a decreasing discharge rate by decreasing availability of remaining biomass for the applied reactants. Biomass discharge courses following this non-linear pattern indicate an optimal mass transport via the coronary system. Consecutively, noticeable limitations of the mass transport appear by courses converging to more linear discharge patterns. Actually we observed those patterns for almost half of the decellularized ovine hearts, while the other half of the organs reveal nonlinear discharge patterns that exhibit noticeable biomass-limitation stages and appear almost congruent with those of rat hearts. We strongly believe that a limited mass transport via the coronary system should be taken as a criterion for exclusion and rejection from the production process because an insufficient integration into blood circulation or respectively its partial disturbance or limitation may hold the risk of vascular clotting with similar consequences as the reported limited *in vivo* survival of decellularized and repopulated livers by blood clotting [37-38].

In addition to these non-disruptive but still downstream or post-process analytical characterization techniques, we investigated the evolving of visco-elasticity in decellularization perfusates as a measurand for debris removal and contrasted this to online detectable fluid-dynamical effects during perfusion based whole heart decellularization. Thereby we could show for the first time a procedural detectability of the progression of the decellularization status. However, this approach still is handicapped by the fact that only ongoing debris removal is revealed while the entire process yet is blind for the level of residual biomass inside the target organ. This latter information has to be derived from parameters specified to the initial wet biomass as shown in 3.1 and may be estimated by calculation of correlations. This problem was recognized by Geerts and colleagues, who took up our basic concept and complemented it by real time computer tomographic scanning of residual DNA during whole organ decellularization [39]. Moreover, the relevance of our method was verified by a roughly contrastable investigational approach, that was published in 2016 by Lee et. al [40]. In this work Lee et. al. introduced flow dynamics through the aorta and pulmonary artery as well as evolving turbidity during whole heart decellularization to characterize the decellularization process.

Continuative to the basic detection of debris via rhelogical measurements in perfusate samples, the observation of the evolving courses of the visoelasiticity and the medial differential quotient of the viscosity (MDQ), an indicator for high molecular structures, while whole-heart decellularization cycles exhibited reproducible characteristic peak-shaped patterns as shown in *3.1 – Fig. 6*. While the instant of time for these peaks varies in between individual processed organs, their occurance is always accompanied by a drastic declining of the protein concentration in the perfusates, whereby this event also comes along with a turnover of the detected accumulated total protein washout. This phenomenon could be due to an emerging of structural cellular components, which in consequence may lead to specific physico-chemical interactions like crosslinking effects of debris fragments or vesicle-formation, potentially also masking proteins from experimental detection. However, actually this is the first ever shown characteristic procedural event of a decellularization procedure at all. Practically it seems to introduce the saturation phase of the decellularization dynamic for particular individual organs. Therefore its detection may be used as a tool for a potentially automated decellularization. But definitely this illustrates the urgent demand for further in depth process analytical elucidation of decellularization processes, while we strive for automated quality controlled pharmaco-industrial production of whole organ scaffolds.

4.2. Bioreactor Design and Biophysical Stimulation for Whole Heart Constructs incl. Bioprocessing

In order to detect and describe the impact of biophysical stimulation to WHC cultivation the first requirement was to develop suitable routines to establish solid proof of principle studies. Thereby the complete whole heart tissue engineering approach had to be deconstructed to preferably short, simple and practicable operations to minimize interferences as illustrated in figure 8. Even so, it still is a quite long composed procedural chain that holds several very specific technical and manual complexities. As a consequence, at this level we aimed rather at stable qualitative information than at quantitative and statistical evidence, so we valued the investment in procedural innovation higher than in applied empiricism. In turn, rising up empiricism as well as expanding the cultivation period are major aspects of consecutively planed optimization studies as outlined in figure 7 in chapter 1.4.

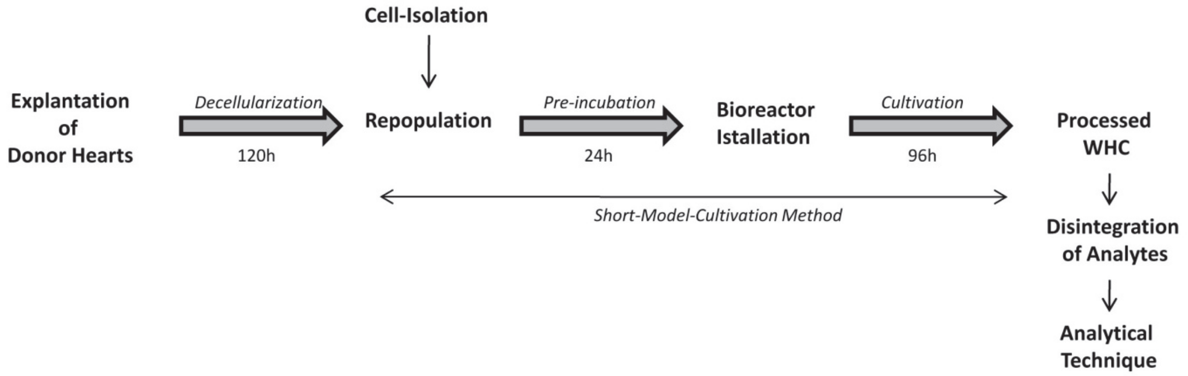

Fig. 8: Work Flow Chart for Proof of Principle Studies. The sequence of whole heart decellularization, repopulation, cultivation and principal investigational evaluation is depicted by manual procedures (bold topics) and technical processes (thick framed arrows). The procedure of the employed short model cultivations is illustrated by the thin double-headed arrow, which shows the corresponding operational procedures.

To start at nearest with the repopulation, in literature the engraftment of seeded cells is investigated and reported as a first relevant aspect of whole organ engineering, especially as the accessible cell-number may be limited. Studies, that have employed the injection method to deliver large cell numbers of 60 to 100 million cells to a decellularized rat heart report an immediate loss of more than 40 % in a span of 20 minutes to 2 hours after injection [2, 6]. By this work, we explored the principles of proliferative invasion vs. high cell density injection involving C2C12 cells (in 3.3) vs. isolated neonatal cardiac cells (in 3.4 & 3.5) and implemented a 24h pre-incubation of freshly repopulated WHC to allow regeneration and adherence before non-adhered cells may be flushed out by perfusion. Both models revealed acceptance of the matrix and affected a dense infiltration of the ECM as shown in *3.3 – fig. 6 and 3.4 – fig. 1A&B*. Interestingly for both models the cells invaded distinct compartments inside of the scaffold resembling certain tracks or pathways. Hence, cells do not spread out in a spatial equipartition but apparently were directed or vectored by the matrix. So even for a proliferative cell source the spatial invasion is obviously limited and the generation of a thoroughly repopulated WHC directly depends on a suitable seeding concept. While for the CMC method, targeting to develop processing strategies, partial repopulation still provides suitable constructs as a biological model, the seeding concept has to be optimized in the course of further process upstream and turns out to require an adequate adaption to the architecture of the ECM.

As stated previously, at the actual state of the art, it still is a major challenge to transfer established concepts of myocardial tissue engineering to the whole heart approach. Key biophysical stimulation concepts, successfully employed to enhance maturation in numerous previous studies, comprise biomechanical stretching and electrophysiological conditioning [24-29]. However, in general either the first or the latter one of these concepts has been used in the past, while their equivalency vs. supremacy of one or their potential summation effects have been hardly investigated and remain unclear [12, 28]. Both biomechanical and electrical stimulation have been proven to enhance sarcomeric organization and contractile functionality [26, 39]. Consequentially we adapted biomechanical stretching as well as electrical field stimulation to whole heart constructs and developed the mentioned CMC method to explore their impact on myocardial development. Actually control based studies were essentially missing in whole heart tissue engineering yet. Thereby we could recover the reported beneficial impact of both biomechanical and electrophysiological stimulation on myocardial constructs for whole heart constructs as described in 3.3, 3.4 and 3.5. And just as a favoring advantage of one stimulation concept as compared to the other could not be reported for conventional 2D and 3D constructs yet, so we observed roughly contrastable effects on sarcomeric and conductive development by qualitative evaluation for biomechanical as well as for electrical stimulation of WHC. Considered in a contrasting confrontation of the found impacts to the myosin heavy-chain ratio for biomechanically vs. electrophysiologically stimulated WHC in relation to the corresponding non-stimulated controls we found ratios of 2.9 ± 1.8 vs. 1.9 ± 1.1 as derived by western blotting (shown in *3.4 – fig.5* and *3.5 – fig. 9A*). As an indicator for the conductive development we found a Cx43 ratio of 3.7 ± 0.7 for bio-mechanically stimulated WHC derived by qRT-PCR in contrast to a ratio of 3.4 ± 3.3 for electrophysiologically stimulated WHC as derived by western blotting (shown in *3.4 – fig. 6A* and *3.5 – fig. 9A*). Of course this is no direct quantitative comparison but it neither even indicates any clearly and apparent predominant impact in between the contrasted biophysical stimulation concepts.

Moreover, electrophysiological functionality could be shown for the WHC model by the detection of spontaneous EP activity via MEA recordings of dissected whole left ventricles after bioreactor cultivation. Although spontaneous EP activity indicates immaturity as a matter of principle, because adult cardiomyocytes need a stimulus to beat [42, 43], a total adolescence cannot be anticipated in a period of 5 days of cultivation. Considering the state of the art, the complete differentiation of such a construct towards an adolescent tissue simply does not appear to be realistic and hence is not a suitable criterion for the success and significance of a processing strategy. As already stated in chapter 1.3, the model of isolated neonatal cardiomyocytes holds the potential for adolescence or maturation as well as dedifferentiation. So first and foremost the proportionate regain of native neonatal characteristics after isolation, repopulation into a new scaffold and a short cultivation-period represents a more consequential assessment. Moreover, spontaneous EP activity is a common investigational characteristic for neonatal cardiomyocytes and has already been shown for WHC [6-7, 30]. In this context, recorded voltage amplitudes could be significantly increased by the impact of electrical field stimulation in contrast to apparently weak amplitudes that were measured by non-stimulated controls. Interestingly, the strongest recorded amplitudes for stimulated WHC, though they occur rather rarely in our recordings at those intensities, revealed voltage values in the range of about 4 mV while direct recording of freshly excised neonatal rat hearts ranged in a span of very similar 1 to 4 mV (*3.5 – fig.3B & fig.6A1*). Following this general methodology, we could also observe a 60 % recovering of native neonatal connexin 43 expression by the impact of left ventricular stretching in contrast to 20 % for the corresponding unstimulated controls.

Generally the investigation of electromechanical functionality is always in the special focus of characterizing myocardial maturation and development as it very simply represents the essence of myocardial function. But beyond that, cellular alignment and metabolic activity are commonly investigated for a complementary characterization [5, 9, 44]. So we picked up and adapted both concepts as well and integrated them into an adaptive investigational concept for processed WHC. Thereby the perfusion based WST-1 assay as established along this thesis and the self-established quantification of alignment by the orientation density have been accepted well in literature as valuable measures, indicated by several citations of the study 3.3 [5, 32, 45-46]. Furthermore, two years after the respective publication which has derived from this thesis, a similar but resazurin based method for the evaluation of metabolic activity has been published by the group of Harald Ott, a well-recognized pioneer in the field of whole organ tissue engineering approach [47]. This clearly puts emphasis on the scientific relevance of this thesis and the herein presented methods.

In a direct contrasting of the impact of biophysical stimulation to metabolic activity of WHC, LV stretching showed clearly oppositional effects on constructs containing C2C12 cells vs. those repopulated with neonatal rat cardiomyocytes. The results of 3.3 when compared to those of 3.4 reveal a decreased metabolic activity for stretched WHC that were repopulated with C2C12 cells and an increased activity for those that were repopulated by neonatal rat cardiomyocytes (*3.3 – fig. 5* vs. *3.4 – fig. 1C*). Hence this may indicate a certain biological sorting-effect of the ECM that has previously been shown impressively by Shamis and colleagues and is frequently discussed as the “dynamic reciprocity” of the matrix [48-50]. In this connection the oppositional effect of LV stretching on neonatal cardiomyocytes vs. C2C12 cells underscores particularly the significance of the ECM´s micro-architecture, especially as biomechanical stretch has been shown to significantly increase the metabolic activity of C2C12 cells [51-52]. Moreover a recent study has shown a deeper analysis of cellular vitality depending on the morphologic features of the cell (shape) during uniaxial stretching of C2C12 cells in 2D and reported a decreasing relative vitality by increasing circularity [53]. So it may be summed up that the preparation of cells prior to repopulation on the one hand and the timing of biomechanical stimulation in dependency on morphology and maturity of the cells on the other hand are potentially important features for a successful stimulation of 3D cardiac constructs.

On the contrary, concerning cellular alignment as quantified by the orientation density, LV stretching resulted in similar values for C2C12 cells exhibiting 0.95 ± 0.21 percent per degree as well as neonatal rat cardiomyocytes exhibiting 1.28 ± 0.26 percent per degree as shown in *3.3 - fig. 7* and *3.4 – fig. 4A*. Interestingly for non-stimulated controls, WHC repopulated with neonatal rat cardiomyocytes exhibit apparently higher OD´s than those composed of C2C12 cells by 0.69 ± 0.07 vs. 0.41 ± 0.06 percent per degree (*3.3 - fig. 7* and *3.4 – fig. 4A*). As a matter of principle this may further confirm the biological sorting effect of the matrix as mentioned above.

5. Conclusion

In an overall conclusion we could successfully complete the first 3 levels of the 4-stage multilevel approach while the 4th level could not be totally completed, but beneficial information could be gathered, that deliver starting points for further optimization. Ultimately, a general process concept could be developed and the impact of biophysical stimulation has been evaluated along the herein presented work.

At the fist level **“Verification of availability of suitable biologic raw-material”** we paved the way by a first process-analytical clarification of decellularization mechanistics that enabled non-destructive quality control of the prepared decellularized scaffolds. Further it may help to refine and optimize a wide range of decellularization strategies that have been established for diverse tissues and organs to this day. Moreover, for the first time we provided a computer-model that offers basic estimations for a mathematical description and *in silico* investigations of decellularization processes (see in detail: *3.1 – 5.*).

Building upon this, the second level “**Enabling of quality control and process automation for a preparative process-upstream**” could be overcome by showing a fast process accompanying detectability of biomass in decellularization perfusates based on the evaluation of rheological characteristics and the resulting fluid-dynamical effects with a direct influence to the variables of pressure controlled perfusion-based decellularization. Actually these methods offer a first proposal for a process-control that enables to individualize decellularization protocols to the single processed organ. Thereby excessive residence times of decellularization agents can be avoided and potentially negative side-effects can be minimized (see in detail: *3.2 – 5.*).

To master the demanding challenge of “**Enabling automation for processing and cultivation methods for production processes**” at the third level, a bunch of technical hurdles had to be faced. In order to accomplish these tasks convincingly, we developed a modular and integrative bioreactor system for whole-heart tissue engineering as a universal tool. According to the current state of knowledge in conventional myocardial tissue engineering, we were able to transfer the well established cultivation and processing concepts of biomechanical and electrophysiological field stimulation to whole heart constructs and to embed them into fully automated processing aided by the bioreactor system. Both, biomechanical stretching and electrophysiological field-stimulation were successfully converted to whole heart constructs for the first time (see in detail: *3.3 – p. 74. & 3.5 – 5.*).

In order to proceed with the aspired “**Development and optimization of bioprocesses for the production**” at the fourth and last level, using the mentioned bioreactor system, another set of very specific scientifically-technical demands had to be solved. Therefore we had to deviate very consciously from the common procedure to aspire as highly developed constructs as possible by every single process. In contrast we successfully deconstructed the entire procedure of whole heart tissue engineering to rather short and robust operations, designed the strategy of short control based model cultivations and used it to investigate and identify essential impacts of biophysical stimulation to the myocardial development in WHC. Thereby our results have shown clear beneficial influence of the integrated biophysical stimulation on myocardial maturation by increasing cellular alignment and spatial organization as well as enhancing specific myocardial protein and gene expression.

Both, the left ventricular stretching system and the principle of an alternating eight-pole field are novel self-developments that delivered completely new options for complex integrated three-dimensional stimulation of whole heart constructs (see in detail: *3.4 – p. 84. & 3.5 – 5.*).

Furthermore to the best knowledge of the author, the corresponding studies represented in this thesis are also the first control-based studies showing comparative investigations of biophysically stimulated WHC. However, the further development of a holistic and optimized production-process based on the findings of the presented proof of principle studies could not be realized within the limits of this thesis.

Finally the scientific relevance of this thesis was validated simply in course of ordinary scientific processing of the particular sub-aspects. In recapitulation for the aspect of **Process Analytics and Process Automation for Whole Heart Decellularization** the basic idea as well as the complete approach was initially picked up and cited explicitly by the well respected Uygun group at the Harvard Medical School [39] (explained in detail in chapter 4.1). Soon afterwards, in the recent past, this subject attracted more scientific attention in terms of a debate concerning our work of 3.2 contrasted to a later study, that assesses flow dynamics in a whole heart throughout the decellularization procedure amongst other evaluations [38, 54] (explained in detail in chapter 4.1).

Last but not least by now also the renowned Prof. Badylak from the McGowan Institute for Regenerative Medicine picked up the aspect of quality assurance for decellularized scaffolds [55]. So it may be assumed that this aspect actually becomes established in the field of whole organ tissue engineering.

Essentially in the same way, the aspects of **Bioreactor and Bioprocess Design for Biophysical Stimulation of Whole Heart Constructs** have shown their relevance due to several citations in subsequent literature. A particular meaningful example is illustrated by the explicitly mentioned bioreactor system for biophysical stimulation (as shown in 3.3) in a review by Luis Tapias and Harald Ott from 2014 [32]. Particular technical solutions were also mentioned in a review by Doris Taylor, Rohan Park and Luiz Sampaio from the Texas Heart Institute [50]. Both reviews can be considered as current standard literature in the field of whole heart tissue engineering.

Finally the approach of left ventricular stretching has been adopted by others and is integrated to one of the most recent studies in the field [5] (*3.4 – p.84*). So it can be assesed, that our contributions to these aspects have been recognized and accepted by the scientific community as well.

While the central working hypothesis of this work was that that neither the scientific advance and state of knowledge, nor the scientific-technical state of the art already complied with the demands of the high scientific level of WHC cultivations under the settings of maximal clinical relevancy, we faced the challenge to make this gap up by working towards a holistic integrative processing concept, that incorporates the well known and established principles of myocardial tissue engineering to the whole heart approach.

We are confident, that the findings of the particular studies in all sub-aspects of this thesis have contributed to the scientific-technical state of the art in this field and thereby may have reduced the rigor of the initial working hypothesis.

6. Outlook

In figure 7, complementary to the description of the study structure, the potential continuative work to pursue the overall effort to strive towards reasonable translational research and finally an approval for clinical trials is illustrated too.
In this sense on the one hand, it seems that the most important and necessary continuation for a potential pharmaco-industrial production of decellularized whole organ scaffolds would be the systematic further development of the process-analytical debris monitoring to a general automation concept, that individualizes particular protocols so single processed organs.
On the other hand, respectively concerning the utilization of the whole heart scaffolds for the generation and processing of WHC, the found beneficial effects of the transferred and established biophysical stimulation methods have to be incorporated into a profound process optimization. Thereby the model have to be scaled up to human sized scaffolds, the cultivation time have to be extended, the empiricism have to be raised and potential summation effects of the left ventricular stretching and the electrophysiological stimulation methods have to be investigated before an optimized process-setting can be determined and be used as a suitable tool for the screening of potentially clinically relevant cell types.

In parallel, in consideration of prospective real pre-clinical *in vivo* transplantations of myocardial patches in an animal model, the seeding technique has to be optimized as well to ensure completely vital replacement tissue. Finally, for a successful integration into the host-tissue, those patches would have to be thoroughly endothelialized as well. This aspect was excluded completely from this work and has to be picked up by external literature.

7. References

List of references that were cited in the chapters 1 and 4 and 6. The studies as presented in 3.1 to 3.5 include their associated reference lists respectively.

1. eurostat (5/4/2016): Todesursachen im Jahr 2013. Über 1 Million Personen starben in der EU an einem Herzinfarkt oder Schlaganfall. Vincent BOURGEAIS, eurostat-pressoffice@ec.europa.eu. Available online at http://ec.europa.eu/eurostat/documents/2995521/7247557/3-04052016-BP-DE.pdf.
2. Ott, Harald C.; Matthiesen, Thomas S.; Goh, Saik-Kia; Black, Lauren D.; Kren, Stefan M.; Netoff, Theoden I.; Taylor, Doris A. (2008): Perfusion-decellularized matrix. Using nature's platform to engineer a bioartificial heart. In *Nature medicine* 14 (2), pp. 213–221. DOI: 10.1038/nm1684.
3. Suuronen, Erik J.; Ruel, Marc (2015): Biomaterials for cardiac regeneration. Cham: Springer.
4. Weinberger, Florian; Mannhardt, Ingra; Eschenhagen, Thomas (2017): Engineering Cardiac Muscle Tissue: A Maturating Field of Research. In *Circulation research* 120 (9), pp. 1487–1500. DOI: 10.1161/CIRCRESAHA.117.310738.
5. Guyette, Jacques P.; Charest, Jonathan M.; Mills, Robert W.; Jank, Bernhard J.; Moser, Philipp T.; Gilpin, Sarah E. et al. (2016): Bioengineering Human Myocardium on Native Extracellular Matrix. In *Circulation research* 118 (1), pp. 56–72. DOI: 10.1161/CIRCRESAHA.115.306874.
6. Tao, Ze-Wei; Mohamed, Mohamed; Hogan, Matthew; Salazar, Betsy; Patel, Nikita M.; Birla, Ravi K. (2015): Establishing the Framework for Fabrication of a Bioartificial Heart. In *ASAIO journal (American Society for Artificial Internal Organs : 1992)* 61 (4), pp. 429–436. DOI: 10.1097/MAT.0000000000000233.
7. Yasui, Haruyo; Lee, Jong-Kook; Yoshida, Akira; Yokoyama, Teruki; Nakanishi, Hiroyuki; Miwa, Keiko et al. (2014): Excitation propagation in three-dimensional engineered hearts using decellularized extracellular matrix. In *Biomaterials* 35 (27), pp. 7839–7850. DOI: 10.1016/j.biomaterials.2014.05.080.
8. Weymann, Alexander; Patil, Nikhil Prakash; Sabashnikov, Anton; Jungebluth, Philipp; Korkmaz, Sevil; Li, Shiliang et al. (2014): Bioartificial heart: a human-sized porcine model--the way ahead. In *PloS one* 9 (11), e111591. DOI: 10.1371/journal.pone.0111591.
9. Lu, Tung-Ying; Lin, Bo; Kim, Jong; Sullivan, Mara; Tobita, Kimimasa; Salama, Guy; Yang, Lei (2013): Repopulation of decellularized mouse heart with human induced pluripotent stem cell-derived cardiovascular progenitor cells. In *Nature communications* 4, p. 2307. DOI: 10.1038/ncomms3307.
10. Maher, Brendan (2013): Tissue engineering: How to build a heart. In *Nature* 499 (7456), pp. 20–22. DOI: 10.1038/499020a.
11. Badylak, Stephen F.; Dziki, Jenna L.; Sicari, Brian M.; Ambrosio, Fabrisia; Boninger, Michael L. (2016): Mechanisms by which acellular biologic scaffolds promote functional skeletal muscle restoration. In *Biomaterials* 103, pp. 128–136. DOI: 10.1016/j.biomaterials.2016.06.047.
12. Tiburcy, Malte; Hudson, James E.; Balfanz, Paul; Schlick, Susanne; Meyer, Tim; Chang Liao, Mei-Ling et al. (2017): Defined Engineered Human Myocardium With Advanced Maturation for Applications in Heart Failure Modeling and Repair. In *Circulation* 135 (19), pp. 1832–1847. DOI: 10.1161/CIRCULATIONAHA.116.024145.
13. Ogle, Brenda M.; Bursac, Nenad; Domian, Ibrahim; Huang, Ngan F.; Menasche, Philippe; Murry, Charles E. et al. (2016): Distilling complexity to advance cardiac tissue engineering. In *Science translational medicine* 8 (342), 342ps13. DOI: 10.1126/scitranslmed.aad2304.

14. Taylor, D. A.; Sampaio, L. C.; Gobin, A. (2014): Building new hearts: a review of trends in cardiac tissue engineering. In *American journal of transplantation : official journal of the American Society of Transplantation and the American Society of Transplant Surgeons* 14 (11), pp. 2448–2459. DOI: 10.1111/ajt.12939.

15. Taylor, Doris A.; Caplan, Arthur L.; Macchiarini, Paolo (2014): Ethics of bioengineering organs and tissues. In *Expert opinion on biological therapy* 14 (7), pp. 879–882. DOI: 10.1517/14712598.2014.915308.

16. Badylak, Stephen F.; Taylor, Doris; Uygun, Korkut (2011): Whole-organ tissue engineering. Decellularization and recellularization of three-dimensional matrix scaffolds. In *Annual review of biomedical engineering* 13, pp. 27–53. DOI: 10.1146/annurev-bioeng-071910-124743.

17. Weymann, Alexander; Loganathan, Sivakkanan; Takahashi, Hiroaki; Schies, Carsten; Claus, Benjamin; Hirschberg, Kristóf et al. (2011): Development and Evaluation of a Perfusion Decellularization Porcine Heart Model. In *Circ J* 75 (4), pp. 852–860. DOI: 10.1253/circj.CJ-10-0717.

18. Akhyari, Payam; Aubin, Hug; Gwanmesia, Patricia; Barth, Mareike; Hoffmann, Stefanie; Hülsmann, Jörn et al. (2011): The quest for an optimized protocol for whole-heart decellularization. A comparison of three popular and a novel decellularization technique and their diverse effects on crucial extracellular matrix qualities. In *Tissue engineering. Part C, Methods* 17 (9), pp. 915–926. DOI: 10.1089/ten.TEC.2011.0210.

19. Aubin, Hug; Kranz, Alexander; Hulsmann, Jorn; Lichtenberg, Artur; Akhyari, Payam (2013): Decellularized whole heart for bioartificial heart. In *Methods in molecular biology (Clifton, N.J.)* 1036, pp. 163–178. DOI: 10.1007/978-1-62703-511-8_14.

20. Price, Andrew P.; Godin, Lindsay M.; Domek, Alex; Cotter, Trevor; D'Cunha, Jonathan; Taylor, Doris A.; Panoskaltsis-Mortari, Angela (2015): Automated decellularization of intact, human-sized lungs for tissue engineering. In *Tissue engineering. Part C, Methods* 21 (1), pp. 94–103. DOI: 10.1089/ten.tec.2013.0756.

21. Hülsmann, Jörn; Aubin, Hug; Kranz, Alexander; Godehardt, Erhardt; Munakata, Hiroshi; Kamiya, Hiroyuki et al. (2013): A novel customizable modular bioreactor system for whole-heart cultivation under controlled 3D biomechanical stimulation. In *Journal of artificial organs : the official journal of the Japanese Society for Artificial Organs* 16 (3), pp. 294–304. DOI: 10.1007/s10047-013-0705-5.

22. Hülsmann, Jörn; Aubin, Hug; Wehrmann, Alexander; Lichtenberg, Artur; Akhyari, Payam (2017): The impact of left ventricular stretching in model cultivations with neonatal cardiomyocytes in a whole-heart bioreactor. In *Biotechnology and bioengineering* 114 (5), pp. 1107–1117. DOI: 10.1002/bit.26241.

23. Hülsmann, Jörn; Aubin, Hug; Wehrmann, Alexander; Jenke, Alexander; Lichtenberg, Artur; Akhyari, Payam (2016): Whole-Heart Construct Cultivation Under 3D Mechanical Stimulation of the Left Ventricle. In *Methods in molecular biology (Clifton, N.J.)* 1502, pp. 181–194. DOI: 10.1007/7651_2015_317.

24. Zimmermann, W. H.; Fink, C.; Kralisch, D.; Remmers, U.; Weil, J.; Eschenhagen, T. (2000): Three-dimensional engineered heart tissue from neonatal rat cardiac myocytes. In *Biotechnology and bioengineering* 68 (1), pp. 106–114.

25. Kofidis, T.; Akhyari, P.; Boublik, J.; Theodorou, P.; Martin, U.; Ruhparwar, A. et al. (2002): In vitro engineering of heart muscle. Artificial myocardial tissue. In *The Journal of Thoracic and Cardiovascular Surgery* 124 (1), pp. 63–69. DOI: 10.1067/mtc.2002.121971.

26. Radisic, Milica; Park, Hyoungshin; Shing, Helen; Consi, Thomas; Schoen, Frederick J.; Langer, Robert et al. (2004): Functional assembly of engineered myocardium by electrical stimulation of cardiac myocytes cultured on scaffolds. In *Proceedings of the National Academy of Sciences of the United States of America* 101 (52), pp. 18129–18134. DOI: 10.1073/pnas.0407817101.

27. Tandon, Nina; Cannizzaro, Christopher; Chao, Pen-Hsiu Grace; Maidhof, Robert; Marsano, Anna; Au, Hoi Ting Heidi et al. (2009): Electrical stimulation systems for cardiac tissue engineering. In *Nature protocols* 4 (2), pp. 155–173. DOI: 10.1038/nprot.2008.183.

28. Miklas, Jason W.; Nunes, Sara S.; Sofla, Aarash; Reis, Lewis A.; Pahnke, Aric; Xiao, Yun et al. (2014): Bioreactor for modulation of cardiac microtissue phenotype by combined static stretch and electrical stimulation. In *Biofabrication* 6 (2), p. 24113. DOI: 10.1088/1758-5082/6/2/024113.

29. Kensah, George; Gruh, Ina; Viering, Jorg; Schumann, Henning; Dahlmann, Julia; Meyer, Heiko et al. (2011): A novel miniaturized multimodal bioreactor for continuous in situ assessment of bioartificial cardiac tissue during stimulation and maturation. In *Tissue engineering. Part C, Methods* 17 (4), pp. 463–473. DOI: 10.1089/ten.TEC.2010.0405.

30. Mohamed, Mohamed A.; Islas, Jose F.; Schwartz, Robert J.; Birla, Ravi K. (2016): Electrical Stimulation of Artificial Heart Muscle. A look into the electrophysiological and genetic implications. In *ASAIO journal (American Society for Artificial Internal Organs : 1992). DOI:* 10.1097/MAT.0000000000000486.

31. Tandon, Nina; Marsano, Anna; Maidhof, Robert; Wan, Leo; Park, Hyoungshin; Vunjak-Novakovic, Gordana (2011): Optimization of electrical stimulation parameters for cardiac tissue engineering. In *Journal of tissue engineering and regenerative medicine* 5 (6), e115-25. DOI: 10.1002/term.377.

32. Tapias, Luis F.; Ott, Harald C. (2014): Decellularized scaffolds as a platform for bioengineered organs. In *Current opinion in organ transplantation* 19 (2), pp. 145–152. DOI: 10.1097/MOT.0000000000000051.

33. Gilpin, Sarah Elizabeth; Guyette, Jacques P.; Gonzalez, Gabriel; Ren, Xi; Asara, John M.; Mathisen, Douglas J. et al. (2014): Perfusion decellularization of human and porcine lungs: bringing the matrix to clinical scale. In *The Journal of heart and lung transplantation : the official publication of the International Society for Heart Transplantation* 33 (3), pp. 298–308. DOI: 10.1016/j.healun.2013.10.030.

34. Guyette, Jacques P.; Gilpin, Sarah E.; Charest, Jonathan M.; Tapias, Luis F.; Ren, Xi; Ott, Harald C. (2014): Perfusion decellularization of whole organs. In *Nature protocols* 9 (6), pp. 1451–1468. DOI: 10.1038/nprot.2014.097.

35. Wainwright, John M.; Czajka, Caitlin A.; Patel, Urvi B.; Freytes, Donald O.; Tobita, Kimimasa; Gilbert, Thomas W.; Badylak, Stephen F. (2010): Preparation of cardiac extracellular matrix from an intact porcine heart. In *Tissue engineering. Part C, Methods* 16 (3), pp. 525–532. DOI: 10.1089/ten.TEC.2009.0392.

36. Weymann, Alexander; Patil, Nikhil Prakash; Sabashnikov, Anton; Korkmaz, Sevil; Li, Shiliang; Soos, Pal et al. (2015): Perfusion-Decellularization of Porcine Lung and Trachea for Respiratory Bioengineering. In *Artificial organs* 39 (12), pp. 1024–1032. DOI: 10.1111/aor.12481.

37. Uygun, Basak E.; Soto-Gutierrez, Alejandro; Yagi, Hiroshi; Izamis, Maria-Louisa; Guzzardi, Maria A.; Shulman, Carley et al. (2010): Organ reengineering through development of a transplantable recellularized liver graft using decellularized liver matrix. In *Nature medicine* 16 (7), pp. 814–820. DOI: 10.1038/nm.2170.

38. Baptista, Pedro M.; Siddiqui, Mohummad M.; Lozier, Genevieve; Rodriguez, Sergio R.; Atala, Anthony; Soker, Shay (2011): The use of whole organ decellularization for the generation of a vascularized liver organoid. In *Hepatology (Baltimore, Md.)* 53 (2), pp. 604–617. DOI: 10.1002/hep.24067.

39. Geerts, Sharon; Ozer, Sinan; Jaramillo, Maria; Yarmush, Martin L.; Uygun, Basak E. (2016): Nondestructive Methods for Monitoring Cell Removal During Rat Liver Decellularization. In *Tissue engineering. Part C, Methods* 22 (7), pp. 671–678. DOI: 10.1089/ten.TEC.2015.0571.

40. Lee, Po-Feng; Chau, Eric; Cabello, Rafael; Yeh, Alvin T.; Sampaio, Luiz C.; Gobin, Andrea S.; Taylor, Doris A. (2017): Inverted orientation improves decellularization of whole porcine hearts. In *Acta biomaterialia* 49, pp. 181–191. DOI: 10.1016/j.actbio.2016.11.047.

41. Wanjare, Maureen; Huang, Ngan F. (2017): Regulation of the microenvironment for cardiac tissue engineering. In *Regenerative medicine* 12 (2), pp. 187–201. DOI: 10.2217/rme-2016-0132.

42. Hirt, Marc N.; Boeddinghaus, Jasper; Mitchell, Alice; Schaaf, Sebastian; Bornchen, Christian; Muller, Christian et al. (2014): Functional improvement and maturation of rat and human engineered heart tissue by chronic electrical stimulation. In *Journal of molecular and cellular cardiology* 74, pp. 151–161. DOI: 10.1016/j.yjmcc.2014.05.009.

43. JACOBSON, S.; PIPER, H. (1986): Cell cultures of adult cardiomyocytes as models of the myocardium. In *Journal of molecular and cellular cardiology* 18 (7), pp. 661–678. DOI: 10.1016/S0022-2828(86)80939-7.

44. Aubin, Hug; Nichol, Jason W.; Hutson, Che B.; Bae, Hojae; Sieminski, Alisha L.; Cropek, Donald M. et al. (2010): Directed 3D cell alignment and elongation in microengineered hydrogels. In *Biomaterials* 31 (27), pp. 6941–6951. DOI: 10.1016/j.biomaterials.2010.05.056

45. Scarritt, Michelle E.; Pashos, Nicholas C.; Bunnell, Bruce A. (2015): A review of cellularization strategies for tissue engineering of whole organs. In *Frontiers in bioengineering and biotechnology* 3, p. 43. DOI: 10.3389/fbioe.2015.00043.

46. Momtahan, Nima; Poornejad, Nafiseh; Struk, Jeremy A.; Castleton, Arthur A.; Herrod, Brenden J.; Vance, Brady R. et al. (2015): Automation of Pressure Control Improves Whole Porcine Heart Decellularization. In *Tissue engineering. Part C, Methods* 21 (11), pp. 1148–1161. DOI: 10.1089/ten.TEC.2014.0709.

47. Ren, Xi; Tapias, Luis F.; Jank, Bernhard J.; Mathisen, Douglas J.; Lanuti, Michael; Ott, Harald C. (2015): Ex vivo non-invasive assessment of cell viability and proliferation in bio-engineered whole organ constructs. In *Biomaterials* 52, pp. 103–112. DOI: 10.1016/j.biomaterials.2015.01.061.

48. Shamis, Yulia; Hasson, Eilat; Soroker, Avigail; Bassat, Elad; Shimoni, Yael; Ziv, Tamar et al. (2011): Organ-specific scaffolds for in vitro expansion, differentiation, and organization of primary lung cells. In *Tissue engineering. Part C, Methods* 17 (8), pp. 861–870. DOI: 10.1089/ten.tec.2010.0717.

49. Sanchez, Pedro L.; Fernandez-Santos, M. Eugenia; Costanza, Salvatore; Climent, Andreu M.; Moscoso, Isabel; Gonzalez-Nicolas, M. Angeles et al. (2015): Acellular human heart matrix: A critical step toward whole heart grafts. In *Biomaterials* 61, pp. 279–289. DOI: 10.1016/j.biomaterials.2015.04.056.

50. Taylor, Doris A.; Parikh, Rohan B.; Sampaio, Luiz C. (2017): Bioengineering Hearts. Simple yet Complex. In *Current stem cell reports* 3 (1), pp. 35–44. DOI: 10.1007/s40778-017-0075-7.

51. Saito, Tsugumichi; Okada, Shuichi; Shimoda, Yoko; Tagaya, Yuko; Osaki, Aya; Yamada, Eijiro et al. (2016): APPL1 promotes glucose uptake in response to mechanical stretch via the PKCzeta-non-muscle myosin IIa pathway in C2C12 myotubes. In *Cellular signalling* 28 (11), pp. 1694–1702. DOI: 10.1016/j.cellsig.2016.07.010.

52. Ilaiwy, Amro; Quintana, Megan T.; Bain, James R.; Muehlbauer, Michael J.; Brown, David I.; Stansfield, William E.; Willis, Monte S. (2016): Cessation of biomechanical stretch model of C2C12 cells models myocyte atrophy and anaplerotic changes in metabolism using non-targeted metabolomics analysis. In *The international journal of biochemistry & cell biology* 79, pp. 80–92. DOI: 10.1016/j.biocel.2016.08.012.

53. Wang, Dong; Zheng, Wenfu; Xie, Yunyan; Gong, Peiyuan; Zhao, Fang; Yuan, Bo et al. (2014): Tissue-specific mechanical and geometrical control of cell viability and actin cytoskeleton alignment. In *Scientific reports* 4, p. 6160. DOI: 10.1038/srep06160.

54. Aubin, Hug; Hülsmann, Jörn; Lichtenberg, Artur; Akhyari, Payam (2017): Comment on "Inverted orientation improves decellularization of whole porcine hearts" by Lee et al. In *Acta biomaterialia* 53, pp. 643–644. DOI: 10.1016/j.actbio.2017.01.067.

55. White, Lisa J.; Taylor, Adam J.; Faulk, Denver M.; Keane, Timothy J.; Saldin, Lindsey T.; Reing, Janet E. et al. (2017): The impact of detergents on the tissue decellularization process: A ToF-SIMS study. In *Acta biomaterialia* 50, pp. 207–219. DOI: 10.1016/j.actbio.2016.12.033.

8. List of Figures

	Title and Legend	Page
Fig.1	**Thematic Diagram.** Illustration of connected thematic fields representing the context of this thesis in a scheme. It describes the overall proceeding by overcoming technical hurdles and industrial barriers to work towards the systematic destination of whole heart constructs as a medical device.	9
Fig.2	**Graphical Abstract of the Process Analytical Strategy**. Native ovine hearts are decellularized by a standard perfusion protocol. Completeness and quality of the decellularization is evaluated by classical disruptive methods, which also resulted in validated benchmark data by biomass balancing. Thereby determined parameters characterize the process and become utilized as complement variables of non-destructive process monitoring. The entire process can be described using these parameters and variables and specific dynamics can be determined.	11
Fig.3	**Perfusion Based WST-1 Assay for Assessment of Metabolic Activity in Repopulated Whole Heart Construct.** The scaffold appears in red caused by the phenol-red pH indicator of the perfused cell culture medium. The contrasted areas macroscopically illustrate injections sites that demonstrate metabolic activity of the repopulated cells by the chromatic formazan product as illustrated by the arrows.	14
Fig.4	**3D Distribution of evaluated circularities and orientation angles for nuclei in confocal microscopic digitalization's of whole heart constructs after specific staining**. Fractions of clearly oriented cell structures (FO) can be identified comparative for stimulated constructs vs. non-stimulated controls. The resulting specific orientation density can further be determined by relating the particular FO to its corresponding angle range (AR).	15
Fig.5	**Graphical Abstract of the Study**. The shown sequence illustrates the processing and following exemplary investigation of the processed whole heart constructs (WHC) to investigate the impact of left-ventricular stretching to myocardial development in WHC.	18
Fig.6	**Hardware Setup of an 8-pole Stimulation Processing Chamber**. The perfusion and processing chamber for WHC is based on a square formed 250 ml flask. There are 6 mm olives added at all 8 edges to insert carbon rod electrodes sealed in by food-silicone. Two more olives are placed centric at the upper and above end of one planar side to connect tubes for the perfusion path and potential medium exchange. The perfused WHC gets mounted in combination with the screw-cap and localizes centrally in between the electrodes.	20
Fig.7	**Study structure**: In accordance to figure 1 industrial barriers are indicated in red and technical hurdles in blue. Here the corresponding methods aiding to overcome these limitations are illustrated by arrows and contrasted by the related works. The wide horizontal arrow in the middle illustrates the central circle of figure 1, showing the procedure of project approach 3 with its design to develop and optimize bioprocessing strategies. In green: achievements contributed by this work. In grey: potential continuative work.	21
3.1 - 1	**Decellularization efficacy of human-scale *in toto* decellularized ovine whole-hearts I.A-C)** Representative macroscopic images of perfusion-based decellularized ovine whole-hearts showing no gross decellularization deficit; (A) back view, (B) front view, (C) cross sections. **D-H)** Representative macroscopic images of standardized sections of *in toto* decellularized ovine hearts, demonstrating consistent homogeneous transparency. **I)** Representative images of HE (1-2,4-5) and	34

DAPI (3,6) stained standardized sections of native (1,4) and *in toto* decellularized ovine hearts (2-3,5-6), showing removal of cell nuclei and cellular remnants, with however remaining DNA traces after whole-heart decellularization. Scale bar, 500 µm. **J)** Quantitative assessment of DNA tissue content in native and *in toto* decellularized ovine hearts normalized to the native control and plotted as relative fractions. Data presented as mean ± SD.

3.1 - 2 **Biomass discharge during ovine whole-heart decellularization I – macroscopic view**. Representative macroscopic images of dry biomass (DBM) of native and perfusion-based *in toto* decellularized ovine hearts. **A**) Left: desiccated native ovine heart. Right: desiccated decellularized ovine heart. **B**) Total DBM of one complete ovine heart after *in toto* decellularization and separation of the gross soluble lipid fraction. **C)** Desiccated native (upper line) and *in toto* decellularized (lower line) rodent hearts. **D-E)** Wet and desiccated standardized ovine myocardial tissue samples before (left) and after non-perfusion-based decellularization (right). 35

3.1 - 3 **Decellularization efficacy of human-scale *in toto* decellularized ovine whole-hearts II.A)** Relative collagenous to non-collagenous protein content of ovine hearts before and after perfusion-based *in toto* decellularization, demonstrating a statistical significant reversal of the ratio after the decellularization process. **B)** Locoregional analysis of relative collagenous to non-collagenous protein content showing consistent values after the decellularization process, independent from the myocardial region. n, native; d, decellularized; LV, left ventricular; RV, right ventricular; S, septum. Data presented as mean ± SD. **C-F)** Representative Western blot signals and corresponding densitometric histograms for desmin and cardiac actin for *in toto* decellularized ovine hearts as compared to native controls, respectively. **G)** Semi-quantitative evaluation of the densitometric signals presented as quota to the signal of the native control (normalized to 100 %), revealing almost full removal of cardiac actin and only marginal detection of residual desmin. $p<0.0001$. 36

3.1 - 4 **Biomass discharge during ovine whole-heart decellularization II - parameters of biomass balancing. A)** Dry biomass (DBM) of ovine (blue) and rodent (green) hearts as well as standardized ovine myocardial tissue samples (red) before and after decellularization, showing the total solid biomass discharge during the process (ΔDBM). For ovine hearts this illustrates the total amount of DBM that is discharged during the decellularization process from the myocardial tissue, excluding the gross soluble lipid fraction originating from the epicardial fat, which is not present in the other two sample types. **B)** Fat-dependent and -independent biomass ratios of ovine hearts, demonstrating the important gross soluble lipid fraction (Fat) of the total DBM after the decellularization process**.** $\mathrm{DBM(WBM)^{-1}}$, illustrates the relation of DBM to WBM with and without Fat after the decellularization process. $\mathrm{Fat(WBM)^{-1}}$, illustrates the relation of Fat to WBM before and after the decellularization process. $\mathrm{Fat/DBM_{fat\text{-}free}}$**,** illustrates the mass ratio of Fat to fat-free DBM in native ovine hearts. **C)** Fat-free biomass ratios of initial DBM (native) and DBM discharge during the decellularization process (ΔDBM) normalized to their corresponding native WBM of ovine (blue) and rodent (green) hearts, as well as standardized ovine myocardial tissue samples (red), revealing comparable values for all samples. **D)** Detectable protein fraction of the discharged solid biomass during the decellularization process of ovine (blue) and rodent (green) hearts, as well as standardized ovine myocardial tissue samples (red), demonstrating a much lower detectable protein fraction for ovine as compared to rodent tissue. 37

3.1 - 5 **Biomass discharge during ovine whole-heart decellularization III - discharge dynamics based on detected total-protein in perfusates**. **A)** Cumulative discharged total protein P_{tot} (t) over time during ovine whole-heart decellularization normed to the WBM of the individual heart. Blue line /grey area, mean/range of standardized detectable protein discharge within the decellularization perfusates per initial tissue weight [P_{tot} $(\Delta\mathrm{DBM\ WBM})^{-1}$]; red line, mean standardized solid 38

3.1 – S3 **Biomass-comparative discharge dynamics & kinetics. A**) Dry biomass (DBM) of ovine (blue) and rodent (green) hearts as well as standardized ovine myocardial tissue samples (red) before and after decellularization in temporal intervals according to the duration of the decellularization process, logistic scale. By temporal parallel transition a simple comprehensive regression could be applied, fitting all datapoints ((R^2) of 0.992). **B**) Dry biomass (DBM) of ovine (blue) and rodent (green) hearts as well as standardized ovine myocardial tissue samples (red) before and after decellularization in temporal intervals according to the duration of the decellularization process, linear scale; showing a virtual comprehensive biomass decomposition course equal for all ranges of biomass represented. 48

3.2 - 1 **Flow chart of the decellularization protocol and sampling operation timetable.** Single arrowheads symbolize single batch-wise perfusion intervals. The durations of each interval and the respective perfusion solution are denoted. The lower arrows symbolize the time point of sample withdrawal of the perfusate at the end of each single interval. The glossary of the samples is indicated by the order of the used solutions and the number of exchanges done. S, solution; X, exchange; SDS/DCA, detergent-based solution containing SDS and sodium desoxycholate (DCA); aqua bidest; double-distilled water; phosphate buffered saline (PBS). 51

3.2 - 2 **Exemplary course of perfusion pressure and the actuating RS-P.** The courses of the value of perfusion pressure (expressed in mmHg, purple line) and the actuating RS-P (rounds per minute, green line) as well as the fix setpoint for the perfusion pressure (black line) are marked with black arrows. The single steps of the protocol are indicated by the bars and the denotation of the used solutions (S1, solution 1; S2, solution 2; S3, solution 3). The feedback control system keeps the perfusion pressure in the range of the setpointwith a very good quality of control (80 mmHg). The black circles mark the events and time points when the pumps occlusion and the regulator parameters were adjusted because the actuating variable reached its maximum range. 53

3.2 -3 **Dry biomass of native versus acellular rat hearts.**(a) Mass of the weighted dried native and acellular hearts (n= 4 for each group), $p< 0.0001$. (b) Representative images of dried native and decellularized hearts demonstrate the remarkable reduction in the volume of the remaining dried ECM in contrast to the whole native heart. 53

3.2 - 4 **Chart of the total protein amount in the perfusates.** Samples of perfusates were obtained at the end of every perfusion interval (while exchanging the perfusion solution) during the decellularization of whole hearts (n= 6). Abbre-viations and sampling operation timetable are according to figure1.Significant protein content was only detected in theperfusates of the first and the second perfusion interval of the first step (SDS/DCA). The underlying measured data of allfollowing samples are close to zero, according to the applied methods. ***$p< 0.001$ for perfusate S1_X1 versus all other perfusates. 54

3.2 -5 (a) Protein content of the perfusates as determined by SDS PAGE. Protein bands were stained with Bio-Rad™Flamingo pink. Presented is a surface plot of the band intensities. Lines represent the perfusate samples: (1)& 10) Ladder (10–250 kDa); the absence of protein bands in lines 4–9 supports the findings demonstrated in figure 4. (b) Time course of cumulatively discharged total protein m_x(t) in [g] standardized to the absolute discharged protein BTM out in [g]. It can be observed that the discharge of total protein seems to reveal an exponential character that reaches a saturation limited by the total cellular protein content of the hearts. (b) Rheological flow curves while perfusion step one (S1_X1). Series of flow curves of the corresponding samples show that detectable evolution of viscosity may not be observed before 4–5 h of perfusion. Colored points display the starting point of each flow curve. 55

the perfusion control data for characteristic events based on effects to fluid dynamical characteristics caused by potentially altering rheological activity of the perfusate (see figure 2)(blue). As an alternative, process-accompanying rheological measurements enable the detection of characteristic process stages to adapt the process-guiding strategy to individual organs (red). The pressure-controlled perfusion circuit is drafted in black, as adopted from previous work [4]. (1) Organ perfusion chamber; (2) perfusion pressure transducer; (3) computer hardware running the custom engineered control software; (4) actuating peristaltic perfusion pump. (a) Rheological characterization of a fresh perfusate sample; (b) algorithm for a stepwise analysis of the progress of decellularization; (c) digital out converter and interface to the valves, governing the inflow of different solutions to the perfusion circuit (d); and (e) reservoirs containing single perfusion solutions, volume renewal and feeding of the perfusion system is organized by draining the needed volume from here.

3.3 -1 **Close-up view of a decellularized rat heart mounted into the processing chamber.** Asterisk ventricular part of the decellularized heart, black arrow upper end of the balloon inserted into the left ventricle via the mitral valve, filled arrow head sealing coat of the pressure pipe, half-filled arrow head pressure pipe (duroplastic tube) 66

3.3 - 2 **Draft of the bioreactor systems functions.** 1 Pump system. The movable cock indicates the composition of a membrane and a syringe pump. So the volume V(t) is adjustable as well as the bursting of the system with volume-pulses of controllable stroke volume V_{hub}(t) and frequency f(t). 2 Un-expandable PTFE tubes conducting the expand-ing-fluid. 3 Pressure transducer to observe the pressure signal of the 3D stretching device fluid. 4 Perfused and stimulated, re-populated decellularized rat heart. The inflatable stretching balloon is inserted to the left ventricle. The aorta is cannulated for perfusion of the coronaries. The transmural pressure inside of the balloon is a function of the filling-volume as well as the elasticity and the form of the ventricle. 5 Pressure transducer for the perfusion pressure inside of the silicone tubing system. 6 Peristaltic pump. Herewith the perfusion pressure is actuated bythe volume flow. 7 Vertex-net as achieved by laser scanning of the surface of a re-populated, perfused and processed whole heart in the bioreactor system. Ao Cannulated aortic root, LV left ventricle, RV right ventricle. Red rows give an impression of differing operation states resulting in differing degrees of stretching. 8 Screenshot of the PCS visualizing flow charts of the stimulation pressure signal (lower) and of the determined pressure amplitude (upper). White arrow indicates the actual pressure ampli-tudes; white arrow with black edge indicates the axis of abscissa, that is scaled to the cycles of the process control system (several pressure peaks are incorporated to one single cycle); black arrow indicates the axis of abscissa of the amplitude control course that is scaled in minutes of process time; black arrow with the white edge shows the line of the amplitude of pressure. 67

3.3 - 3 **Surface scanned processed rat heart.** Detail-picture of subitem 7 of Fig. 2. The heart is displayed by a vertex-net as achieved by laser scanning of the surface of a re-populated, perfused and processed whole heart in the bioreactor system. Ao Cannulated aortic root, LV left ventricle, RV right ventricle. Red rows give an impression of differing operation states resulting in differing degrees of stretching. 67

3.3 - 4 **Lateral view of the culture chamber.**Based on a commercially available reagent bottle, a custom-made and application-adoptedculture chamber was constructed. 1 250 ml flask; 2 thin planar glass panel for optical accessibility and high precision optical analysis; 3 modified GL 45 2-Port lid; 4 cut-off cocks of the pressure pipes; 5 bubble trap; 6 pt-100 temperature sensor; 7 filter-equipped (0.2 lm) connection for pressure compensation; 8 pressure pipes for balloon expansion. 68

3.3 - 5 **Increase of cellular metabolism after cultivation by WST-1 cell proliferation reagent.** Cellular metabolism was measured by perfusion application of 1/3 concentrated WST-1 cell proliferation reagent assay. The assay was applied before the initiation of the mechanical stimulation (24 h after seeding) and after finishing the process (96 h after seeding) both for stimulated and non stimulated hearts. The diagram depicts the percentage of augmentation of measured cellular metabolism after 96 h of cultivation relative to the activity after 24 h of cultivation. The calculated percentaged increase of metabolism is depicted in bars representing the arithmetic average with error bars representing the standard deviation. Two stars represent p \ 0.01 for control vs. stimulated group. 70

3.3 - 6 **Confocal microscopic visual analysis of cellular orientation and arrangement of the cultivated cells inside of the hearts ECM.** Representative images of repopulated hearts with C2C12-myoblast, demonstrate viable cellular networks with aligned cells. While in nonstimulated hearts cellular orientation can be observed along ECM fibers following the anisotropy of the matrix, mechanically stimulated hearts show a higher 3D spatial orientation with more elongated cell bodies and nuclei. Nuclei and cytoplasmatic nuclear acids are presented in green by acridine orange staining, while the cytoskeleton is presented in red by F-Actin staining. Representative pictures of nonstimulated and stimulated hearts are depicted in paired columns marked by the dashed rectangles. Nonstimulated hearts: marked blue (I, III and V); mechanically stimulated hearts: marked red (II, IV and VI). Rows A, B and C show the acridine orange, the F-actin and the merged signals respectively. White dotted rows in row I and II indicate the different preferred orientational axis of the pictured cells in the different layers. Bars 50 µm. 71

3.3 - 7 **Specific orientation density (OD) of cells inside of stimulated vs. nonstimulated constructs.** OD representing the ratio between the fraction of clearly oriented cells (FO) and angle range of the concerning FO (AR) is depicted for the stimulated vs. the nonstimu-lated constructs, demonstrating a significantly greater alignment for the stimulated group (p = 0.0128). 72

3.4 - 1 **Repopulation and metabolic activity.** (A) DAPI stained LVW of repopWHC. Spatially widespread DAPI signal (blue) indicates injected cells with a high depth of infiltration into the matrix cavity. (B) Differential spatial spreading of injected cells in the LVW of repopWHC. Image from a representative DAPI stained cross section has been converted to grayscale to highlight the spatial distribution of the cells. Dashed lines illustrate the main axes of different clustered strands. (C) The diagram depicts the gain of measured absorbance of the applied WST-1 stain after 96 h of bioreactor cultivation relative to the initial activity as measured 24 h after injection for stimulated versus non-stimulated constructs. (D and E) Repopulated and metabolic active areas become macroscopically visible after staining by WST-1 reagent. 78

3.4 - 2 **Cellular vitality of repopWHC.** (A) Quantitative evaluation of the fractions of living and dead cells. At 24 h after injection living cells account for 83.3 10.4%, of all cells, with an increase to 89.3 8% and 86.5 15% after additional 96 h of static cultivation (non-stimulated) or cultivation with biomechanical stimulation of the left ventricle (stimulated), respectively. High cell vitality showing vast infiltration of the ECM. (B–D): Representative confocal images of LIVE/DEAD staining of LV specimens of repopWHC after 24 h of repopulation (B), and after additional 96 h of bioreactor cultivation under static conditions (C), or under LV biomechanical stimulation (D), respectively. Green, vital cells; red, non-vital cells. 79

3.4 - 3 **Myocardial functionality of the repopWHC model.** (A) Electrophysiological voltage mapping of isolated neonatal cardiomyocytes as control in a multielectrode array (MEA) set-up. Isolated neonatal cardiomyocytes were seeded on glasdiscs and put onto a 2D glass MEA. (B) Electrophysiological voltage mapping of cultivated repopWHC using the same experimental set-up. The presence of functional, electrophysiologal active cardiomyocytes can be detected by patterns of spontaneous frequent activity. 80

3.4 - 4 **Cellular organization of repopWHC.** (A) Orientation density (OD) of living cells inside was calculated for freshly repopulated WHC in contrast to repopWHC after 96 h of cultivation under biomechanical stimulation versus non-stimulated (static) controls. (B–D) Histograms demonstrate the distribution of measured angles of orientation of cells in freshly repopoulated WHC (B), and in repopWHC cultivated under control conditions (C) versus stimulated conditions (D). (E–G) Histograms demonstrate the distribution of measured circularity of cells in freshly repopoulated WHC (E), and in repopWHC cultivated under control conditions (F) versus stimulated conditions (G). 81

3.4 - 5 **Densitometric evaluation cardiac myosin heavychain (MHC) blot signals:** (A) The diagram shows the relative MHC signal intensity in normalized IOD [IOD g ^{1}] of the WHCs. Levels 1–4 identifies the different pairs, while (+) indicates the stretched repopWHC, and (-) the non-stretched control of each pair. (B) The diagram shows the total protein signal intensity of the 223 kDa protein band, what represents the molecular weight of MHC. (C) Depiction of the corresponding MHC-blot-bands 81

3.4 - 6 **Selective gene expression of repopWHC.** (A) Relative expression level of connexin 43: Pair wise comparison of Cx43 expression for stretched repopWHC versus non-stretched control. For all pairs the stretched repopWHC exhibit at least a 2.5-fold increased Connexin 43 expression with an average of more than 3. (B) Ratio of Connexin 43 expression in contrast to adult and neonatal native controls: Ration of Cx43 expression in repopWHC with or without biomechanical stimulation and with respect to adult and neonatal native controls. 82

3.4 - 7 **Immunodetection of Cx43 and MHC in repopWHC.** Fluorescence microscopic image of immune stained whole left ventricular walls. (A) Non-stimulated repopWHC.Cx43 signals appear in a grainy pattern located in spots, surrounding cell bodies. (B) Stimulated repopWHC. Here, the Cx43 signals appear more intense and more densely distributed all over the repopulated area. The signal arrangement further displays the patterns of oriented strands that get superposed by DAPI stained nucleic structures. (C) Stimulated repopWHC at higher magnification. Cx43 signals appear as a conjunctive interstice (indexed by black arrows) between cell bodies, that can be distinguished by the shadow-nuclei (indexed by blue dashed circles), (D) Single image of the 546 nm channel corresponding to the overlay in B showing the isolated MHC signal for stimulated repopWHC. The MHC signal is present in the Cx43 positive areas, when compared to B. 82

3.5 - 1 **Processing Chamber and Electrical Field. A:** Perfusion and processing chamber for WHC based on a square formed 250 ml flask. There are 6 mm olives added at all 8 edges to insert carbon rod electrodes. Two more olives are placed centric at the upper and above end of one planar side to connect tubes for the perfusion path and potential medium exchange. **B:** Depiction of the 8 pole electrical field, spanned by the carbon rod electrodes. **C:** Perfusion and stimulation installation at work placed inside a CO_2 Incubator. The blue arrows points at the mounted and processed repopulated WHC. **D:** Measured resulting current under applied field stimulation as shown in B. The current was measured in x, y and z direction (as shown in B) in warm cell culture medium (37°C) resulting to applied alternating voltage with pulse durations of 1 to 50 ms. **E:** same diagram as D but shown for pulse durations of 1 to 200 ms. 94

3.5 - 2 **Combining the Particular Oriented Current Flows in Arithmetic Mean Values.** A: Bar Plot of the resulting current flow provoked by alternating voltage at 3, 5 and 8 V for pulse durations of 1 to 200 ms. The particular oriented current flows in x, y and z direction are combined into one arithmetic mean value complemented by its standard deviation to illustrate the spatial uniformity of the current establishment in the three-dimensional eight-pole setting. 95

9. List of Tables

Title and Legend **Page**

10. Declaration on oath / Eidesstattliche Erklärung

Hiermit verischere ich, Jörn Hülsmann, an Eides Statt, dass die Dissertation von mir selbständig und ohne unzulässige fremde Hilfe unter Beachtung der „Grundsätze zur Sicherung guter wissenschaftlicher Praxis an der Heinrich-Heine-Universität Düsseldorf“ erstellt worden ist.

11. Acknowledgements

First and foremost I am greatly indebted to Prof. Dr. Artur Lichtenberg and Prof. Dr. Payam Akhyari for accepting my application back in 2008 to join their team. Initially as a master student, then as a staff-member and finally as a doctor student, it have been eight eventful and moving years of cooperation, that enabled me to learn and gather experience in the fascinating field of tissue engineering and to familiarize within the world of cardiovascular science. In this time I always found receptive ears and great support for the development and advance of my projects by my supervisor and mentor Prof. Dr. Akhyari. Very special thanks are due to him for the trust and confidence he placed in me and for the time and his commitment that he invested in our meetings and discussions. Likewise, I am very grateful to Prof. Dr. Eckhard Lammert and Prof. Dr. Lichtenberg for their friendly and professional supervision.

I also would like to thank Dr. Hug Aubin for the fruitful collaboration in our working group. Further many thanks are due to the whole crew of the *Research Group for Experimental Surgery* and especially Dr. Andreas Weber, Dr. Mareike Barth and Dr. Alexander Jenke for the continuous scientific exchange and the kind and open minded working environment. Not at least my fellow doctoral-students deserve a special mention in the same sense.

This work would not have been possible without the sponsorship by the Susanne Bunnenberg-Stiftung at the Düsseldorf Heart Center and my stipend from the Schmeil-Stiftung, Heidelberg, for which I am very grateful.

Finally my gratitude is dedicated to my whole family, which always has supported me on my journey as an absolute constant.